

THE UNIVERSITY OF HULL

Barscale morphodynamics through the tidal-fluvial transition

being a Thesis submitted for the Degree of Doctor of Philosophy

in the University of Hull

by

Claire Elizabeth Keevil MSci

April 2016

Abstract

A complex transitional zone within river-estuary systems exists between fully-fluvial and fully-tidal conditions. This zone varies both spatially and temporally across a range of scales. The resultant sedimentary transport and depositional characteristics are, at present, poorly understood and a robust model that links processes to products across this complex zone is presently lacking.

Process-product relationships were investigated in two distinctive tidal-fluvial systems: the high fluvial flux mesotidal Columbia River estuary (USA), and the smaller fluvial flux macrotidal River Severn (UK). Spatially and temporally distributed three-dimensional flow and bed morphology data within the two transitions were coupled to sub-surface geophysical and core information.

High resolution bathymetric measurements collected within the Columbia River estuary transition zone allowed investigation of the variations in bedform and bar morphology. The dominant fluvial flow steers asymmetrical bedforms around local barforms, decreasing in size with increasing tidal influence. Barforms commonly have an apparently tidally-influenced lobate planform, however, investigations around a single bar indicated a fluvial origin, with tidal modification restricted to smaller-scale bedforms. Deposition within the River Severn appears fluvial, but the presence of a large tidal bore and strong flood tide is shown to hinder larger scale meander bend migration processes, also resulting in characteristic soft sediment deformation within bar deposits. The deformation may be important for palaeogeographical system reconstruction as tidal bores only form under limited conditions.

Investigations within these two very different systems reveal that both are fluvially-dominated, but with some tidal influence. Although the barforms and surrounding bedforms appear to be fluvial they contain important, although subtle, evidence of the tidal nature of the system. This may be spatially limited and could be hard to detect in both cores and/or geophysical measurements. Careful analysis of the smaller-scale features of ancient lowland fluvial systems is required to observe evidence of this subtle tidal influence.

Acknowledgements

Firstly I must thank Dan Parsons for all his help and supervision throughout the last four years, but in particular I must thank him for allowing me the opportunity to carry out this work! I also thank the many people in Hull who I have shared the last few years with: Chris U, Jordan, Kevin, Leiping, Dave, Xuxu, Laura, Rita, Chloe, Hao, Arjan, Steve, Sally, Chris S and Annie. Particular thanks must go to Rob Thomas for all his help along the way and helpful nudges which have taken me to places I hadn't ever thought about.

Fieldwork on the Columbia River was carried out as part of the NERC funded TIFZ project with Phil Ashworth, Jim Best, Greg Sambrook Smith, Andrew Nicholas, Chris Simpson, Eric Prokocki, Rob Strick, Kiyomi Holman, Pat Killion and Jesse. I was able to take part in the second field season thanks to the British Sedimentological Research Group who granted me a Farrell award.

Fieldwork on the Severn was possible thanks to generosity of Jeff Williams and the Minsterworth Waterski Club who allowed me to use their slipways. Matt, Joe, Brendan, Mike, Leiping, Xuxu and Gareth were all extremely generous with their time and assistance during the work. I must also thank Hubert Chanson, David Reungoat and Pierre Lubin for being so generous with their time and fieldwork whilst introducing me to the wider world of tidal bores.

My family have been a great support during my studies, for which I am extremely grateful: thanks to my Mum (and also for the extensive use of your garage as a base for fieldwork), my sister Kate, Auntie Barbara and the Keevils (Wiltshire and Texan branches). I also need to acknowledge the people who I wish had been able to watch my progress but are no longer here: my Dad, Granny and Nanna – I know that they would all have been very proud and interested in my work. Thanks must also go to Emma and Luca for regular visits and the Sinfonia of Leeds for my Monday evenings of sanity.

Finally, and most importantly, I would like to thank Gareth Keevil. Your help, support and love over the last four years have made it possible for me to do this, even when I doubted I could. Revenge at last!

Contents

| | |
|---|-----------|
| Abstract | i |
| Acknowledgements | ii |
| Contents | iii |
| Figures | vii |
| Tables | xvii |
| Nomenclature | xviii |
| Declaration of authorship | xx |
| 1 Introduction to flow around tidal barforms | 1 |
| 1.1 Context | 1 |
| 1.2 Importance and implications | 4 |
| 1.3 Conceptual models of the tidal-fluvial zone | 6 |
| 1.3.1 Tidally-dominated, fluvially-influenced | 7 |
| 1.3.2 Balanced tidal-fluvial | 8 |
| 1.3.3 Fluvially-dominated, tidally-influenced | 9 |
| 1.4 Tidal bores | 12 |
| 1.5 Thesis aims and objectives | 12 |
| 1.6 Thesis summary | 13 |
| 2 Depositional patterns arising from tidally-influenced flow in a fluvially-dominated system | 15 |
| 2.1 Introduction | 15 |
| 2.2 Field methods | 17 |
| 2.2.1 Field location: the Columbia River Estuary | 17 |
| 2.2.2 Methodology | 22 |
| 2.2.2.1 Bathymetric surveys | 22 |
| 2.2.2.2 Flow measurements | 25 |
| 2.3 Results | 28 |
| 2.3.1 Bathymetry surveys | 28 |
| 2.3.1.1 Northern Channel | 28 |
| i) Desdemona North | 28 |
| 2.3.1.2 Navigation Channel | 28 |
| i) Desdemona South | 31 |
| ii) Bridge | 34 |
| | iii |

| | |
|--|-----------|
| iii) Taylor Sands – FS1 | 34 |
| iv) Taylor Sands – FS2 | 37 |
| v) Jubilee | 42 |
| vi) Wills | 44 |
| 2.3.1.3 Prairie Channel | 44 |
| i) Prairie Channel – FS1 | 47 |
| ii) Prairie Channel – FS2 | 47 |
| iii) Sandee/Snag Island – FS1 | 47 |
| iv) Sandee – FS2 repeat | 51 |
| 2.3.2 Sandee flow data | 54 |
| i) Cross-section A | 54 |
| ii) Cross-section B | 55 |
| iii) Cross-section C | 56 |
| iv) Cross-section D | 56 |
| 2.4 Discussion | 57 |
| 2.4.1 Variations in flow | 58 |
| 2.4.2 Bedform morphology | 59 |
| 2.4.3 Bedform scale | 61 |
| 2.4.4 Variations in bedform morphology with location | 64 |
| 2.5 Conclusions | 68 |
| 3 Flow around a tidal barform | 70 |
| 3.1 Introduction | 70 |
| 3.2 Field Methods | 72 |
| 3.2.1 Field Location: Wood Bar, the Columbia River Estuary | 72 |
| 3.2.2 Methodology | 73 |
| 3.3 Results | 77 |
| 3.3.1 Bathymetry | 77 |
| 3.3.2 Repeat Bathymetry | 80 |
| 3.3.3 Internal bar sedimentology | 87 |
| 3.3.4 Relationship between flow and bar morphology | 87 |
| i) Cross-section A | 87 |
| ii) Cross-section B | 92 |
| iii) Cross-section C | 94 |
| iv) Cross-section D | 95 |
| 3.4 Discussion | 98 |
| 3.4.1 Bedform morphology | 98 |
| 3.4.2 Bedform migration | 102 |
| 3.4.3 Flow patterns | 105 |

| | | |
|----------|---|------------|
| 3.4.4 | Bar formation | 108 |
| 3.5 | Conclusions | 110 |
| 4 | Three-dimensional meander bend flow within the tidally-influenced fluvial zone | 112 |
| 4.1 | Abstract | 112 |
| 4.2 | Introduction | 113 |
| 4.3 | Methods | 116 |
| 4.3.1 | Field Area | 116 |
| 4.3.2 | Field Methods | 118 |
| 4.4 | Results | 119 |
| i) | High River – Neap Tide (HRNT) | 120 |
| ii) | Low River – Spring Tide (LRST) | 122 |
| iii) | Repeated Bend Apex measurements at LRST | 125 |
| 4.5 | Discussion | 128 |
| 4.6 | Conclusions | 132 |
| 5 | The influence of tidal bores on bar morphology | 134 |
| 5.1 | Introduction | 134 |
| 5.2 | Field location | 137 |
| 5.3 | Field methods | 139 |
| 5.4 | Results | 146 |
| 5.4.1 | Flow measurements | 146 |
| 5.4.2 | Deposits | 152 |
| i) | Core A – landward bar region | 153 |
| ii) | Core B – Channel adjacent to bar centre | 156 |
| iii) | Core C – Bar centre | 160 |
| iv) | Core D – Seaward bar region | 163 |
| 5.5 | Discussion | 168 |
| 5.6 | Conclusions | 177 |
| 6 | Discussion | 179 |
| 6.1 | Tidal modification of fluvial flow within fluvially-dominated systems | 179 |
| 6.2 | Steering of tidally-influenced flows | 181 |
| 6.3 | Variations in bedform morphology | 183 |
| 6.4 | Effects of system morphology on perceived tidal influence | 189 |
| 7 | Conclusions | 194 |
| 7.1 | Further work | 195 |
| 8 | References | 197 |

| | |
|--|-----|
| Appendix I Reungoat <i>et al.</i> (2015) | 212 |
| Appendix II Keevil <i>et al.</i> (2015a) | 224 |

Figures

| | | |
|----------|---|----|
| 1 | Introduction to flow around tidal barforms | |
| 1.1 | Movement of the turbidity maximum, Gironde Estuary, France (redrawn from Fenies <i>et al.</i> , 1999). | 3 |
| 1.2 | Reconstruction of the McMurray Formation, Athabasca, Canada (Fustic <i>et al.</i> , 2012). | 5 |
| 1.3 | i) Variations in river currents, tidal currents and waves with position within a tidal-fluvial system; ii) Schematic map of a tide-dominated estuary with funnel shape translating into a “straight-meander-straight” geometry (redrawn from Dalrymple and Choi, 2007). | 7 |
| 1.4 | Flow transport around an elongate bedform in a tidal channel (Dalrymple and Choi, 2007). | 9 |
| 2 | Depositional patterns arising from tidally-influenced flow in a fluvially-dominated system | |
| 2.1 | Modulation of river currents by tides (redrawn from Dalrymple and Choi, 2007). | 16 |
| 2.2 | Map of tidal Columbia River, USA. Study area is within the red box. | 18 |
| 2.3 | June flow at The Dalles, 1879-1989. Adjusted flow estimates flow which would have occurred without the presence of dams (observed flow plus monthly corrections); Virgin flow estimated by Bonneville Power Administration prior to represent flow without presence of large settlements (redrawn from Naik and Jay, 2005). | 19 |
| 2.4 | Region studied of the Columbia River Estuary. Bar complexes are found throughout the region, some of which are vegetated. Fluvial flow is from the east. | 21 |
| 2.5 | Locations of MBES data collected during the present work. Data was collected at 9 separate locations in FS1 and FS2. Data from Wood Bar is presented in Chapter 3. | 22 |
| 2.6 | Reson SeaBat 7125 head, in transport position on boat. The transmitter is located underneath the head (black unit visible in the upright portion of the image), whilst the receiver is at the front of the head underneath a metal protective cover (facing ground in image). | 24 |
| 2.7 | Position of ADCP cross-sections collected at Sandee Bar (Location 9 on Figure 2.5). Fluvial flow from top right of image. Dark blue shows the | 26 |

| | | |
|------|--|----|
| | position of MBES data collected during FS1. | |
| 2.8 | Arrangement of beams in a three beam ADCP (redrawn from Szupiany <i>et al.</i> , 2007) | 27 |
| 2.9 | Bathymetry measurements collected at Desdemona North during FS1 (Location 1 on Figure 2.5) – see text for details of bedforms. | 29 |
| 2.10 | Desdemona North dune profiles derived from MBES data (Location 1 on Figure 2.5), where 0 m is at the seaward end of the profile (fluvial flow from right of figure). Profile 7 is the southern most profile, collected at the northern edge of Desdemona Sands, while Profile 1 was collected in the channel to the north of the bar. | 30 |
| 2.11 | Bathymetry measurements collected to the south of Desdemona Sands (Desdemona South; Location 2 on Figure 2.5) – see text for details of bedforms. | 32 |
| 2.12 | Desdemona South (Location 2 on Figure 2.5) dune profiles derived from MBES data (Figure 2.11), where 0 m is at the seaward end of the profile (fluvial flow from right of figure). Profile 10 is the northern most profile, collected at the southern edge of Desdemona Sands, while Profile 1 was collected in the navigation channel to the south of the bar. Profile 4 is located on the featureless slope observed in the MBES data. | 33 |
| 2.13 | Bathymetry measurements collected at the northern edge of the Navigation Channel, east of the Astoria-Megler Bridge during FS2 (Location 4 on Figure 2.5) – see text for details of bedforms. | 35 |
| 2.14 | Bathymetry measurements of the region around Taylor Sands collected during FS1 (Location 3 on Figure 2.5). The southern edge of the section lies within the Navigation Channel. See text for details of bedforms. | 36 |
| 2.15 | Profile traces collected from seaward region of the Navigation Channel adjacent to Taylor Sands derived from bathymetry data (Figure 2.14; Location 3 on Figure 2.5), where 0 m is at the seaward end of the profile (fluvial flow from right of figure). Profile 10 is the northern most profile, collected at the adjacent to Taylor Sands, while Profile 1 was collected in the navigation channel to the south of the bar. | 38 |
| 2.16 | Profile traces collected from landward region of the Navigation Channel adjacent to Taylor Sands derived from bathymetry data (Figure 2.14; Location 3 on Figure 2.5), where 0 m is at the seaward end of the profile (fluvial flow from right of figure). Profile 9 is the northern most profile, collected on the bar top, while Profile 1 was collected in the Navigation Channel to the south of the bar. | 39 |
| 2.17 | Bathymetry measurements of the northern region of Taylor Sands collected | 40 |

| | | |
|------|---|----|
| | during FS2 (Location 3 on Figure 2.5) – see text for details of bedforms. | |
| 2.18 | Profile traces within the centre of the scour feature measured at Taylor Sands (Location 3 on Figure 2.5) showing variations between FS1 (2012) and FS2 (2013): i) northern profile; ii) central profile; iii) southern profile. | 41 |
| 2.19 | Bathymetry measurements of Jubilee collected during FS1 (Location 6 on Figure 2.5) – see text for details of bedforms. | 43 |
| 2.20 | Jubilee channel dune profiles derived from bathymetry data (Figure 2.19; Location 6 on Figure 2.5), where 0 m is at the seaward end of the profile (fluvial flow from right of figure). Profile 10 is the most southern of the profiles, adjacent to the bar top. | 45 |
| 2.21 | Bathymetry measurements collected around Wills bar during FS1 (Location 5 on Figure 2.5) – see text for details of bedforms. | 46 |
| 2.22 | Bathymetry measurements collected at the southern extent of Prairie Channel during FS1 (Location 7 on Figure 2.5) – see text for details of bedforms. | 48 |
| 2.23 | Bathymetry measurements collected at the southern extent of Prairie Channel during FS2 (Location 7 on Figure 2.5). These measurements repeat a subsection of the measurements made during FS1 (Figure 2.22) – see text for details of bedforms. | 49 |
| 2.24 | Bathymetry measurements collected around Sandee Bar and Snag Island at the landward limit of Prairie Channel during FS1 (Location 9 on Figure 2.5) – see text for details of bedforms. | 50 |
| 2.25 | Bedform profiles derived from bathymetry data collected during FS1 at Sandee (Location 9 on Figure 2.5), where 0 m is at the seaward end of the profile (fluvial flow from right of figure). Profile 1 is located within the shallower region to the south of the channel, with Profile 2 in the deepest region of the channel. Profile 4 is located on the channel shelf. Profiles 5-8 are located on the bar top. | 52 |
| 2.26 | Bathymetry measurements collected around Sandee Bar at the landward limit of Prairie Channel during FS2 (Location 9 on Figure 2.5). This is a repeat of the landward extent of the data collected during FS1 (Figure 2.25) – see text for details of bedforms. | 53 |
| 2.27 | Flow data collected at cross-section A (located on Figure 2.7). Fluvial flow is oriented out of the page: i) shows primary flow velocity (zsd) at lower-low water; ii) primary flow velocity (zsd) at lower-high water; iii) secondary flow velocity (zsd) at lower-low water; iv) secondary flow velocity (zsd) at lower-high water. | 54 |
| 2.28 | Flow data collected at cross-section B (located on Figure 2.7). Fluvial flow is | 55 |

| | | |
|----------|---|----|
| | oriented out of the page: i) shows primary flow velocity (zsd) at lower-low water; ii) primary flow velocity (zsd) at lower-high water; iii) secondary flow velocity (zsd) at lower-low water; iv) secondary flow velocity (zsd) at lower-high water | |
| 2.29 | Flow data collected at cross-section C (located on Figure 2.7). Fluvial flow is oriented out of the page: i) shows primary flow velocity (zsd) at lower-low water; ii) primary flow velocity (zsd) at lower-high water; iii) secondary flow velocity (zsd) at lower-low water; iv) secondary flow velocity (zsd) at lower-high water. | 56 |
| 2.30 | Flow data collected at Transect D (located on Figure 2.7). Fluvial flow is oriented out of the page: i) shows primary flow velocity (zsd) at lower-low water; ii) primary flow velocity (zsd) at lower-high water; iii) secondary flow velocity (zsd) at lower-low water; iv) secondary flow velocity (zsd) at lower-high water. | 57 |
| 2.31 | Changes in bed elevations between FS1 and FS2 at Sandee. Regions highlighted in blue show erosion between the two sets of measurements, whilst the red shows deposition | 58 |
| 2.32 | Image of the Columbia River estuary showing sand bars present close to the water surface. Note the elongated tails visible at the seaward end of several bars. Fluvial flow is from the east. | 60 |
| 2.33 | Scale dependent flow orientations observed at: i) Bridge; ii) Taylor Sands. Large blue arrows show flow directions of large bedforms, red arrows flow directions of superimposed bedforms | 62 |
| 2.34 | Comparison of bedforms found at -4 m TP_MSL throughout study area. Relative depth between each profile is 2 m | 63 |
| 2.35 | Distribution of bedform lengths within the study area. Local flow direction is also shown. | 67 |
| 2.36 | Bedform distributions from side-scan sonar measured in June 1980 (Sherwood and Creager, 1990). | 68 |
| 3 | Flow around a tidal barform | |
| 3.1 | Location of Wood Bar in the Columbia River estuary. | 73 |
| 3.2 | Location of data collection around Wood Bar. Blue represents location of main MBES survey, with location of repeated MBES measurements shown in grey; ADCP transects (A-D) are shown as black lines; GPR transects shown in red. Fluvial flow is from the top right of the section. | 74 |
| 3.3 | Collection times of ADCP surveys relative to tide data at the Tongue Point gauge. All times shown are in UTC. Cross-section A shown in red; cross-section B shown in dark blue; cross-section C shown in green; cross-section | 75 |

| | | |
|------|---|----|
| | D shown in pale blue, locations of cross-sections shown in Figure 3.2. | |
| 3.4 | Common offset reflection surveys R = Receiver, T = Transmitter (Neal, 2004). | 77 |
| 3.5 | Bathymetry measurements of Wood Bar (location shown in Figure 3.1). Highlighted regions are shown in Figure 3.5. Fluvial flow is from the top right of figure. | 78 |
| 3.6 | Features of Wood Bathymetry – see text for details. | 79 |
| 3.7 | Initial surface collected during Epoch 1. Fluvial flow is from the top right corner. | 80 |
| 3.8 | Repeat surface collected during Epoch 2. Fluvial flow is from the top right corner. | 81 |
| 3.9 | Plots to show erosion and deposition occurring between Epoch 1 and Epoch 2: i) Difference map created by subtracting Epoch 1 (Figure 3.7) from the repeat surface collected on Epoch 2 (Figure 3.8). Erosion and deposition scale by +/- 5.3 m; ii) Profile collected along line A-B on figure i, showing development and seaward migration of bedforms from Epoch 1 to Epoch 2 | 82 |
| 3.10 | Repeat surface collected during Epoch 3. Fluvial flow is from the top right corner. | 83 |
| 3.11 | Plots to show erosion and deposition occurring between Epoch 2 and Epoch 3: i) Difference map created by subtracting Epoch 2 (Figure 3.8) from the repeat surface collected during Epoch 3 (Figure 3.10). Erosion and deposition scale by +/- 5.3 m; ii) Profile collected along line A-B on figure i, showing development and landward migration of bedforms from Epoch 2 to Epoch 3. | 84 |
| 3.12 | Repeat surface collected during Epoch 4. Fluvial flow is from the top right corner. | 85 |
| 3.13 | Plots to show erosion and deposition occurring between Epoch 3 and Epoch 4: i) Difference map created by subtracting Epoch 3 (Figure 3.10) from the repeat surface collected during Epoch 4 (Figure 3.12). Erosion and deposition scale by +/- 5.3 m; ii) Profile collected along line A-B on figure i, showing development and significant seaward migration of bedforms from Epoch 3 to Epoch 4. | 86 |
| 3.14 | GPR traces collected on Wood Bar. Yellow highlights indicate undulating reflections (large-scale dune stratification); orange highlights indicate low angled reflections (smaller scale dune stratification); blue highlights indicate sharply angled reflections (laterally accreting bar margin); purple highlights indicate concave reflections (channels). Green horizons highlight interpreted reactivation surfaces. Fluvial flow shown by black arrow. | 88 |

| | | |
|------|---|-----|
| 3.15 | Longitudinal GPR traces collected on Wood Bar. Yellow highlights indicate undulating reflections (large-scale dune stratification); orange highlights indicate low angled reflections (smaller scale dune stratification); blue highlights indicate sharply angled reflections (laterally accreting bar margin); purple highlights indicate concave reflections (channels). Green horizons highlight interpreted reactivation surfaces. Fluvial flow illustrated by black arrow. | 89 |
| 3.16 | Flow data collected at cross-Section A (located on Figure 3.2). Seaward flow is oriented out of the page: i & v) at lower-low water; ii & vi) after lower-low water; iii & vii) before lower high water; iv & viii) after lower high water. | 91 |
| 3.17 | Flow data collected at cross-Section B (located on Figure 3.2). Seaward flow is oriented out of the page and the barhead is emergent at low water: i & vii) Lower-low water across bar; ii & viii) Lower-low water in eastern channel; iii & ix) midway between lower-low water and lower-high water across bar; iv & x) midway between lower-low water and lower-high water in the eastern channel; v & xi) lower-high water; vi & xii) after lower-high water. | 93 |
| 3.18 | Flow data collected at cross-section C (located on Figure 3.2). Seaward flow is oriented out of the page and the barhead is emergent at low water. i & v) Lower-low water across the bar; ii & vi) after lower-low water in the eastern channel; iii & vii) midway between lower-low water and high water across the bar; iv & viii) before lower-high water within the eastern channel. | 95 |
| 3.19 | Flow data collected at cross-section D (located on Figure 3.2). Seaward flow is oriented out of the page: i & v) After lower-low water; ii & vi) midway between lower-low water and lower-high water; iii & vii) before lower-high water; iv & viii) lower-high water. | 97 |
| 3.20 | Crestlines of bedforms observed within the bathymetry data at Wood Bar; fluvial flow is from top right corner of the image (shown by black arrow). Green lines highlight longitudinal crests which are oriented perpendicular to flow from within the channel to the south of Sandee Bar (not yet adjusted to presumed local flow); blue highlights main dune crest orientation, consistent with flow in this area; black dashed lines highlight sharp changes in bathymetry at the edge of the bar top; black lines highlight dominant crest lines of superimposed bedforms; white highlight dune spurs. | 99 |
| 3.21 | Morphological features of transverse bedforms (redrawn from Allen, 1982). | 100 |
| 3.22 | Spur asymmetries, showing variations in slope asymmetries. Central region is directly landward of the barhead, whilst northern region lies at the north of the bathymetry measurement zone. | 101 |
| 3.23 | Dune crest migration at the repeat bathymetry location (Location shown in | 104 |

| | | |
|----------|---|-----|
| | Figure 3.2): i) central bathymetry profiles (0 m is at landward end of profiles); ii) variations of crestline locations (fluvial flow from top right of image). | |
| 3.24 | Depth averaged flow patterns at the 4 cross-sections measured at: i) lower-low water; ii) after lower-low water; iii) between lower-low water and lower-high water; iv) lower-high water; v) after lower-high water. | 107 |
| 3.25 | Summary of bar position in aerial surveys carried out by the USDA. Bar shows migration in a seaward direction consistent with fluvial dominance. | 109 |
| 4 | Three-dimensional meander bend flow within the tidally-influenced fluvial zone | |
| 4.1 | Map of tidal Severn Estuary showing study bend. Outer estuary extends from Barry (B) - Minehead (M) to Severn Bridge (SB). Inner estuary ends at Maisemore Weir (MW). E shows the location of the Environment Agency gauge at Epney. ADCP measurement cross-sections are shown on the inset of the study bend | 117 |
| 4.2 | Base river flow measured at Epney Gauge (Site ID – 2059). Red dashed lines show the dates of the fieldwork reported on here. <i>Contains Environment Agency information © Environment Agency and database right.</i> | 119 |
| 4.3 | Stage data collected every 15 minutes by Environment Agency Epney Gauge (site ID – 2059). The dotted line shows data for 12:00 11/07/2012 to 12:00 13/07/2012; solid line shows data for 12:00 24/04/2013 to 12:00:26/04/2013. <i>Contains Environment Agency information © Environment Agency and database right</i> | 121 |
| 4.4 | Flow velocities at six cross-sections at high river-neap tide conditions: i-vi show primary flow velocities (zero secondary discharge) in ms^{-1} ; vii-xii show secondary flow velocities (zero secondary discharge), also shown as black arrows. Cross-section A is shown in i and vii; cross-section B in ii and viii; cross-section C in iii and ix; cross-section D in iv and x; cross-section E in v and xi; cross-section F in vi and xii. Flow is in a seaward direction at all cross-sections. Locations of the cross-sections are shown in Figure 4.1. | 123 |
| 4.5 | Flow velocities at three cross-sections, landward of the bend apex at LRST conditions: i-iii show primary flow velocities (zero secondary discharge) in ms^{-1} , where flow is in a landward (reversed) direction due to the incoming flood tide; iv-vi show secondary flow velocities (zero secondary discharge), also shown as black arrows. Cross-section A is shown in i and iv; cross-section B is shown in ii and v; cross-section C is shown in iv and vi. Flow is in a landward direction (reversed to normal river flow) at all cross-sections. Locations of the cross-sections are shown in Figure 4.1. | 124 |

| | | |
|---|--|-----|
| 4.6 | Flow velocity collected close to the position of cross-section D (Figure 4.1) during one spring tidal cycle at low river discharge. i-iv show primary flow velocities (zero secondary discharge) in ms ⁻¹ ; v-vii show secondary flow velocities (zero secondary discharge). Cross-sections were collected 20 minutes after tidal bore, where flow is in a landward direction (i and v); 100 minutes after tidal bore, when seaward flow had re-established (ii and vi); 155 minutes after tidal bore (iii and vii); 200 minutes after tidal bore (iv and viii). Gaps in the data are due to high suspended sediment concentrations during data collection. | 127 |
| 4.7 | Regions of highest flow velocity within the bend measured, relative to the centreline (shown as grey dashed line) showing bed bathymetry. Landward of the bend at high river-spring tide flow is adjacent to the inner bank, whilst at low river-high tide flow is adjacent to the outer bank. | 129 |
| 5 The influence of tidal bores on bar morphology | | |
| 5.1 | Location of Longney Sands, River Severn, UK. The bar is located 3 km seaward of the bend investigated in Chapter 4. River flow is from the North. | 137 |
| 5.2 | Evolution of Longney Sands shown via Google Earth imagery: i) shows a single bar with 2 channels; ii) the bar has become bank attached to the east with the western channel cutting through the previous bar; iii) the bar is now bank attached to the west with a wider eastern channel, smaller surface channels are also visible; iv) the bar is now centralised again. | 139 |
| 5.3 | Stage data measured at Environment Agency Epney Gauge (Site ID – 2059): i) Base river flow for the period 01/01/2012 – 10/10/2014- red dashed line shows the fieldwork reported on here (08-09/09/2014); ii) Stage data collected every 15 minutes for the period of the present work 00:00 08/09/2014 to 00:00 10/09/2014. <i>Contains Environment Agency information © Environment Agency and database right.</i> | 140 |
| 5.4 | Locations of field measurements. Cores are red circles, the current meter as a green circle. ADCP transects are shown as blue lines, with the blue circle showing the mooring location during the tidal bore. | 141 |
| 5.5 | ADCP setup: i) Teledyne RD Instruments Rio Grande 1200 Hz ADCP; ii) schematic of instrument setup showing position of instrument and data collection bins. | 142 |
| 5.6 | Midas ECM current meter: i) Instrument before deployment; ii) Instrument in situ; iii) Instrument in situ at time of recovery; iv) Instrument following recovery. | 144 |
| 5.7 | Coring rig set up: i) the pipe driving rig using a moveable clamp with a concrete poker head attached; ii) shows the measurements taken; iii) the | 145 |

| | | |
|------|--|-----|
| | retrieval rig using a ratchet winch with the cable passed over the top of a fixed frame. | |
| 5.8 | Depth averaged ADCP measurements: i) prior to the arrival of the tidal bore, ii) during flow reversal following tidal bore, iii) following re-establishment of flow in a seaward direction. | 147 |
| 5.9 | ADCP velocity data collected during the first 15 minutes of the passage of a tidal bore from an anchored boat. Initial anchor position is shown in Figure 5.4, following which the boat was carried landward by the incoming tide. Positive downstream velocity is in a seaward direction whilst positive cross-stream velocity is towards the western bank. | 148 |
| 5.10 | Flow data collected by the Midas ECM (location shown in Figure 5.4). Downstream flow is in i-iii, cross-stream flow in iv-vi (data in blue is from the first tide, data in red from the second tide). Data from the full deployment is shown in i and iv; the first 1000 seconds of data following the arrival of a tidal bore are shown in ii and v (dashed box on i and iv); the full tide comparison is shown in iii and vi (dotted box on i and iv). | 149 |
| 5.11 | Pressure measurements from the Midas ECM: i) all data measured; ii) comparison of the arrival of both tidal bores (data in blue is from the first tide, data in red from the second tide); iii) the full incoming tide for both tides (start point of tidal bore and tide plots is the same). | 150 |
| 5.12 | Salinity measurements from the Midas ECM: i) all data measured; ii) comparison of the arrival of both tidal bores (data in blue is from the first tide, data in red from the second tide); iii) the full incoming tide for both tides (start point of tidal bore and tide plots is the same). | 151 |
| 5.13 | Temperature measurements from the Midas ECM: i) all data measured; ii) comparison of the arrival of both tidal bores (data in blue is from the first tide, data in red from the second tide); iii) the full incoming tide for both tides (start point of tidal bore and tide plots is the same). | 152 |
| 5.14 | Core retrieved at landward end of bar (Core A on Figure 5.4). | 154 |
| 5.15 | Grain size statistics for the landward core showing D_{10} , D_{50} and D_{90} . | 155 |
| 5.16 | Core retrieved within channel, 300 m from seaward end of bar (Core B on Figure 5.4). | 157 |
| 5.17 | Grain size statistics for the central channel core (Core B) showing D_{10} , D_{50} and D_{90} . | 159 |
| 5.18 | Core retrieved at bar centre, 300 m from seaward end of bar (Core C on Figure 5.4). | 161 |
| 5.19 | Grain size statistics for the core collected at the centre of the bar, 300 m from the seaward end of the bar (Core C) showing D_{10} , D_{50} and D_{90} . | 163 |

| | | |
|----------|---|-----|
| 5.20 | Core retrieved at seaward end of bar (Core D on Figure 5.4). | 164 |
| 5.21 | Grain size statistics for the seaward core showing D_{10} , D_{50} and D_{90} . | 165 |
| 5.22 | Bedforms observed on the bar top: i) 2D ripples; ii) 3D ripples; iii) ripples showing coal detritus; iv) gravel lags; v) rip up clasts; vi) overlaying fluid muds. | 166 |
| 5.23 | Combined ADCP and ECM flow data | 168 |
| 5.24 | Sedimentary structures associated with tidal bores in the Qiantang Estuary, China. ES: erosion surfaces, ES_P/U: planar/under ES, MB: Massive bedding, PL: parallel laminations, ISP: invasive sand patches, LFS: load-flame structures, PS: pipe-like structures, SD: sand dykes (Figure 3 from Fan <i>et al.</i> , 2014). | 171 |
| 5.25 | Shear stress calculated from ADCP data. | 172 |
| 6 | Discussion | |
| 6.1 | Summary diagram of expected bedforms within the fluviably-dominated region of the tidal-fluvial transition. Active channel is shown in grey. | 184 |
| 6.2 | Variations in perceived flow energies with grain-size. Fluvial flow is the same for all tidal conditions. As tidal influence decreases coarser material is not reworked and evidence of tidal influence decreases. | 188 |
| 6.3 | Comparison of the tidal-fluvial influences observed at both the Columbia River and River Severn. Arrows show the dominant flow directions. Whilst the tidal and fluvial flows are balanced at both locations, overall system flows are very different. Adapted from Figure 1.3 (Dalrymple and Choi, 2007). | 190 |
| 6.4 | Summary of the variations in perceived tidal influence arising due to bedform size within identical tidal systems (fluvial input, grain-size, planform geometry) with varying tidal energy. TD = Tidal dominance, FD = Fluvial dominance. | 191 |

Tables

| | | |
|----------|---|-----|
| 2 | Depositional patterns arising from tidally-influenced flow in a fluvially-dominated system | |
| 2.1 | Tidal constituent ratios calculated from 7 months of data at Tongue Point (from Jay <i>et al.</i> , 1990). | 20 |
| 2.2 | Datums for the Tongue Point gauge, 9439040, Astoria OR (NOAA, 2014). | 21 |
| 2.3 | Methodology to convert Caris HIPS and SIPS BASE surface to Raster object in ArcMap 10. | 25 |
| 2.4 | ADCP data collected at Sandee Bar. Date and time in UTC. | 26 |
| 3 | Flow around a tidal barform | |
| 3.1 | Times of repeated bathymetry measurements (all times UTC) | 74 |
| 3.2 | ADCP data collected at Wood Bar. Date and time in UTC. | 76 |
| 3.3 | Mean discharges collected at the Beaver Army Terminal river gauge (USGS 14246900). | 102 |
| 3.4 | Trough migration rates along central transect profile. | 105 |
| 4 | Three-dimensional meander bend flow within the tidally-influenced fluvial zone | |
| 4.1 | Data collection times at high river-neap tide (HRNT) and low river-spring tide (LRST). Flow was reversed (primary velocities in a landward direction) during the first four measurements at LRST. | 120 |
| 5 | The influence of tidal bores on bar morphology | |
| 5.1 | Timings of ADCP data | 143 |
| 5.2 | Cores recovered. Locations are shown on Figure 5.4. | 152 |
| 5.3 | Suspended sediment samples | 167 |

Nomenclature

Nomenclature

| | |
|-----------|--|
| <i>b</i> | length of magnetic conductor (m) |
| <i>B</i> | Magnetic flux density (T) |
| <i>E</i> | Electromagnetic field (V) |
| \bar{v} | average velocity of conducting fluid (ms ⁻¹) |

Acronyms

| | |
|-----------------|--|
| ADCP | Acoustic Doppler Current Profiler |
| BASE | Bathymetry Associated with Statistical Error |
| D ₁₀ | 10 th percentile of grain size data – fine grained fraction |
| D ₅₀ | 50 th percentile of grain size data – mean grain size |
| D ₉₀ | 90 th percentile of grain size data – coarse grained fraction |
| DEM | Digital Elevation Model |
| dGPS | Differential Global Positioning System |
| DSLR | Digital single-lens reflex |
| ECM | Electromagnetic Current Meter |
| GPR | Ground Penetrating Radar |
| HRNT | High river-neap tide |
| IMU | Inertial Measurement Unit |
| LED | Light emitting diode |
| LRST | Low river-spring tide |
| MBES | Multibeam Echosounder |
| NE | North east |
| NERC | Natural Environment Research Council |
| NW | North west |
| PSU | Practical Salinity Units |
| RTK | Real time kinematic |
| SE | South east |
| SW | South west |
| swg | Standard wire gauge |
| T20 | Flow measurements collected 20 minutes after flood tide |

| | |
|--------|---|
| T100 | Flow measurements collected 100 minutes after flood tide |
| T155 | Flow measurements collected 155 minutes after flood tide |
| T200 | Flow measurements collected 200 minutes after flood tide |
| TIFZ | Tidally-influenced fluvial zone |
| TP_MSL | Water depth corrected relative to Mean Sea Level at the Tongue Point Tide Gauge (NOAA station 9439040) |
| UTC | Co-ordinated universal time |
| VTG | Vector track and speed over ground |
| zsd | Zero secondary discharge |

Declaration of authorship

The candidate confirms that the work submitted is her own, except where work has formed part of a jointly-authored publication.

Fieldwork on the Columbia River and reported in Chapters 2 and 3 was carried out in conjunction with the NERC funded Tidally-Influenced Fluvial Zone (TIFZ) project - NE/H007954/1. All bathymetry and flow data collected during this fieldwork was processed and interpreted by Claire Keevil. GPR data presented in Figures 3.14 and 3.15 was processed and interpreted by Professor Phil Ashworth and Dr Greg Sambrook Smith.

The work in Chapter 4 has been published as:

Keevil, C.E., Parsons, D.R., Ainsley, M. and Keevil, G.M. (2015). Three-dimensional meander bend flow within the tidally-influenced fluvial zone. In: Parsons, D.R., Ashworth, P.J. and Best, J.L. (Eds.) *Developments in Sedimentology 68: Fluvial-Tidal Sedimentology*, 127-148

All data was processed and interpreted by Claire Keevil. Ideas were shaped during discussion with co-authors.

Chapter 1

Introduction to flow around tidal barforms

1.1 Context

Within river-estuary systems there exists a complex transitional zone between fully-fluvial and fully-tidal conditions. The varying fluvial and tidal flow magnitudes acting in this zone result in a region of complex flow and sediment transport processes which may be 10s to 100s of km in length (Dalrymple *et al.*, 1992; Dalrymple and Choi, 2007; van den Berg *et al.*, 2007; Fustic *et al.*, 2012). Increases in fluvial flow due to seasonal variations such as increased rainfall or snow melt will move the tidal-fluvial boundary seaward, increasing the length of the region of fluvial dominance, whilst during periods of low fluvial flow the boundary will move landward. Incoming tidal flows will be able to move further landward during the highest tides, which will vary according to the tidal cycle. Close to the sea tidal flows are dominant and in regions of high tides may act to stop or reverse fluvial flows. The furthest inland incursion of the tide, the tidal limit, is dependent on local river levels, tidal range and estuary geometry. This occurs within the region of fluvial dominance, at which point fluvial flows are slowed, or modulated, to show a slight rise in flow depth. As such, the position of the tidal-fluvial boundary will vary within the transitional zone due to flow fluctuations on daily, seasonal, annual and lunar scales. The resultant sedimentary transport and depositional characteristics within the transition zone are, at present, poorly understood.

The criteria used for the definition of estuaries can vary, depending on the area of study and may include physical characteristics, tidal influence, salinity or biological assemblages (Dyer, 1997; Elliott and McCluskey, 2002; Gingras and MacEachern, 2015). Prichard (1967) describes an estuary as “a semi-enclosed coastal body of water which has free access to the ocean and within which seawater is measurably diluted by freshwater from land drainage”. A more geological definition was proposed by Dalrymple *et al.* (1992) who state that an estuary is “the seaward portion of a drowned valley system which receives sediment from both fluvial and marine sources and which contains facies influenced by tide, wave and fluvial processes. The estuary is considered to extend from the landward limit of tidal facies at its head to the seaward limit of coastal facies at its mouth”. Estuaries are subject to tidal, fluvial and to a lesser extent wave influence, which in turn control the morphodynamics and sedimentology (Dyer, 1997). Systems are generally tidally-dominated or wave-dominated; fluvially-dominated systems generally do not show estuarine architecture (Boyd *et al.*, 1992).

When described with reference to salinity distributions a four part classification is formed: well-stratified (Type A) estuaries have minimal tidal influence and have a salt wedge at the base of the flow which tapers upstream; partially stratified (Type B) systems possess a gradual salinity gradient as the top of the wedge is destroyed by tidal interactions; well mixed (Type C) estuaries have no salt wedge due to increasing tide action (Dyer, 1997). Within an estuarine system density differences arising from the increased salinity and the temperature difference of the incoming tide can drive local circulation (Uncles, 2002).

The present work considers the processes which occur within tidally-dominated estuaries. Estuaries with a tidal range of less than 2 m are termed microtidal; these estuaries do not generally show much tidal influence. Tidal ranges of 2-4 m are found in mesotidal estuaries, and the resulting morphodynamics exhibit a mix of tidal, wave and fluvial influence. Macrotidal estuaries have a tidal range greater than 4 m, with those showing a range over 8 m termed megatidal or hypertidal. These will show a strong tidal signature (Dalrymple *et al.*, 1992; Kirby, 2010; Longhitano *et al.*, 2012). The geometry of estuarine systems will also act to amplify the tidal range at the landward end of the system (Dalrymple and Choi, 2007; Chanson, 2012; Longhitano *et al.*, 2012)

The variation in tidal and fluvial influence can be illustrated by the relative position of the location of maximum sediment suspension within an estuary, the turbidity maximum, such as within the Gironde Estuary, France shown in Figure 1.1 (Fenies *et al.*, 1999). The high sediment concentrations found within the turbidity maximum is formed due to the combination of incoming tidal flows eroding sediment with flocculation caused by the incoming salt water wedge (Dalrymple and Choi, 2007). Similarly, Uncles *et al.* (1998) found that the turbidity maximum within the Humber Estuary, UK varied seasonally by up to 60 km. This has also been observed via the movement of the position of a freshwater plume with increased river flow in the Snohomish River, WA, USA (Yang and Khangaonakar, 2008). Variations of freshwater discharge in tropical estuaries during extreme wet and dry seasons, such as those in northern Australia may also affect the position of tidal influence, where tidal transport and deposition is dominant except during freshwater floods (Bryce *et al.*, 1998). This movement of the position of the tidally-influenced region means that there will be no single zone of tidal, marine or mixed facies, as the interface between them will be gradual both spatially and temporally.

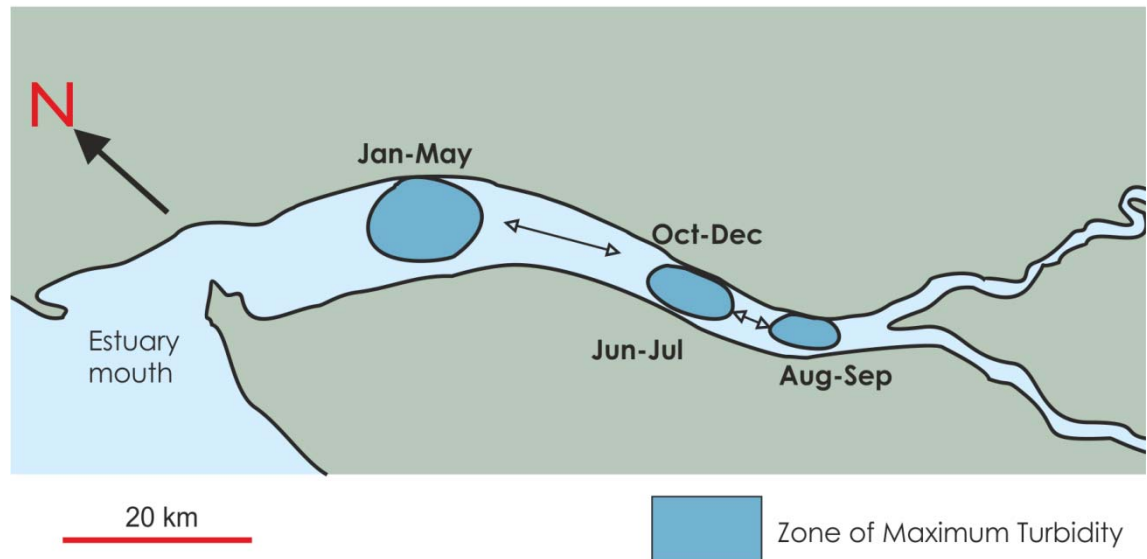


Figure 1.1 Movement of the turbidity maximum, Gironde Estuary, France (redrawn from Fenies *et al.*, 1999).

Within multidirectional flows, such as a river-estuary system, the direction of transport will be dependent on the grain size of material and can occur in different directions within the same region. Bedload will usually be transported in the direction of the dominant flow direction, whilst suspended sediment is carried by the estuarine circulation driven by saline and fresh water density differences (Dalrymple and Choi, 2007). The sediment load in estuaries generally fines in a seaward direction, with fine cohesive muds dominating at the freshwater/saltwater interface (van Rijn, 2007). Comparisons of 44 estuaries by Uncles *et al.* (2002) showed that the amount of suspended particulate matter contained within estuaries was directly related to their tidal range and estuary length. Specifically, long estuaries with a high tidal range had a higher suspended sediment concentration than short, highly tidal estuaries or long estuaries with weaker tides.

The most commonly preserved evidence of tidal influence is a series of stacked heterolithic strata which are both sand and mud rich, where mud rich horizons were deposited during periods of low flow. Laminations may preserve flow structures which are uni-directional in nature (where either tidal or fluvial flow dominates), bi-directional herringbone cross-stratification or tidal bundles which preserve coarsening or fining sequences as relative flow strengths vary (Longhitano *et al.*, 2012). These laminations may form throughout river-estuary systems as the internal structure of dunes or sandbars or on channel margins. Variations in the relative thickness of these laminations may be used to reconstruct historic tidal cycles and may preserve information on daily, monthly or annual scales (Longhitano *et al.*, 2012).

In addition to the varying sedimentation arising from the movement of the turbidity maximum, seasonal variations in sedimentation may also be preserved. Holocene sedimentation in the Severn Estuary was investigated for seasonal signatures by Dark and Allen (2005). They found that fine grained bands within the deposit contained spring to summer flowering pollen, whilst the coarser bands appeared to contain pollen which had flushed through the system during the winter months (Dark and Allen, 2005), so showing the variation of depositional facies with tidal-fluvial interface migrations throughout the year. Allison *et al.* (1995) found that extensive overbank deposits of fine muds were deposited annually on tidal mud flats in the Amazon system during the 6 months of peak flow but that these muds were reworked by high flow events in the rest of the year, leading to lenses of fine grained mud above the level of mean high water. These seasonal variations in sedimentation are not directly related to the movement of the tidal-fluvial boundary, but result in further sedimentary signatures (e.g., Allison *et al.*, 1995; Dark and Allen, 2005) which must be considered during palaeogeographical system reconstruction (e.g., Fustic *et al.*, 2012; Shiers *et al.*, 2014).

1.2 Importance and implications

Although tidally-influenced features such as estuaries have a high preservation potential, as they contain large amounts of sediment and are contained within older valleys, they have not always been recognized within the geological record (Dalrymple *et al.*, 1992). Following the formulation of more comprehensive facies models (e.g., Boyd *et al.*, 1992; Dalrymple *et al.*, 1992; Dalrymple and Choi, 2007) their signatures are now being recognized more frequently. The reconstruction of ancient deposits is dependent on the understanding of modern processes, with modern analogues providing an important insight (e.g., Olariu *et al.*, 2015). Ancient deposits only record a relatively short time period within the existence of a system, with early deposition reworked and redeposited by later processes. Variations in sea-level will result in the movement of the tidal-fluvial transitional zone, with an initially fluvially-dominated location becoming tidally-dominated during a marine transgression. Estuaries are often found in transgressive regions resulting in variable degrees of preservation, with significant facies variations (Dalrymple *et al.*, 1992; Longhitano *et al.*, 2012; Webb *et al.*, 2015). Understanding the range of facies occurring within the tidal-fluvial transition is also therefore of great importance for the reconstruction of palaeosea-levels. Additional interest arises due to the formation of tar sands, such as the Athabasca Sands in Canada, within regions of tidal influence which are now being exploited as a major source of hydrocarbons (e.g., Gray *et al.*, 2009; Fustic *et al.*, 2012).

This will have implications for understanding deposits relative position within a sequence and their adjacent deposits, as well as their exploitation.

Whilst the facies arising within fully-fluvial and fully-tidal environments have been studied in some detail (e.g., Allen, 1991a; Bridge, 1993; van den Berg *et al.*, 2007; Kostaschuk *et al.*, 2010; Rennie and Church, 2010; Uncles, 2010; Blanckaert, 2011), the more complex tidal-fluvial transitional zone has yet to be fully explained. Broad depositional facies models have been described in modern settings (e.g., Allen, 1991a; Dalrymple *et al.*, 1992; Dalrymple and Choi, 2007; van den Berg *et al.*, 2007; Dalrymple *et al.*, 2012; Dalrymple *et al.*, 2015; La Croix and Dashtgard, 2015; Carling *et al.*, 2015). However, this is complicated by the broad range of modern systems studied, with variations in tidal range, fluvial flow, sediment content and geometries.

The low-lying, wide planform of tidal-fluvial systems mean that they are often the location of large areas of population and industry (Xie *et al.*, 2009). This means that they are at increased risk to effects of climate change, sea-level rise and storminess (Xie *et al.*, 2009; Kirby, 2010; Phillips and Crisp, 2010; Uncles, 2010). Considerable resources are utilised to protect these regions of high economic importance, with the creation of costly defensive structures. Understanding of system dynamics and the relative influence of tidal and fluvial flows is therefore of high economic importance, allowing the modelling of potential areas of risk and the targeting of any defences.

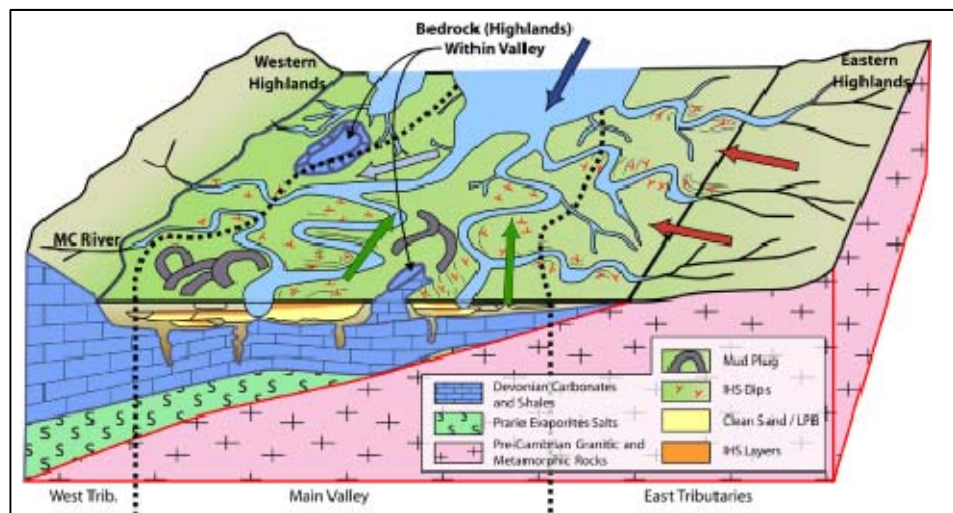


Figure 1.2 Reconstruction of the McMurray Formation, Athabasca, Canada (Fustic *et al.*, 2012).

1.3 Conceptual models of the tidal-fluvial zone

The tidal-fluvial zone is present within tidally-dominated estuarine systems. These systems have commonly been divided into a three part model corresponding to a high tidal energy outer estuary, an intermediate middle estuary and a fluvially dominated inner estuary (Dalrymple *et al.*, 1992). These models have been formulated using both modern and ancient analogues (e.g., Rahmani, 1988; Allen, 1991a; Reinson, 1992; Archer, 2013) as well as remote sensing methods (Archer, 2013). One such model describes the fluvial-estuarine transition based on deposition within the Gironde Estuary, considering only three distinct regions: fluvial, upper estuarine (sinuous) channels and the estuary funnel itself (Allen, 1991a). A three region model is also proposed by Rahmani (1988), based on ancient deposits in Alberta, Canada, consisting of a lower, middle and upper estuary. This model is characterised by variations in grain-size as the estuary becomes less tidal in nature where the lower estuary fill is predominantly sandy in nature, the middle estuary muddy and the upper estuary sandy (Rahmani, 1988). Archer (2013) studied hypertidal systems, classifying them into three sedimentological zones: an outer zone of longitudinal bars; a middle zone with extensive sand flats; an inner tidal zone marking the limit of tidal flows and the formation of estuarine point bars. Broadly these zones would appear to correspond to those of Allen (1991a), although the innermost zone of Archer (2013) is tidally-influenced while this region is described as fluvial within Allen (1991a). Again, the transition from tidal to fluvial influence in the sand flat region will be lost within the broadly defined middle zone.

Whilst these models may be of interest when characterising general estuarine facies they do not describe the tidal-fluvial transition in detail as this lies within a more general middle estuary region. The most detailed model of the tidal-fluvial transition, formulated by Dalrymple *et al.* (1992) and expanded by Dalrymple and Choi (2007), describes the variations in system planform and facies within both tide-dominated deltas and estuaries (Figure 1.3). The flow patterns and arising bedforms within the tidal-fluvial transition vary along its length due to the variations in relative flow magnitudes. Fluvial flow strength decreases in a seaward direction due to a decrease in the hydraulic gradient and the splitting of the flow into an increasing number of channels. Tidal flow strength peaks landward of the mouth of the system, due to amplification effects arising from the narrowing system width and decreasing bathymetry (Figure 1.3).

The resultant transition zone contains variations in system bathymetry and geomorphology, sediment transport mechanisms, rate of sediment transport

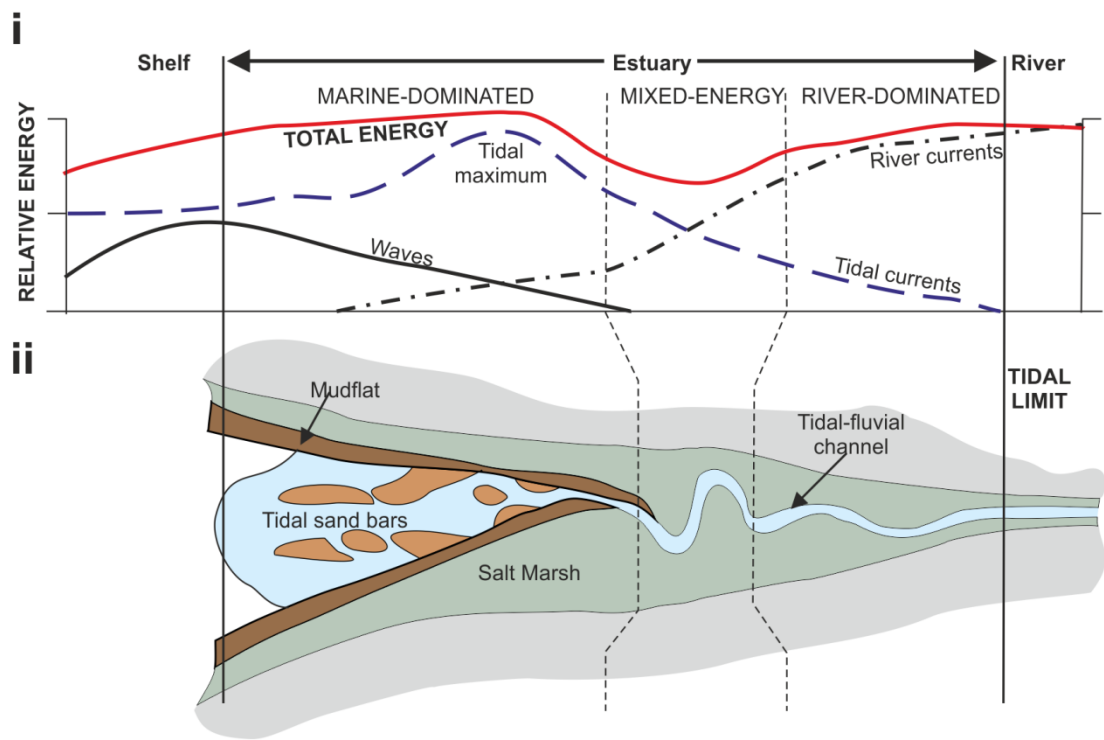


Figure 1.3 i) Variations in river currents, tidal currents and waves with position within a tidal-fluvial system; ii) Schematic map of a tide-dominated estuary with funnel shape translating into a “straight-meander-straight” geometry (redrawn from Dalrymple and Choi, 2007).

and system salinity. These variations result in directly observable changes in sedimentology including grain-size characteristics and their distributions, volumes of suspended sediment, and the resultant sedimentary structures at varying scales (Dalrymple and Choi, 2007). Rahmani (2000) considers the model of Dalrymple and Choi (2007) to be of limited use when considering ancient facies as it considers smaller scale features and is not reliant on grain-size. However, the widespread adoption of this model by workers within both ancient and modern systems would suggest that this is not the case (e.g., Davis, 2012; Hubbard *et al.*, 2011; Fustic *et al.*, 2012; Shiers *et al.*, 2014; Carling *et al.*, 2015; Olariu *et al.*, 2015; Prokocki *et al.*, 2015).

1.3.1 Tidally-dominated, fluvially-influenced

At the mouth of tidally-dominated estuary systems a series of elongated tidal bars will form, with their morphology controlled by the bi-directional flows acting upon them (Allen, 1991a; Dalrymple *et al.*, 1992; Dalrymple *et al.*, 2015). Bars with a more lobate planform may also be found arising from the amalgamation of elongate bars, or with a delta-like planform resulting in locally protected areas, with flood-dominance occurring in some regions and ebb-dominance in others (Hayes, 1975; Billy *et al.*, 2012; FitzGerald *et al.*, 2012). Distinct ebb-flood channel pairings may exist, giving rise to

bedforms with differing directional biases within the same region (Dalrymple *et al.*, 2012), although a main ebb channel with flood regions at the edges may also form. These axial regions may show well-developed tidal rhythmites (Archer, 2004; Dalrymple *et al.*, 2012). This region is expected to be dominated by coarse grained deposits (Rahmani, 1988; Dalrymple and Choi, 2007).

1.3.2 Balanced tidal-fluvial

Regions of balanced tidal and fluvial flows commonly have a tightly meandering planform as this is the lowest energy part of the system (Dalrymple *et al.*, 1992). The finest grain sizes are found here in the region of bedload convergence (Dalrymple and Choi, 2007). This is also the site of the turbidity maximum, with the deposition of finer material as mud drapes over underlying bedforms becoming more common as tidal influence increases, slowing the fluvial flow (e.g., Allen, 1991a; Fenies *et al.*, 1999). Where coarse material dominates flaser bedding will form as finer material settles into ripple troughs during periods of low flow such as slack water. Lenticular bedding (discontinuous lenses of coarse material within a fine matrix) will form when finer material dominates deposition (Reineck and Wunderlich, 1968).

Two-way sediment transport is possible in this region due to the mixing of fluvial and tidal flows; the dominant transport direction of bedload may not be the same as for suspended sediment within the same channel (Culver, 1980; Dalrymple and Choi, 2007). Indicators of the dominant tide may be misleading as preferential erosion may occur on the dominant flood tides, with deposits on the weaker ebb tide being preserved (Figure 1.4), emergent tidal bars may start to form showing clay drapes only present in dune bottomsets and over run-off ripples which run against the dominant tidal flow (Fenies *et al.*, 1999). Again, uni-directional tidal channels may begin to form (Dalrymple and Choi, 2007), but flow is commonly forced through a single channel, resulting in herringbone crossing bedding and sets which are thicker in the dominant fluvial direction (van den Berg *et al.*, 2007).

It should be noted that this tightly meandering region corresponds to the Upper Estuarine Channel of Allen (1991a), which is described as containing estuarine point bars. This region contains extensive rippled sands on the bordering sand flats, interspersed with flaser deposits, although the variation with waning tidal influence is not described in detail, as is also described within the middle zone of Archer (2013). Although the description of the Gironde Estuary notes extensive intertidal regions adjacent to these meanders, the resultant model does not consider these and appears to be channelised (Allen, 1991a). This may be as a result of over-simplification, but further

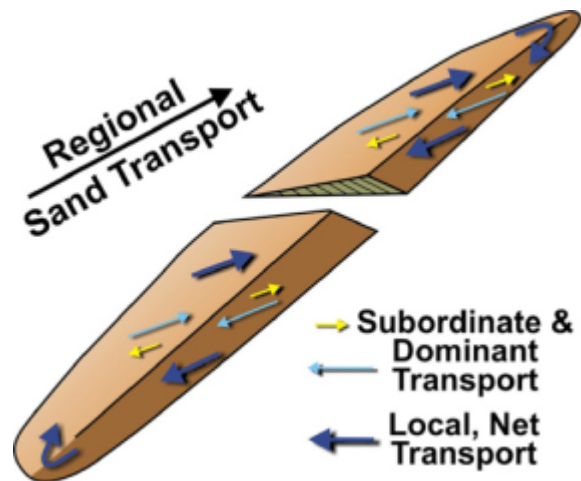


Figure 1.4 Flow transport around an elongate bedform in a tidal channel (Dalrymple and Choi, 2007).

confuses the transition to a more fluviually-dominated regime. Rahmani (1988) described the channel fill of the middle estuary region as predominantly muddy in character, resulting from estuarine (tidally-influenced) processes, which is in agreement with the region of bedload convergence described by Dalrymple and Choi (2007).

1.3.3 Fluviually-dominated, tidally-influenced

The facies trends described by Dalrymple and Choi (2007) within their tidal-fluvial transition model are noted to occur within tide-dominated systems. Whilst the processes and resultant deposition within the regions of tidal dominance and tidal-influence are described in detail, those occurring in the most landward region of the tidal-fluvial transition are not described. In the summary figure it is clear that uni-directional flow is expected landward of the maximum tidal incursion (Figure 1.3). It would be expected that deposition within this region would show a fluviually-dominated pattern, but as the tidal-fluvial transition is known to move it is unclear if any tidal influence would be expected to be preserved. The presence of bedforms within the channel which are constantly reworked by reversing tidal flows are discussed, but only in reference to preserved grain-size variations due to the movement of the brink point (Dalrymple and Choi, 2007). Van den Berg *et al.* (2007) investigated the tidal-fluvial transition in detail, describing outcrop scale sedimentary features. However, they did not collect data at the most landward region where there is a small amount of tidal-influence, as noted within their own discussion, which also highlights the difficulties of interpreting the difference between tidally-influenced cross-stratification and re-activation of fluvial surfaces (van den Berg *et al.*, 2007). Allen (1991a), describing

the Gironde Estuary, noted that this region transgresses from fluvial deposits above the tidal limit to more estuarine point bars, with fluvial point bars becoming more estuarine in nature, with increased clay lamina. The ancient upper estuary channel fills described by Rahmani (1988) were noted to be coarser grained than the middle estuary, with a fluvial source to the sediments.

Flow conditions in all natural systems will not maintain a constant velocity and direction at all times. Bedforms will adjust to attempt to maintain equilibrium with the flow (Baas, 1994). As flows increase scouring and erosion of existing bedforms will occur followed by formation of bedforms with increased height and wavelength. Decreased flow will erode the tops of existing bedforms and shorter wavelengths will form (Baas, 1994). If the bedforms in a flow have not yet reached equilibrium, larger bedforms than would be expected for the local conditions will be present and may have lower flow bedforms superimposed upon them. These superimposed bedforms may pre-sort the sediment available to the larger bedforms (Reesink and Bridge, 2009).

Dalrymple *et al.* (2015) describe a series of tidal-fluvial outcrops with varying degrees of tidal and fluvial influence. However, even within this framework the example with the least tidal influence, the Middle Jurassic Lajas Formation in Argentina, although fluvially-dominated in parts of the section has been interpreted as having a high degree of tidal influence (Dalrymple *et al.*, 2015). The formation is dominated by periods of high fluvial flow, with interflood deposits which are interpreted as tidal in nature due to the ichofossils present. Whilst useful in interpretation of fluvial systems producing river-flood dominated deposits within regions of tidal influence, this is of less use when compared to other systems.

It is known that tidal dunes scale with water depth in estuaries as a result of the maximum current speeds, with the largest dunes occurring in bottom of channels (Dalrymple *et al.*, 2012). The largest dunes (over 10 m in wavelength) are 2D in nature, with smaller dunes superimposed on them, while smaller dunes are simple in form. Care must also be taken when interpreting the formation timescales of preserved bedforms, as although these may be formed during a single flood event (Bridge, 1993), the size of the flood may not be as important as the overall system geometry. Sambrook Smith *et al.* (2010) studied the effects of a 1 in 40 year flood on the South Saskatchewan River, Canada. They found that although the system was extensively scoured, the new bedforms created were of the same scale as bedforms created in previous smaller scale floods, so did not leave a distinct signature in the deposits. They noted that at this point the system consisted of a 30m wide incised channel lying within a 150m wide flood plain. This geometry allowed the flood to expand into the flood plain resulting in bedforms in scale with smaller floods, but in a more constrained system there may be

more of a record due to deepening of the flow (Sambrook Smith *et al.*, 2010). Seasonal flooding of melt water will also create a flood pulse which may leave a trace in the system. As previously noted, the location of the tidal-fluvial transition is highly variable, moving with landward and seaward as a consequence of varying tidal and fluvial flows. These variations in flow depth and speed will result in a range of bedforms sizes and morphologies which although locally consistent (Villard and Church, 2005), may also show evidence of the variations in tidal and fluvial flow.

The existing models of the transitional region between fully-tidal and fully-fluvial flows discuss in detail the region of tidal dominance, where tidal influence in both flow and deposition is readily recognised (Rahmani, 1988; Allen, 1991a; Dalrymple *et al.*, 1992; Dalrymple and Choi, 2007; Davis, 2012; Longhitano *et al.*, 2012; Archer, 2013; Dalrymple *et al.*, 2015; Dashtgard and La Croix, 2015). Whilst the details of these models vary they broadly agree when describing grain-size distributions and the variations in morphology. However, the region of fluvial dominance has to date been less studied. Studies often rely on satellite imagery to interpret similar planform geometries, with very little data collected on the bedforms present within systems and the flows which occur (Billy *et al.*, 2012; Archer, 2013). Studies such as that of van den Berg *et al.* (2007) present extensive descriptions of facies arising within this region (although as noted previously not the most landward), but do not present any corresponding flow data. The model of Dalrymple and Choi (2007) presents clear data for more tidal regions of the transition, but within the fluvially dominated region merely describes a few small features which may show some tidal influence whilst warning:

“The bottom line is that care must be taken not to over-interpret the presence of tidal deposits on the basis of a few, scattered, pseudo-tidal features.” (Dalrymple and Choi, 2007 page 166)

However, this neglects the possibility that a small degree of tidal influence may result in modification of apparently fluvial bedforms and relies on the appearance of bedforms without any quantification of the relative tidal and fluvial flows at this location. As the position of the tidal-fluvial transition is known to be highly mobile, this flow data is necessary to understand the processes forming these bedforms. Repeated use of bedform morphology data without reference to flow dynamics will result in the propagation of inaccurate models of the region of tidally-influenced fluvial dominance, leading to inaccurate reconstruction of ancient systems.

Biological markers are often used to reconstruct the salinity of ancient deposits, and thus interpret the relative tidal influence (e.g., Hubbard *et al.*, 2011; Gingras and

MacEachern, 2012; Dalrymple *et al.*, 2015). However within a fluviially-dominated setting the length of incursion and duration of the salt wedge is highly variable, which may result in the observation of less brackish markers in some parts of the section whilst more tidally-influenced deposition is short-lived in nature and does not allow the relevant assemblages to become established.

1.4 Tidal bores

In systems with a shallow bathymetry, rapidly narrowing planform and a high tidal range (>6 m) the incoming tides may become amplified, forming a mobile hydraulic jump which propagates in a landward direction as a tidal bore (Chanson, 2012; Fielding and Joeckel, 2015; Bonneton *et al.*, 2016). These tidal bores form a series of waves which may be undular or breaking in nature, dependent on the location within the system. Tidal bores of varying heights have been described at locations around the world, with the amount of fluvial flow acting as an additional control on their size and landward incursion (Bartsch-Winkler and Lynch 1988; Chanson, 2012). At times of low fluvial flow and high tides, larger bores will form which travel further landward than bores forming at times of higher fluvial flow.

The interaction of tidal bores with the underlying sediment surface has been described in a few field locations, but the number of descriptions to date are limited (Tessier and Terwindt, 1994; Greb and Archer, 2007; Fan *et al.*, 2014). This interaction may give rise to erosion surfaces, folding, flame structures and sediment dewatering. In addition there have been two descriptions of ancient tidal bore deposits (Martinius and Gowland, 2011; Fielding and Joeckel, 2015). The limited conditions under which tidal bores form mean that their presence within sedimentary deposits is an important palaeomorphological indicator. Indeed, it could be suggested that the passage of a tidal bore may be the only indicator of tidal influence within a fluviially-dominated system. As such, understanding the interaction of tidal bores with underlying substrates and the resultant deposits within modern systems is of clear importance if they are to be understood within ancient systems.

1.5 Thesis aims and objectives

This thesis aims to examine whether there is evidence at the barscale of tidal influence within the fluviially-dominated region of the tidal-fluvial transition zone. As previously discussed, common indicators of tidal influence within this region are represented by smaller, ripple scale deposition. Examining features which scale with the system itself, such as bars, allows a fuller understanding of the region. It will do this by:

- Examination of the flow patterns within the region of interest to establish the relationship between tidal and fluvial flow;
- Investigation of the variations in bedform and barform morphologies arising due to variations in tidal and fluvial flow;
- Investigation of the interaction of tidal and fluvial flows with local barforms.

1.6 Thesis Summary

This thesis examines the flows and bar morphologies arising within the fluvially-dominated tidally-influenced region of two different river-estuary systems. Chapters 2 and 3 investigate the mesotidal Columbia River estuary, Oregon, USA. The Columbia River has the largest drainage basin in the northwest USA, entering the Pacific Ocean close to Astoria, Oregon. Chapter 2 investigates the region of tidal influence, examining the bedform distributions within the system and comparing them to the local flow patterns. The variations in flow around a single barhead across the tidal cycle is reported, further examining the importance of barform geometries and position of the tidal-fluvial interface on bedform morphology. Chapter 3 examines the flow and resultant bedforms around a large lobate barform in the landward region of the tidally-influenced Columbia River. The interaction of the bedforms with the flow is investigated to assess whether the tidal flow has any influence on deposition at this landward location. The shape and formation the barform are also assessed to study any topographic forcing which may arise and the nature of the bar itself. As previously discussed, tidal bars may have a variety of planforms and the lobate shape of the barform is usually described in terms of tidal flows (Hayes, 1975; Dalrymple and Rhodes, 1995; Billy *et al.*, 2012). However, the bar studied herein lies within a region of fluvial dominance with some tidal influence which will affect the method of formation.

The second system studied is reported in Chapters 4 and 5. The River Severn, UK is a macrotidal estuary with the second highest tidal range measured globally. The field sites reported herein lie within the inner estuary in a region of fluvial dominance, but with a regularly reported tidal bore, illustrating the tidal influence present. Chapter 4 investigates the flow around a symmetrical meander bend at two river conditions: during a period of high river flow during neap tides, when the tidal-fluvial boundary lies seaward of the field location; during a period of low river flow during spring tides, when the tidal-fluvial boundary lies landward of the field location. The variations in flow pattern at a single location are examined in detail and the consequence for point bar formation and meander migration assessed. Chapter 5 examines the flow and deposition at a single mid-channel bar located landward of the meander bend

previously reported during a tidal bore. The importance of the incoming tide and the tidal bore to the local depositional patterns is discussed, along with the variations in flow patterns of a single bore at locations at the bar tail and within the adjacent channel.

The differing tidal and fluvial signatures and resultant bedforms and barforms observed within both the Columbia River and River Severn are discussed in detail in Chapter 6. Although the systems are of differing geometry, fluvial and tidal input, the resultant bedform and barform morphology appears to be fluvially-dominated with only subtle indications of tidal influence present. In contrast the flow data collected reveal both systems to have a significant tidal influence. Conclusions to the thesis and a discussion of further work are presented in Chapter 7.

In addition to the work presented in this thesis, further fieldwork was carried out during the course of the author's studies examining the flow and suspended sediment characteristics of a tidal bore on the Garonne River. The papers arising from this work are presented as an appendix to the thesis (Reungoat *et al.*, 2015; Keevil *et al.*, 2015a).

Chapter 2

Depositional patterns arising from tidally-influenced flow in a fluvially-dominated system

2.1 Introduction

The complex transition within river-estuary and river-delta systems from fully-fluvial to fully-tidal occurs at a range of temporal and spatial scales. At a given time, the position of the tidal limit will vary dependent on local river levels, tidal range and system geometry (Dalrymple *et al.*, 1992). Increases in fluvial flow due to seasonal variations or increased rainfall will act to move the transition in a seaward direction, whilst increases in tide height due to daily, monthly or annual tidal cycles will move the transition landward. The maximum landward incursion of the tide, the tidal limit, occurs within the fluvially-dominated region of the river-estuarine system, at which point the fluvial currents are only slowed and modulated by high tides. Closer to the ocean tidal influence increases and fluvial flow will stop or can be reversed (Figure 2.1; Dalrymple and Choi, 2007). The resultant flows and sediment transport processes within the tidal-fluvial transition, whilst sharing characteristics, will reflect the environment in which they formed (e.g., Bridge, 1993; Best *et al.*, 2003; Martinius and Gowland, 2011; Fustic *et al.*, 2012). Sediment transport and deposition will vary through this region as the fluvial flow is modulated or reversed (Dalrymple and Choi, 2007; Dalrymple *et al.*, 2015).

The region of tidal influence has been studied far less than the other parts of river-estuary systems. It can be considered to be the region between the limits of tidal reversals at high and low river discharge (Martinius and Gowland, 2011). The region can be 10s or 100s of kilometres long (van den Berg *et al.*, 2007), and contain the only signatures of both the tidal and fluvial inputs to the system. This influence will often be cryptic, especially within the backwater region, an area which shows little tidal influence (Martinius and Gowland, 2011). Van den Berg *et al.* (2007) define the tidal-fluvial zone as:

“that part of the river which lies between the landward limit of observable effects of tidally induced flow deceleration on fluvial cross-bedding at low river discharge, and the most seaward occurrence of a textural or structural fluvial signature at high river stage.” (page 289)

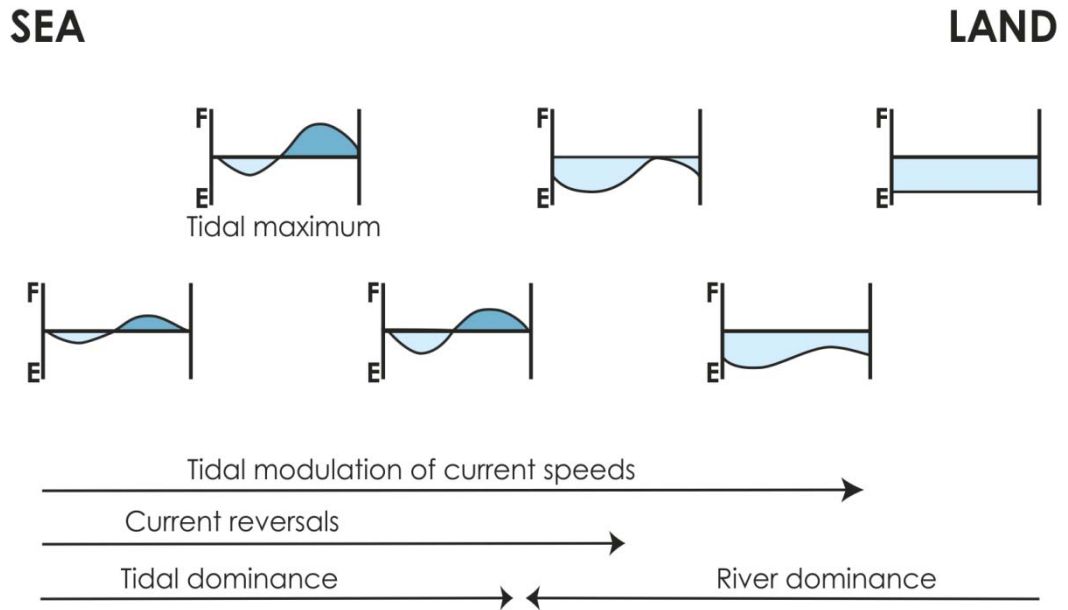


Figure 2.1 Modulation of river currents by tides (redrawn from Dalrymple and Choi, 2007).

Work on modern systems has allowed the description of broad depositional facies zones within a variety of tidal-fluvial environments (Dalrymple and Choi, 2007; van den Berg *et al.*, 2007; Dalrymple *et al.*, 2012; Dalrymple *et al.*, 2015; Dashtgard and La Croix, 2015; Keevil *et al.*, 2015b; Carling *et al.*, 2015). However, the broad range of geometries, tidal range, fluvial flux and sediment content further complicates the creation of a facies model. For example, shallow systems may often have a shorter tidal-fluvial zone due to the slowing of the incoming tide by increased friction (Dalrymple *et al.*, 2015). La Croix and Dashtgard (2015) investigated the sedimentology, ichnology, palynology and geochemical signatures at several locations in the Fraser River and found that only the sedimentology and ichnology could reliably be used to determine position within the tidal-fluvial transition.

Distinct ebb-flood channel pairings may exist within more estuarine settings, giving rise to bedforms with differing directional biases within the same region (Dalrymple *et al.*, 2012), although a main ebb channel with flood dominated regions at the edges and on the top of inundated bars may also form (van den Berg *et al.*, 2007). These axial regions may show well-developed tidal rhythmities (Archer, 2004; Dalrymple *et al.*, 2012). Two-way sediment transport is possible in this region due to the mixing of fluvial and tidal flows; the dominant transport direction of bedload may not be the same as for suspended sediment within the same channel (Culver, 1980; Dalrymple and Choi, 2007). The interaction between flood and ebb dominated channels may result in a braiding pattern, where the maximum tidal currents occur at the highest water level and maximum fluvial currents occur at the lowest water levels resulting in equal patterns of erosion (Hibma *et al.*, 2004). These channels remain distinct from each

other resulting in a braided pattern (Hughes, 2012). In more fluviially-dominated but tidally-influenced settings these straight flood channels do not form, with fluvial channels instead widening in a seaward direction with the landward weakening tidal flows contained within them (van den Berg *et al.*, 2007).

Tidal dunes are known to scale with water depth in estuaries as a result of the maximum current speeds, with the largest dunes occurring in bottom of channels (Dalrymple *et al.*, 2012). The largest dunes (over 10 m in wavelength) are 2D in nature, with smaller dunes superimposed on them, while smaller dunes are simple in form. Investigations were made into the reaction of sand dune morphology to increases in fluvial discharge and tidal range in the Fraser Estuary, Canada (Kostaschuk and Best, 2005). Dune lengths were found to be stable and often not in equilibrium to the flow velocities. However, dune height and steepness were found to vary, with dune tops eroded at the highest measured velocities but showing distinct patterns of hysteresis.

The present study investigates the variations in deposition within a 15 km region of the Columbia River Estuary, Oregon, USA. The region of interest lies within the lower river which while fluviially-dominated experiences tidal modification of flow, as revealed by detailed flow measurements reported herein. Extensive sand bars complexes have formed within the study area, with bathymetry measurements made around several bars across the full extent of the study reach. Large-scale bedforms are found throughout the study region and were measured both within the main channels and subsidiary channels adjacent to the main flow. The variation in bedform morphologies throughout the field area will be reported and the relationship to tidal modification, flow depth and interactions with local barforms assessed.

2.2 Field methods

2.2.1 Field location: the Columbia River Estuary

The Columbia River is the largest river on the Pacific coast of North America, with a drainage basin of 660,480 km², an area which includes parts of British Columbia, Canada, Idaho, Oregon and Washington (Simenstad *et al.*, 2011). The river flows for 2,000 km from Columbia Lake in British Columbia before entering the Pacific Ocean near to Astoria in Oregon, US (Simenstad *et al.*, 2011; Figure 2.2), with an average discharge of 6,700 – 7,300 m³s⁻¹ and a maximum tidal range of 3.6 m (Sherwood and Creager, 1990; Fain *et al.*, 2001). Over 90% of the total basin area is arid, supplying 75% of the basin runoff as spring snow melt (Fain *et al.*, 2001). The system was chosen for this study due its highly dynamic nature, revealed in aerial surveys of the Columbia

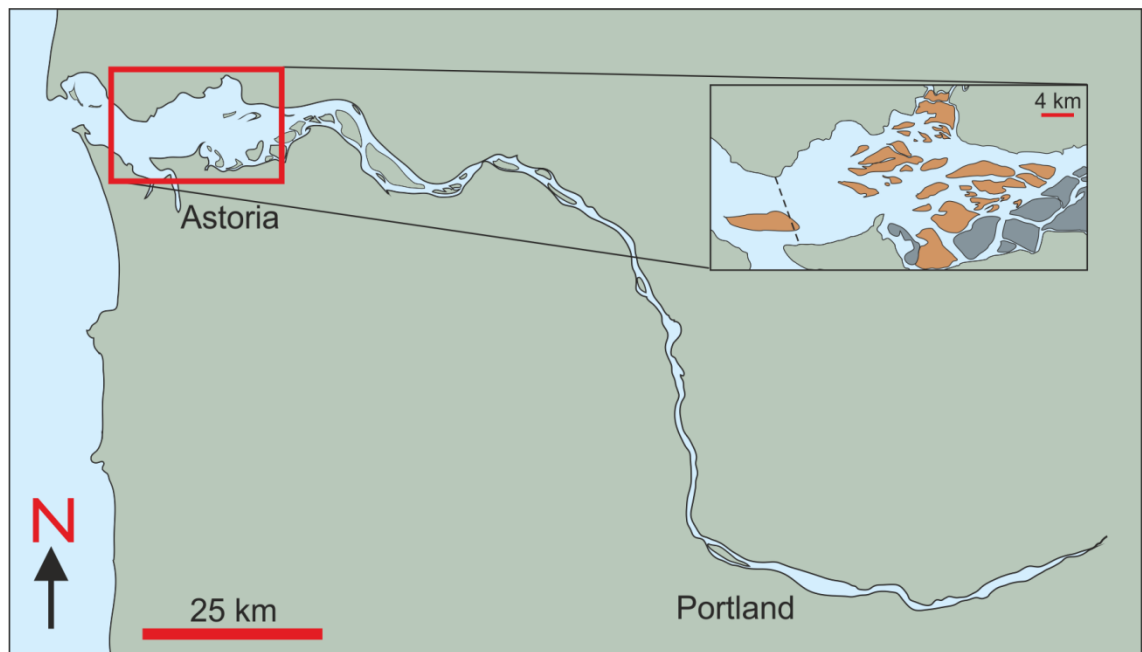


Figure 2.2 Map of tidal Columbia River, USA. Study area is within the red box.

River Estuary carried out by the United States Department of Agriculture (USDA) with barforms which migrate over periods of several years. It has a well defined tidal-fluvial transition, with real time flow gauges and historical records allowing further understanding of the system.

The Columbia River is of economic importance and is used for large-scale merchant transport to Portland, OR. Early surveys show shifting patterns of channels and shoals within the estuary, and for navigation purposes the southern channel began to be engineered from the 1880s to maintain its stability and suitability for shipping. This has slightly isolated previously important channels such as Prairie Channel from the main flow. The navigation channel was 10.7 m deep in 1935, deepened from an initial depth of 3-6 m and has been further deepened to ~16 m by the 1980s (Sherwood *et al.*, 1990; Jay *et al.*, 2011). The estuary region itself has undergone many changes, with the construction of salmon canneries and logging from ~1850 (Sherwood *et al.*, 1990), with abandoned pilings and jetties still visible at the present time.

Continuous daily records of river flow have been made at The Dalles, landward of the Bonneville Dam since 1878, with annual peak flows recorded from 1858 (Naik and Jay, 2005). This shows that at this point in the river the virgin flow (estimated flow with no anthropogenic effects) in June has dropped by 37% from 12,964 m³ s⁻¹ (1903-70) to 8,196 m³ s⁻¹ (1971-1989) (Figure 2.3; Naik and Jay, 2005). The remaining river flow is sourced from the western sub-basin, where the highest flows occur in winter from rain-on snow events (Sherwood *et al.*, 1990; Naik and Jay, 2011). The periods of highest

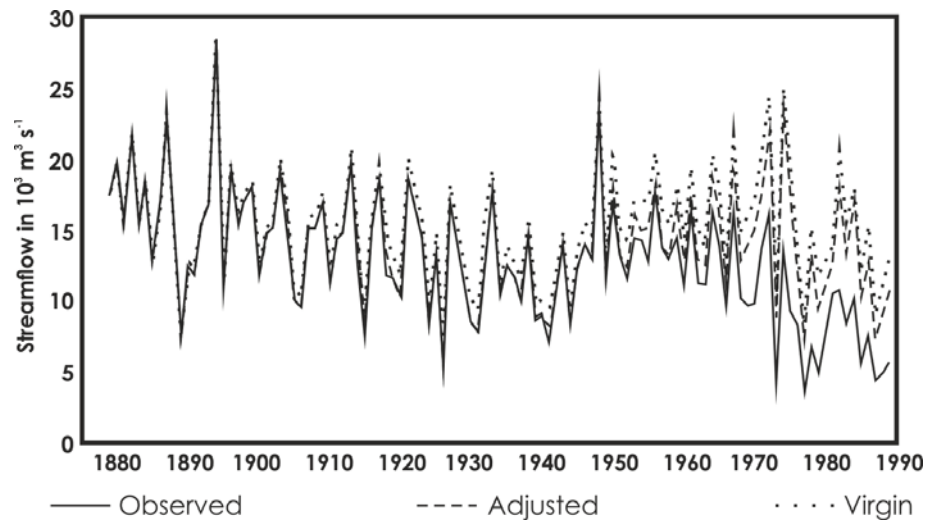


Figure 2.3 June flow at The Dalles, 1879-1989. Adjusted flow estimates flow which would have occurred without the presence of dams (observed flow plus monthly corrections); Virgin flow estimated by Bonneville Power Administration represents flow without presence of large settlements (redrawn from Naik and Jay, 2005).

flow, caused by the freshet is in May-July (Jay *et al.*, 2011), however the flow has decreased due to engineering projects further up the river. Changes in river management, such as extraction for irrigation and power production, have resulted in a reduction in river flow, as well as a 10 day delay to the arrival of the freshet (Naik and Jay, 2011). Sediment supply has been reduced by 80% by the dams further upstream, while further sediment has been removed for channel maintenance and developments (Jay *et al.*, 2011).

The Columbia River estuary has mixed diurnal and semidiurnal tides, with the semidiurnal dominance increasing upstream (Jay *et al.*, 1990). Jay *et al.* (1990) list the principal tidal constituents at Tongue Point, which is within the study area (Figure 2.4). The semidiurnal tidal components acting at this point are:

- M_2 – Principal lunar semidiurnal tidal constituent
- S_2 – Principal solar semidiurnal tidal constituent
- N_2 – Larger lunar ecliptic

while the diurnal constituents are:

- O_1 – Lunar diurnal
- K_1 – Lunar-solar diurnal

The ratios of these tidal constituents are shown in Table 2.1, with a ratio of semidiurnal to diurnal tides of ~1.8 in the Astoria area (Jay *et al.*, 2011). The tidal effect can be felt at Portland, 170 km upstream from the estuary mouth and during periods of low riverine flows ~245 km upstream at Bonneville Dam (Jay *et al.*, 2011).

Table 2.1 Tidal constituent ratios calculated from 7 months of data at Tongue Point (from Jay *et al.*, 1990).

| M ₂ | S ₂ : M ₂ | N ₂ : M ₂ | M ₄ : M ₂ | MK ₃ : M ₂ | K ₁ : M ₂ | O ₁ : M ₂ | O ₁ : K ₁ | M ₂ +S ₂ + N ₂ : O ₁ +K ₁ + P ₁ |
|----------------|------------------------------------|------------------------------------|------------------------------------|-------------------------------------|------------------------------------|------------------------------------|------------------------------------|--|
| 0.947 | 0.247 | 0.189 | 0.012 | 0.025 | 0.423 | 0.252 | 0.596 | 1.81 |

Local tidal data is available for the Tongue Point Tide Gauge, NOAA station 9439040, (NOAA, 2014) located next to a small headland near the town of Astoria (Figure 2.4). The station datums are shown in Table 2.2, all water depths presented for fieldwork are corrected relative to the Mean Sea Level at Tongue Point (TP_MSL). The WGS84 ellipsoid height of the tide gauge is -22.91 m.

Within the estuary there are two deeper tidal channels, at the north and south of the river estuary, both of which show reversing of flow due to tides (Simenstad *et al.*, 1990), although the northern channel is more marine in character (Fain *et al.*, 2001). The southern channel of the river has been artificially deepened to form the navigation channel (Jay *et al.*, 2011). As a result, the routing of fluvial flow and sediment supply is predominantly into the southern channel (Fain *et al.*, 2001). The area of tidal influence studied herein is near Astoria, OR about 15 km landward of the mouth (Jay *et al.*, 2011). The northern channel becomes insignificant within this region, with the southern channel continuing landward as the navigation channel. The study region contains a relatively shallow bay with extensive sand bars which are submerged at mean lower-low water (Prokocki *et al.*, 2015); the main navigation channel runs through the middle of the region, while a secondary deep channel forms to the south (Figure 2.4).

Sediments are fluvial in origin, with marine sediments forming a small mouth bar region (Sherwood and Creager, 1990). The study area contains extensive sand bar and island complexes, typical of the tide-dominated delta model described by Dalrymple and Choi (2007). According to this model the region will show some bidirectional flow, with flow in an ebb direction (i.e. seaward) dominating. However, dating of a series of cores collected by Prokocki *et al.* (2015) in a transect across the landward region of the field area suggests that the lower Columbia River forms an entrenched fluvial system, resulting in the preservation of tidally-modified fluvial sediments rather than estuarine deposits. Prokocki *et al.* (2015) found that the bars within the study region predominantly lie in a subtidal region, with only tidal reworking of the top surfaces. Sediments are mainly fluvially-derived and form stacked small-scale ripple crossbeds on the bar surface.

Table 2.2 Datums for the Tongue Point gauge, 9439040, Astoria OR (NOAA, 2014).

| Datum | Value (m) | Description |
|-------|-----------|-------------------------|
| MHHW | 3.305 | Mean Higher-High Water |
| MHW | 3.099 | Mean High Water |
| MTL | 2.068 | Mean Tide Level |
| MSL | 2.054 | Mean Sea Level |
| DTL | 1.993 | Mean Diurnal Tide Level |
| MLW | 1.036 | Mean Low Water |
| MLLW | 0.681 | Mean Lower-Low Water |

Investigations were made of the Columbia River estuary by Sherwood and Creager (1990) using side-scan sonar. They found that bedforms throughout the region were fluviially dominated, often with smaller superimposed bedforms. However, the larger bedforms in the seaward area of the estuary have smaller superimposed bedforms which show a bi-directional influence. These studies were predominantly carried out seaward of the Astoria-Megler Bridge within the northern and southern (navigation) tidal channels, with one section in the upper region of the estuary, within the navigation channel. The landward limit of these studies corresponds to the landward limit of the Navigation channel shown in Figure 2.4. The variation of bedforms due to the weakening of the tidal influence was not investigated further and there were no measurements made around any of the large barforms landward of the bridge, so their growth and influence were not investigated. All were carried out in the deeper channels and no investigation was made of the effects of flow around shallower barforms (Sherwood and Creager, 1990).

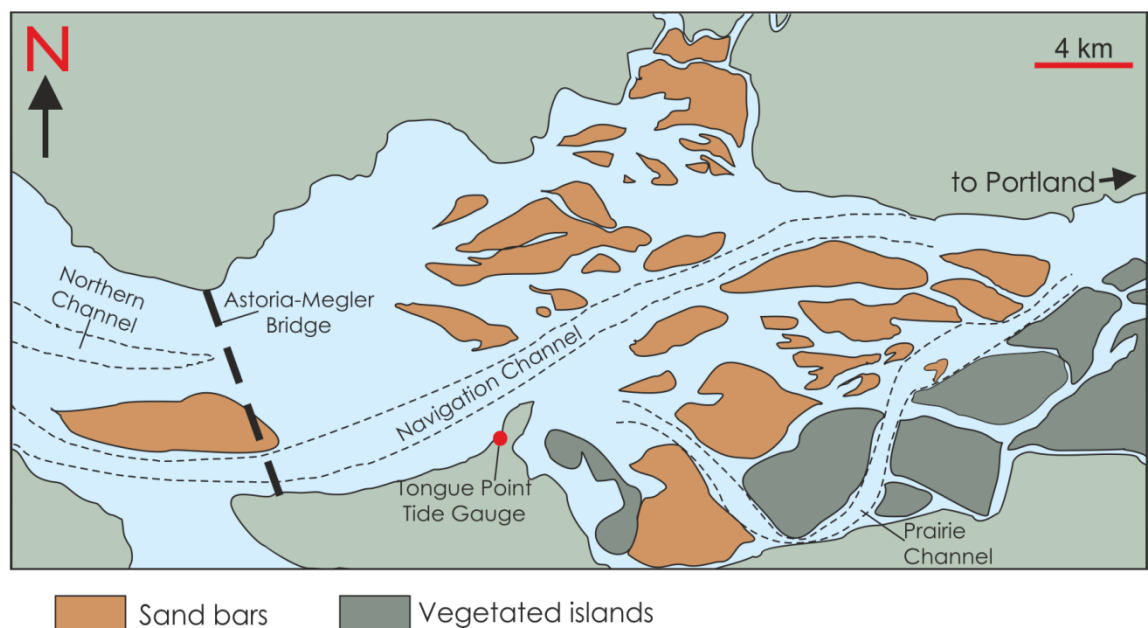


Figure 2.4 Region studied of the Columbia River Estuary. Bar complexes are found throughout the region, some of which are vegetated. Fluvial flow is from the east.

2.2.2 Methodology

Fieldwork was carried out within the Columbia River estuary during two field seasons. In June 2012 (FS1), bathymetry surveys were made throughout the lower Columbia River estuary, whilst flow measurements were made around a bar head at the landward end of the field area. In May-June 2013 (FS2) further bathymetry surveys were conducted, repeating some of the earlier surveys.

2.2.2.1 Bathymetric surveys

Multibeam Echosounder (MBES) surveys were carried out during two field seasons, covering areas within a 15 km length of the Columbia River Estuary. These were located throughout the region of tidal influence and concentrated on the areas around several large sandbars. During FS1 measurements were made at six different locations; in FS2 another six surveys were made, three of which repeat locations from the previous field season (Figure 2.5).

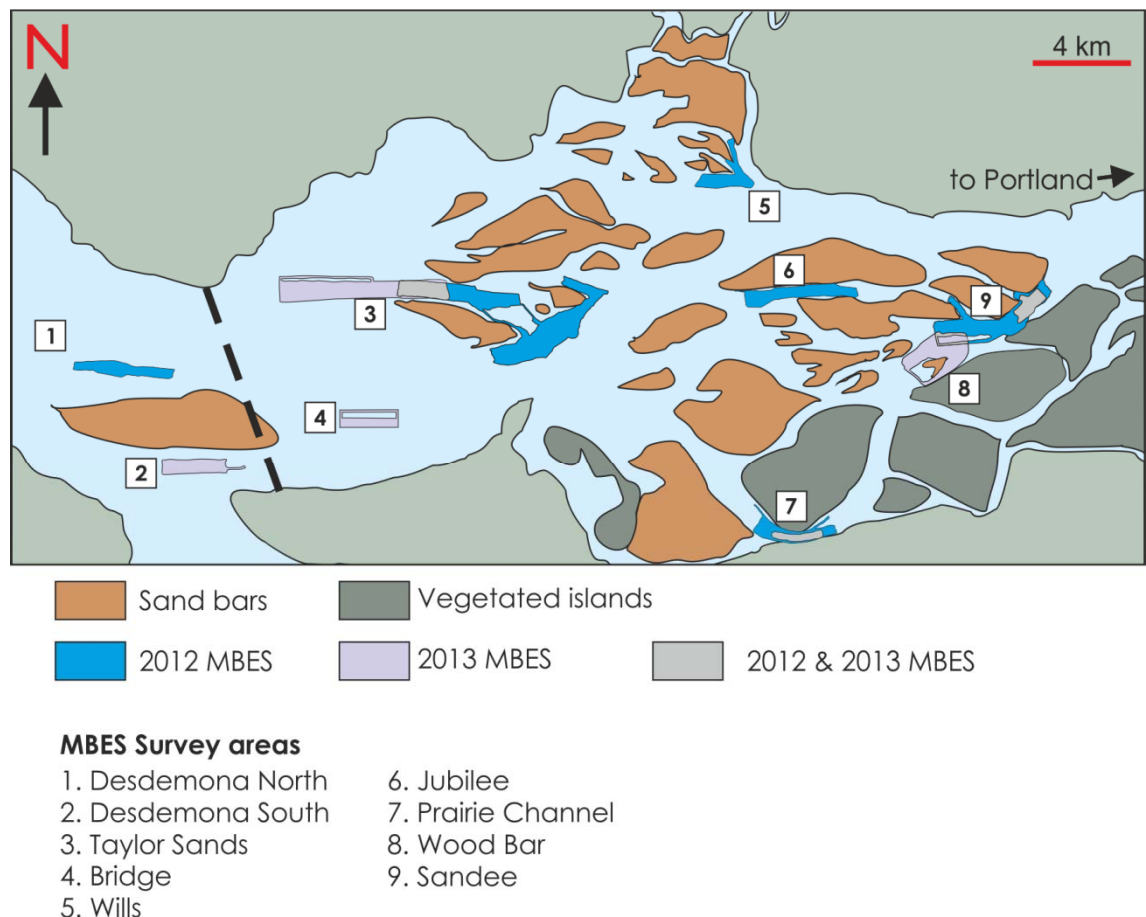


Figure 2.5 Locations of MBES data collected during the present work. Data was collected at 9 separate locations in FS1 and FS2. Data from Wood Bar is presented in Chapter 3.

MBES is an acoustic technique used to create three-dimensional topographic images of river and sea bed morphology (Parsons *et al.*, 2005; Simmons *et al.*, 2010). A sonar head emits pulses of acoustic energy and listens for reflections from the bed and within the water column (Parsons *et al.*, 2005). MBES allows high resolution bathymetric mapping of surfaces to a resolution of centimetres allowing bedforms to be observed at a range of scales (Simmons *et al.*, 2010). The collection of repeat surveys allows the development of bedforms and their reaction to local flow conditions to be assessed. Nittrouer *et al.* (2008) carried out repeated MBES surveys in the lower Mississippi River over a range of river discharge conditions. At several locations they took pairs of surveys 24 hours apart to quantify the bedform migration occurring during this time. This allowed them to estimate the annual bedform flux in the region of the Mississippi. Franzetti *et al.* (2013) carried out similar comparisons of dune migrations in the English Channel.

In the present work MBES data was collected from a small survey boat using a Reson SeaBat 7125 system (Figure 2.6); spatial positioning was calculated using a differential Global Positioning System (dGPS) system with real time kinematic (RTK) correction. The Reson SeaBat 7125 is a 400 kHz system with an array of 512 beams covering a swath angle of up to 128° (Reson, 2007). It can operate in water depths from 1-200 m, with pulses in the rate of 10-300 μ s and a ping rate of up to 50 per second (Reson, 2007). The sonar system was controlled using the Reson 7K Control Center software, whilst data acquisition was carried out using Reson PDS2000 software. During the current work, MBES surveys were carried out in water depths of 1-20 m using the maximum ping rate and pulses of approximately 60 μ s. Full motion correction for the system was obtained using an Applanix Pos MV system, which collects real-time motion and directional data for the survey boat using an Inertial Measurement Unit (IMU) connected to 2 fixed GPS antennas. The positioning data was corrected using a live RTK correction: in FS1 the correction used was the Washington State Reference Network; in FS2 the correction used was the Oregon Real-Time GPS Network.

Processing of the MBES data was carried out using Caris HIPS and SIPS version 7.1.2. The raw output files are imported into the programme and checked for errors in navigation. A tide correction was generated from the instantaneous GPS height data recorded using the Caris GPSHeight utility, which was further filtered to one point per minute. Using the Caris tide utility this tide file was cleaned to remove peaks in the tide data and then applied to the processed data file. Although sound velocity profiles were recorded during the MBES surveys using a Reson SVP-15, no sound velocity correction was applied to the data as Caris HIPS and SIPS version 7.1.2 has an algorithm for sound velocity correction using the sound velocity profile used at the time of data collection by

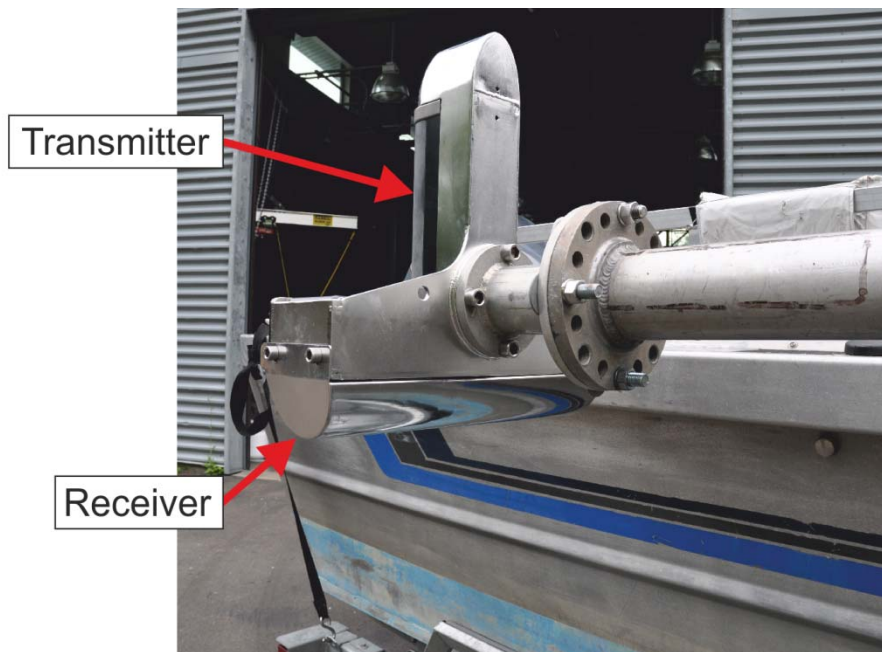


Figure 2.6 Reson SeaBat 7125 head, in transport position on boat. The transmitter is located underneath the head (black unit visible in the upright portion of the image), whilst the receiver is at the front of the head underneath a metal protective cover (facing ground in image).

the SeaBat 7125 (Caris, 2013). Once a sound velocity profile has been applied to a profile it cannot be removed, so any MBES data which has been processed in earlier versions of Caris HIPS and SIPS cannot be further processed in version 7.1.2 as the system recognises that a correction has been made but no longer applies this, but at the same time does not apply the SeaBat 7125 correction. The MBES profiles were then merged in Caris HIPS and SIPS and a Bathymetry Associated with Statistical Error (BASE) surface generated. This surface allows further quality control of the data to be carried out using a visual interpretation of the data (Caris, 2012). Data spikes and regions where navigation errors still persisted were removed and the BASE surface exported to a point cloud file at a resolution of 0.5 m, to allow further interpretation.

As Caris HIPS and SIPS records depths as positive values below the surface, whilst ArcGIS 10 requires the use of negative values a correction to the point cloud file was made using a custom script in Matlab prior to importing the data. Following the import of the point cloud file into ArcMap 10, the data was converted into a Raster object using the methodology in Table 2.3. Once a raster surface has been created profiles through the data can be output for further analysis using the Bedform Tracking Tool (van der Mark and Blom, 2007; van der Mark *et al.*, 2008). Differences between repeated surfaces can also be output using the Math function of the Spatial Analyst Toolbox, allowing regions of deposition and erosion to be highlighted.

Table 2.3 Methodology to convert Caris HIPS and SIPS BASE surface to Raster object in ArcMap 10.

| | | |
|---|--|--|
| 1 | Export BASE surface to point cloud (xyz) data | Caris HIPS and SIPS 7.2 |
| 2 | Convert bathymetry values to negative downward | Custom Matlab script |
| 3 | Import point cloud data to ArcMap 10 | Add Data |
| 4 | Extract point separations | 3D Analyst Toolbox> Conversion> From File> Point File Information |
| 5 | Convert point file into ArcMap Feature | 3D Analyst Toolbox> Conversion> From File> ASCII3D to Feature Class |
| 6 | Create Raster object in ArcMap | Conversion Tools Toolbox> To Raster> Point to Raster |

2.2.2.2 Flow measurements

During FS1 flow data was collected at 4 cross-sections landward of the bar head of Sandee Bar (location 9 on Figure 2.5) using a Teledyne RD Instruments RioGrande 1200 Hz Acoustic Doppler Current Profiler (ADCP) (Figure 2.7). One of the cross-sections was located within the shallow channel between two sub-aerial bars, where there was limited exposure. The data were collected during one tidal cycle, at lowest low water and lowest high water on 23-24/06/2012 (Table 2.4). Data was collected at a rate of ~1 Hz in vertical data bins of 0.25 m through the water column; the blanking distances due to instrument deployment and acoustic interference effects were 0.61 m down from the water surface and 0.5 m up from the base of measurements. Corrections must be made to boat motion relative to the water column using a connected GPS system, as the velocities returned will be a combination of those of the water column and the vessel (Yorke and Oberg, 2002; Parsons *et al.*, 2005). The present measurements were performed using a vector track and speed over ground derived (VTG-derived) dGPS correction for the boat velocity.

All ADCP data were post-processed in Matlab using the Velocity Mapping Toolbox and were rotated to remove lateral flux through the cross section using the zero-net secondary discharge (zsd), where the cross-section is re-oriented so that there is no lateral flux through the cross-section (Parsons *et al.*, 2013). This method was chosen as it allows improved visualisation of the cross-stream flow patterns, without the complication of any residual cross-stream discharge being within the rotation. For each cross-section two reciprocal ADCP transects were measured; this was due to the length of the cross-sections (up to 900 m) and the rapidly changing tidal conditions which

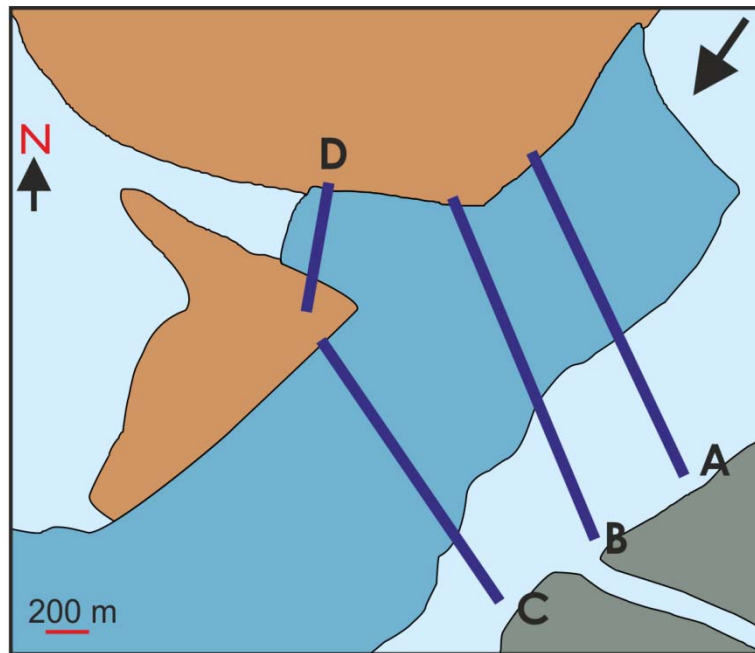


Figure 2.7 Position of ADCP cross-sections collected at Sandee Bar (Location 9 on Figure 2.5). Fluvial flow from top right of image. Dark blue shows the position of MBES data collected during FS1.

were being compared (Table 2.4). When collecting ADCP data it is recommended that more transect repeats than this are measured (e.g. Yorke and Oberg, 2002; Muste *et al.*, 2004a; Muste *et al.*, 2004b; Szupiany *et al.*, 2007), but this would not allow direct comparison of the tidal data in the present case.

ADCPs are commonly used to measure an instantaneous three-dimensional velocity field in a vertical profile (Szupiany *et al.*, 2007). Acoustic pulses are transmitted at a

Table 2.4 ADCP data collected at Sandee Bar. Date and time in UTC.

| Time | Cross-section | ADCP Transect | Condition |
|---------------------|---------------|-----------------------|------------------|
| 18:19 23/06/2012 | A | Trans001- Trans002 | Lower-low water |
| 23:41 23/06/2012 | A | Trans011- Trans012 | Lower-high water |
| 18:46 23/06/2012 | B | Trans003- Trans004 | Lower-low water |
| 00:09 24/06/2012 | B | Trans013- Trans014 | Lower-high water |
| 19:26 23/06/2012 | C | Trans005- Trans006 | Lower-low water |
| 00:40 24/06/2012 | C | Trans015- Trans016 | Lower-high water |
| 20:01 23/06/2012 | D | Trans007- Trans008 | Lower-low water |
| 23:27 23/06/2012 | D | Trans009- Trans010 | Lower-high water |

fixed frequency along beams within a water column. The echoes from suspended particles within the water column are processed to find the Doppler shift between the pulse and the echo, and so the difference in velocity between the ADCP and the water (Muste *et al.*, 2004b; Yorke and Oberg, 2002). The echoes are grouped into set intervals along the beam path based on time of return called cells or bins. At least three beams are needed to measure the entire velocity field, arranged at precise angles (120° in three beam instruments (Figure 2.8), 90° in four beam instruments) to allow full 3-dimensional measurement (Muste *et al.*, 2004b; Yorke and Oberg, 2002). The frequency of the pulses emitted varies according to the instrument used, with a wide range available. The frequency used is chosen according to the depth of the system being measured, as higher frequencies have greater attenuation of the signal and so a shorter usable range (Yorke and Oberg, 2002). A 300 kHz system is suitable for measurements up to a depth of 120m, whilst a 1200 kHz system such as the one used herein can only take measurements up to a depth of 20 m (Yorke and Oberg, 2002).

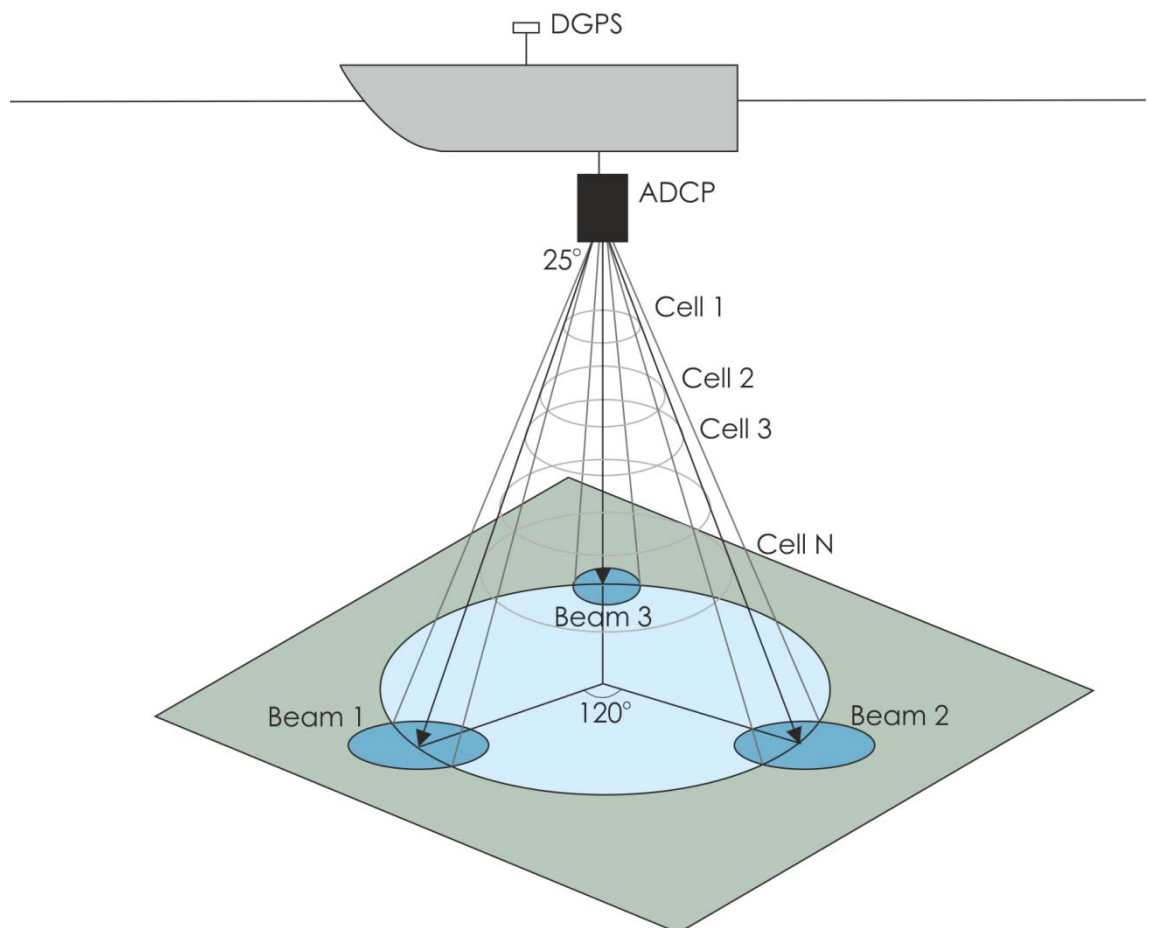


Figure 2.8 Arrangement of beams in a three beam ADCP (redrawn from Szupiany *et al.*, 2007).

2.3 Results

2.3.1 Bathymetry surveys

2.3.1.1 Northern Channel

The northern channel described by Sherwood and Creager (1990), extends landward to the region of the Astoria-Megler Bridge (Figure 2.4). Bathymetry measurements were collected seaward of this adjacent to Desdemona Sands. A second region, landward of the bridge and connected to Taylor Sands, is described in that section below.

i) Desdemona North

The most seaward section of bathymetry data collected, this section is 2.7 km long and up to 400 m wide on the northern edge of Desdemona Sands, seaward of the Astoria-Megler Bridge within the upper section of the northern tidal channel (Location 1 on Figure 2.4). This section was measured during FS1. The section varies in depth by only 7.2 m, ranging from -2.05 m at the edge of Desdemona Sands to -9.24 m (Figure 2.9). The deeper region at the north of the section (-6 m) forms the upper extent of a channel spur. Within this there are seaward oriented scours, ranging in size from 2 to 10 m in length; there are no regular bedforms observed within the channel itself (Figure 2.9iii). As the section shallows to the south onto the edge of Desdemona Sands, uniform dunes can be seen with laterally extensive crests (up to 150 m) oriented perpendicular to the channel direction. These dunes have very shallow crests (0.1-0.2 m) with crest separations of up to 5 m (Figure 2.9i), whilst on the bar top the dunes have a 10 m wavelength, with crests 0.5 m high (Figure 2.9ii).

The variation with depth of a series of dunes on the bar edge is shown in Figure 2.10. The profiles vary in depth from -2.6 m at the bar edge to -6 m TP_MSL within the channel. The shallowest profile contains highly asymmetrical dune crests oriented with flow in a seaward direction, 0.35 m in height with mean crest separations of 13 m. The bedforms observed in the deepest profile are much smaller in size (0.1 m high, mean crest separation of 8 m) and have a more rounded, symmetrical appearance.

2.3.1.2 Navigation Channel

The main navigation channel within the lower Columbia River forms the southern channel west of the Astoria-Megler Bridge; to the east of this it forms the main channel through the system. The navigation channel has been dredged to allow shipping to pass landward to Portland, OR. Bathymetry surveys were carried out at several locations varying from seaward of the Astoria-Megler Bridge, to the northern region of the channel within the measurement region.

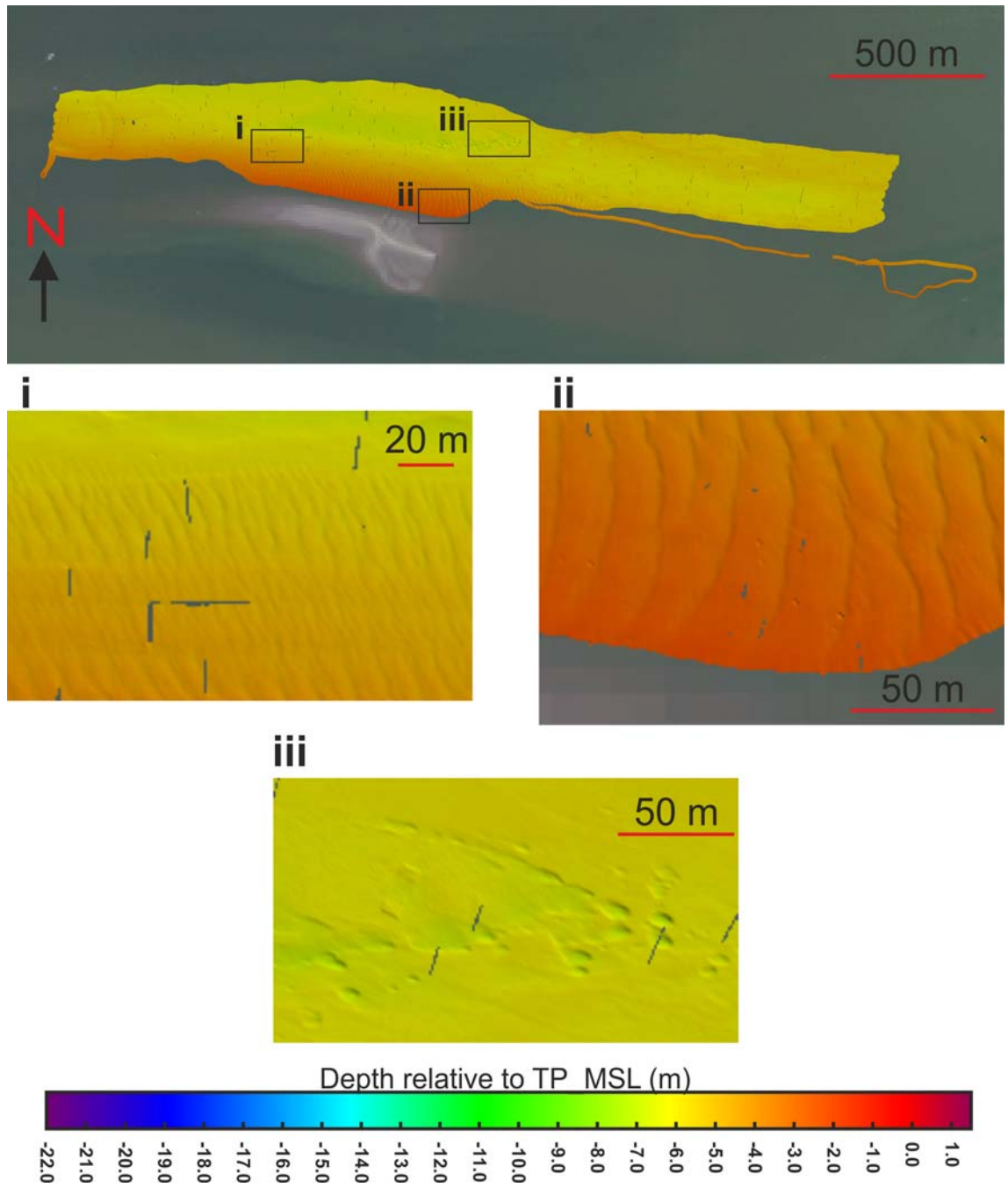


Figure 2.9 Bathymetry measurements collected at Desdemona North during FS1 (Location 1 on Figure 2.5) – see text for details of bedforms.

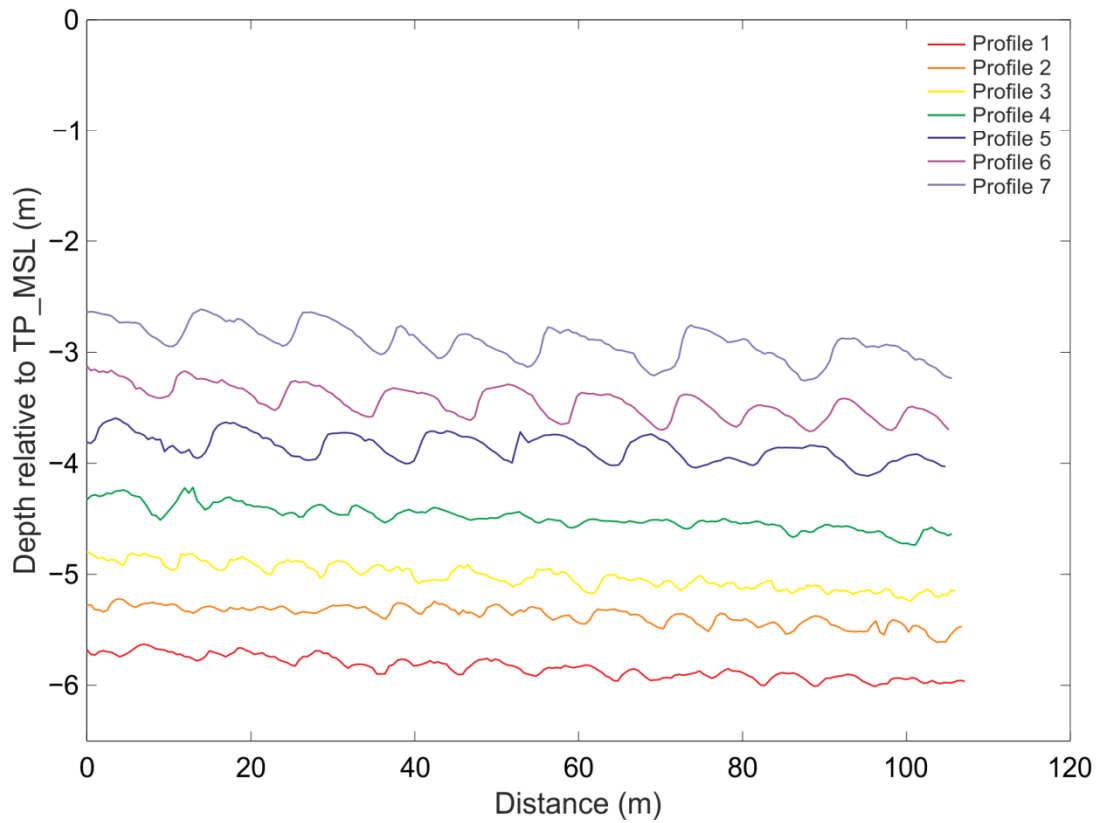
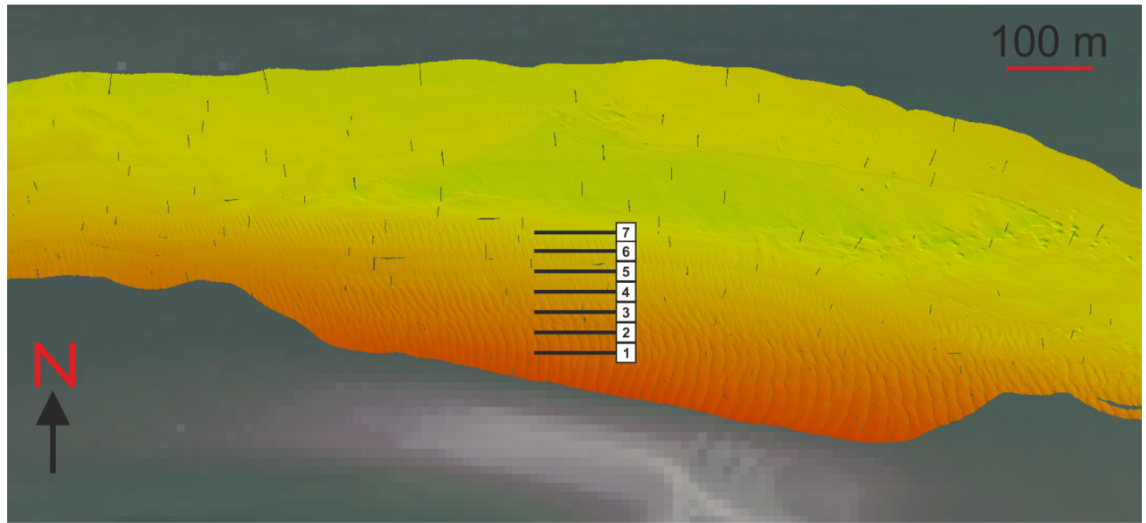


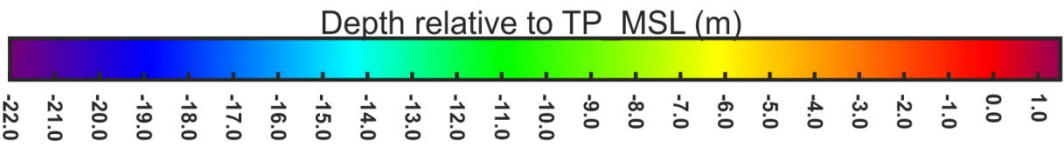
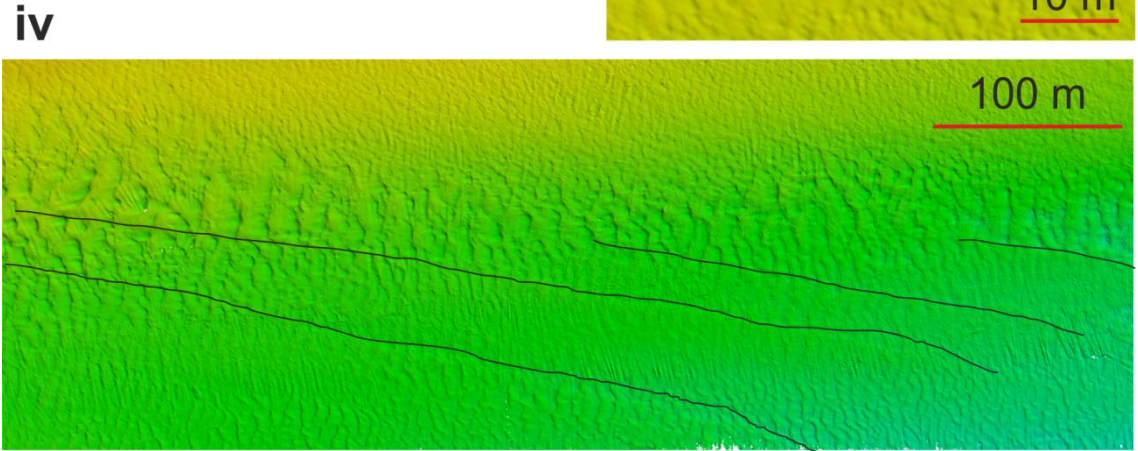
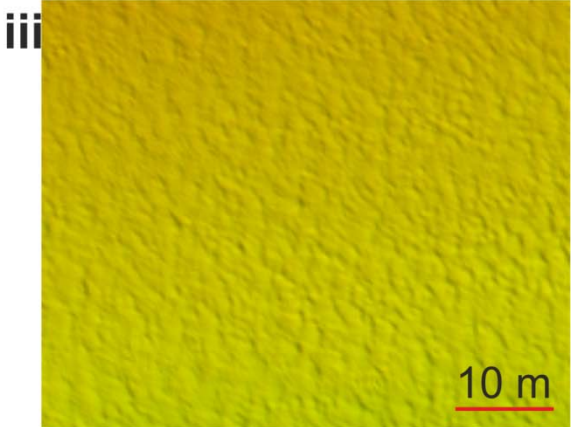
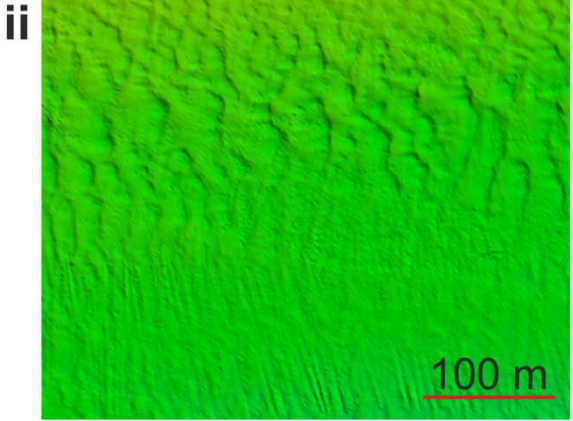
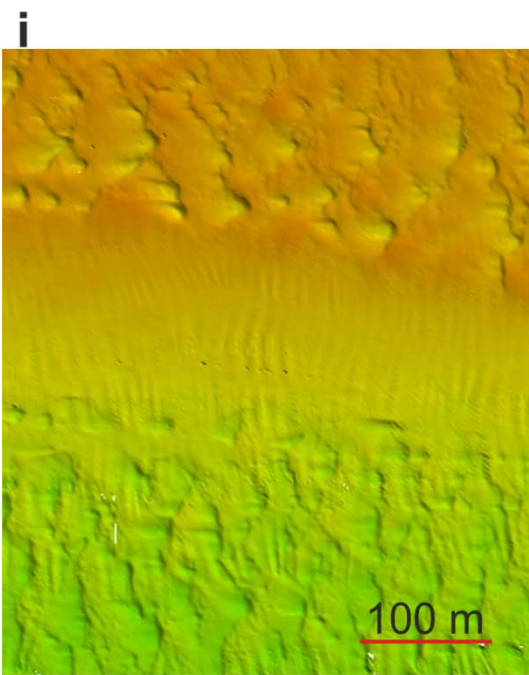
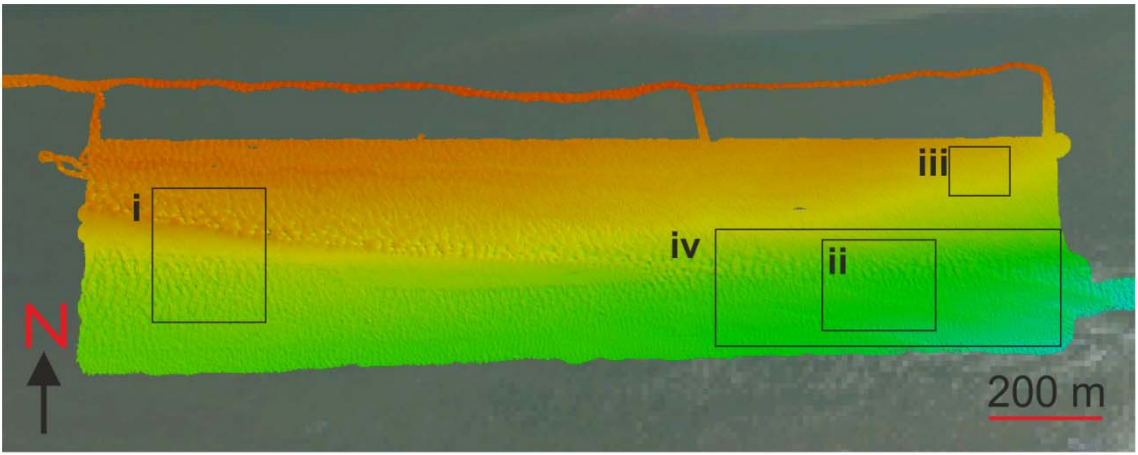
Figure 2.10 Desdemona North dune profiles derived from MBES data (location 1 on Figure 2.5), where 0 m is at the seaward end of the profile (fluvial flow from right of figure). Profile 7 is the southern most profile, collected at the northern edge of Desdemona Sands, while Profile 1 was collected in the channel to the north of the bar.

i) Desdemona South

The second Desdemona Sands section was measured during FS2. This section was collected to the south of Desdemona Sands, seaward of the Astoria-Megler Bridge on the northern edge of the navigation channel (Location 2 on Figure 2.4). The section is 1.8 km long by 400 m wide and varies in depth from -2.1 m TP_MSL at the northern margin to -9.8 m TP_MSL at the south (Figure 2.11). On the shallower margin of Desdemona Sands dunes with up to 20 m separation and relative crest heights of 0.3 m are observed. On the bar top the dunes become less pronounced moving landward (Figure 2.11iii). Within the deeper section adjacent to the Navigation Channel the dunes are smaller, with straighter crest lines. Between the two regions of dunes is a steeper slope up to 70 m wide with no bedforms present: at the most seaward point the north-south slope is 2.85 %; in contrast on the bar top the slope is 0.05 %, while the slope of the deepest region is 1 % (Figure 2.11i). At the landward end of this slope more pronounced dunes are seen than in any other part of this section, with relative crest heights of up to 0.8 m (Figure 2.11ii). A series of ridges are observed adjacent to the bar edge in the landward region, one of which appears to be an extension of the smoother bar slope. These ridges are <1 m high with separations of <50 m and are angled obliquely to fluvial flow (Figure 2.11iv).

A series of 200 m long profile traces from the centre of the bathymetry measurements were made at ~40 m intervals, oriented parallel to fluvial flow and ranging from within the channel (-10 m TP_MSL) to the southern edge of Desdemona Sands (-4 m TP_MSL) (Figure 2.12). The relatively bedform free slope observed in Figure 2.11, is observed in Profile 4. Dune crests are asymmetrical throughout the profiles, although not as pronounced as those within the slightly shallower northern Desdemona profiles (Figure 2.10). The deepest profile contains dunes which have 8 m crest separations, with crest heights of 0.35 m. The largest dunes are observed at the edge of the bar to the north of the bar slope in Profile 5. This profile contains bedforms with crest separations of 18 m and crest heights of 5.5 m. The shallowest profiles contain dunes with similar crest separation to those observed in the channel (8 – 9 m), but smaller crest heights (0.2 m).

Figure 2.11 (next page) Bathymetry measurements collected to the south of Desdemona Sands during FS2 (Desdemona South; Location 2 on Figure 2.5) – see text for details of bedforms.



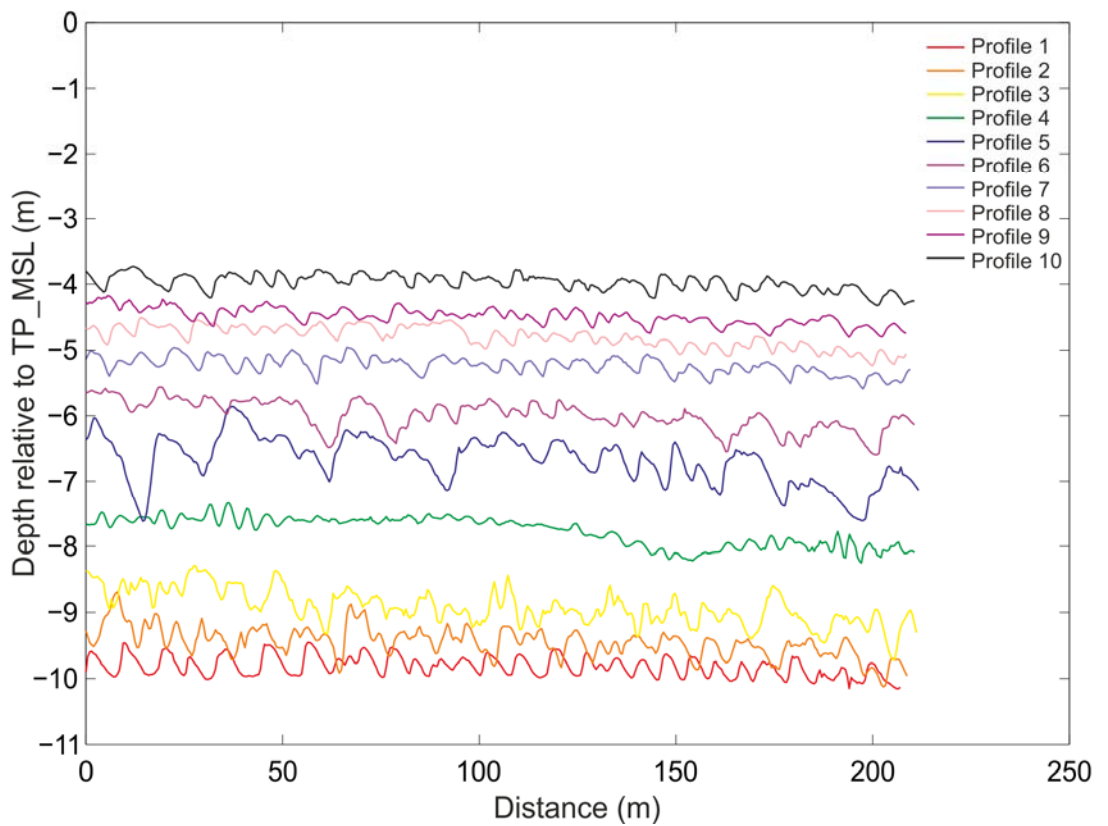
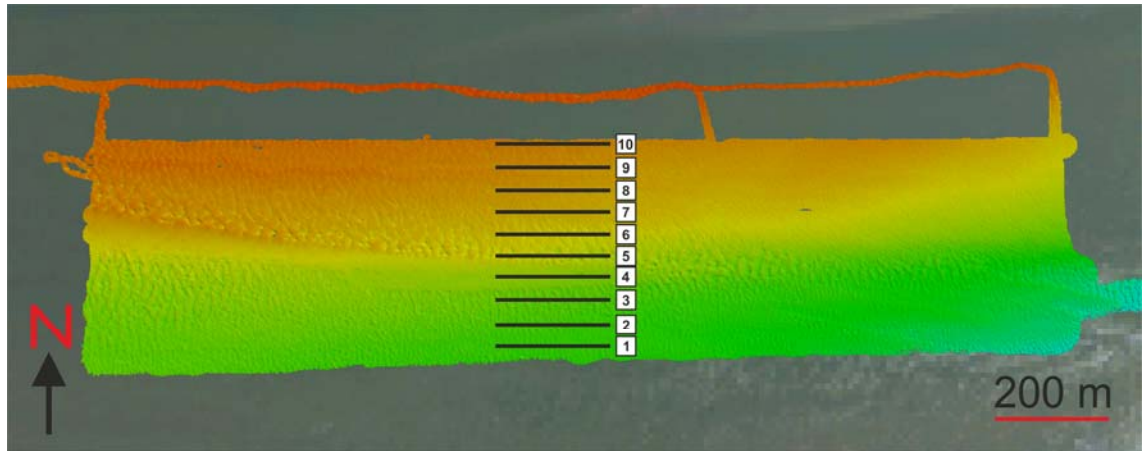


Figure 2.12 Desdemona South (Location 2 on Figure 2.5) dune profiles derived from MBES data (Figure 2.11), where 0 m is at the seaward end of the profile (fluvial flow from right of figure). Profile 10 is the northern most profile, collected at the southern edge of Desdemona Sands, while Profile 1 was collected in the navigation channel to the south of the bar. Profile 4 is located on the featureless slope observed in the MBES data.

ii) Bridge

The Bridge section is 2 km landward of the Astoria-Megler Bridge (3.5 km landward of the Desdemona South section), on the northern edge of the navigation channel (Location 4 on Figure 2.4). Measurements were collected during FS2. The section is 1.6 km long by 500 m wide and is between -4.2 m TP_MSL at the north western corner and -11.36 m TP_MSL at the south east (Figure 2.13). There are several large scale bedforms with a wavelength of 350 m and a relative crest height of 0.6 m (Figure 2.13iii). Superimposed on these bedforms are smaller dunes which are aligned at 90° to the larger bedforms (Figure 2.13ii). In the main measurement section these superimposed dunes have sinuous crests with a relative crest height of 0.05 m in shallower sections and <0.2 m in deeper sections. The shallowest region of measurement in the northwest shows more defined dunes with crest heights of up to 0.9 m and wavelengths of 25 m (Figure 2.13i).

iii) Taylor Sands – FS1

Measurements were made around the Taylor Sands bar complex during both FS1 and FS2, with some overlap of data. This was the largest section measured during FS1 with a total east-west length of 5.9 km by 2.5 km (Figure 2.14). The southern edge of the section is located on the northern slope of the navigation channel around the Taylor Sands complex directly north of Tongue Point (Location 3 on Figure 2.5). There are three distinct regions within the measured section: the edge of the navigation channel; the channel region north of Taylor Sands; the bar top.

The edge of the navigation channel is a section 3.5 km long and 700 m wide. At its deepest the section is -10.5 m TP_MSL; as the section shallows towards the bar top several large scale dune features can be seen with a wavelength of 300 m and smaller superimposed dunes. These are aligned normal to the edge of the bar, not to the implied channel position from aerial images (Figure 2.14iii).

The channel to the north of Taylor Sands is 2.5 km long and 450 m wide. The middle region is a uniform depth of -8.5 m TP_MSL and does not contain any large scale bedforms; there is a large scour feature -16.84 m TP_MSL, which is 170 m wide at the seaward end (700 m from the head of the scour). This scour contains a second deep section 240 m seaward of the initial scour (Figure 2.14i). The landward region contains large scale dunes with 2D crests normal to the channel and wavelengths of 40 – 50 m. The region seaward of the scour contains dunes of a similar scale, but the dunes are not so clearly aligned. At the edges of the channel dunes with up to 50 m separation between crests can be seen, these are aligned at ~45° to the edges of the channel

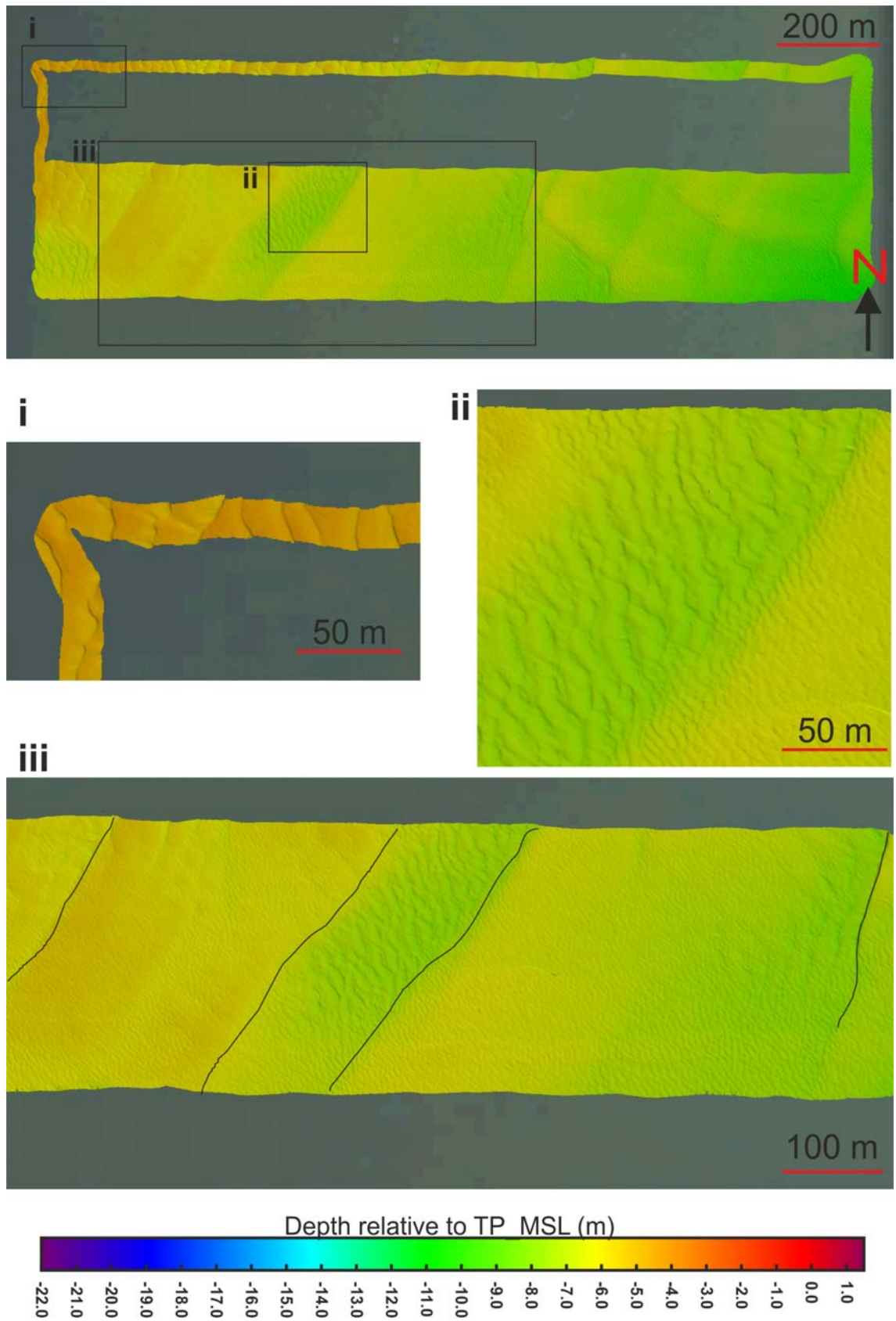


Figure 2.13 Bathymetry measurements collected at the northern edge of the Navigation Channel, east of the Astoria-Megler Bridge during FS2 (location 4 on Figure 2.5) – see text for details of bedforms.

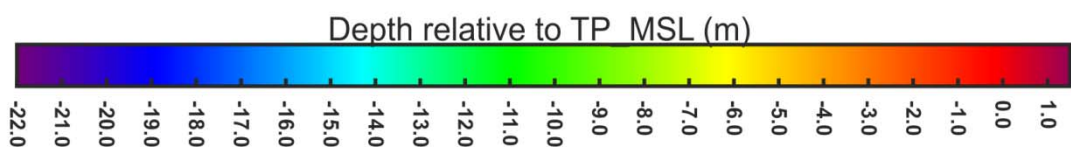
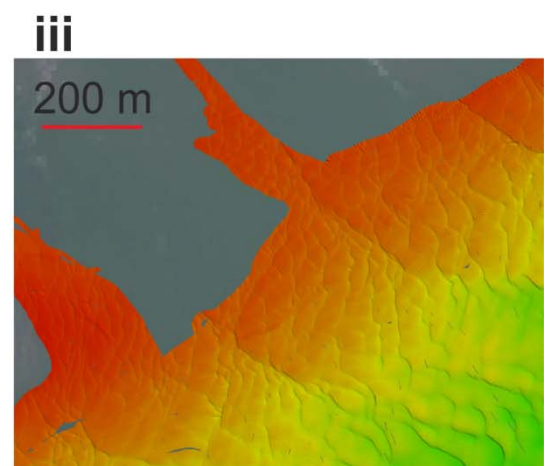
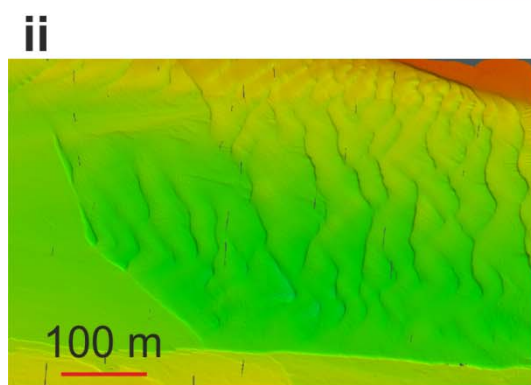
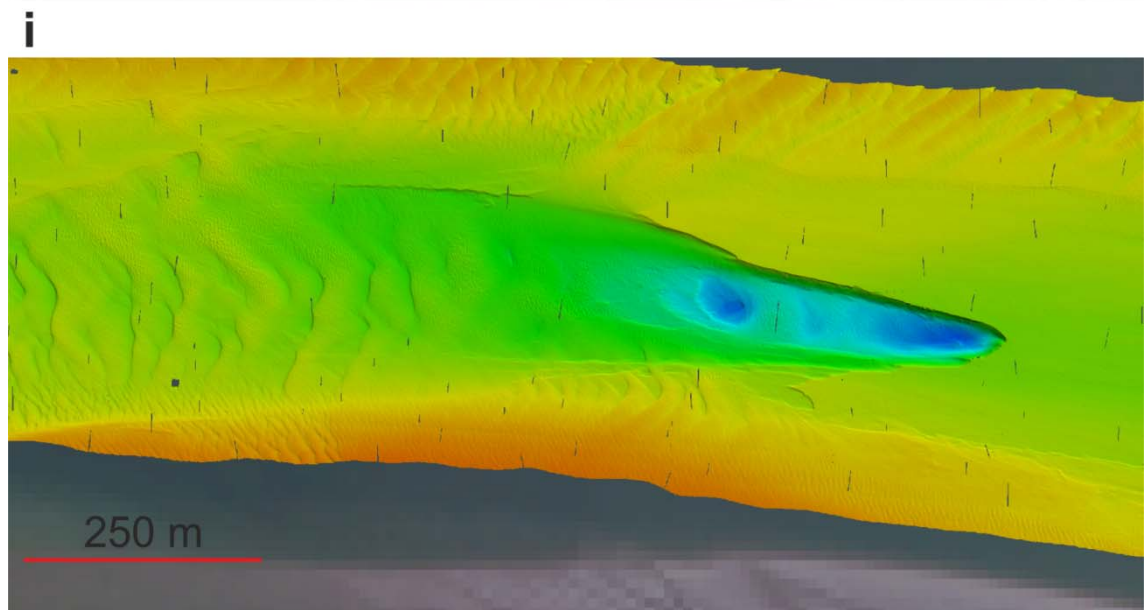
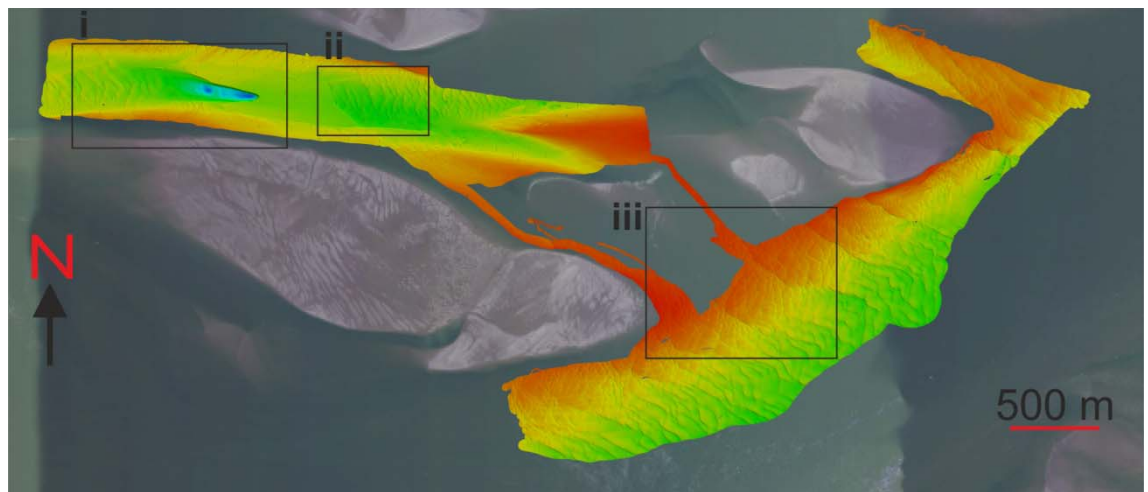


Figure 2.14 Bathymetry measurements of the region around Taylor Sands collected during FS1 (Location 3 on Figure 2.5). The southern edge of the section lies within the Navigation Channel. See text for details of bedforms.

(Figure 2.14ii). The bar top region consists of MBES data collected around the bar complex, when tidal conditions allowed measurements to be made. The surface is generally up to -3 m TP_MSL, but in some areas is 0.45 m above TP_MSL. Where large bedforms are seen these generally have a crest separation of 5 – 10 m; most areas show much smaller scale features (Figure 2.14iii).

The second set of profile traces were made further upstream, again oriented parallel to fluvial flow and ranging from the bar top to the base of the Navigation channel slope with a separation of ~100 m (Figure 2.16). The bedforms at the base of the slope have a similar morphology to those seen at the seaward section (Figure 2.15), whilst the bedforms at the top of the slope have smaller crest heights. Smaller superimposed bedforms are seen at the crest of all profiles and on the landward slopes, rather than throughout the profiles as observed at the seaward traces.

iv) Taylor Sands – FS2

The FS2 section is to the east of the Astoria-Megler bridge, landward of the secondary tidal channel, and to the north of Taylor Sands (Location 3 on Figure 2.5), overlapping the eastern section of Taylor Sands measured during FS1. The section is 4.7 km long and 500 m wide (Figure 2.17). In this extended section the channel previously observed at the west during FS1 shallows in a seaward direction to -4.1 m TP_MSL (Figure 2.17ii). Dunes on a similar scale can be seen, becoming more sheet-like as the section moves seaward with sickle shaped crests extending across the whole section width (Figure 2.17i).

To the west of this is a deeper channel section, the centre of which is -10.25 m TP_MSL, containing sinuous crested dunes up to 6 m in wavelength and relative crest heights of about 0.2 m. At the margins of this channel the section shallows and contains 2D dunes up to 15 m in wavelength with relative crest heights of 0.6 m (Figure 2.17iii). All dunes have an asymmetrical profile indicating flow dominance in a seaward orientation.

The region of overlap between the two field seasons is 1.3 km long, corresponding to the area containing a large scour hole. A profile trace measured through this scour reveals that the landward edge of the scour did not move significantly between the two field seasons and that although there has been some erosion on the seaward surface (<1 m in some regions) there has been no significant erosion or deposition within the scour feature itself, maintaining a depth of -17 m TP_MSL (Figure 2.18). The bedforms observed on the seaward edge do not differ in size or morphology between the two field seasons.

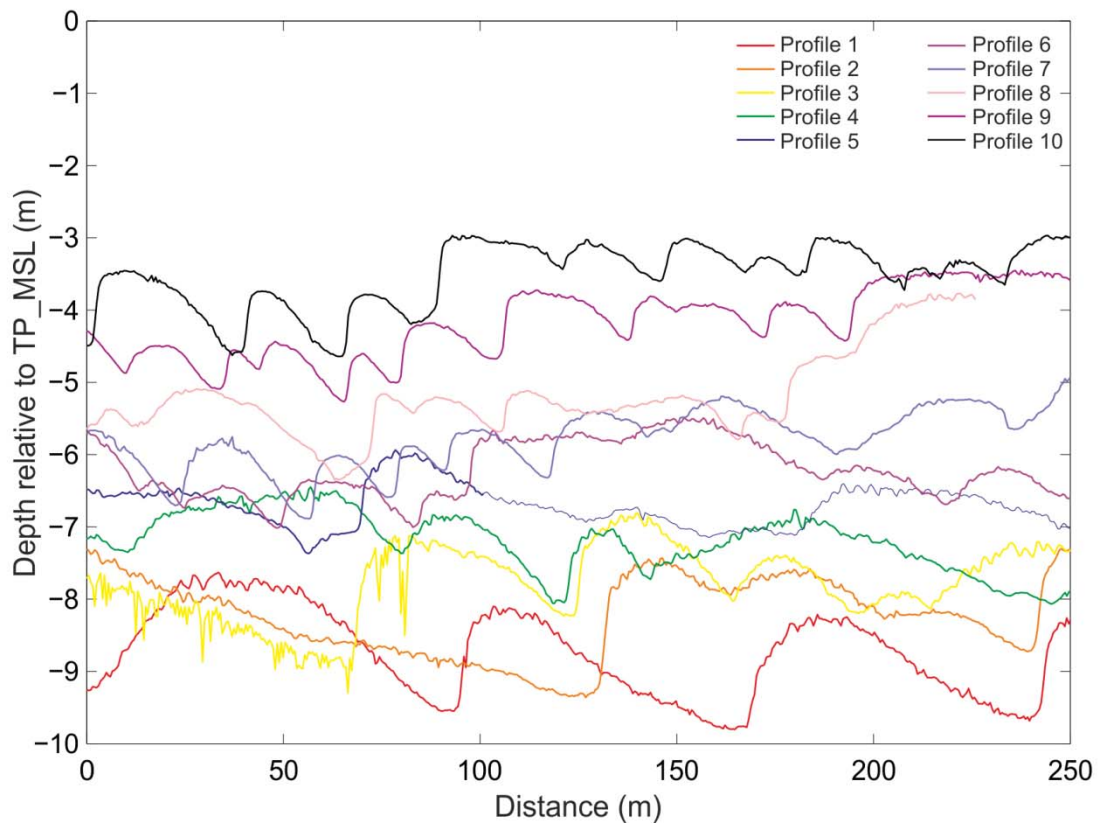
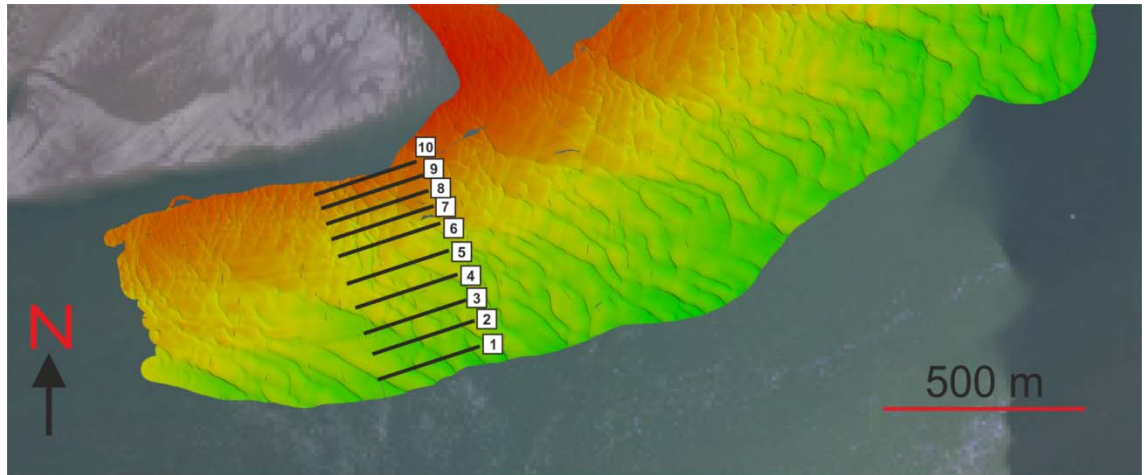


Figure 2.15 Profile traces collected from seaward region of the Navigation Channel adjacent to Taylor Sands derived from bathymetry data (Figure 2.14; Location 3 on Figure 2.5), where 0 m is at the seaward end of the profile (fluvial flow from right of figure). Profile 10 is the northern most profile, collected at the adjacent to Taylor Sands, while Profile 1 was collected in the navigation channel to the south of the bar.

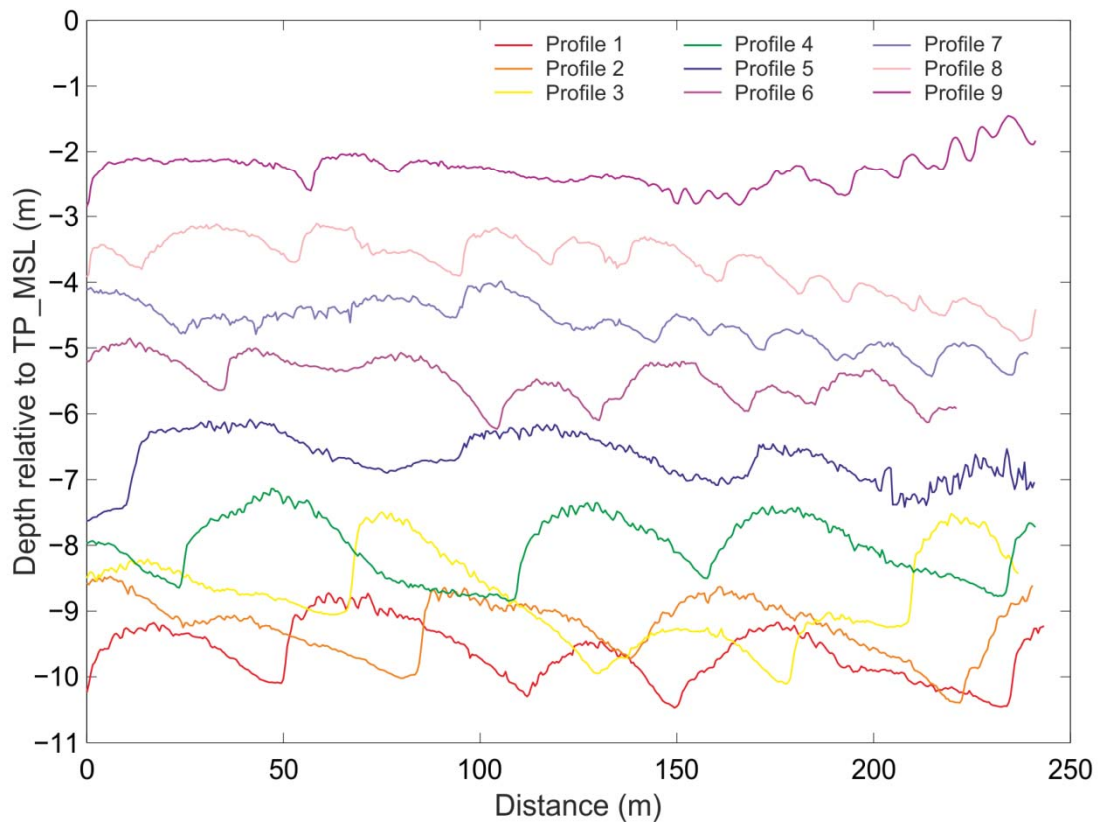
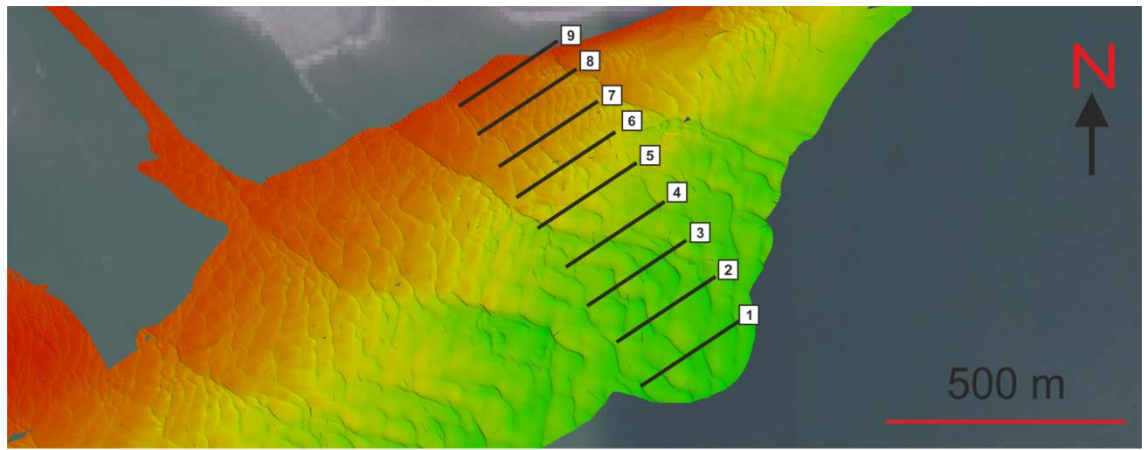
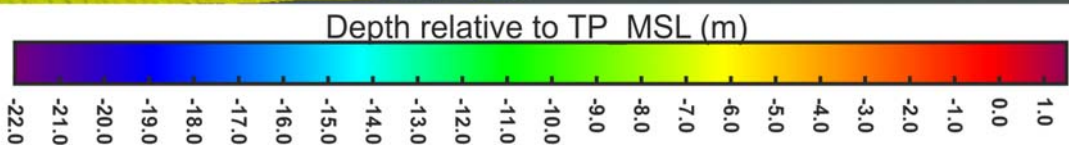
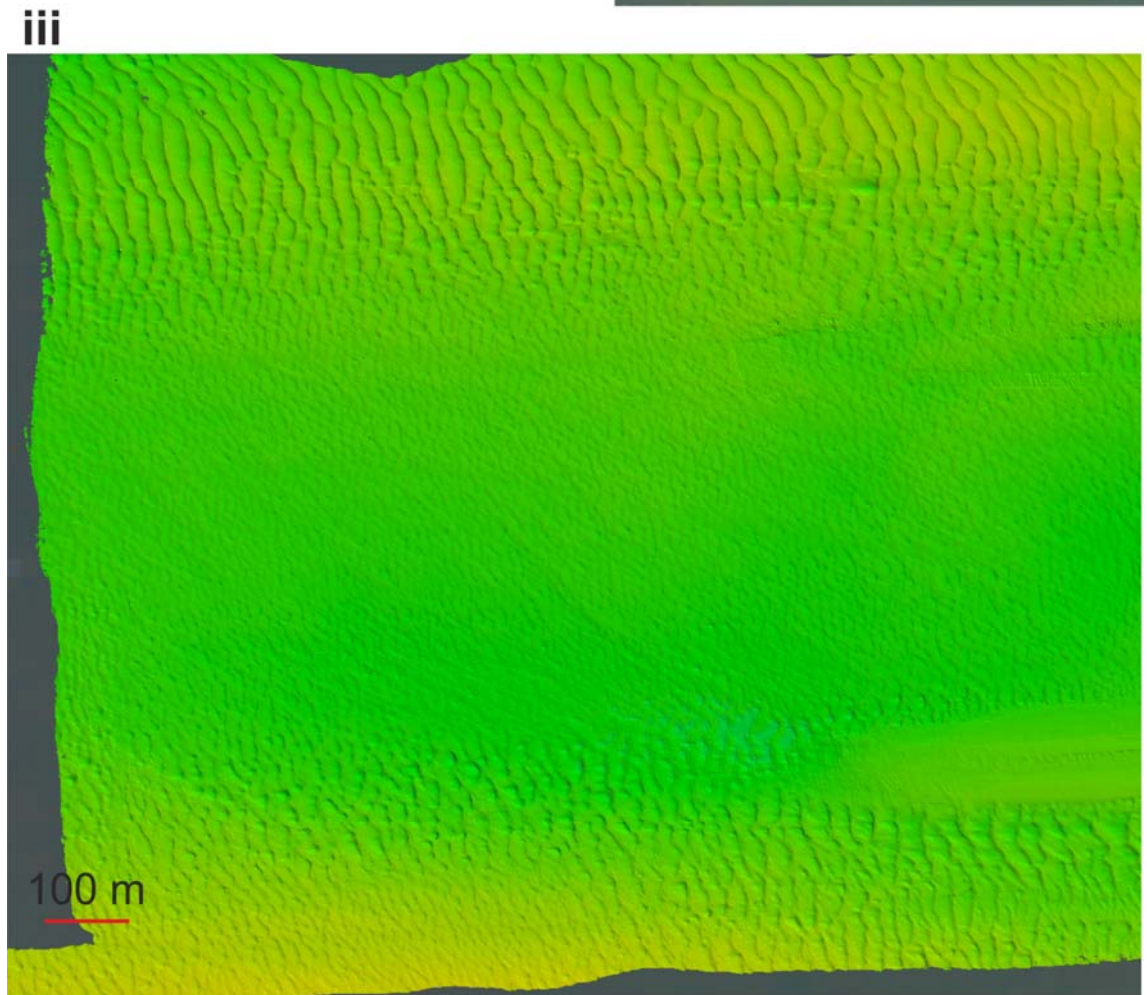
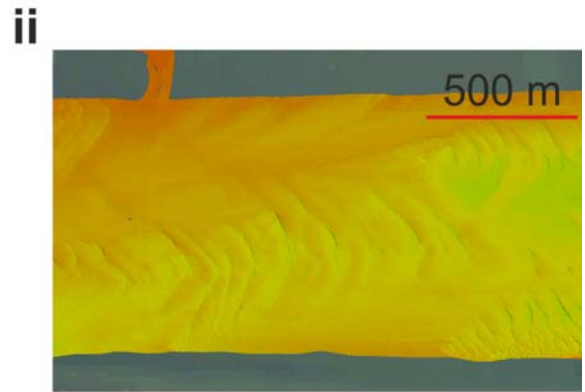
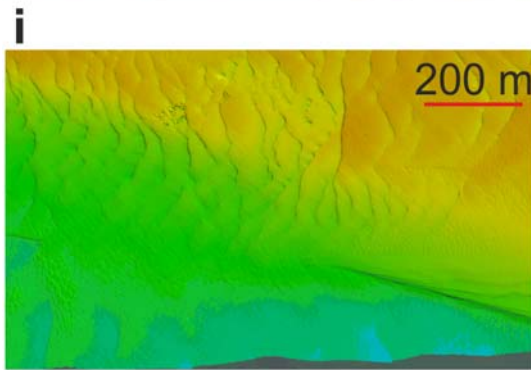
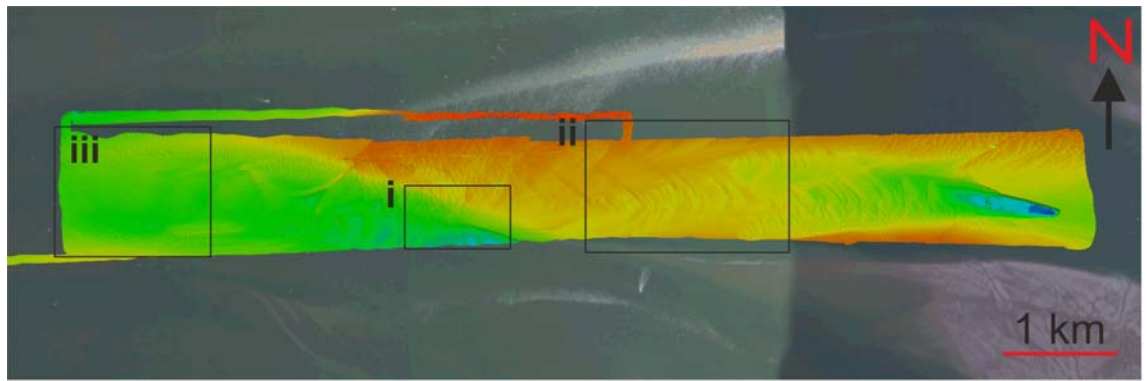


Figure 2.16 Profile traces collected from landward region of the Navigation Channel adjacent to Taylor Sands derived from bathymetry data (Figure 2.14; Location 3 on Figure 2.5), where 0 m is at the seaward end of the profile (fluvial flow from right of figure). Profile 9 is the northern most profile, collected on the bar top, while Profile 1 was collected in the Navigation Channel to the south of the bar.

Figure 2.17 (next page) Bathymetry measurements of the northern region of Taylor Sands collected during FS2 (Location 3 on Figure 2.5) – see text for details of bedforms.



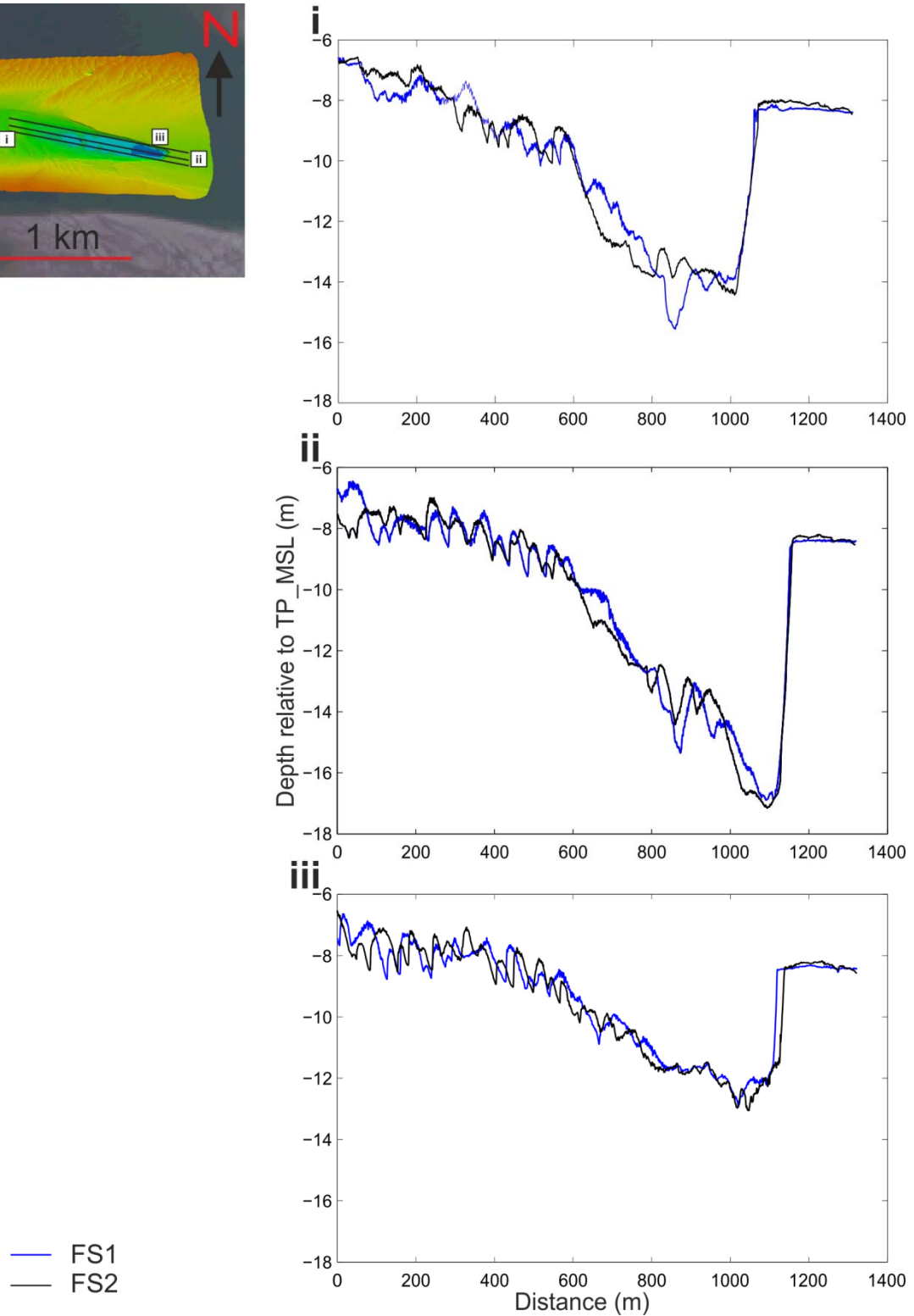
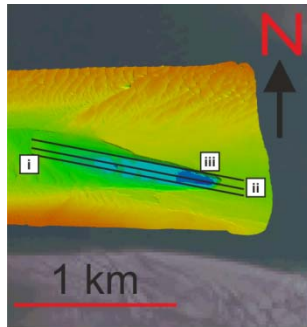


Figure 2.18 Profile traces within the centre of the scour feature measured at Taylor Sands (Location 3 on Figure 2.5) showing variations between FS1 (2012) and FS2 (2013): i) northern profile; ii) central profile; iii) southern profile.

v) Jubilee

This section was collected during FS1 and lies to the south of the navigation channel, separated from it by Miller Sands to the north (Figure 2.19). The section measures a channel between Miller Sands and sand bars to the south and is 3.1 km long by 300 m wide (Figure 2.19). At the northern boundary with Miller Sands there is a steep shelf dropping about 5 m; the southern edge of the section consists of a gradually shallowing sand bar margin. The western part of the section is covered with dunes up to 5 m in wavelength with relative crest heights of up to 0.2 m; these bedforms are superimposed on all other features seen in this region. The northern part of this subsection (600 m in length) is -6.5 m TP_MSL and contains larger dunes up to 50 m in wavelength with relative crest heights of up to 1.5 m; these dunes have sinuous crest lines up to 200 m in length. Dune crests are oriented normal to flow in a seaward direction. To the south the section shallows onto the margin of a sand bar (Figure 2.19i).

A large scour, 4 m deep and 140 m long can be seen within this section (Figure 2.19ii), located seaward of two large sheet features. These extend the width of the channel, linking from Miller Sands to the sandbar at the southern margin. The sheets do not have many superimposed bedforms on them and shelve against the direction of flow indicated by the surrounding bedforms, i.e. the deepest section is at the landward edge suggesting flow in a landward direction.

The central section of the Jubilee measurements is 1.5 km long and shows a channel section to the north with the margin of a sandbar to the south (the southern margin was determined by local tidal conditions during data collection). The northern channel section is -6 to -8 m TP_MSL and contains straight crest dunes 40 m in wavelength with relative crest heights of 0.5 – 1 m (Figure 2.19iii). These have superimposed bedforms of a similar scale to those seen in the seaward section. As the section shallows to the south, to a minimum depth of -2 m TP_MSL, the crest lines become straighter and separation of the dunes becomes shorter (~15 m) with relative crest heights of less than 0.5 m. At the landward end of the section the shallow margin becomes featureless with a small region of shallow scours.

The landward section of the Jubilee measurements contains a deep channel (-12 m TP_MSL) at the north and a shallower channel (-7.5 m TP_MSL) to the south separated by a shallow (-0.24 m TP_MSL), featureless sand bar with sharp margins. The northern channel does not contain any bedforms, while the southern channel contains some dunes on a similar scale to those seen in the central section (Figure 2.19iv).

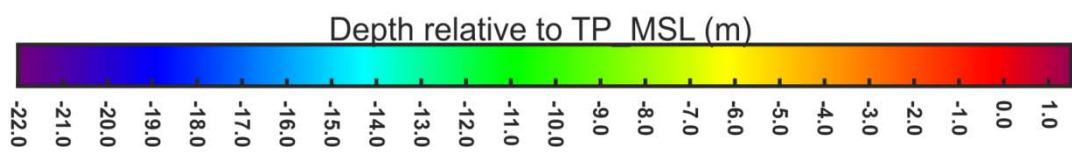
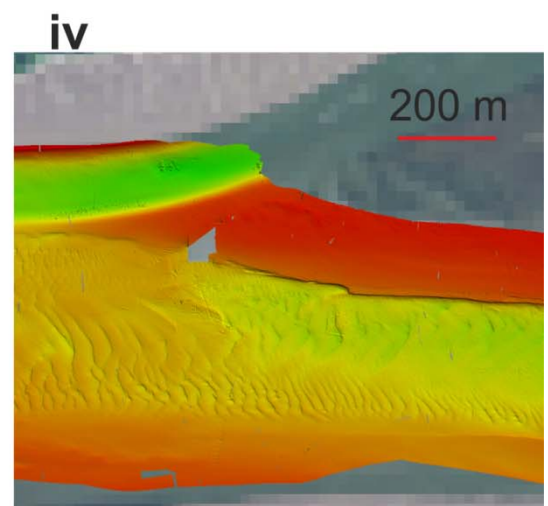
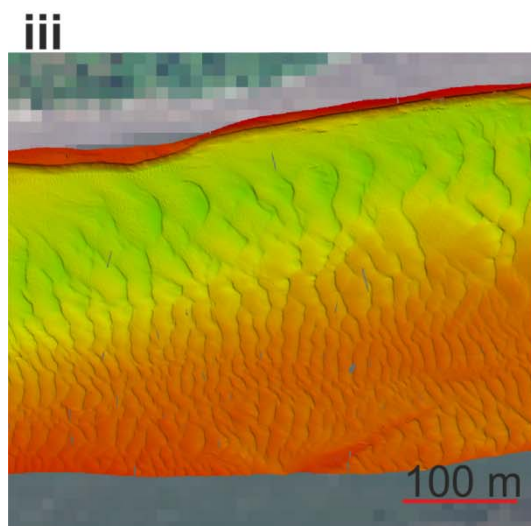
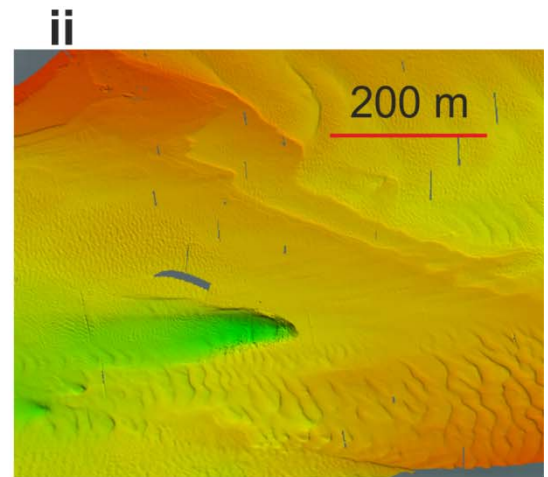
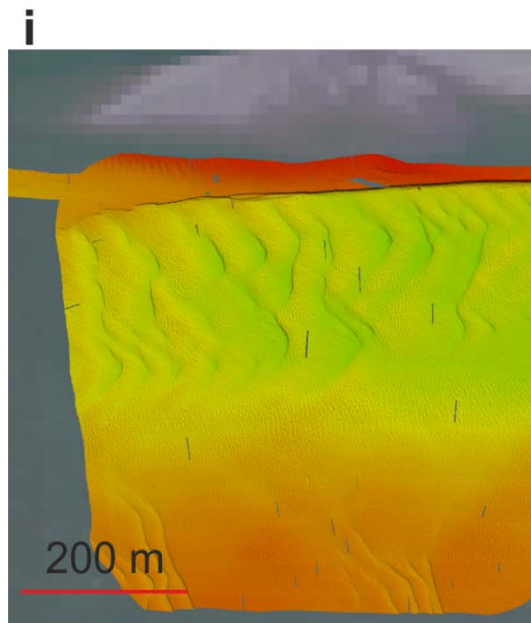
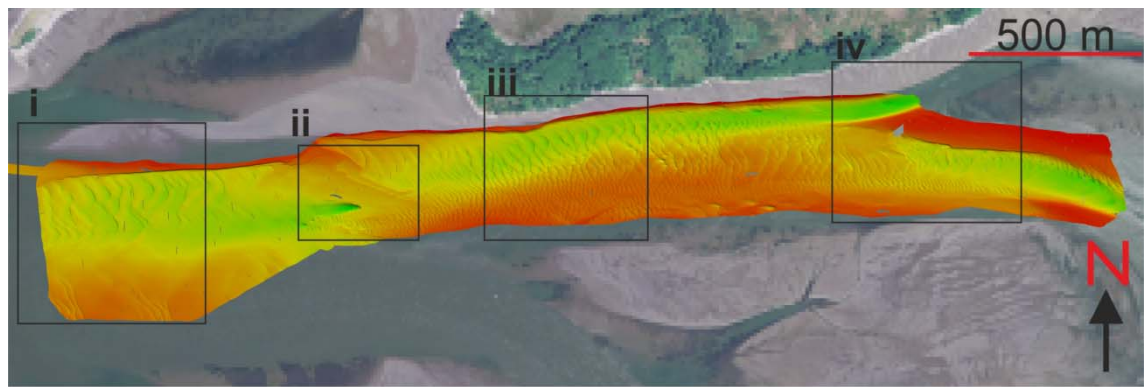


Figure 2.19 Bathymetry measurements of Jubilee collected during FS1 (location 6 on Figure 2.5) – see text for details of bedforms.

Bed profiles obtained from the central region of the channel, adjacent to the southern bar show variations in bedforms with depth (Figure 2.20). Within both the deepest and shallowest profiles the seaward oriented bedforms can be seen to be more rounded than at previous locations, with the most symmetrical forms seen at the deepest profile.

vi) Wills

This section is to the north of the navigation channel to the west of the headland where the Columbia River begins to narrow; there are the remains of early 20th century piers directly to the east of the measured section (Location 5 on Figure 2.5). The section measures around the head of two large bars and contains 3 “limbs” measuring 1.5 km by 400 m, 1.4 km by 150 m and 300 m by 100 m (Figure 2.21); the section varies in depth from -0.2 m to -15.14 m TP_MSL, with the deepest section at the landward end where it meets the navigation channel. The largest limb measured is oriented east-west and contains large elongated dunes oriented in a northeast-southwest orientation; these dunes have a crest separation of between 20 – 50 m and 0.5 m in height (Figure 2.21i). These dunes are rounded with an asymmetric profile (lee:stoss length ratio ~1:5), indicating flow in a seaward direction. Moving landward towards the barhead the dune crest orientation begins to rotate to a direction normal to the barhead (Figure 2.21iii); in the deeper section the dunes also show this change in orientation (Figure 2.21iv). The intermediate channel is up to -2 m TP_MSL and is dominated by smaller scale features up to about 2 m in size. The centre of this section contains some larger dunes up to 10 m long, but with crest height differences of about 0.2 m. The northern limb contains straight crested bedforms aligned normal to flow around the bar (Figure 2.21ii). These crests become more sinuous further in the seaward region.

2.3.1.3 Prairie Channel

Landward of the Astoria-Megler Bridge a second deep channel has formed to the south of the main navigation channel. Bathymetry measurements were made at three locations within this channel, two of which are reported in this chapter. The third is reported in Chapter 4.

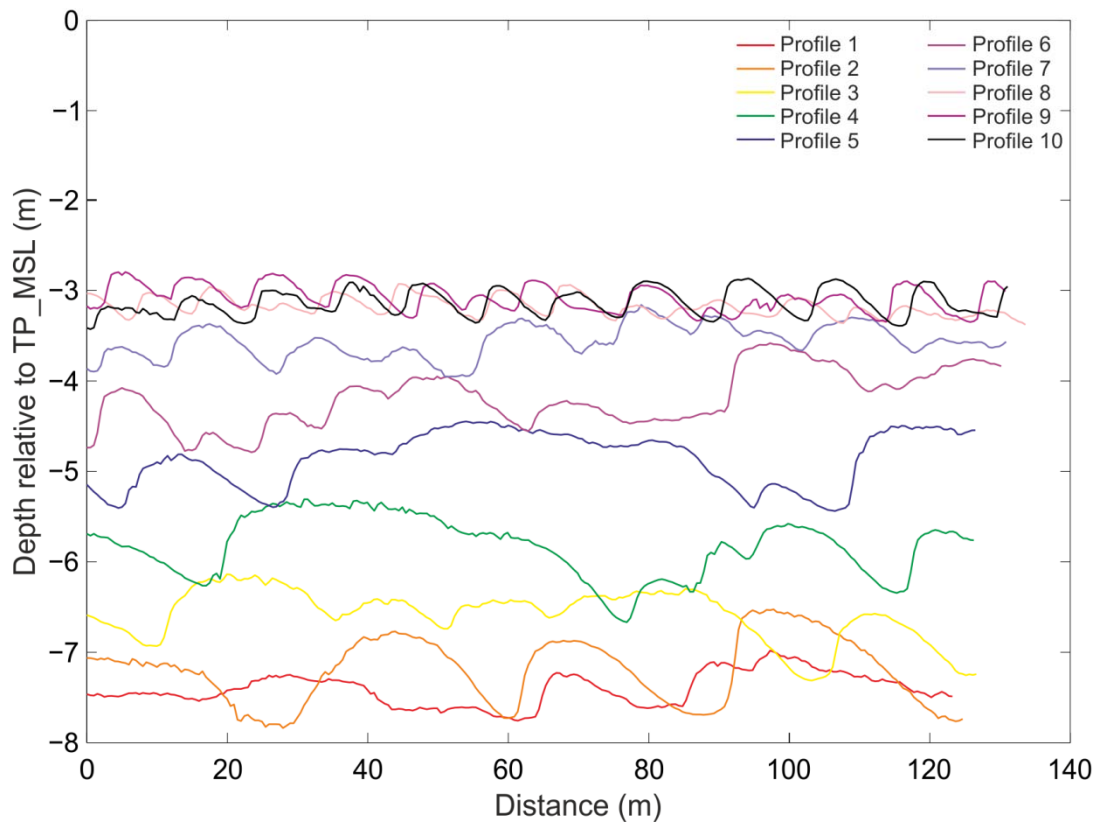
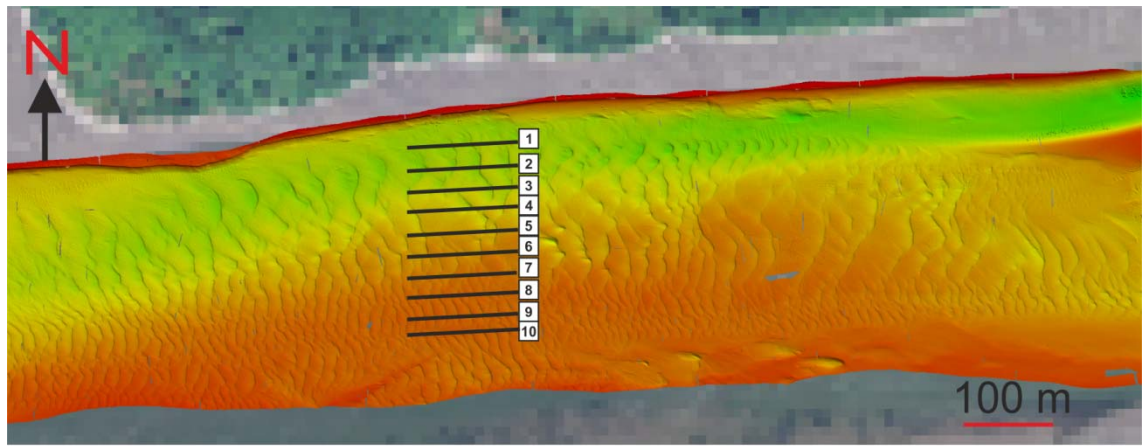
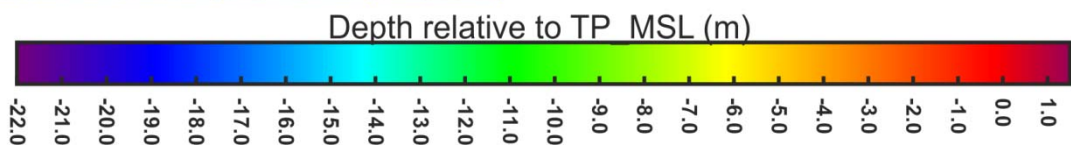
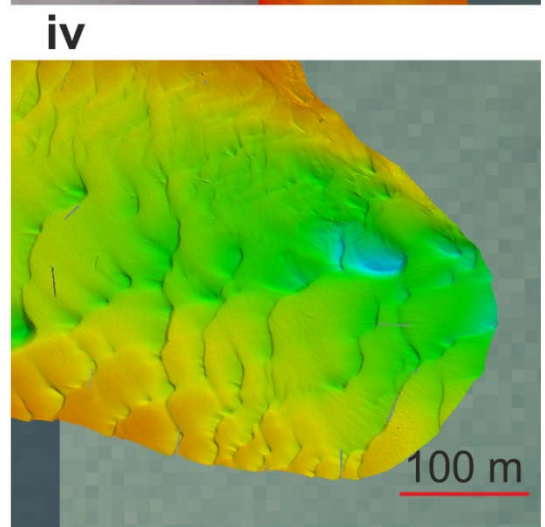
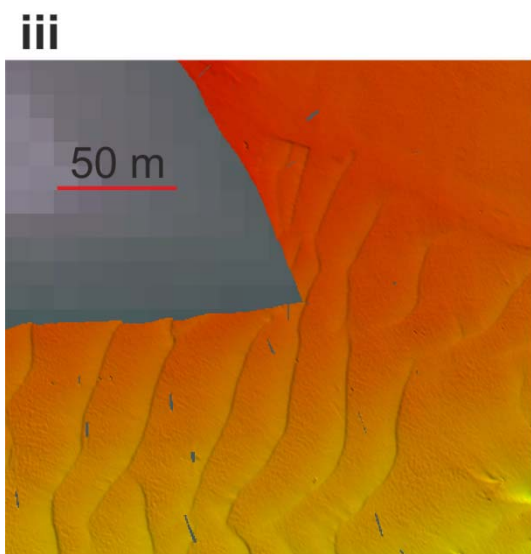
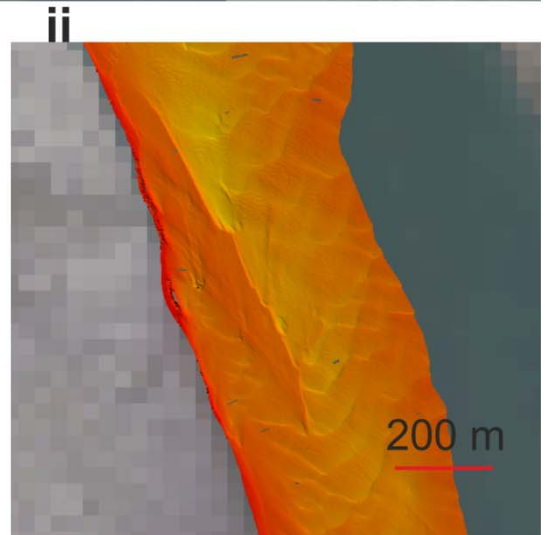
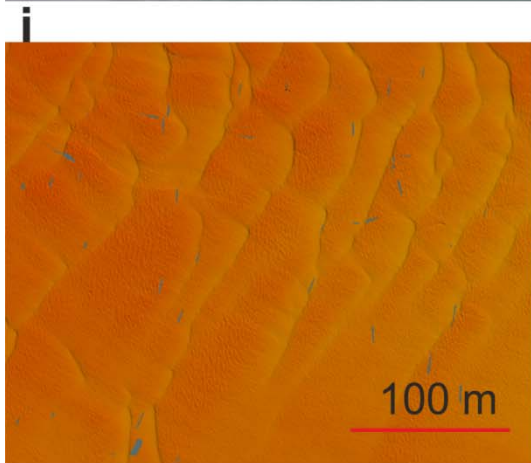
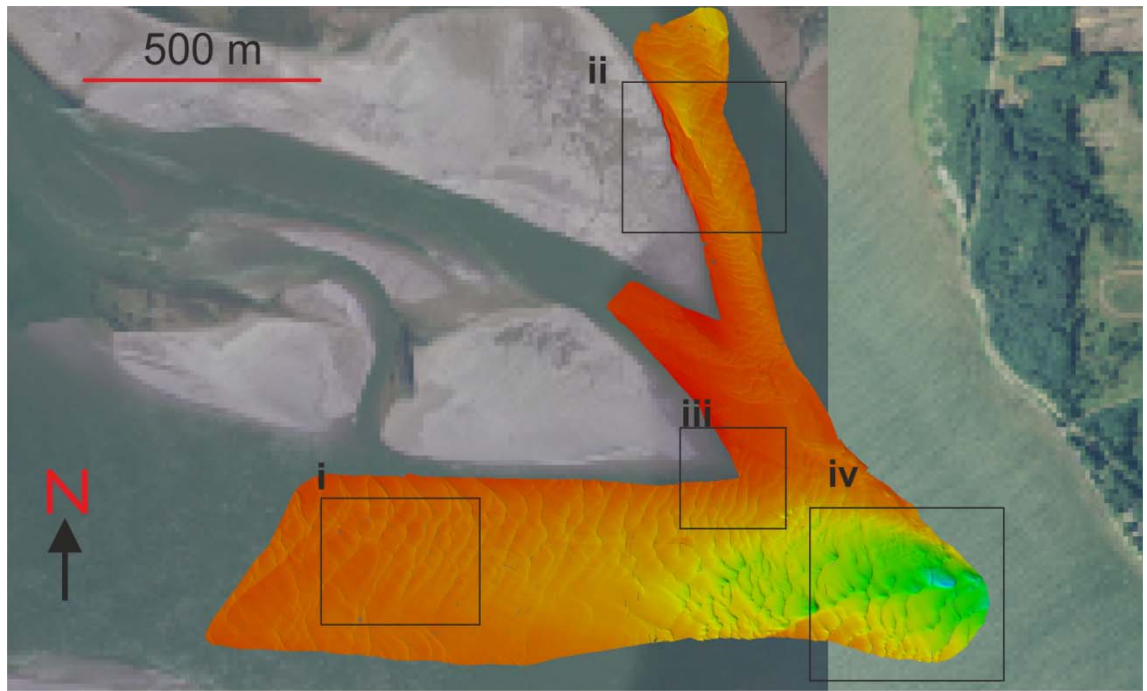


Figure 2.20 Jubilee channel dune profiles derived from bathymetry data (Figure 2.19; Location 6 on Figure 2.5), where 0 m is at the seaward end of the profile (fluvial flow from right of figure). Profile 10 is the most southern of the profiles, adjacent to the bar top.

Figure 2.21 (next page) Bathymetry measurements collected around Wills bar during FS1 (Location 5 on Figure 2.5) – see text for details of bedforms.



i) Prairie Channel – FS1

This is the most southerly section measured and is within Prairie Channel, the deep subsidiary channel in the Columbia River Estuary (Location 7 on Figure 2.5). The section measured is 2.3 km long and 400 m wide, with steep boundaries onto the surrounding vegetated islands (Figure 2.22). In general the shallow boundaries do not show any bedforms, although there are some dunes seen at the landward end where a sandbar has formed within the channel (Figure 2.22ii). The channel depth is -13.5 m TP_MSL and contains sinuous dunes the width of the section. Within shallower regions (-9 m TP_MSL) these have crest separations of 30 – 40 m (Figure 2.22i) and 60 – 90 m in the deeper regions (Figure 2.22iii). Relative crest heights in the shallower regions are up to 1.2 m, whilst in the deeper regions they are 3.5 m. There are few superimposed bedforms and dune orientation shows flow in a seaward direction (fluvially-dominated).

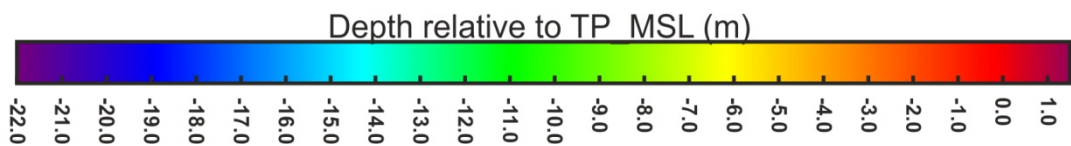
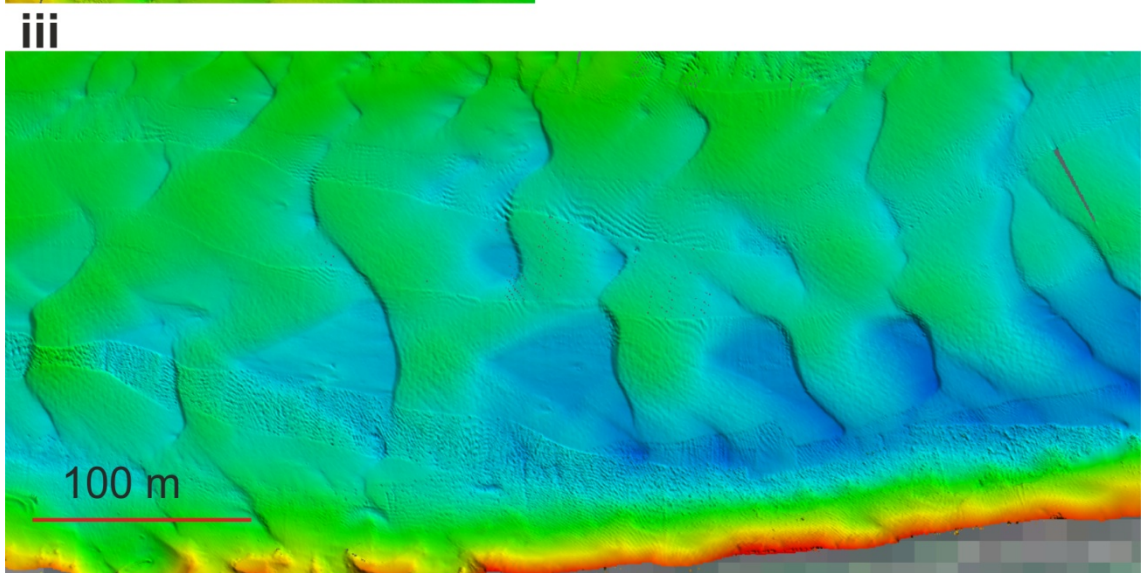
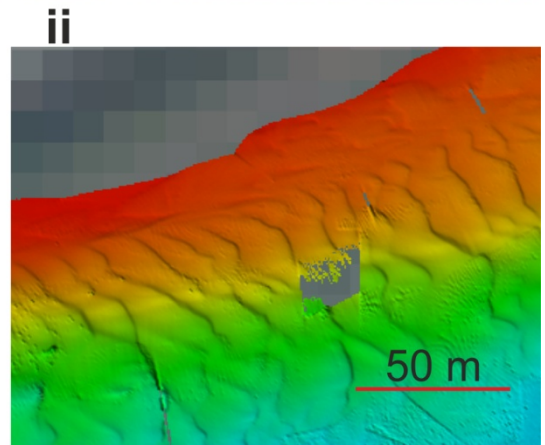
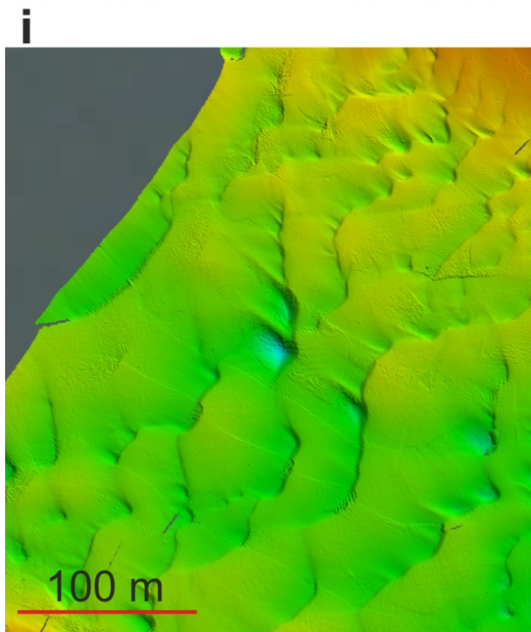
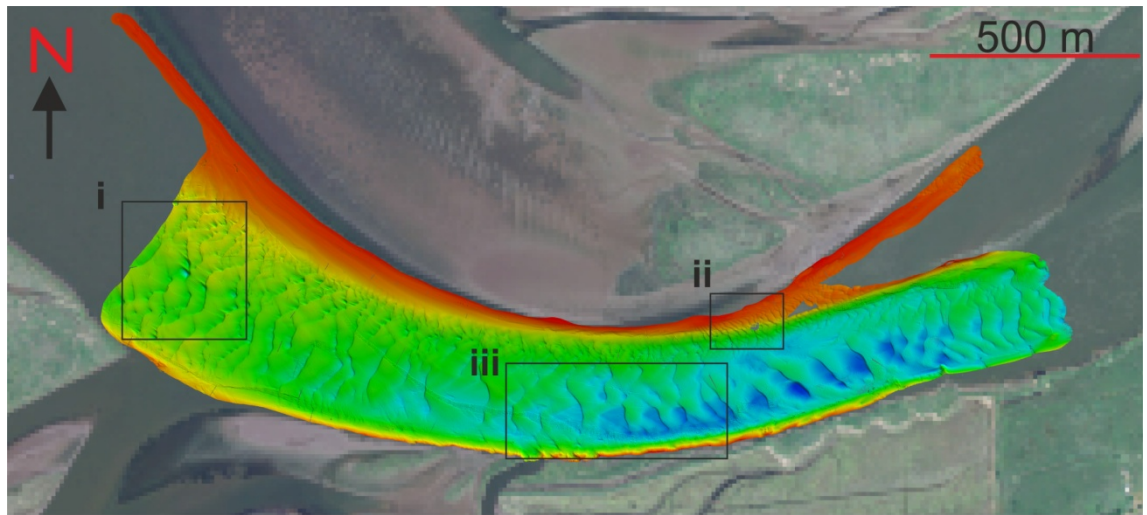
ii) Prairie Channel – FS2

A smaller subsection of the one measured in FS1 (Figure 2.22), the FS2 survey covered only the deep central section 1.4 km by 400 m (Figure 2.23). As in FS1 there are large scale dunes oriented with the fluvial flow, with crest separations of about 60 m and relative crest heights of 3.5 m. There are smaller superimposed bedforms on the upper sections of the dunes that are about 2 m in wavelength.

iii) Sandee/Snag Island – FS1

This section is at the landward end of Prairie Channel, 1.5 km south of its divergence from the main navigation channel; it is the furthest inland of all the sections measured (Location 9 on Figure 2.24). The section is approximately 3.5 km in length and 500 m wide, with measurements around the bar heads of Sandee and Snag Island (Figure 2.24). The section is shallower on its northern edge (the bar top) with a deeper section to the south where it intersects Prairie Channel. Section depths range from 1.13 m to -18.36 m TP_MSL, the extent of the shallow depth survey was controlled by local tidal conditions at the time of data collection (Figure 2.24).

Figure 2.22 (next page) Bathymetry measurements collected at the southern extent of Prairie Channel during FS1 (Location 7 on Figure 2.5) – see text for details of bedforms.



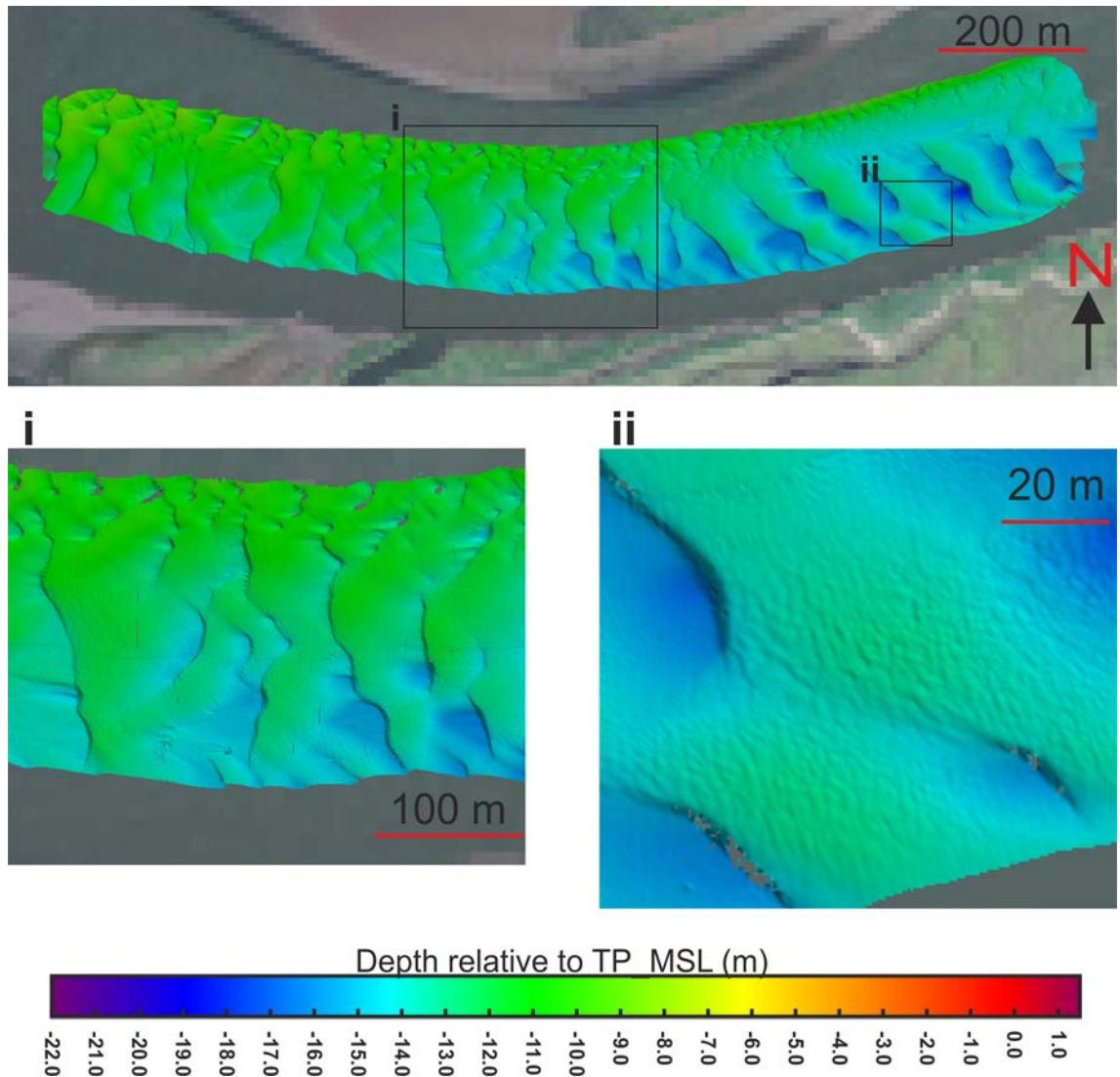


Figure 2.23 Bathymetry measurements collected at the southern extent of Prairie Channel during FS2 (Location 7 on Figure 2.5). These measurements repeat a subsection of the measurements made during FS1 (Figure 2.22) – see text for details of bedforms.

The most landward section of the bar top shows variations in bedform distributions. Adjacent to the channel shelf are a series of 2D dunes, oriented normal to the flow. These have crest separations of ~ 10 m with crest heights of up to 0.8 m (Figure 2.24iv), with the asymmetric shape of the dunes indicating flow in a seaward direction. The central region of the bar top contains no significant bedforms and contains a wide relatively shallow channel (2 m deep, 20 m wide) across the bar top (Figure 2.24iv). The shallow channel measured between the two eastern subaerial bars again shows variation in crest orientation as they steer around the western bar head (Figure 2.24iv). At the seaward end of the measured section (Figure 2.24i) the larger 3D dunes in the

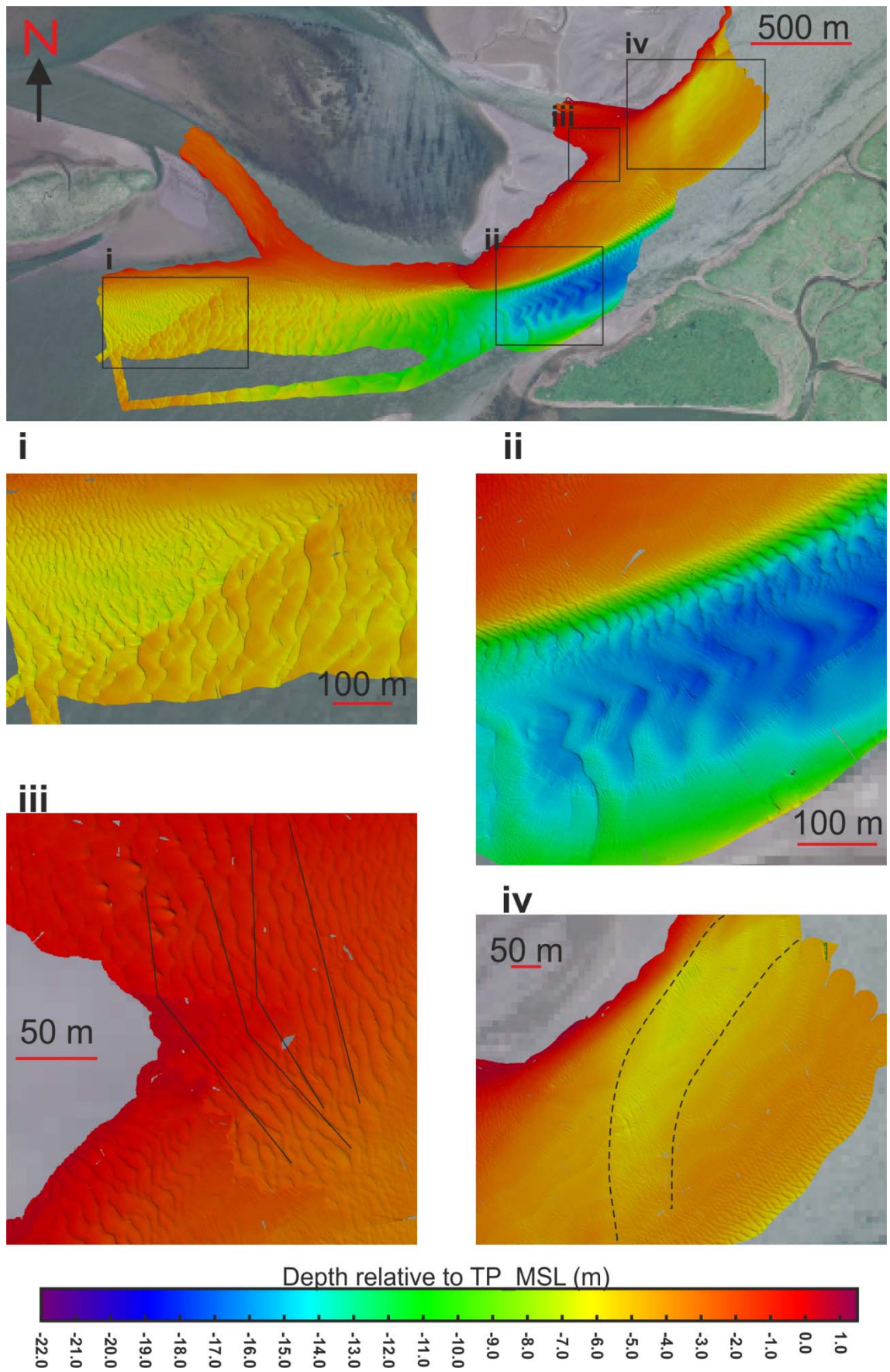


Figure 2.24 Bathymetry measurements collected around Sandee Bar and Snag Island at the landward limit of Prairie Channel during FS1 (Location 9 on Figure 2.5) – see text for details of bedforms.

deeper channel (1.5 m high, 150 m wavelength) begin to change orientation. The dune crests become more 2D and the dunes decrease in size (0.5 m high, 15 m wavelength), marking the landward extent of a new channel forming to the west of this region.

Within the deeper channel at the south of the section (Prairie Channel) larger bedforms are observed with crest separations of 45 m and crest heights of 1 m. A series of bedform profiles oriented parallel to the channel are shown in Figure 2.25. These show the fluviially-dominated nature of the bedforms within both the channel and on the bar top. Within the channel bedforms are <1 m high with a wavelength of up to 80 m, whilst on the bar top bedforms are <20 m in length and 0.5 m high. There are few superimposed bedforms at this location.

iv) Sandee – FS2 repeat

A subsection of the shallowest landward region of the FS1 bathymetry measurements were repeated during FS2. The measured section is 1 km long by 400 m wide (Figure 2.26) predominantly on the bar top, with some measurements extending into the deeper channel (-17.2 m TP_MSL) at the southern edge where there is a drop of 10 m in height over 30 m. The section is oriented north-east to south-west, with river flow entering at the northeastern edge. Large scale dunes are seen throughout the section, with 2D dune crests oriented normal to the predominant flow direction (north-west to south-east for the majority of the section). At the landward end of the section the dunes have a relative crest height of 0.15 – 0.5 m and a wavelength of 10 – 15 m (Figure 2.26ii). This region contained no large scale bedforms when measured in FS1 (Figure 2.24). The bar top has increased in height in the centre of the measurements. At the seaward end the dune crests become more 3D and sinuous with relative crest heights of 0.6 – 0.8 m and a wavelength of 30 m (Figure 2.26iii). Around the bar head a shallower section is seen (+0.376 m TP_MSL) with dune crests oriented normal to the bar head (Figure 2.26i). The dune crests are closer, with a separation of 10 m, and relative heights of 0.1 m.

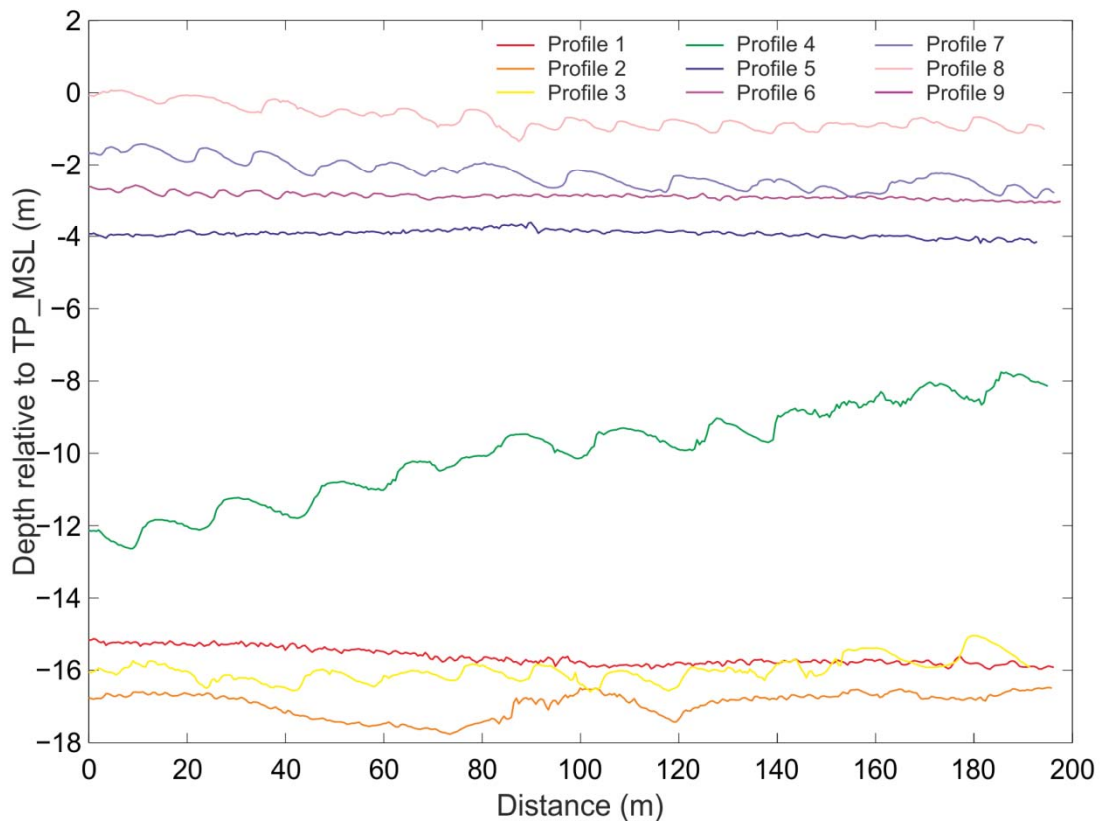
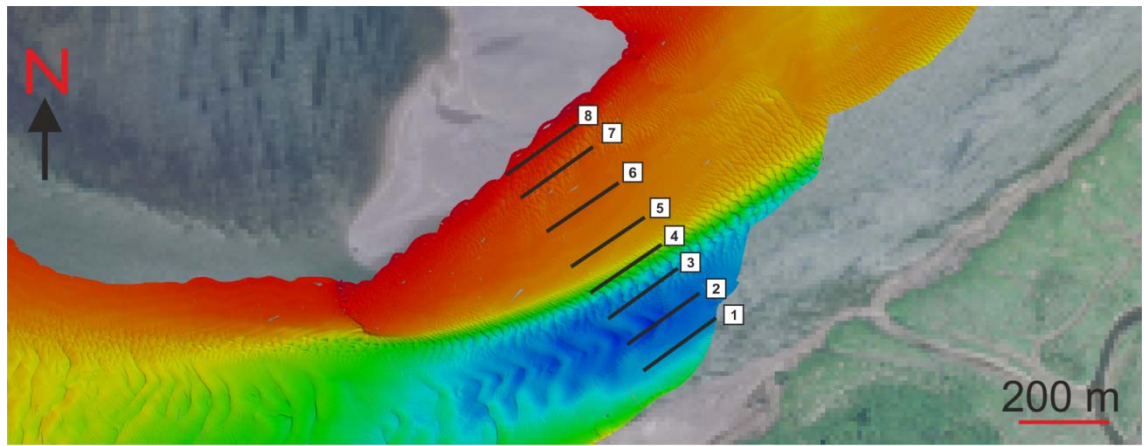
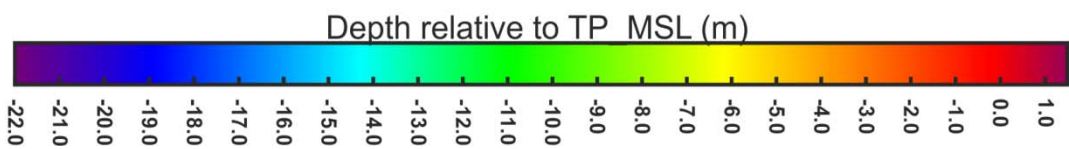
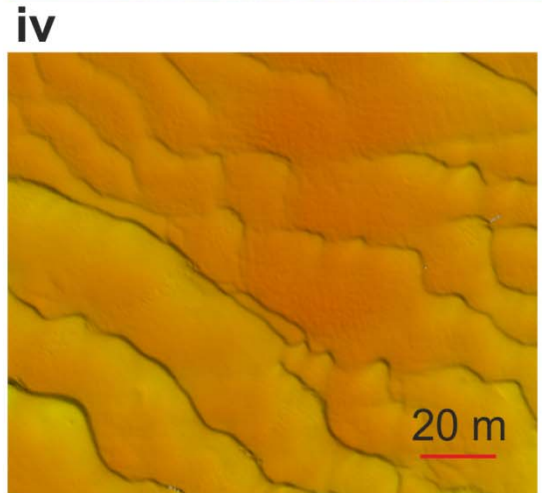
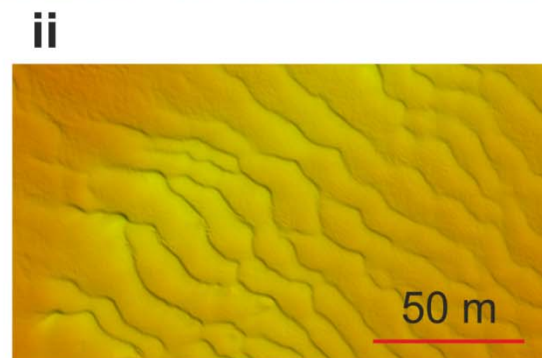
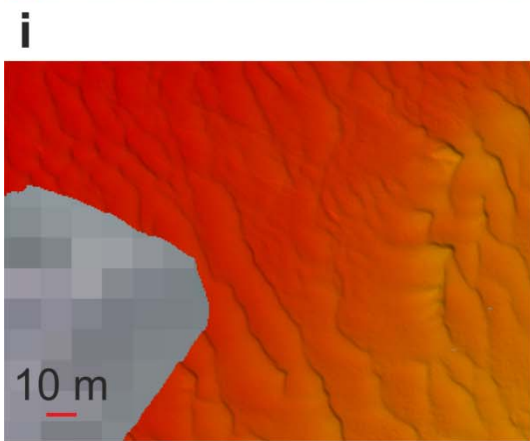
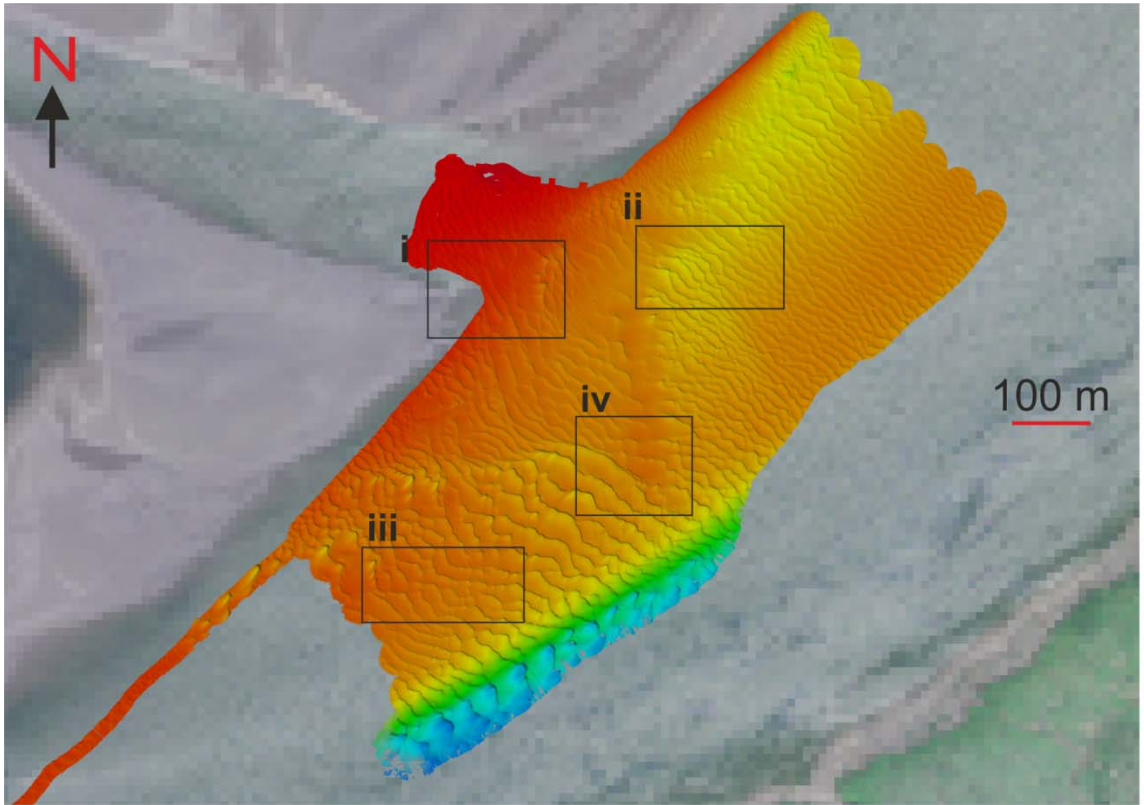


Figure 2.25 Bedform profiles derived from bathymetry data collected during FS1 at Sandee (Location 9 on Figure 2.5), where 0 m is at the seaward end of the profile (fluvial flow from right of figure). Profile 1 is located within the shallower region to the south of the channel, with Profile 2 in the deepest region of the channel. Profile 4 is located on the channel shelf. Profiles 5-8 are located on the bar top.

Figure 2.26 (next page) Bathymetry measurements collected around Sandee Bar at the landward limit of Prairie Channel during FS2 (Location 9 on Figure 2.5). This is a repeat of the landward extent of the data collected during FS1 (Figure 2.25) – see text for details of bedforms.



2.3.2 Sandee flow data

i) Cross-section A

Cross-section A is the furthest landward of the cross-sections collected around Sandee bar (Figure 2.7). The cross-section is ~800 m in length, consisting of a deep channel to the southeast (19 m deep at high tide, 250 m wide), a shallower (<9 m) central section 400 m wide and a shallow region to the west where the bar has been submerged at high tide. At lower-low water (Trans001-Trans002) flow is in a strongly seaward direction, with a region of slower flow at the margins (Figure 2.27i). The highest flow velocities are seen in the centre of the channel where flow is up to 1.1 ms^{-1} , with some small reversals of flow at the eastern edge of the deeper channel (-0.2 ms^{-1}). Cross-stream flows of $<0.2 \text{ ms}^{-1}$ are observed with flows towards the east on the bar top. A 20 m region to the west of the bar top shows flow towards the exposed bar top, whilst the deeper channel flows are predominantly towards the west (Figure 2.27iii). At lower-high water (Trans011-Trans012) this flow has slowed considerably with a maximum velocity of only 0.18 ms^{-1} , and with some small reversals of flow within the channel (Figure 2.27ii). There are no clear patterns of secondary circulation at lower-high water (Figure 2.27iv), although a region of circulating flow can be observed within the shallower channel on the bar top.

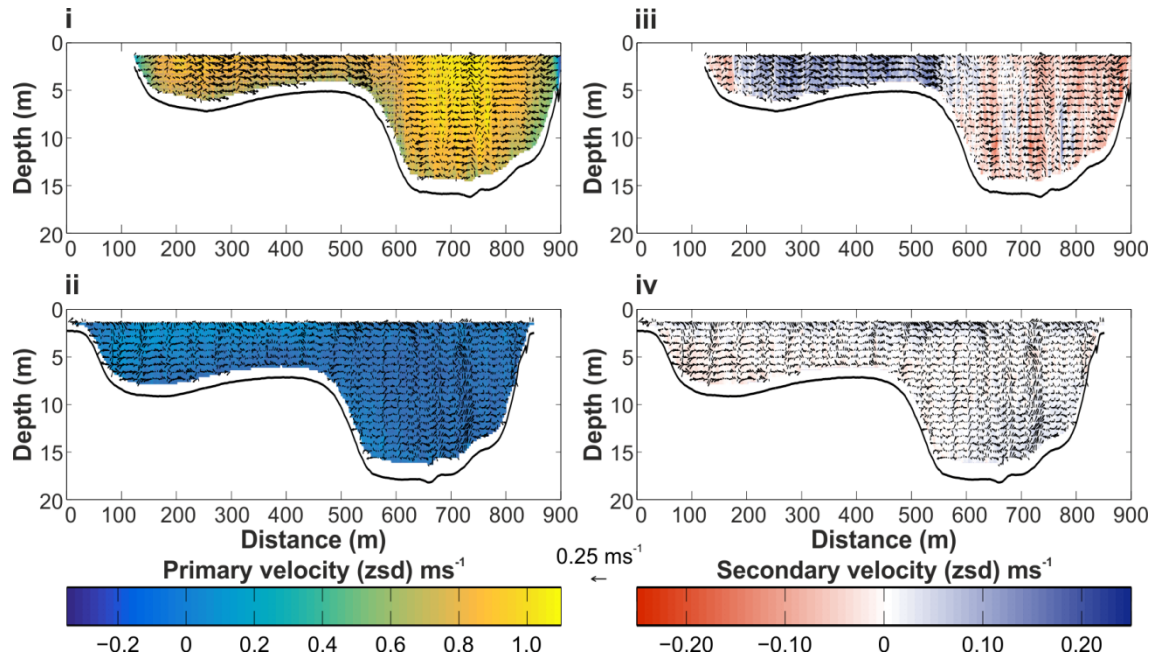


Figure 2.27 Flow data collected at cross-section A (located on Figure 2.7). Fluvial flow is oriented out of the page: i) shows primary flow velocity (zsd) at lower-low water; ii) primary flow velocity (zsd) at lower-high water; iii) secondary flow velocity (zsd) at lower-low water; iv) secondary flow velocity (zsd) at lower-high water.

ii) Cross-section B

Cross-section B is located 200 m seaward of cross-section A (Figure 2.7). The channel to the south east has widened to 300 m, and no measurements have been made of the submerged bar top at high tide. At lower-low water (Trans003-Trans004) there is a deeper edge to the deep channel (5 m deeper, 10 m wide at base) which shows strong landward flow ($<0.31 \text{ ms}^{-1}$), and strong secondary circulation (Figure 2.28i and iii). The edge of this transect intersects a small channel entering the main channel (seen at the end of the transect marker in Figure 2.7), so this landward flow is probably a consequence of flow outward from the channel. Flow in the main channel is in a seaward direction ($<1.1 \text{ ms}^{-1}$), with regions of slower flow in the shallower region ($\sim 0.45 \text{ ms}^{-1}$) with faster flow towards the surface. Secondary flow velocities show the same patterns as observed at cross-section A, with divergent flows observed in the shallower bar-top region (Figure 2.28iii). At lower-high water (Trans013-Trans014) flow has again slowed to a maximum of 0.25 ms^{-1} (Figure 2.28ii), some flow reversal is observed adjacent to the tributary channel at the east of the section but this is not significant. Secondary flows have a maximum cross-stream velocity of 0.25 ms^{-1} with no clear flow cells developing (Figure 2.28iv).

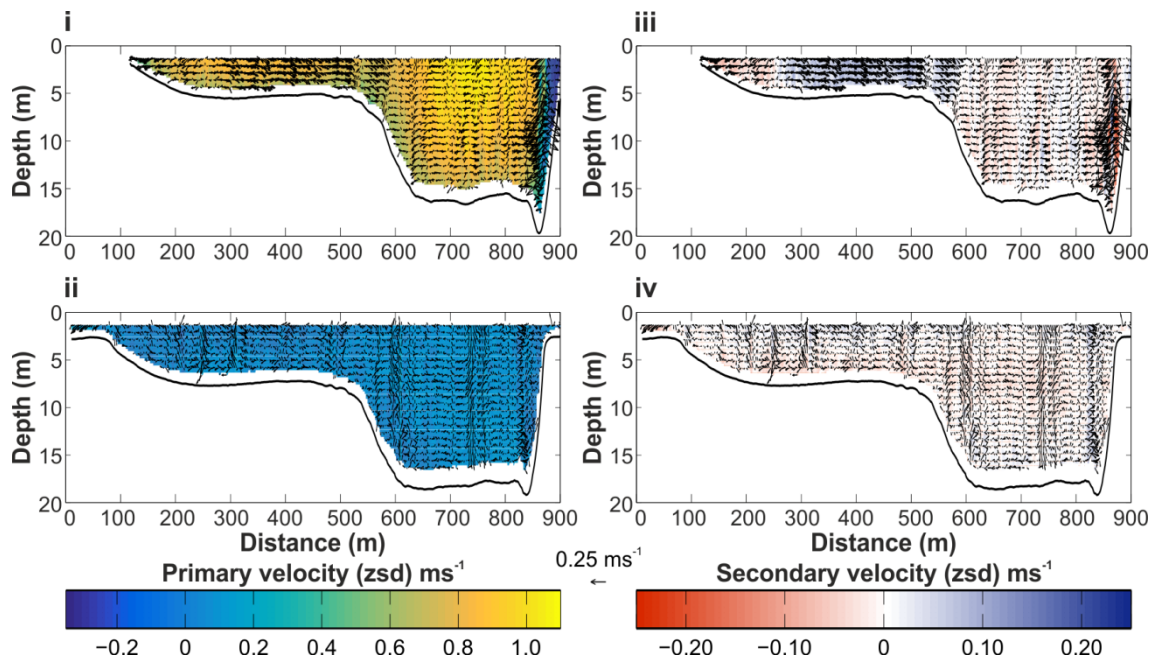


Figure 2.28 Flow data collected at cross-section B (located on Figure 2.7). Fluvial flow is oriented out of the page: i) shows primary flow velocity (zsd) at lower-low water; ii) primary flow velocity (zsd) at lower-high water; iii) secondary flow velocity (zsd) at lower-low water; iv) secondary flow velocity (zsd) at lower-high water.

iii) Cross-section C

Cross-section C is located within the main channel seaward of the barhead of Sandee bar (Figure 2.7). The cross-section is 700 m wide, with the deeper channel 350 m wide at this point, and a narrower shelf region. At lower-low water (Trans005-Trans006) flow velocities of $<1 \text{ ms}^{-1}$ are again seen within the deeper channel, with slower flow observed at each end of the cross-section and in localised regions on the shallower shelf (Figure 2.29i). There is strong cross-stream flow from the bar top into the channel, with small regions of re-circulation within the channel itself (Figure 2.29iii). At lower-high water (Trans015-Trans016) flow has slowed to $\sim 0 \text{ cms}^{-1}$ with small regions of seaward flow ($<0.37 \text{ ms}^{-1}$), but no reversal in flow is observed (Figure 2.29ii). There is a small amount of cross-stream flow ($<0.15 \text{ ms}^{-1}$), but this is localised in nature (Figure 2.29iv).

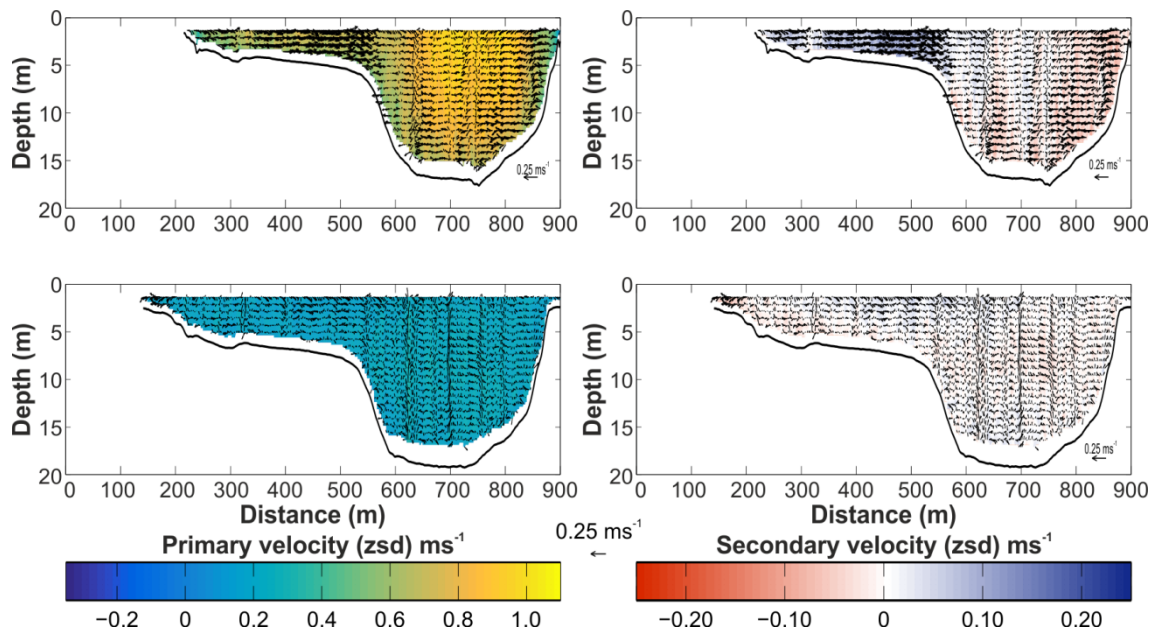


Figure 2.29 Flow data collected at cross-section C (located on Figure 2.7). Fluvial flow is oriented out of the page: i) shows primary flow velocity (zsd) at lower-low water; ii) primary flow velocity (zsd) at lower-high water; iii) secondary flow velocity (zsd) at lower-low water; iv) secondary flow velocity (zsd) at lower-high water.

iv) Cross-section D

Cross-section D measures flow with the smaller channel between Sandee bar and Snag Island (Figure 2.7). The section is only 300 m wide at lower-high water, and due to the depth of water a section of $<50 \text{ m}$ was measured at lower-low water (Figure 2.30). The cross-section has a 40 m wide channel at the northern end, and a flatter bar section to the south. At lower-low water only a small section could be measured showing fluvial flow velocities of $<0.4 \text{ ms}^{-1}$ (Figure 2.30), with no clear secondary circulation. At lower-

high water the seaward velocities have decreased slightly to $\sim 0.3 \text{ ms}^{-1}$, but there is no significant secondary circulation present.

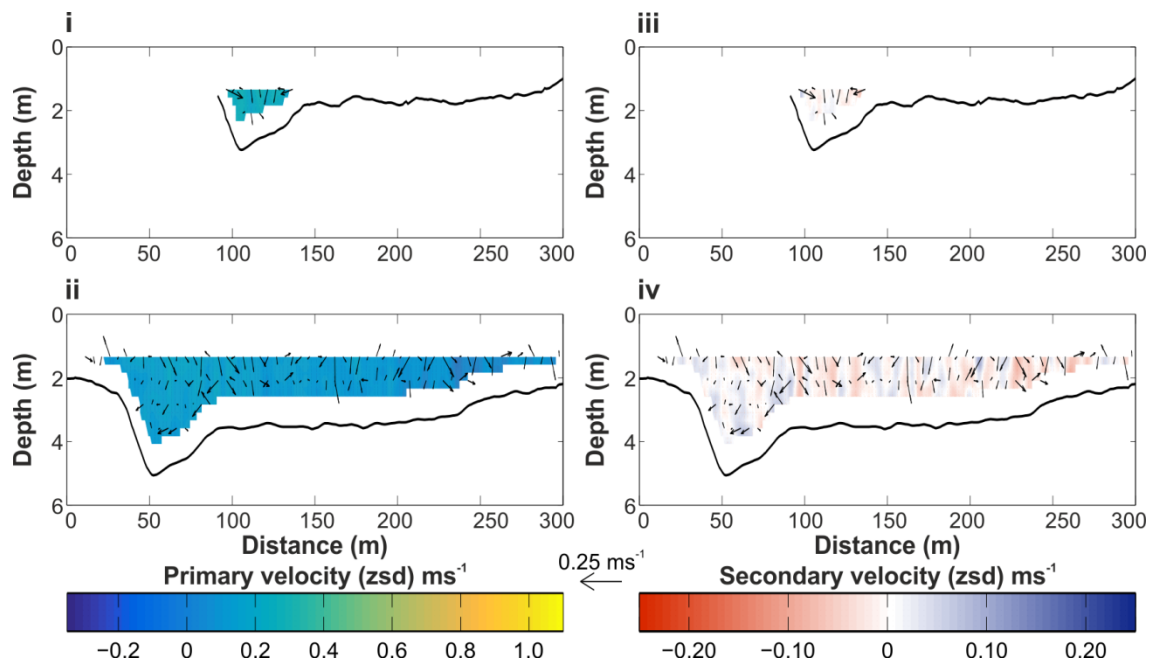


Figure 2.30 Flow data collected at Transect D (located on Figure 2.7). Fluvial flow is oriented out of the page: i) shows primary flow velocity (zsd) at lower-low water; ii) primary flow velocity (zsd) at lower-high water; iii) secondary flow velocity (zsd) at lower-low water; iv) secondary flow velocity (zsd) at lower-high water.

2.4 Discussion

The varying bathymetry around a braided sandbar complex was examined within the lower Columbia River, OR, USA over the course of two field seasons a year apart. Both field seasons were carried out during periods of high fluvial flow (immediately following or during the freshet). These sandbars lie within a 15 km region which is fluvially dominated but undergoes some modulation of flow due to incoming tides. Measurements were made within the dominant and secondary fluvial channels, but also within subsidiary channel in the braided complex to assess the variance of tidal influence on deposition in this region. In addition, flow measurements were made close to the landward limit of the bar complex to assess amount of tidal modification to flow.

The bathymetry measurements made at Prairie Channel show little variation between FS1 and FS2 (Location 7 on Figure 2.5). There is some migration of bedforms, but bedform size and morphology do not vary significantly. However, the two sections measured at the most landward position within the Prairie Channel, at Sandee bar, show distinct differences (Location 9 on Figure 2.5). The FS2 measurement section is much smaller (1 km in length), and is located at the landward end of the bar top section (Figure 2.26). In the FS1 data this region is relatively featureless, with no large-scale

bedforms present and a wide, shallow channel on the bar top adjacent to the region exposed at low tide; linear dune crests with a spacing of 10 m are observed as the edge of the bar is approached (Figure 2.24). The linear dunes observed adjacent to the channel edge now cover the entire bar top, overprinting the shallow channel observed in FS1. The bar top itself has grown onto the shelf, with a region in the middle of the measurements showing a 1 m decrease in bathymetry (Figure 2.31). Associated with this is a deepening adjacent to the shallower bar regions, in both landward and seaward directions.

2.4.1 Variations in flow

The flow data collected around the bar at Sandee during FS1 reveals that although fluvial flow was relatively high, the incoming tide at the landward end of a secondary channel within system was able to slow the seaward velocity significantly (from a maximum of 1.1 ms^{-1} to a maximum of 0.2 ms^{-1}) although no reversal of flow was observed (Figure 2.27 - Figure 2.30). The tidal nature of the Columbia River acts to modify fluvial flow at the landward end of the section, but with no flow reversals

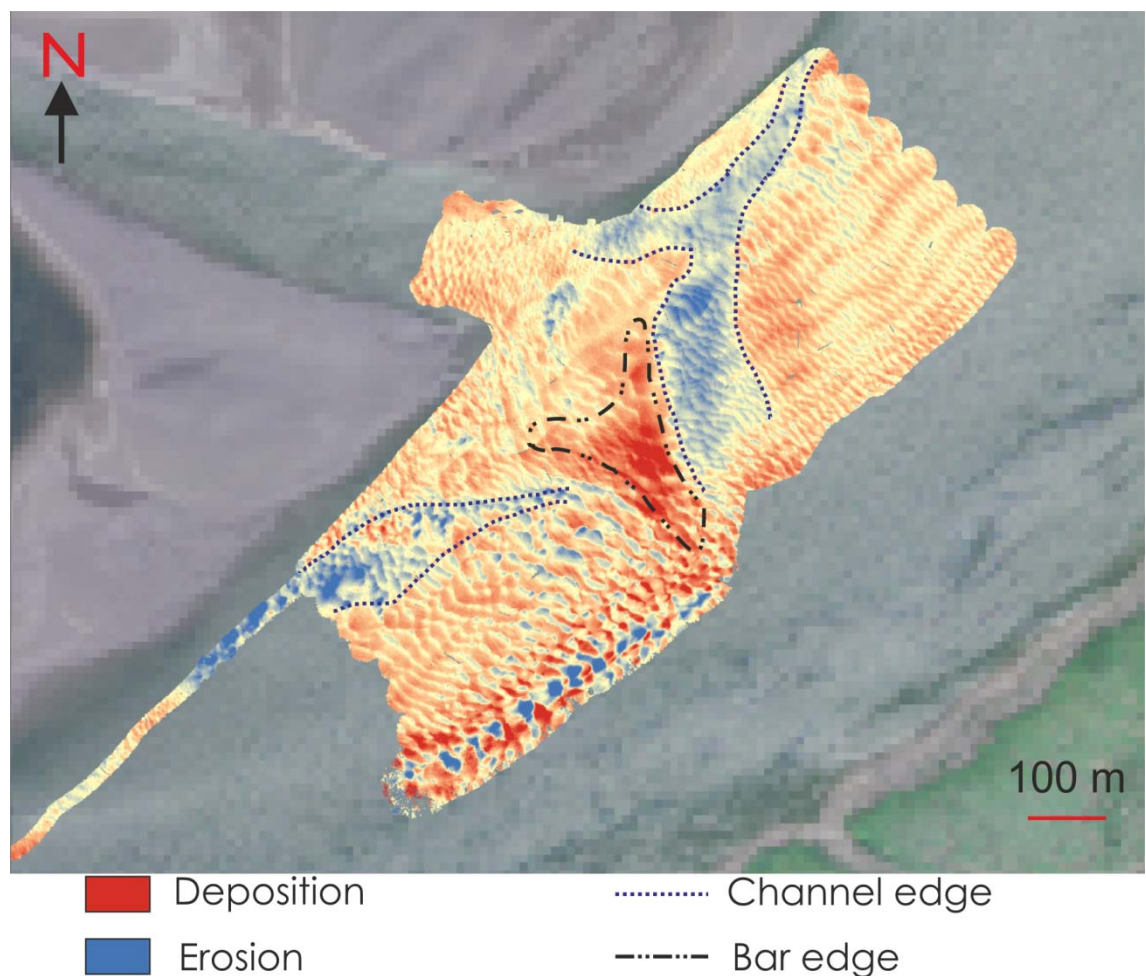


Figure 2.31 Changes in bed elevations between FS1 and FS2 at Sandee. Regions highlighted in blue show erosion between the two sets of measurements, whilst the red shows deposition.

observed within this subsidiary channel during the relatively high river flows measured herein. Measurements on the bar top at lower-low water reveal a splitting of secondary flow across the bar top within cross-sections A and B. This is due to flow separating around the barhead and is reflected in the steering of the bedforms observed in Figure 2.24iii, although flow in the channel itself is fairly minor. At lower-high water this splitting of the secondary circulation is no longer observed due to the inundation of the bar top as seen at the edges of the cross-sections. This variation in flow patterns illustrates the steering of flow around the bar, with flow divergence occurring several hundred metres landward of the bar head. At the eastern edge of cross-section B a small region of reversed flow is observed due to the interaction of a subsidiary channel which cuts between two vegetated bars draining into the main channel at this point (Figure 2.28). The flows observed adjacent to this channel were slower than the main fluvial flows observed (-0.35 ms^{-1} whilst main channel flow was 1.1 ms^{-1}), however as the minor channel is fixed by the stabilised bars it can be expected that they would act to modify the local bedforms within the channel. Unfortunately the bathymetry data does not overlap this region.

Steering of bedforms around local barforms is observed in several locations, notably at Sandee (Figure 2.24iii), Wills (Figure 2.21iii) and the landward region of Taylor Sands (Figure 2.14). This steering is seen where bedforms interact with the landward side of large barforms, indicating topographic forcing of fluvial flow. In regions where the seaward end of barforms are observed, such as in Jubilee (Figure 2.19ii and iv) and within the northern channel at Taylor Sands (Figure 2.14) no steering is observed, only deposition at the bar tail. The flow data at Sandee show that at high fluvial flow the incoming tides act to modulate flow rather than reverse it, hence the barforms are able to influence steering of bedforms moving from a landward direction, but as there is no significant landward flow, and hence sediment transport in a landward direction, there is no comparable steering at the seaward end of barforms. The region of cross-stream flow divergence observed at Sandee lies landward of the region bedform steering, suggesting that there is a lag between bedform migration and local flow. However, barforms throughout the system can be seen to have a tidally influenced shape *sensu* Hayes (1975) even though they are fluvially dominated (Figure 2.32). This will be discussed in more detail in Chapter 3 which investigates the flow and bedform morphology surrounding a single bar within the Columbia River.

2.4.2 Bedform morphology

The variation of bedform morphology across the Columbia River results from the variation in tidal energy within the system. The most seaward bathymetry sections were collected to the north and south of Desdemona Sands, a year apart (Figures 2.9-2.12).



Figure 2.32 Image of the Columbia River estuary showing sand bars present close to the water surface. Note the elongated tails visible at the seaward end of several bars. Fluvial flow is from the east.

The northern section lies within the northern channel, which was identified as more marine in character by Fain *et al.* (2001). This channel is shallower than the main navigation channel to the south of the same bar. Comparison of the profile traces shows that at -6 m TP_MSL, which corresponds to the channel in the northern section (Figure 2.10) and the top of the bar slope in the southern section, the bedform morphologies are different. The northern channel contains rounded bedforms 1 m high, with crest separations of 7.8 m, whilst to the south the bedforms have crests 1.2 m high with a mean separation of 14.5 m. Comparison of the bar top also reveals a difference in the bedform morphology. Within the more tidally-influenced northern channel the balance of tidal and fluvial forces act to form bedforms ~10 m in wavelength, which have a total height of 0.4 m and a rounded profile. However, in the navigation channel at the same depth larger bedforms are found with wavelengths up <20 m in length. It is known that the northern channel becomes less pronounced upstream of the Astoria-Megler Bridge (Figure 2.4), therefore most fluvial flow within the Columbia River is routed through the navigation channel. The larger bedforms to the south of Desdemona Sands shows this large fluvial flux with some reworking by a more minor tidal component of flow. North of Desdemona Sands the reduced fluvial flow results in smaller bedforms which

are more extensively reworked by tidal flow. The flood and ebb flows are more balanced at this location resulting in a more symmetrical bedform morphology.

Investigations into the flow patterns of the Columbia River by Jay (1984) found that most seaward flow occurs within the southern/navigation channel, whilst tidal flows are greatest within the northern channel; this finding is supported by the bedform morphologies discussed herein. Whilst mutually evasive ebb and flood channels are known to be a common feature of fluvial-tidal systems (e.g. van den Berg *et al.*, 2007; Dalrymple and Choi, 2007) the subtle differences in flow occurring within these two bi-directional channels which are located at a similar position within the estuary may be of importance to the reconstruction of similar ancient deposits. In isolation they would be interpreted to have formed at different positions within a single channel in the tidal-fluvial transition.

Less asymmetric bedforms are also found in the channel at Jubilee, a relatively minor channel within the sand bar complexes to the south of the navigation channel (Location 6 on Figure 2.5). These rounded bedforms are found at all the profiles measured in the central region of the bathymetry (Figure 2.20). Landward of the profiles the channel splits, with the deeper region to the north forming a single channel and the bar edge to the south forming a shallower channel. Bedforms lying seaward of the deeper channel are less asymmetric than in the shallower profiles. This would imply that any tidal flow or tidal modulation within this region is preferentially diverted into the deeper northern channel and resulting in mixed bedform profiles. Cores collected by Prockocki *et al.* (2015) within the channel at Jubilee show cross-laminated current ripples indicating uni-directional flow in a seaward direction. The presence of finer beds was inferred to be caused by weakening flow rather than the interaction with flood tides. The cores were collected at the southern margin of the Jubilee channel, not within the deeper channel to the north and this weakening flow may be as a consequence of the divergence discussed previously. This would suggest that the variations in depth and braided patterns of channels result in a more complicated model of tidal modulation within this small region. Cores collected in the same work at Taylor Sands also show cross-bedding, but here the presence of fine sand and silt drapes was interpreted to arise from the slowing of unidirectional fluvial flows by tidal modulation (Prockocki *et al.*, 2015).

2.4.3 Bedform scale

Throughout the survey region bedforms are observed on multiple scales, with smaller bedforms often superimposed on larger ones. These bedforms do not necessarily form due to flow in a single direction. At the Bridge section (Figure 2.13) large scale dunes

are observed up with crest heights of 0.6 m and 350 m wavelength. Superimposed on these are much smaller bedforms of variable scale; within the troughs of the larger bedforms the superimposed bedforms have crest heights <0.2 m, whilst on the dune crests the superimposed bedforms have crest heights of only 0.05 m. The alignment and asymmetry of the largest dune crests suggests flow in an east-south-east to west-north-west direction; however, the morphology of the smaller superimposed bedforms suggest flow from northeast to southwest (Figure 2.33i). Similar variations in flow orientations are observed adjacent to the Navigation channel at Taylor Sands (Figure 2.14iii), where large dunes reflect steering around the sand bars at Taylor Sands, whilst smaller superimposed bedforms (0.05-0.2 m height) show flow in a northeast-southwest direction within the channel (Figure 2.33ii). The superimposed bedforms at Taylor Sands show a more rounded profile, suggesting that they are more tidally-influenced than the larger scale dunes. This suggests that the largest scale bedforms reflect the mean flow within this region of the Columbia River, whilst the smaller bedforms represent a temporal “snapshot” of the flow at the time of the bathymetry measurements. The smaller bedforms would appear to have reached equilibrium with local flow conditions as shown by the variations in size with flow depth.

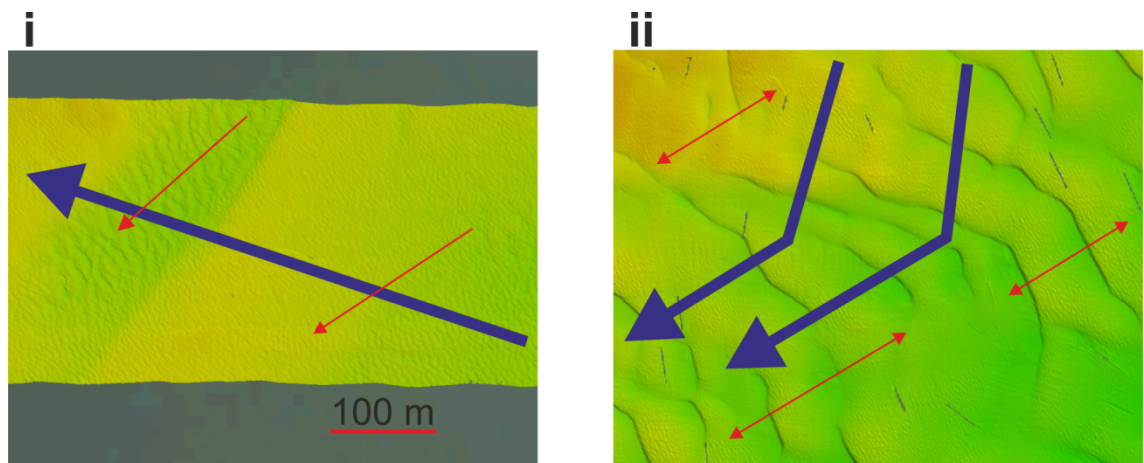


Figure 2.33 Scale dependent flow orientations observed at: i) Bridge; ii) Taylor Sands. Large blue arrows show flow directions of large bedforms, red arrows flow directions of superimposed bedforms.

Comparison of bedform profiles at a mean depth of -4 m TP_MSL are shown in Figure 2.34, illustrating the variations in bedform length and height throughout the study area. Bedform morphology at this depth does not appear to be linked to local topography: Desdemona South (Profile 10 on Figure 2.12), the seaward Taylor Sands (Profile 10 on Figure 2.15) and landward Taylor Sands (Profile 8 on Figure 2.16) profiles are located adjacent to the deeper navigation channel, but have very different morphologies (Figure 2.34). Instead, morphology appears to be linked to position within the field area with the furthest seaward sections collected north and south of

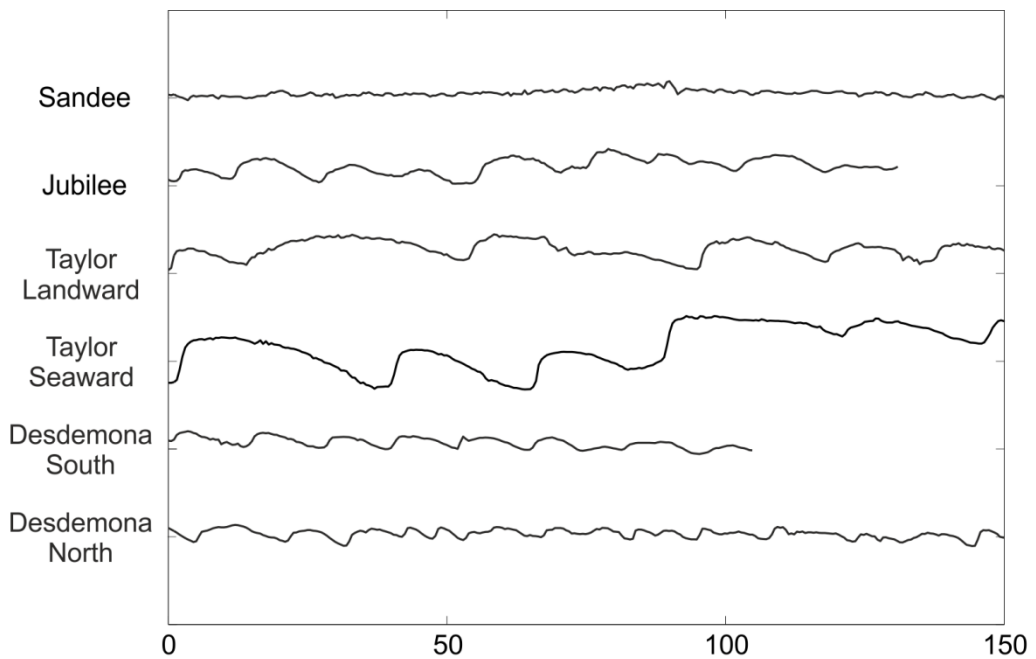


Figure 2.34 Comparison of bedforms found at -4 m TP_MSL throughout study area. Relative depth between each profile is 2 m.

Desdemona Sands having similar scale and shape (even with varying tidal influence), whilst the sections at Taylor Sands and Jubilee Channel have a similar crest separation and are both located within the centre of the field area; the smallest bedforms observed are at Sandee, the most landward section.

The most landward bathymetry data collected at Sandee corresponded to the edge of a submerged barform adjacent to Prairie Channel and has very small bedforms, less than 0.1 m in height, with crest separations of ~1 m (Profile 5 in Figure 2.25). The profile collected at Jubilee, lies within a smaller channel in the braided section of the study reach (Profile 7 on Figure 2.20). Bedforms at this location are 0.4 m high, with mean crest separations of 21 m. Local changes in bathymetry may result in variations in flow depth even at the same relative vertical position within the system with a localised high resulting in the diversion of flow from a measurement location. However, the bathymetry at Desdemona South (Figure 2.11) and Taylor Sands (Figure 2.14) does not show any such sheltering of the profiles discussed and the maximum and minimum bathymetries adjacent to the profiles are of similar magnitude.

Comparison of the two Taylor Sands bedforms and Desdemona South show that within this system, bedform height cannot be used to estimate flow depth, as the variations in tidal flow and modulation of the fluvial flow have resulted in very different bedform scales. A higher degree of tidal influence at Desdemona South has resulted in the reworking of fluvial bedforms and prevented their growth to a morphology closer to those observed at Taylor Sands. The landward profiles at Taylor Sands appear to have

undergone more reworking than the bedforms further seaward as although they have a comparable bedform length they have a more truncated shape and are smaller in height with smaller bedforms superimposed (Figure 2.34). The main navigation channel is the primary conduit for fluvial flow and so contains larger bedforms within the central region measured at Taylor Sands. Where there is more tidal modification at Desdemona Sands these bedforms are not able to grow to the same scale, being eroded by tidal flows although they appear more fluvial in nature than those within the northern channel.

Kostaschuk and Best (2005) reported on bedform hysteresis within the Fraser Estuary, in a region of tidal modulation at spring tides, finding that bedform lengths were not in equilibrium with the surrounding flows but that dune height and steepness reacted to variations in tidal and fluvial flows. The dunes measured at that location were <2 m in height, with lengths of 25-50 m and typically 2 dimensional in shape, comparable to the dunes reported at the edge of Taylor Sands (Figure 2.34). However, it should be noted that the dunes reported by Kostashuk and Best (2005) were located at the base of a channel ~15 m deep; the bedforms discussed here are located at a depth of 4 m and increase in size becoming more 3D in planform at greater depths. This suggests that the scale of bedforms is related to the interaction of tidal and fluvial flows, not to flow depth as is usually suggested (Kostaschuk and Best, 2005).

2.4.4 Variations in bedform morphology with location

The distribution of bedforms sizes observed within the bathymetry data throughout the field area is summarised in Figure 2.35. This shows that the largest bedforms (>50 m in length) are located within the deepest channels throughout the system, as would be expected, although some larger bedforms are observed seaward of the large scour at Taylor Sands (located above “3” in Figure 2.35). This corresponds to the presumed locations of high fluvial flow, which although tidally modulated do not slow sufficiently or reverse and prevent the seaward transport of sediment. Bedforms 25-50 m in length are observed at bar tops in regions of high fluvial flow such as Sandee and at bar edges in more modulated flow regions. Smaller bedforms (10-25 m) are observed on the edges of bar forms within the most seaward bar complexes at Desdemona and Taylor Sands, but also on the bar edge at Jubilee and within Prairie Channel. These are regions of bi-directional flow, whether due to tidal flow reversals as at Desdemona North or on bar tops where they are affected by the uncovering and submergence of the bar with the tides. The smallest bedforms (<10 m) were located within a 10 m deep channel seaward of Taylor Sands and show a very symmetrical profile. This region probably reflects the true location of the northern channel and the full extent of its landward incursion.

The field area was previously surveyed by Sherwood and Creager (1990), whose reported bedforms following the freshet are summarised in Figure 2.36. Bedforms in this earlier work were classed as <14 m or above in size, so on a different scale to the presentation in Figure 2.35. However, the distribution of bedforms, where the two surveys overlap are in general agreement. The present work does not report any regions of flood dominant bedforms, however the survey does not extend as far seaward as Sherwood and Creager (1990), so is confined to the tidally-influenced fluvially-dominated region only. The interaction of tidal and fluvial flows with barforms adjacent to the main channel has resulted in a range of bedform sizes and morphologies. The complex region of braided bars which is the focus of this study has resulted in a pattern of deposition which is more complicated than would be observed within a single channel system and results in more subtle indicators of the influence of local tidal flow. This may have implications for the reconstruction of similar ancient systems. The river flood dominated but tidally-influenced Lajas Formation, shows large-scale fluvial flood deposition, with fine-grained bioturbated interflood deposits which are interpreted as tidally-influenced due to the presence of saline influenced ichnofossils (Dalrymple *et al.*, 2015). The section described does not appear to have any modulation of the fluvial bedforms due to tidal-influence, as it comprises a series of large-scale fluvial flood events. Although the Columbia River experiences high fluvial flow during the freshet (Jay *et al.*, 2011), the bedforms are revealed to be continually modulated by both tidal and fluvial flows.

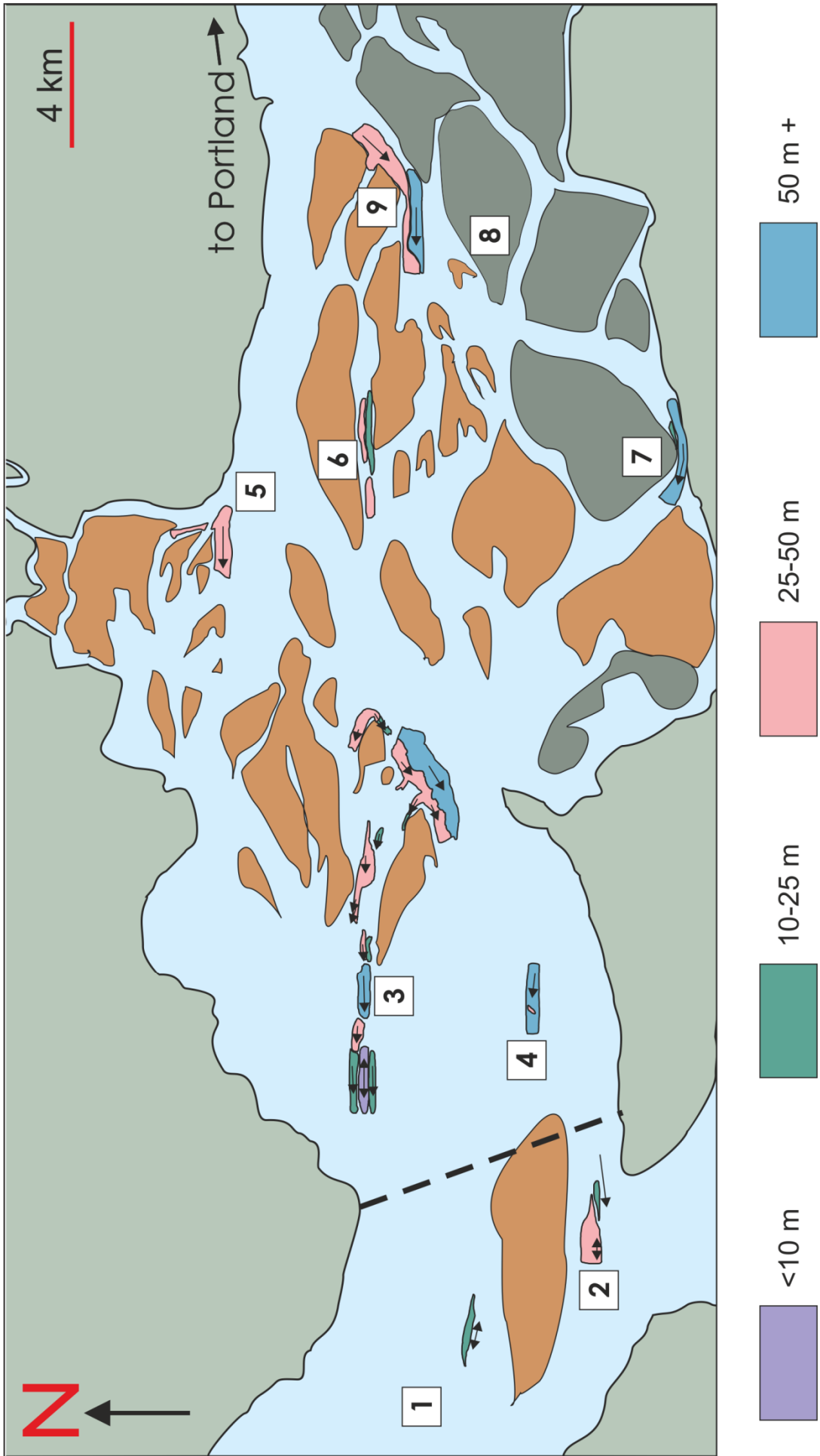
There is a 1.3 km overlap between the two sections measured at Taylor Sands in FS1 and FS2. This region contains a large scour hole, with a maximum depth of -18 m MSL_TP. This scour hole is present in both years, and appears to be a relatively stable feature, showing little migration (20 m migration in a landward direction at the southern edge). A second deeper section observed in the northern region of the scour in the FS1 profile which has been infilled (1.5 m in depth) before the FS2 measurements; this material has been transported from the seaward slope. There is some migration of the bedforms observed, but they do not change in magnitude or morphology between the two field seasons. Whilst this implies that there is some tidal influence within this scour region, the effects appear to be relatively weak in comparison to the fluvial flow as there has been little effect on the scour morphology.

Within Jubilee channel there are large landward oriented shelves observed across the width of the channel, with a small scour at the seaward edge (Figure 2.19ii). These appear to correspond to the failure of the edge of the large bar to the north of the channel, which is largely composed of dredging waste from the navigation channel and has been reworked by tidal flows within the channel. The large scour at Taylor Sands

also lies seaward of a landward oriented featureless structure. This sheet cross-cuts the dune crests which lie to the east (landward), although smaller superimposed bedforms have been transported in a landward direction from these truncated dunes onto the smoother sheet (Figure 2.14ii). Deep scour holes have been observed in tidal environments at the confluence of two tidal channels with balance flow (Kjerfve *et al.*, 1979; Ginsberg and Perillo, 1999). However, the large scours observed at Taylor Sands and within Jubilee Channel although both lying seaward of a channel confluence are too distant to have been affected by the confluence in this way. There are numerous regions of small-scale scour throughout the study area (e.g. Desdemona North; Figure 2.9), which all lie within areas which do not contain widespread dunes.

All bathymetry measurements collected in the present work lie below the local mean sea level, as the Columbia River estuary is actively infilling (Prokocki *et al.*, 2015). The large scour at Taylor Sands is significantly deeper than the surrounding channel (-17 m TP_MSL in a channel -8 m TP_MSL), and is comparable to the depth of Prairie Channel. However, the presence of these deep erosive channels and scours might be interpreted in isolation as an indicator of sea-level change. Interpretation of similar scour surfaces in ancient deposits may be used as evidence of sea-level fall, although Best and Ashworth (1997) suggest that this is only the case when the erosive surface is more than 5 times the mean channel depth; the present scours are not deep enough to be suggestive of this type of sea-level change. Core data reveal that local sea-level has been rising by ~1 mm/year for the last 2,000 years (Prokocki *et al.*, 2015), illustrating that the entrenched nature of this system has resulted in a morphology which may result in misinterpretation if observed in ancient deposits. As observed previously, bedform morphology varies with tidal influence rather than depth at the present location, which might result in scours of this type being misinterpreted as resulting from sea-level fall if viewed in isolation within ancient deposits with the same morphology.

Figure 2.35 (next page) Distribution of bedform lengths within the study area. Local flow direction is also shown.



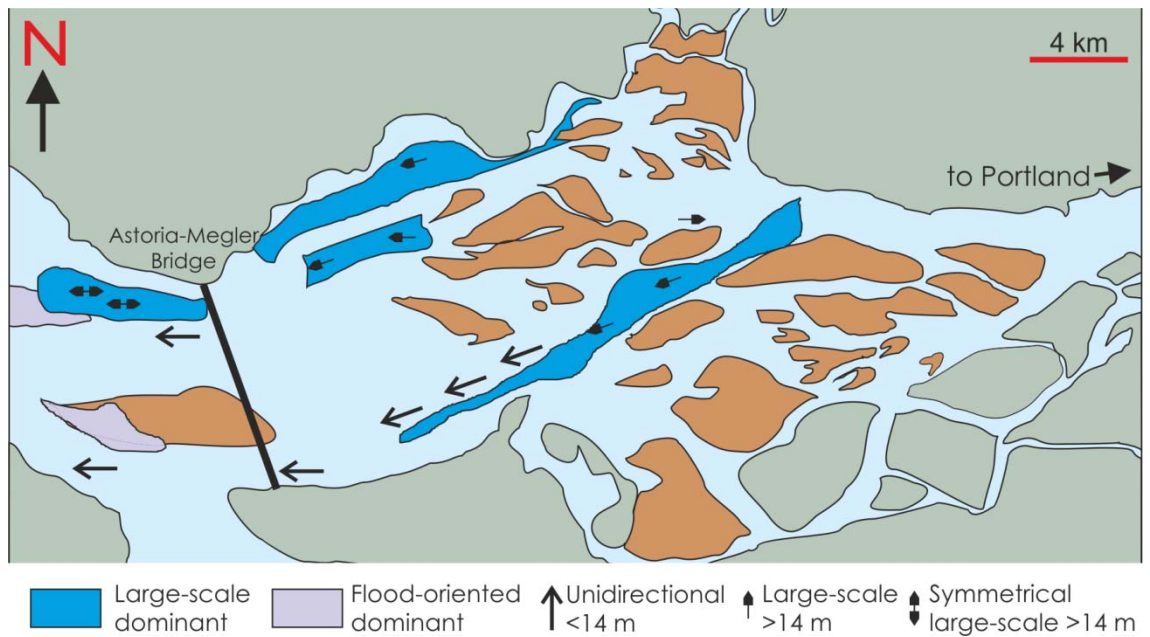


Figure 2.36 Bedform distributions from side-scan sonar measured in June 1980 (Sherwood and Creager, 1990).

2.5 Conclusions

Investigations were made of the bathymetry within the Columbia River estuary, Oregon, USA. Measurements were made in a region of braided sandbars cut by a deep channel in a region which is fluvially dominated but has a degree of tidal influence. Bedforms within study region vary in scale from <10 m in length to 100 m and often have smaller bedforms superimposed upon them. The bedforms appear to be fluvial in nature, but detailed analysis of bedform distribution and size reveal the increasing tidal influence in the seaward region of the study.

1. The largest bedforms reveal the mean flow patterns of the Columbia River, being slow to erode. The balance of tidal to fluvial flows is revealed in the predominantly fluvial nature of the bedforms
2. Smaller superimposed bedforms reveal a temporal “snapshot” of conditions during measurement, with preservation of more tidal flow patterns at a different orientation to the dominant fluvial flow.
3. Whilst bedforms may appear to be entirely fluvial in origin, the decrease in size in more seaward locations reveals a greater degree of tidal modulation.
4. The steering of bedforms around the large barforms reveals flow to be predominantly in a seaward direction as no steering is observed at the seaward end of bars.

5. Evidence of flow in a landward direction is seen in areas of bar collapse where channel wide sheets showing transport in a landward direction is observed. This suggests that any landward flows are sediment starved and deposition and transport is only possible in regions with large amounts of available sediment. These sheets do not contain any large bedforms and are maintained for over a year. They are often associated with large scour features which occur at the seaward end of the sheet.

Comparison to the model of tidal-fluvial transition would suggest that the bedforms observed within the studied region of the Columbia River would be placed within a region of fluvial-dominance, perhaps with no tidal influence (Dalrymple and Choi, 2007). However, the flow observations made herein reveal that this fieldwork was carried out within a region of significant tidal influence (Figure 2.27-30). Although fluvial in appearance the systematic variations of bedform morphology with position highlighted are an indicator of tidal influence, despite the absence of more commonly described tidal markers. This would suggest that further refinement of the fluvial region of tidal-fluvial transition models such as that of Dalrymple and Choi (2007) or Archer (2013) is necessary, as they are currently too simplistic within the region of fluvial dominance or describe large scale fluvial flood events (Dalrymple *et al.*, 2015). A more systematic investigation of bedform scale with tidal influence would inform the addition of this subtle marker of tidal influence to such models. While broad zones of bedform types and grain-size distributions are presently described within their longitudinal variations as a marker of tidal influence has not been considered to date.

Chapter 3

Flow around a tidal barform

3.1 Introduction

The balance between the varying fluvial and tidal inputs into river-estuary and river-delta systems results in a complex transition zone, which will vary spatially and temporally. Variations in fluvial flow due to seasonal or anthropogenic effects will act to move the boundary between fully-fluvial and fully-tidal, with increased fluvial flux pushing the boundary further seaward. The natural variations in the tidal cycle will act to move the boundary in a landward direction during the highest tides. However, whilst tides act to reverse flow in more seaward regions they may also modulate fluvial flows within the zone of river dominance landward of the maximum tidal incursion, acting to slow fluvial currents (Dalrymple and Choi, 2007; Dalrymple *et al.*, 2015; Figure 2.1). Due to the length of many large rivers the tidal-fluvial transition may represent a region hundreds of kilometres long; recognition of the distinct facies arising from the varied nature of flow within this transition is essential for accurate palaeogeographic reconstructions. This complex region of tidal-fluvial transition will exhibit varying sediment transport and depositional patterns throughout its length, with tidal processes dominating at the seaward and fluvial processes at the landward end (e.g., Dalrymple *et al.*, 1992; Bridge, 1993; Best *et al.*, 2003; van den Berg *et al.*, 2007; Martinius and Gowland, 2011; Fustic *et al.*, 2012). There is increased interest in the region of the tidal-fluvial transition as it has been identified as a potential petroleum reservoir source (e.g., Dalrymple *et al.*, 2015; Webb *et al.*, 2015). The distinction between compound tidal dunes (crests normal to tidal currents, flow oriented accretion) and tidal bar deposits (parallel to tidal currents, lateral accretion) is therefore important for the creation of facies models (Martinius and Gowland, 2011; Fustic *et al.*, 2012; Olariu *et al.*, 2012).

Within the tidal-fluvial transition zone there will be variation in bar planform with system position. Planforms may result from the amalgamation of several smaller bars and may form at varying angles to the main flow direction. Barform size is scaled to flow width rather than depth as is the case with dunes (Dalrymple and Rhodes, 1995). In the most seaward region of both estuaries and deltas elongate tidal bars commonly form. With high tidal range these bars will develop a linear planform and vary in size depending on tidal and fluvial currents (Dalrymple and Rhodes, 1995). These elongate bars migrate laterally rather than with flow due to bi-directional deposition acting on

both bar edges (Dalrymple *et al.*, 1992; Dalrymple and Choi, 2007; Figure 1.4). Towards the system mouth these bars may become detached from channel edges and two elongate bars may become connected forming a U-shaped bar within larger bar complexes (Dalrymple and Choi, 2007).

Whilst elongate bars are common at the mouth regions of estuaries, bars with a lobate planform are also observed (Hayes, 1975; Billy *et al.*, 2012; FitzGerald *et al.*, 2012). The bi-directional flow acting upon these bars results in a compound barform: flood ramps and channels interact with a higher ebb shield which acts to protect the flood ramp from fluvial flows (Hayes, 1975). These delta-like barforms are often found at regions of flow expansion and have been suggested to arise from the modification of more elongate barforms and may be tidally-dominated and wave-influenced or tidally-dominated but fluvially-influenced depending on their location within the tidal-fluvial system (Dalrymple and Rhodes, 1995; Billy *et al.*, 2012). In regions of mixed tidal-fluvial influence the seaward end of large bars may become sheltered from fluvial flow forming flood barbs, straight channels through which the incoming tide is able to flow (van den Berg *et al.*, 2007). Further landward, in areas which are more fluvially-dominated, the system will develop a more sinuous planform which is associated with relatively balanced tidal and fluvial flow (Dalrymple *et al.*, 1990). Flow is contained within a single channel, with no separation into flood and ebb dominated channels (van den Berg *et al.*, 2007). Bank attached point bars and alternate bars are commonly found within this region, particularly within straighter channels (Dalrymple and Rhodes, 1995; Dalrymple and Choi, 2007; Blondeaux and Vittori, 2011; Carling *et al.*, 2015).

Barform initiation and development was studied within the tidal reach of the Fraser River estuary by Villard and Church (2005). This field location is regularly dredged, allowing the formation of barforms within a region devoid of pre-existing bedforms to be assessed. It was found that dunes within the channel varied in size according to variation in discharge, with dune size following the high flows during the freshet re-establishing to scale with channel depth. Bar growth was found to be linked to local sediment transport from large-scale dunes, with the bar acting as a sediment sink during periods of high flow.

In contrast to regions of tidal-fluvial mixing, within fluvial settings mid-channel bars have been shown to form downstream of bar confluences, representing the re-deposition of material eroded from a confluence scour (Ashworth, 1996). Lobate patterns may be observed within more fluvial settings due to the amalgamation of several smaller barforms; these compound bars have a slower migration rate than their constituent barforms. Flow around an evolving braid bar within a fluvial setting was

investigated by McLelland *et al.* (1999). Flow was found to diverge around the barhead and converge at the bar tail; helical flow cells were not induced during this divergence, instead flow was parallel to the channel thalweg. At later stages of bar development flow began to cut across the bar top, causing an asymmetric planform to develop.

The present work will investigate the morphology and flow characteristics of a large bar within an area of tidal influence in the fluvially-dominated Columbia River estuary. Bathymetry measurements were made adjacent to the bar to build a full picture of the depositional signatures which result from this flow, along with subsurface geophysical imaging of the bartop itself. Repeated bathymetry measurements made at a smaller sub-section of the submerged bar top also allows the rate of bedform migration on the subtidal bartop to be investigated. In addition, high resolution flow measurements were made throughout the tidal cycle, allowing the flow dynamics around this bar to be understood in detail and the morphology of the bedforms to be understood within the context of this flow.

3.2 Field Methods

3.2.1 Field location: Wood Bar, the Columbia River Estuary

The Columbia River lies on the Pacific coast of North America, draining an area of over 660, 480 km² (Simenstad *et al.*, 2011). The estuarine reach of the river is modified by mixed diurnal and semidiurnal tides, with tidal modification of river flow heights for over 200 km (Simenstad *et al.*, 2011; Prokocki *et al.*, 2015). The landward region of the Columbia River estuary is highly complex with multiple channels and braid bars present (Figure 3.1). However, the region of tidal dominance lies seaward of the main braided reach of the system (Figure 2.3). As discussed in Chapter 2, the Columbia River estuary is an entrenched fluvial system, with shallow water bays containing intertidal bars (Prokocki *et al.*, 2015). As such, flow within the Columbia River estuary is fluvially-dominated in nature but undergoes some tidal modification which is not sufficient to fully reverse flow throughout the system.

The field data reported on here comprises a sub-section of the main Columbia River data discussed in Chapter 2. Bathymetry and flow measurements were collected around a bar 950 m by 400 m which is in the landward region of Prairie Channel, 1 km seaward of the Sandee Section (Figure 3.1; Location 8 on Figure 2.7). This bar has a lobate planform and lies within a region of fluvial dominance with tidal modulation (Chapter 2). The presence of lobate bars within the tidal-fluvial transition was discussed by Billy *et al.* (2012), who noted the Columbia River estuary as a location where these were observed. Multibeam Echosounder (MBES) bathymetric surveys and acoustic Doppler

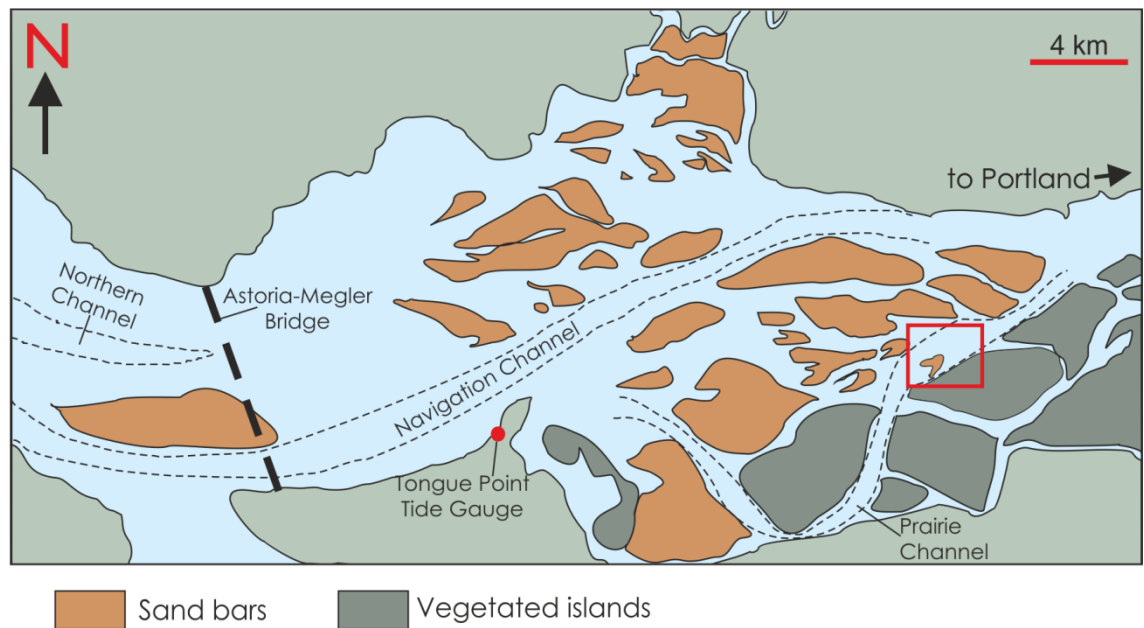


Figure 3.1 Location of Wood Bar in the Columbia River estuary.

current profiler (ADCP) flow data were collected using the same methods as previously outlined in Chapter 2 and processed in the same way.

3.2.2 Methodology

Repeated MBES surveys were carried out to allow the development of the local bedforms to be investigated, in the manner of Nittrouer *et al.* (2008) and Franzetti *et al.* (2013). In addition to the main bathymetry data a series of repeated MBES measurements were made at a single location to the north of Wood Bar (Figure 3.2). Repeat data collection was carried out over several days and at different points within the tidal cycle (Table 3.1). The subsection is 300 m long and 150 m wide and contains several different bedforms. The landward region consists of large dunes (~20 m in wavelength) with smaller superimposed dunes, whilst the seaward section contains only the smaller dunes. After data processing within Caris HIPS and SIPS the repeat surfaces were exported as point cloud files. This data was then imported into ArcMap 10 and a digital elevation model (DEM) created. Using the Raster Maths function a difference map of the successive surfaces was created and output to show the relative deposition and erosion which had occurred between section repeats. Profiles were also collected along a central transect to compare the movement of bedforms.

Flow data was collected using an acoustic Doppler current profiler (ADCP) along 4 cross-sections surrounding the bar, two of which were bifurcated by the bar: B at low water only; C at all times (Figure 3.2). Cross-section transects were collected between

Table 3.1 Times of repeated bathymetry measurements (all times UTC)

| Repeat | Date | Start Time | River Condition | Time since previous |
|---------|------------|------------|------------------------|---------------------|
| Epoch 1 | 28/05/2013 | 00:42 | Lower-high water | |
| Epoch 2 | 28/05/2013 | 18:24 | Lower-low water | 18 hours |
| Epoch 3 | 29/05/2013 | 17:48 | Before lower-low water | 23.5 hours |
| Epoch 4 | 02/06/2013 | 16:18 | Lower-high water | 94.5 hours |

29/05/2013 and 01/06/2013 with repeats at different stages of the tidal cycle (Table 3.2; Figure 3.3). These transects were then used to examine the changes in flow through the tidal cycle at each position.

In addition to the bathymetry and flow data collected around the bar, subsurface data was collected using a pulseEKKO 100 MHz Ground Penetrating Radar (GPR) along 16 transects on the exposed bar top at low water. Traces were collected every 0.1 m, triggered by an odometer wheel on the system carrier. Transects locations were surveyed using a Leica GPS1200 differential GPS (dGPS) to accurately position the surveys and allow topographic reconstruction. Transects were collected across the width of the bar and also longitudinally (Figure 3.2). Processing and interpretation of this data was carried out as part of the TIFZ project (NERC NE/H007954/1).

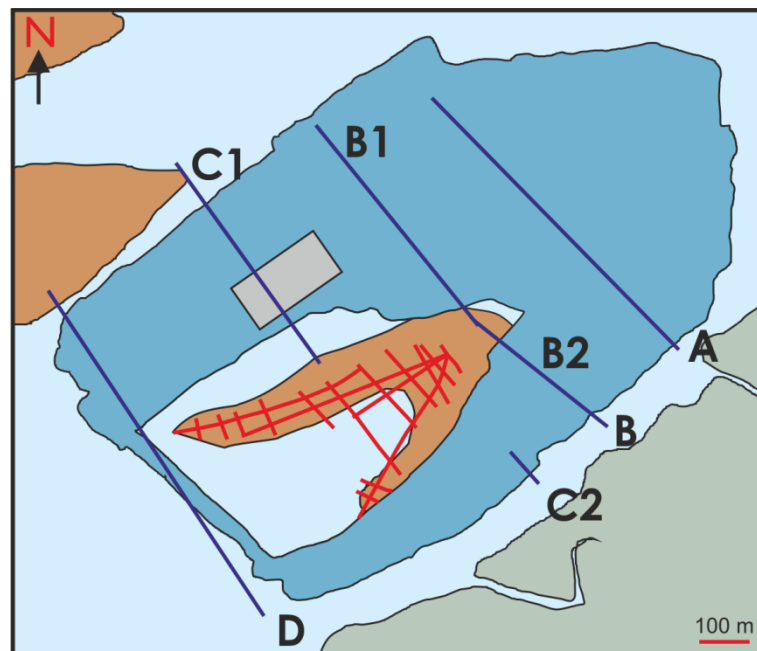


Figure 3.2 Location of data collection around Wood Bar. Blue represents location of main MBES survey, with location of repeated MBES measurements shown in grey; ADCP cross-sections (A-D) are shown as black lines; GPR transects shown in red. Fluvial flow is from the top right of the section.

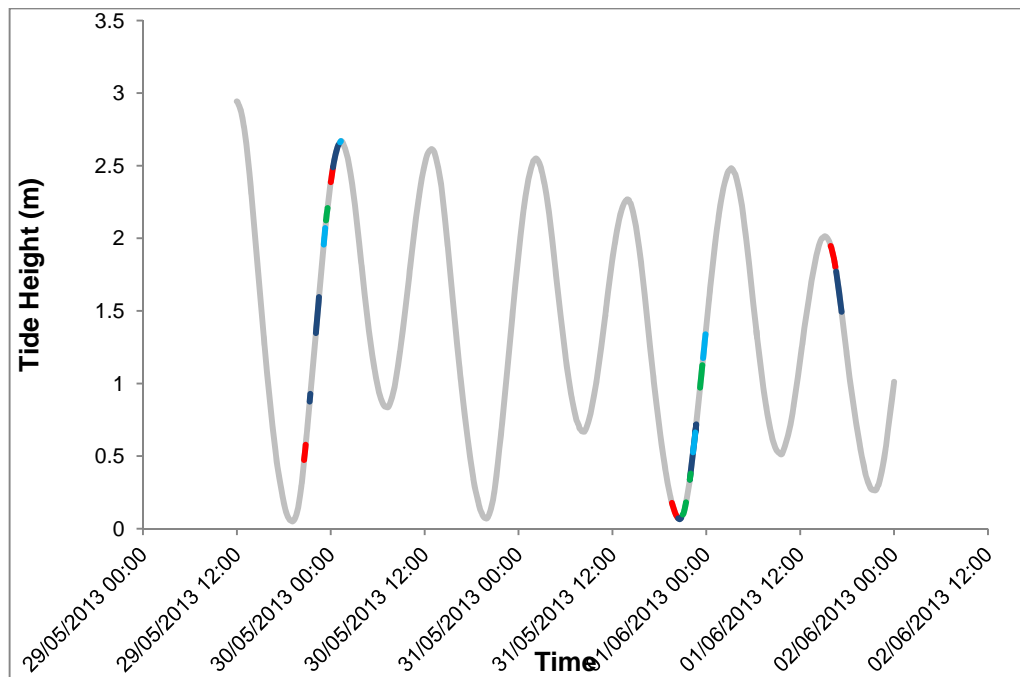


Figure 3.3 Collection times of ADCP surveys relative to tide data at the Tongue Point gauge. All times shown are in UTC. Cross-section A shown in red; cross-section B shown in dark blue; cross-section C shown in green; cross-section D shown in pale blue, locations of cross-sections shown in Figure 3.2.

GPR is a non-invasive technique used to visualise near surface sedimentary structures (Bristow and Jol, 2003; Neal, 2004; Sambrook Smith *et al.*, 2006). It has also been used to study ice thickness, water depth in lakes, bedrock depth, soil stratigraphy, and water table depth (Davis and Annan, 1989). Electromagnetic pulses are generated by the equipment, electrical discontinuities alter the velocity of the pulse as it travels through the substrate and will reflect the pulse when there is a discrete boundary. The water content of the strata alters its electrical properties, so volumetric water changes (caused by variations in packing of particles) will cause differing reflections (Davis and Annan, 1989). The strength of reflections observed and their velocity will show the depth of the structure and variations in sediments forming it, along with the local groundwater level (Neal, 2004). The nature of the sediments cannot be determined from a GPR trace alone; a core must be taken which can then be used for correlation. Table 1 in Neal (2004) highlights the wide range of sedimentary facies on which GPR studies have been carried out, including fluvial, glacial, coastal, aeolian, deltaic and volcanic environments.

GPR systems commonly use a fixed transmitter and receiver system to allow a common offset, with two antennas arranged perpendicular to each other (Figure 3.4). The system is moved along the ground either by dragging or by moving in fixed steps and a horizontal trace is built up showing the reflections received (Neal, 2004). A short pulse of electromagnetic energy in the range of 10-1000 MHz, depending on the system used,

Table 3.2 ADCP data collected at Wood Bar. Date and time in UTC.

| Cross-section | River condition | ADCP Transect | Date | Start Time |
|---------------|---|---------------|------------|------------|
| A | Lower-low water | Trans019 | 31/05/2013 | 19:32 |
| | | Trans020 | 31/05/2013 | 20:02 |
| A | After lower-low water | Trans000 | 29/05/2013 | 20:36 |
| A | Before lower-high water | Trans014 | 30/05/2013 | 00:02 |
| A | After lower-high water | Trans037 | 01/06/2013 | 15:55 |
| | | Trans038 | 01/06/2013 | 16:11 |
| B1 | Lower-low water | Trans021 | 31/05/2013 | 20:25 |
| | | Trans022 | 31/05/2013 | 20:39 |
| B2 | Lower-low water | Trans026 | 31/05/2013 | 21:38 |
| B1 | Midway between lower-low water and lower-high water | Trans005 | 29/05/2013 | 22:06 |
| | | Trans006 | 29/05/2013 | 22:17 |
| B2 | Midway between lower-low water and lower-high water | Trans003 | 29/05/2013 | 21:18 |
| B | Lower-high water | Trans015 | 30/05/2013 | 00:21 |
| | | Trans016 | 30/05/2013 | 00:43 |
| B | After lower-high water | Trans039 | 01/06/2013 | 16:34 |
| | | Trans040 | 01/06/2013 | 17:00 |
| C1 | Lower-low water | Trans023 | 31/05/2013 | 20:57 |
| | | Trans025 | 31/05/2013 | 21:15 |
| C2 | After lower-low water | Trans029 | 31/05/2013 | 21:56 |
| C1 | Midway between lower-low water and lower-high water | Trans033 | 31/05/2013 | 23:13 |
| | | Trans034 | 31/05/2013 | 23:24 |
| C2 | Before lower-high water | Trans011 | 29/05/2013 | 23:26 |
| | | Trans012 | 29/05/2013 | 23:33 |
| D | After lower-low water | Trans031 | 31/05/2013 | 22:19 |
| D | Midway between lower-low water and lower-high water | Trans035 | 31/05/2013 | 23:37 |
| D | Before lower-high water | Trans010 | 29/05/2013 | 23:06 |
| D | Lower-high water | Trans017 | 30/05/2013 | 01:11 |

is generated and the reflections collected by the receiver (Davis and Annan, 1989; Neal, 2004).

The electrical properties of sediments control the way the sediments react when an alternating electric field is applied to them, and how much of the field is transmitted through the medium (Neal, 2004). The main properties considered are the dielectric permittivity (a measure of a material's ability to store electrical charge), electrical conductivity (transport of an applied electrical field) and magnetic permeability (magnetic energy stored and lost by induced magnetisation). Attenuation of the signal by the material through which it is travelling will affect the maximum depth it is possible to survey (Davis and Annan, 1989). This is a problem when working within estuarine environments as the presence of saline water present rapidly degrades the signal and allows only shallow surveys (Neal, 2004).

Following collection of GPR survey data a post-processing routine must be carried out to remove background noise: Band pass filtering to remove noise at the high and low end of the amplitude selected; Dewow filtering was applied to remove low frequency noise which may obscure features (Woodward et al., 2003).

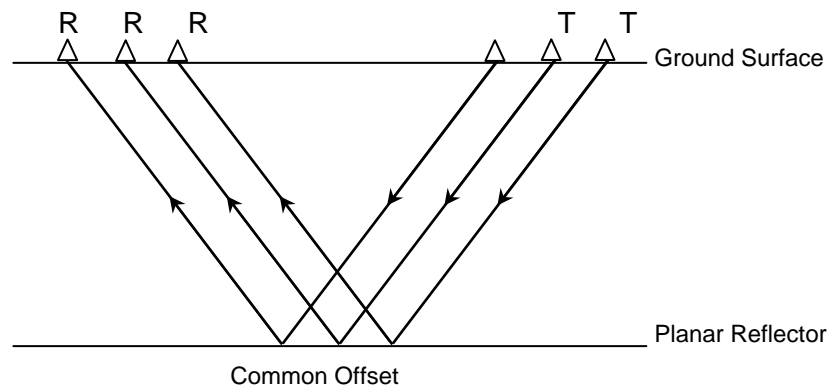


Figure 3.4 Common offset reflection surveys R = Receiver, T = Transmitter (Neal, 2004).

3.3 Results

3.3.1 Bathymetry

MBES measurements were made of a region 1.9 km by 1 km surrounding Wood Bar, which measures 950 m by 400 m (Figure 3.5). The measurement zone mainly consists of a shallowing sand bar with surrounding channels, whilst at the southern edge is a deep channel -9.5 m deep relative to TP_MSL with sinuous dunes up to 4m in length. The deeper section at downstream edge of the northern margin is -7 m deep relative to TP_MSL and contains large dunes 40 m in length and with a relative crest height of 0.9 m. Smaller bedforms are superimposed on the dune crests.

At the seaward edge of the bar, adjacent to the deeper channel to the east, the bar edge is steeply cut (Figure 3.6i and ii). However, at the western edge the bar gradually deepens into the channel with no break in the crestlines of the bedforms, although the orientation does vary in this channel (Figure 3.6iii). At the landward end of the bar there is no distinct bar edge, with the bathymetry shallowing and bedform crests becoming less widely spaced and steering around the bar head (Figure 3.6iv). The shallowest regions around the bar are -1.1 m deep relative to TP_MSL. These areas do not show any large-scale dunes, but contain dunes up to 2 m in wavelength in slightly deeper regions.

The region landward of the barhead contains several northeast – southwest oriented longitudinal dune crests up to 200 m wide, with the crests oriented to the west and crest heights of approximately 1.5 m (Figure 3.6v). Cross cutting these dunes are large sinuous dunes, with crest lines continuing across the sheet margins. These dunes are

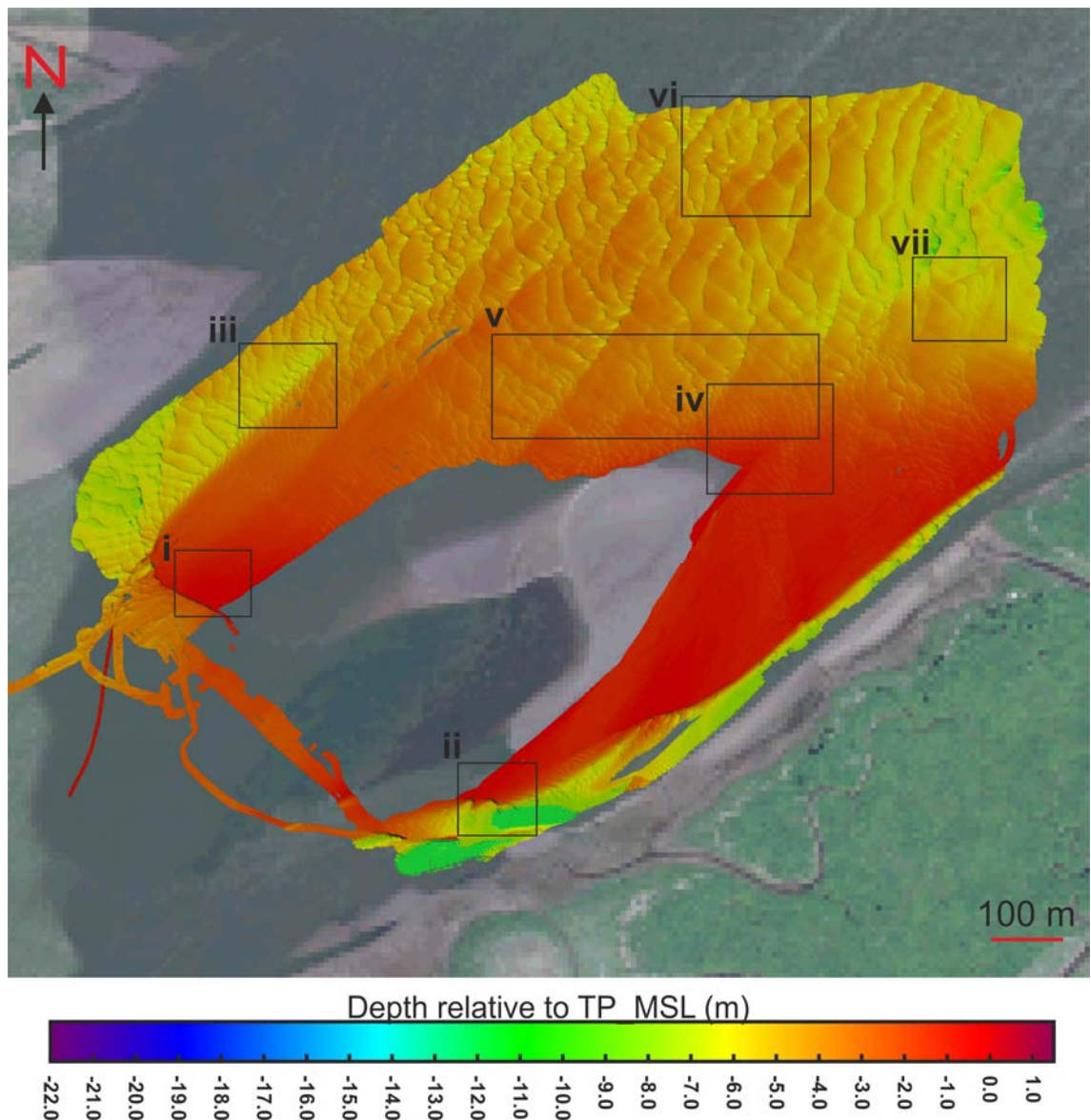
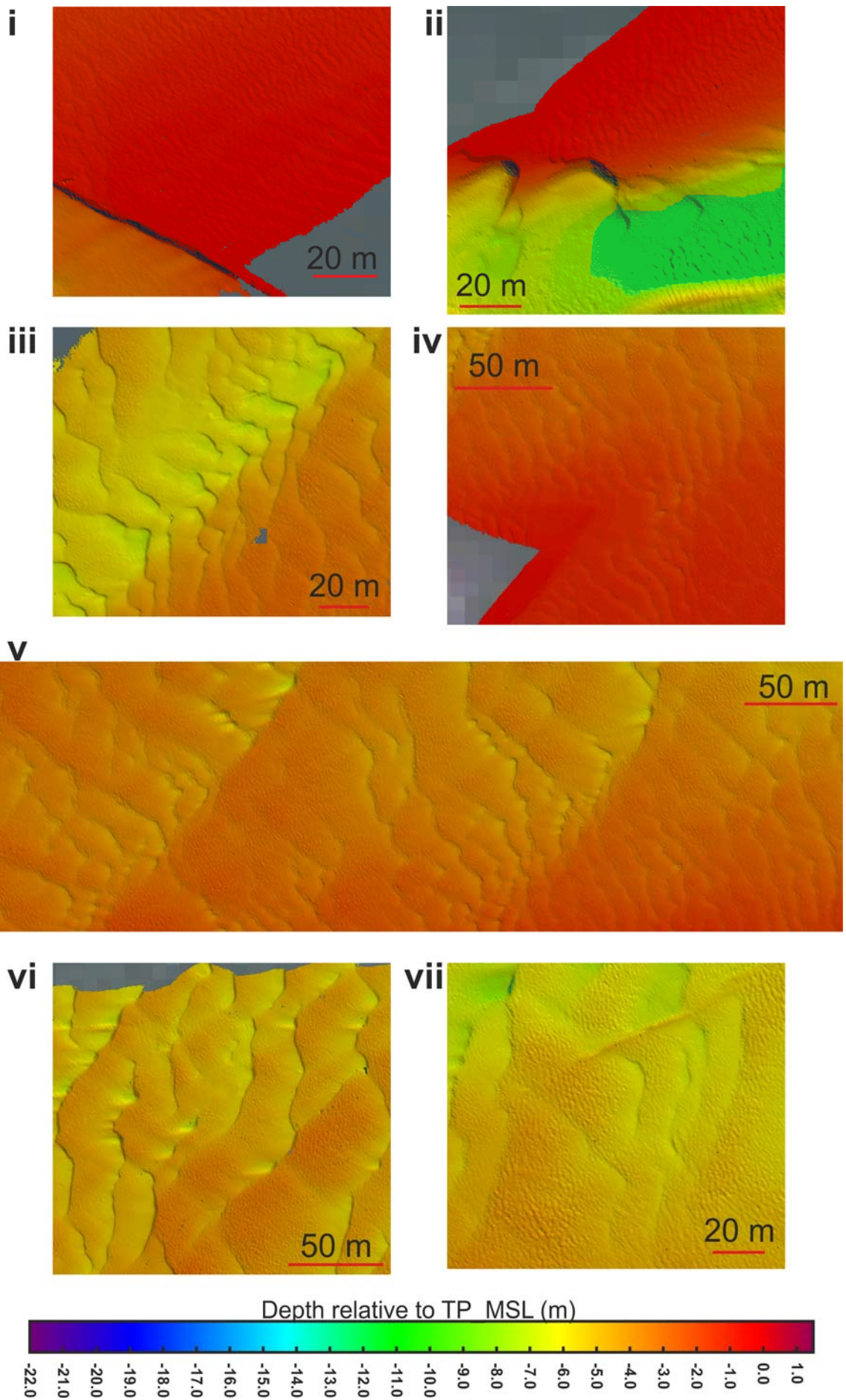


Figure 3.5 Bathymetry measurements of Wood Bar (location shown in Figure 3.1). Highlighted regions are shown in Figure 3.6. Fluvial flow is from the top right of figure.

approximately 40 m in wavelength with relative crest heights of 0.9 m; superimposed on the dunes crests are smaller dunes. In the landward region of the bathymetry there is an elongated linear high (0.5-1.5 m), approximately 5 m wide and visible for 500 m (Figure 3.6vii). This feature is oriented northeast-southwest, parallel to the edge of the channel and has a distinct edge to the northeast. Angled obliquely to the larger bar crest lines are smaller linear features <20 in length (Figure 3.6v and vi). Similar features were observed at Prairie Channel (Figures 2.23 and 2.24). These are found throughout the landward region of the bathymetry measurement zone. Smaller scale dunes are superimposed on the crests of the large dunes throughout the bathymetric measurements.

Figure 3.6 (next page) Features of Wood Bathymetry – see text for details.



3.3.2 Repeat Bathymetry

To investigate bedform development and migration, a subsection of the bathymetry data was re-surveyed (location shown in Figure 3.2; timings in Table 3.1). The first repeat section, Epoch 1, was collected just after lower-high water (Figure 3.7). The landward region contains several large dunes with an initial crest separation of approximately 20 m and a relative crest height of 0.5 m. The seaward region does not contain any large dunes and is -2.6 m TP_MSL. Smaller 3D dunes up to 2 m in wavelength with relative crest heights of 0.6 m initially are present on the bar top to the seaward end of the section and on the dune crests at the landward end. Crest orientations of the both the large dunes and the superimposed bedforms are aligned normal to fluvial flow around the bar. Both scales of bedforms have an asymmetrical profile suggesting fluvially-dominated flow.

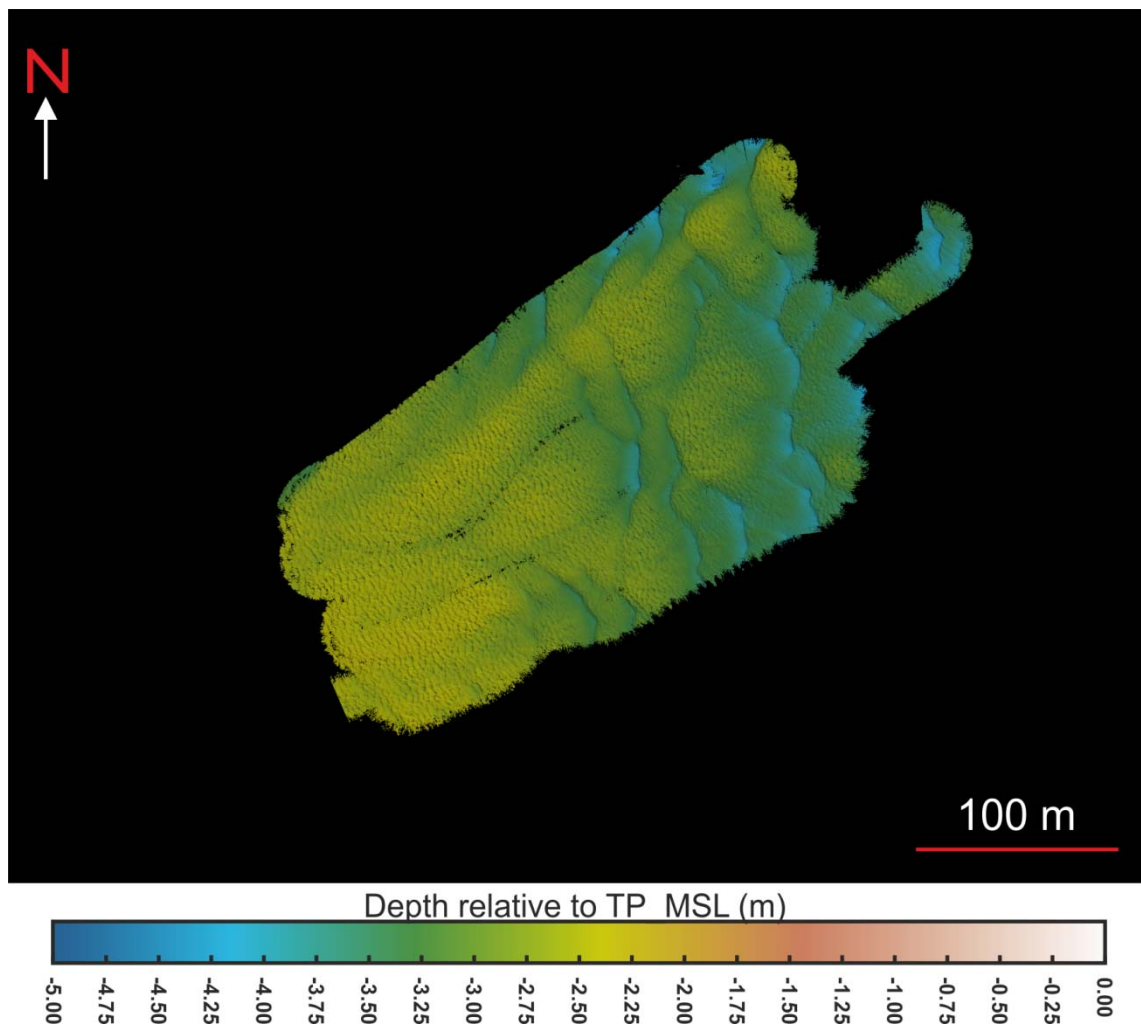


Figure 3.7 Initial surface collected during Epoch 1. Fluvial flow is from the top right corner.

A second bathymetry measurement, Epoch 2, was collected at the same location 18 hours later, just after lower-low water (Figure 3.8). Bedforms of a similar scale to the first section are observed, with large asymmetrical dunes and superimposed smaller

bedforms. A comparison of the two surfaces is shown in Figure 3.9i, showing localised variations in deposition and erosion between the two bathymetry measurements. The difference plot between Epoch 1 and Epoch 2 shows a significant amount of localised erosion, with regions of deposition along the dune crests (Figure 3.9i). At the centre of the bathymetry measurements, parallel to the fluvial flow, a profile line was output from the data (Figure 3.9ii). The profile line shows that there has been no significant erosion of dune troughs, but in some areas of the seaward region 0.2 m of erosion of the dunes tops has occurred. The larger landward dunes can be seen to have migrated in a seaward direction.

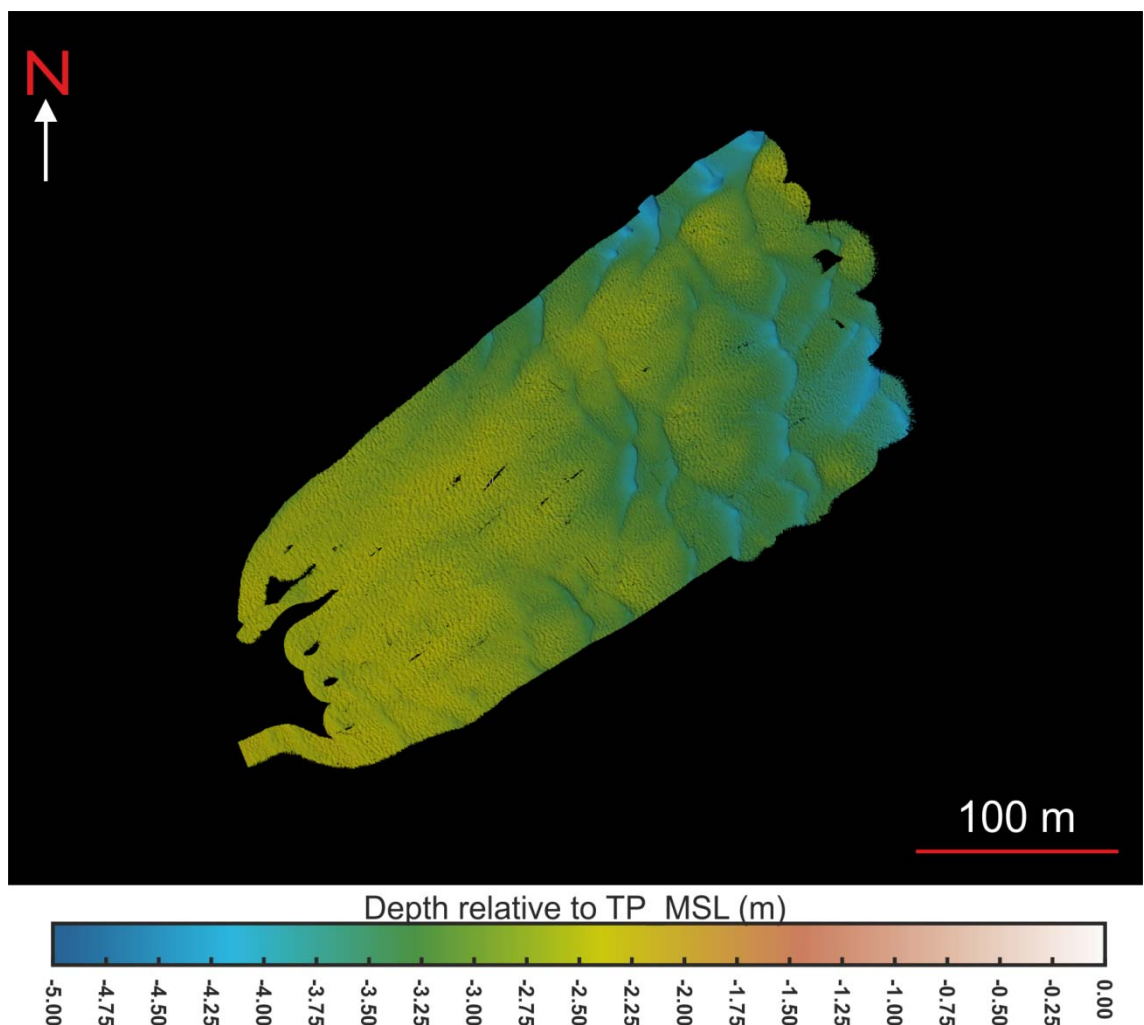


Figure 3.8 Repeat surface collected during Epoch 2. Fluvial flow is from the top right corner.

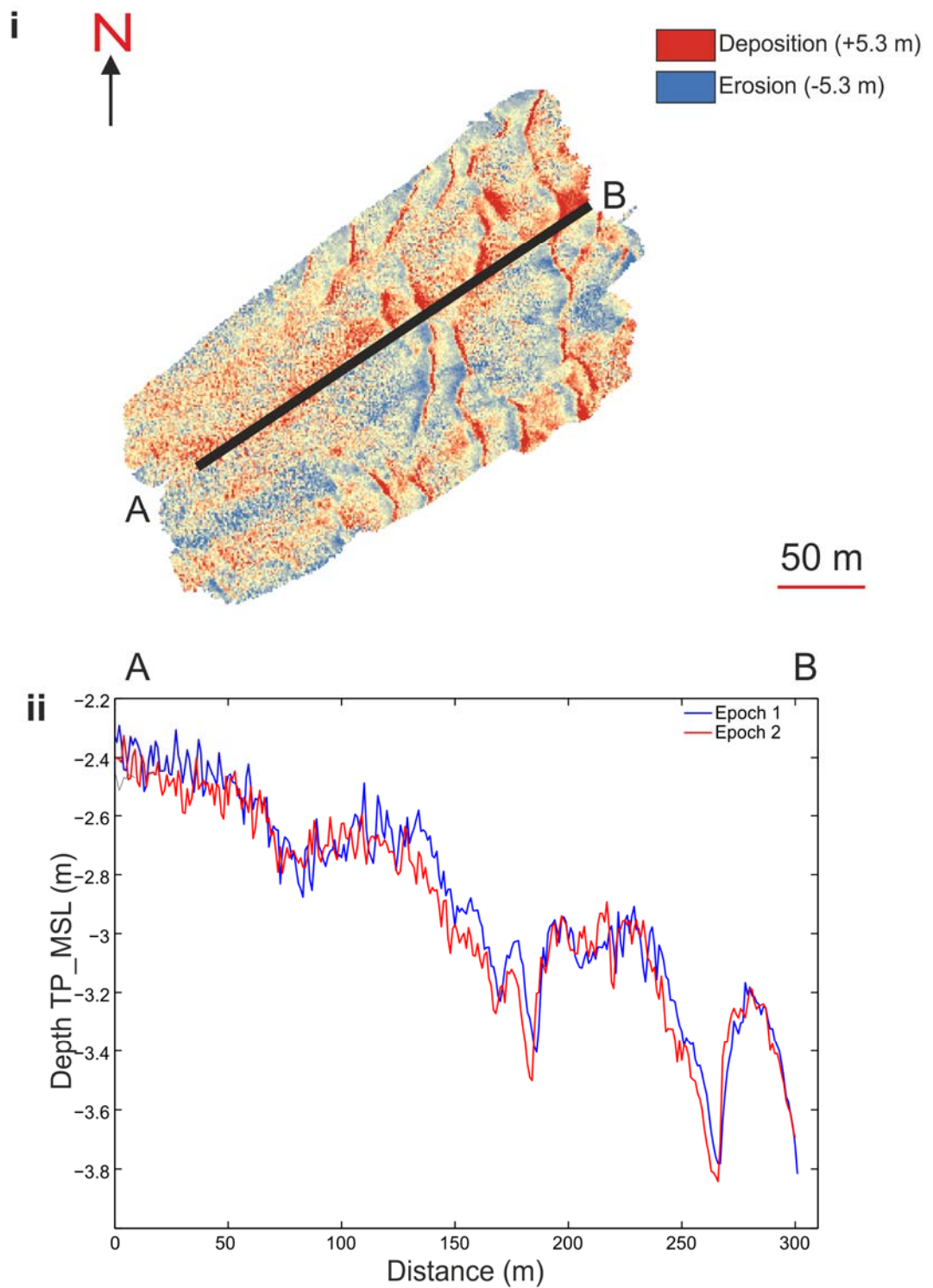


Figure 3.9 Plots to show erosion and deposition occurring between Epoch 1 and Epoch 2: **i)** Difference map created by subtracting Epoch 1 (Figure 3.7) from the repeat surface collected on Epoch 2 (Figure 3.8). Erosion and deposition scale by ± 5.3 m; **ii)** Profile collected along line A-B on figure i, showing development and seaward migration of bedforms from Epoch 1 to Epoch 2.

23.5 hours later, just before low water a third bathymetry measurement, Epoch 3, was collected. Again, this shows a similar pattern of bedforms to those seen in Epoch 1 and Epoch 2, with the section shallowing in a seaward direction and large dune crests present in the landward region (Figure 3.10). The difference plot shows that although there has been widespread erosion and deposition in the seaward region, with larger regions of deposition and erosion in the landward area (Figure 3.11i). The profile line shows that there has been widening and landward migration of dune troughs, but no change in dune height in the landward region, whilst deposition has occurred in the seaward region (Figure 3.11ii).

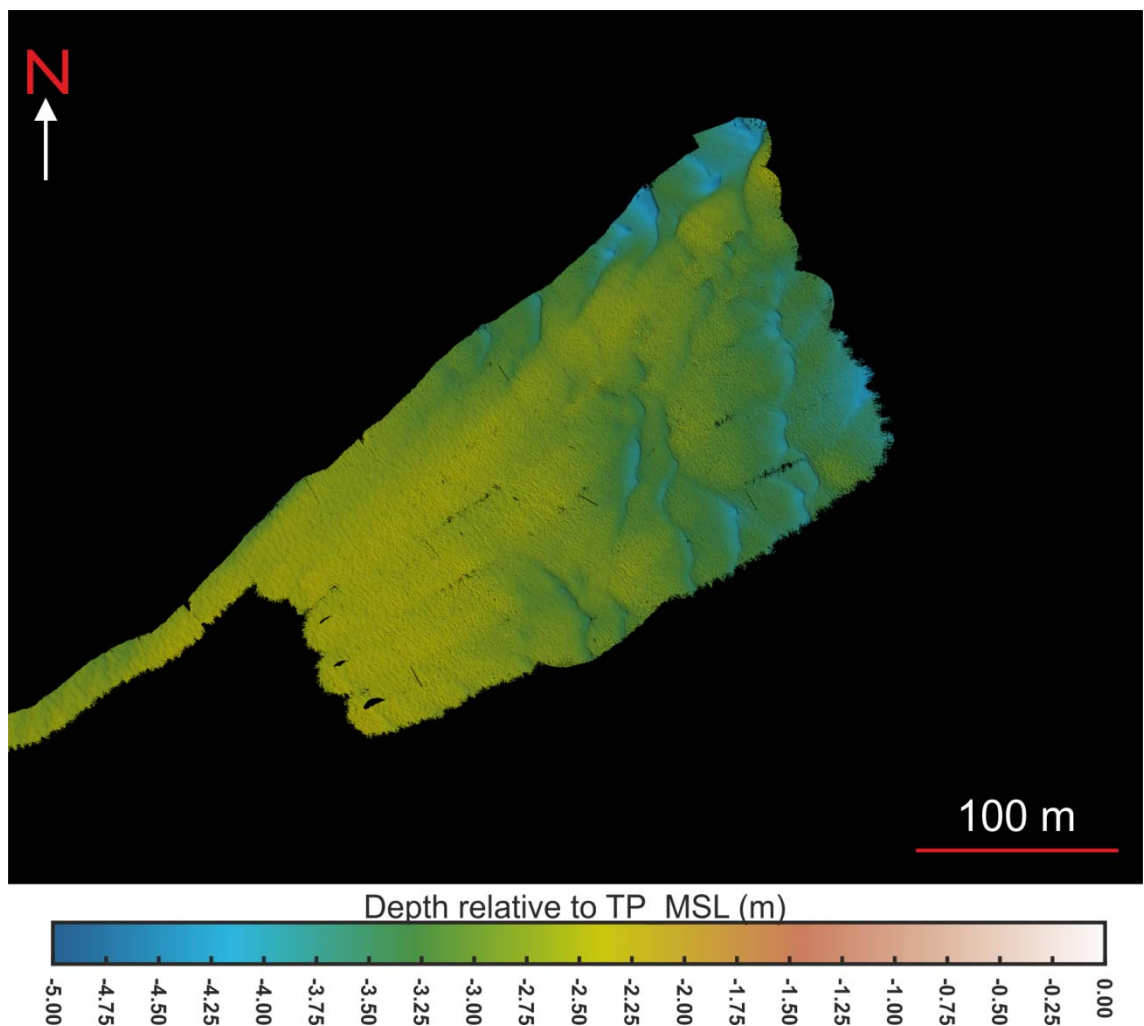
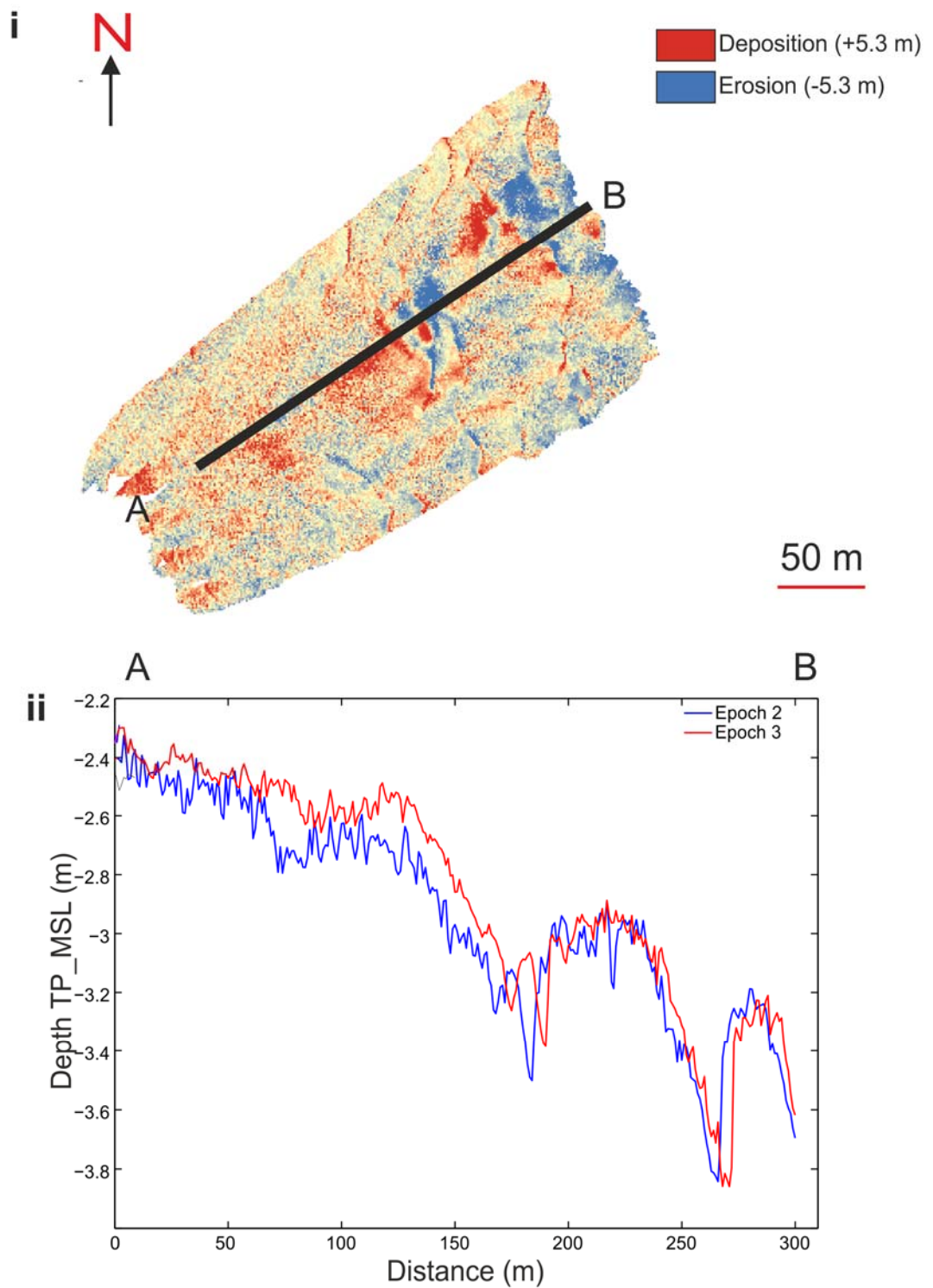


Figure 3.10 Repeat surface collected during Epoch 3. Fluvial flow is from the top right corner.

The final bathymetry repeat, Epoch 4, was carried out 94.5 hours later (4 complete tidal cycles) just before lower-high water. The smaller scale bedforms seen in the seaward region and superimposed on the large dunes at the landward end of the section have disappeared, forming a much smoother surface than seen previously (Figure 3.12). The larger bedforms are of a similar scale and morphology to the previous measurements.



The difference plot shows that there has been erosion of most of this surface, with erosion of the dune crests at the landward end of the surface (Figure 3.13i). The large-scale dunes at the landward end of the section have migrated seaward by up to 20 m, as seen in both the difference plot and the profile lines (Figure 3.13ii). Dune length has remained the same as has the crest height, although there has been erosion on the stoss side of the dune crests.

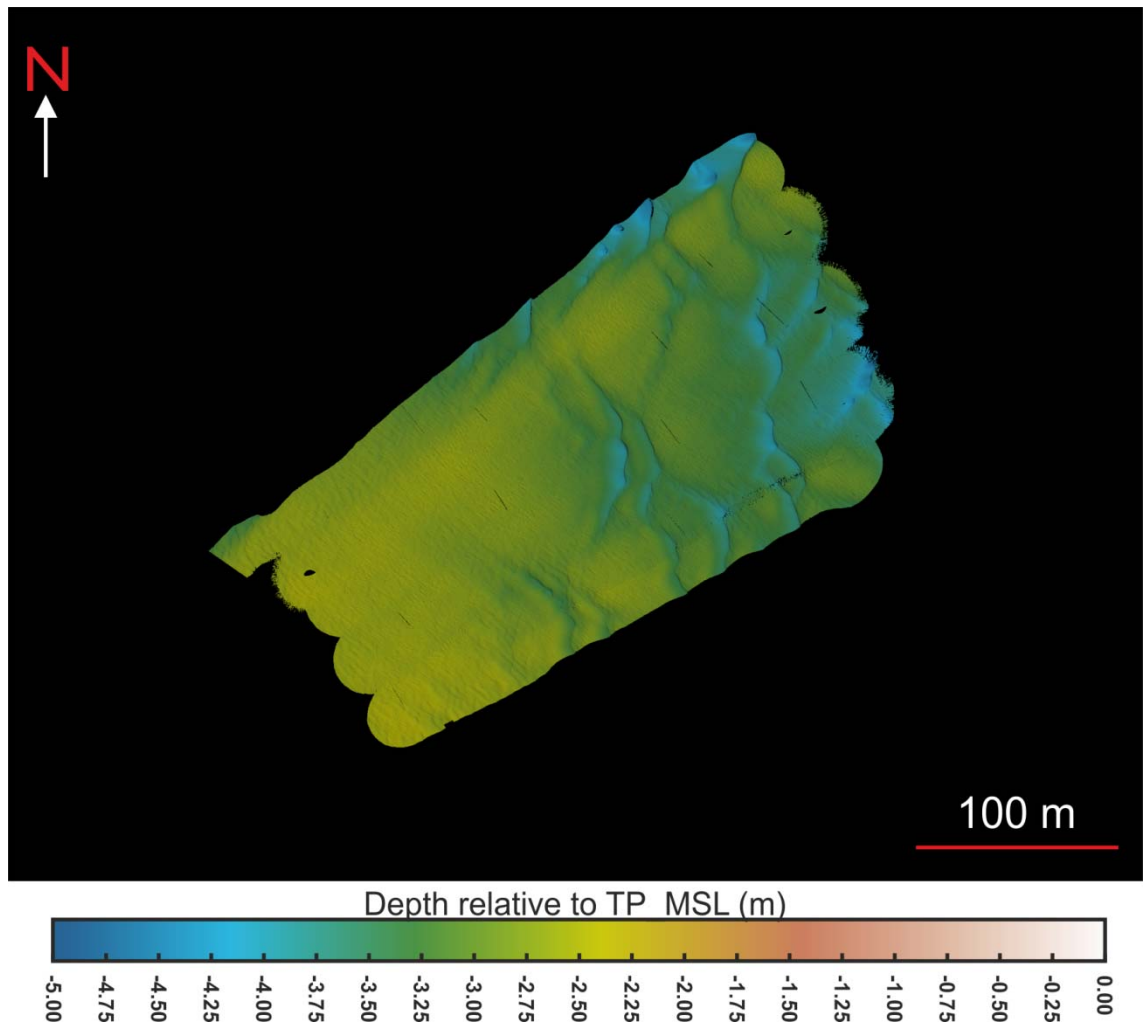


Figure 3.12 Repeat surface collected during Epoch 4. Fluvial flow is from the top right corner.

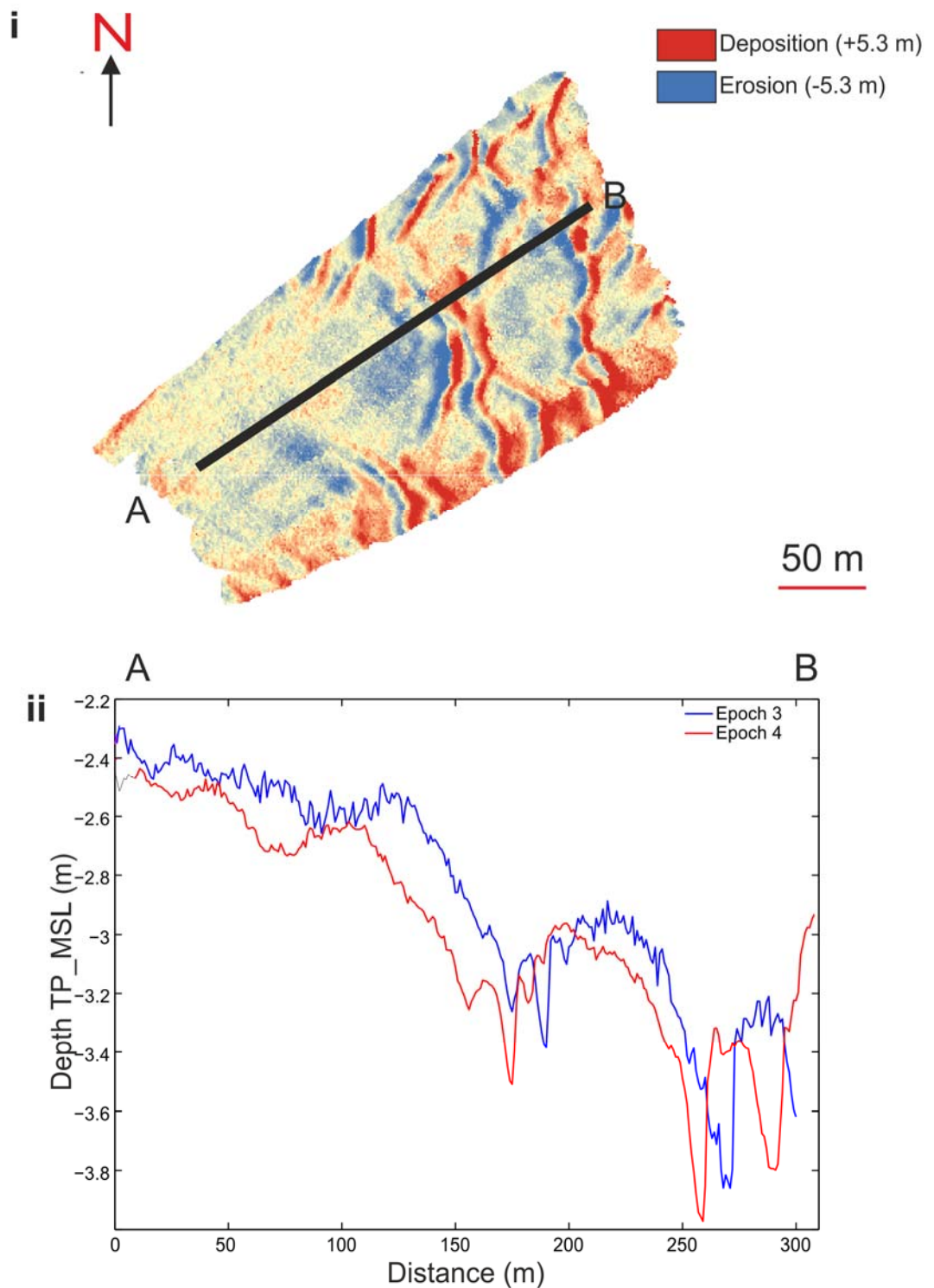


Figure 3.13 Plots to show erosion and deposition occurring between Epoch 3 and Epoch 4: **i)** Difference map created by subtracting Epoch 3 (Figure 3.10) from the repeat surface collected during Epoch 4 (Figure 3.12). Erosion and deposition scale by +/- 5.3 m; **ii)** Profile collected along line A-B on figure i, showing development and significant seaward migration of bedforms from Epoch 3 to Epoch 4.

3.3.3 Internal bar sedimentology

GPR imaging was made of the bar subsurface along several transects as part of the TIFZ project (NERC NE/H007954/1). The data presented here was processed and interpreted as part of that project. The maximum penetration of the GPR at this location was 8 m, comparable to the deepest MBES measurements made within the channel at the southwest of the bar (Figure 3.5). The GPR data shows that the surface of the bar is dominated by gently dipping horizons which thicken to ~4 m in the landward end at north-western edge of the bar (Figure 3.14). These are overlain by large-scale dunes at the eastern edge of the bar (WDX6), which show reactivation surfaces ~2 m below the present bar top. The western bar tail is formed of steep laterally accreting horizons, indicating bar migration to the west (WDX6, WDX12 and WDX13). The remnants of two channels <15 m wide and 2 m deep are observed at the landward end of the bar (WDX2 and WDX3). These channels are overlain by large-scale dune stratification and at the surface low angled smaller scale dune stratification. Four transects were also collected along the longitudinal axis of the bar (Figure 3.15). These reveal that the bar subsurface horizons are gently dipping in a seaward direction, with steep surfaces at the bar tail.

3.3.4 Relationship between flow and bar morphology

A series of ADCP cross-sections were collected around the bar throughout the tidal cycle to investigate the variations in flow patterns. These four cross-sections were located landward of the bar (Cross-section A), cross-cutting the bar (Cross-sections B and C) and seaward of the bar (Cross-section D). Their locations are shown on Figure 3.2.

i) Cross-section A

Cross-section A is the furthest landward of the data collected, upstream of the bar head and was fully submerged during all ADCP data collection (Figure 3.2). Four repeats of the data were collected ranging from lower-low water to just after lower-high water (Table 3.2; Figure 3.16). The cross-section is 1100 m in length and measures across the shallow bar head to the edge of the deeper channel in the east. Large bedforms are

Figure 3.14 (next page) GPR traces collected on Wood Bar. Yellow highlights indicate undulating reflections (large-scale dune stratification); orange highlights indicate low angled reflections (smaller scale dune stratification); blue highlights indicate sharply angled reflections (laterally accreting bar margin); purple highlights indicate concave reflections (channels). Green horizons highlight interpreted reactivation surfaces. Fluvial flow shown by black arrow.

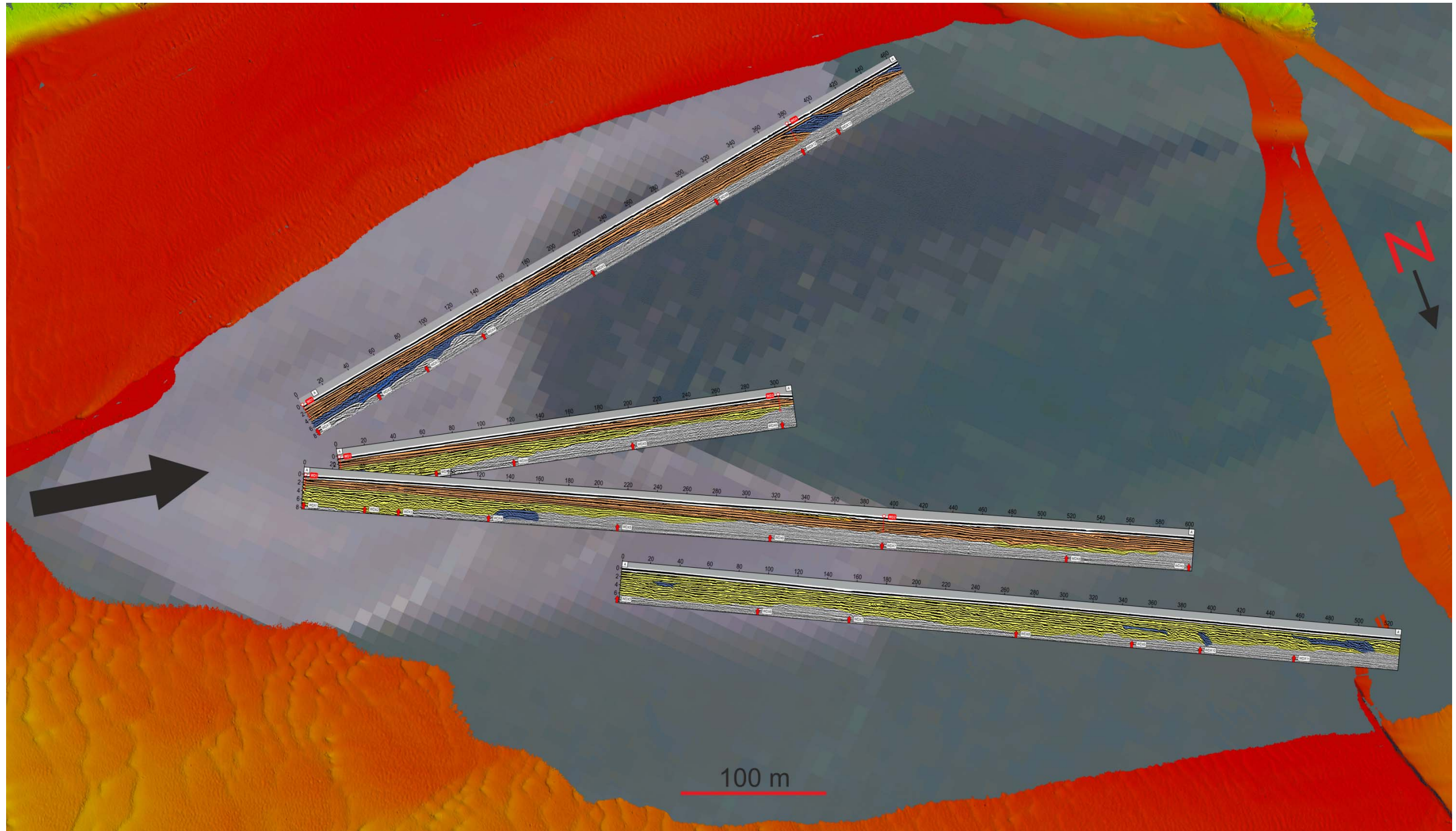


Figure 3.15 Longitudinal GPR traces collected on Wood Bar. Yellow highlights indicate undulating reflections (large-scale dune stratification); orange highlights indicate low angled reflections (smaller scale dune stratification); blue highlights indicate sharply angled reflections (laterally accreting bar margin); purple highlights indicate concave reflections (channels). Green horizons highlight interpreted reactivation surfaces. Fluvial flow illustrated by black arrow.

visible with heights of up to 2 m and wavelengths of up to 100 m. As the cross-section moves 1000 m from north-west to south-east it shallows by ~4 m until a deeper channel is reached at the south-eastern end of the cross-section, 5 m deeper and 50 m wide (Figure 3.16).

The lower-low water data (Trans019-Trans020) shows seaward flow with a maximum velocity of 1.0 ms^{-1} . The highest ebb velocities were observed in the flatter, central region of the cross-section upstream of the bar head. Lower velocities occur in the deeper channel to the east, with the lowest velocities (0.4 ms^{-1}) at the boundary between the flatter region and the deep channel (Figure 3.16i). There is strong secondary flow observed ($< 0.55 \text{ ms}^{-1}$), which diverges around the bar head, with strong flows towards each end of the cross-section (Figure 3.16v); this divergence occurs within a region 150 m wide in the centre of the cross-section (500-600 m from northwest edge), at a depth of ~6 m. This area is directly landward of the bar, as observed in Figure 3.2.

After lower-low water (Trans000) ebb flow velocities remain in a similar range, with velocities in the deeper channel increasing slightly to 1.22 ms^{-1} (Figure 3.16ii). Although the primary flow velocities show little change, secondary flow is much less uniform (Figure 3.16vi). Secondary flow velocities have increased to 0.65 ms^{-1} , the highest observed in any of the cross-sections measured. Whilst flow is still diverted around the bar head, smaller circulation cells have formed over the crests of the large-scale bedforms.

The third cross-section (Trans014) was collected before lower-high water. Seaward flow across the bar head has slowed to almost 0 ms^{-1} , with some localised patches of landward and seaward flow of up to 0.5 ms^{-1} occurring at the crests and troughs of the large-scale bedforms (Figure 3.16iii). Secondary flow is weaker than in the previous cross-sections, reaching a maximum of 0.22 ms^{-1} (Figure 3.16vii). There is little flow divergence observed, with flow across the bar top towards the eastern end of the cross-section. Some circulation cells similar to those present at the lowest low water measurements, but these are again much weaker.

The final cross-section (Trans037-Trans038) was collected following lower-high water, although due to the timings of cross-section measurements this tide was of a lower magnitude than the third repeat (Table 3.2). There is limited flow at this cross-section with some seaward directed flow of 0.24 ms^{-1} in the central region (Figure 3.16iv). There is also very little cross-stream flow measured (up to 0.1 ms^{-1}), with flow mainly directed to the west, with eastern flow corresponding to the downstream flow seen in Figure 3.16iv (Figure 3.16viii).

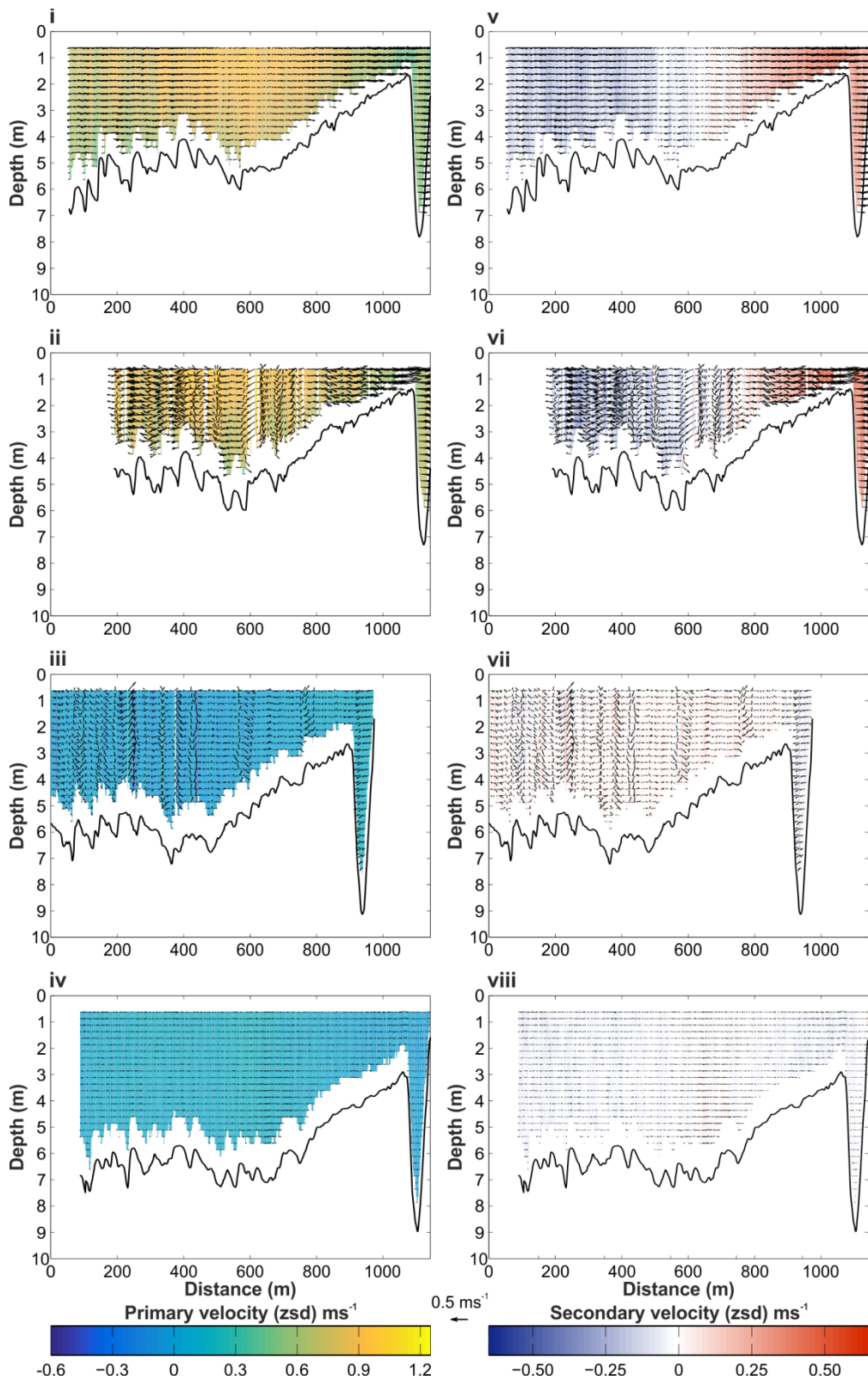


Figure 3.16 Flow data collected at cross-section A (located on Figure 3.2). Seaward flow is oriented out of the page: i & v) at lower-low water; ii & vi) after lower-low water; iii & vii) before lower-high water; iv & viii) after lower-high water.

ii) Cross-section B

300 m seaward of the first set of measurements, cross-section B measures the flow at the head of Wood Bar (Figure 3.2). Data was collected between lower-low water and just after lower-high water (Table 3.2; Figure 3.17). The total cross-section length is 1150 m and at low tides the bar is emergent at this point, as seen in the two sets of partial cross-sections (Figure 3.17i-iv & vii-x).

The lower-low water repeats (Trans021-Trans022 and Trans026) have 200 m of emergent bar between the measurement sections (Figure 3.17i-ii). Flow is in a seaward ebb direction, ranging from 0.2 – 1.0 ms⁻¹, with higher velocities observed in the deeper channel (Figure 3.17i-ii). Secondary flow is slower than observed at cross-section A, with flow <0.2 ms⁻¹ across the bar head and <0.35 ms⁻¹ within the deeper channel (Figure 3.17vii-viii). This secondary flow is diverted by the large bedforms (<100 m in length) in the western section, with flow diverted westward over the crests of the bedforms and small regions of flow diverted to the east in the bedform troughs (Figure 3.17vii). Within the deeper channel a small region of recirculation is visible, with flow appearing to drain into the deeper channel off the bar top (Figure 3.17viii).

Midway between lower-low water and lower-high water the second repeat was collected (Trans005-Trans006 and Trans003). This repeat again shows a region of emergent bar (Figure 3.17iii-iv). Flow velocities in the deeper channel are of a similar magnitude to those seen in the first transect (Figure 3.17iv). In the larger transect to the west seaward flow velocities have slowed to 0.4–0.6 ms⁻¹ (Figure 3.17iii). Secondary flow was stronger during these measurements (<0.44 ms⁻¹), again showing some small regions of recirculation around bedform crests, but no regional flow patterns (Figure 3.17ix). Within the eastern channel the flow again shows a weak recirculation cell (Figure 3.17x).

The repeat collected at the lower-high water (Trans015-Trans016) measures the complete cross-section width as the bar has been sufficiently submerged to allow a survey (Figure 3.17v). Flow is still in a seaward direction (<0.4 ms⁻¹), with some small regions of flow reversal at the base of flow towards the western end of the section and localised flow variations over bedform crests (Figure 3.17v). Secondary flow velocities, of a similar magnitude to lower-low water (0.17 ms⁻¹), also show these localised flow variations, but reveal the flow diverging around the barhead seaward of the cross-section (Figure 3.17xi). This flow divergence occurs 750 m from the north-west end of the section, where there is a 1 m drop in the height of the bed. Comparison to the bathymetry data in Figure 3.5 shows that this drop in height marks the southern edge of the bar top.

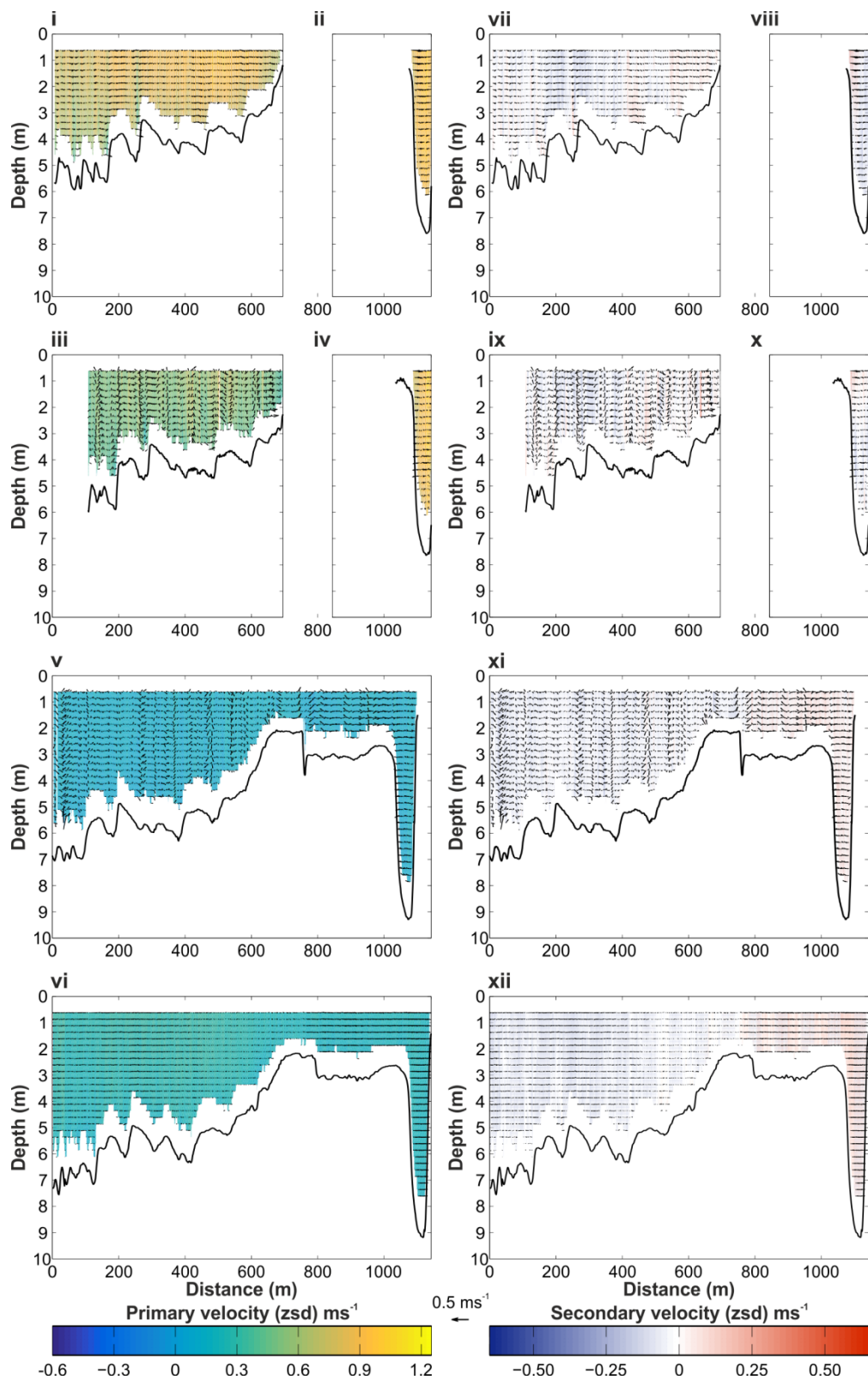


Figure 3.17 Flow data collected at cross-section B (located on Figure 3.2). Seaward flow is oriented out of the page and the barhead is emergent at low water: i & vii) Lower-low water across bar; ii & viii) Lower-low water in eastern channel; iii & ix) midway between lower-low water and lower-high water across bar; iv & x) midway between lower-low water and lower-high water in the eastern channel; v & xi) lower-high water; vi & xii) after lower-high water.

The final repeat was collected at just after lower-high water (Trans039-Trans40), and shows seaward velocities of a similar magnitude to those at lower-high water ($<0.35 \text{ ms}^{-1}$), although there are no regions of flow reversal (Figure 3.17vi). Secondary flow velocities are also of a similar magnitude to lowest high water ($<0.15 \text{ ms}^{-1}$) and again show divergence around the bar head, but there is very little interaction with the bedforms in the cross-section (Figure 3.17).

iii) Cross-section C

250 m seaward of cross-section B, this cross-section measures the flow either side of the fully emergent bar (Figure 3.2; Figure 3.18). The western sub-section is 600 m in length and measures flow across the bar edge, whilst the smaller eastern sub-section measures flow in the 100 m wide eastern channel.

At lower-low water measurements were made at the western subsection (Trans023-Trans025). Flow was in a seaward direction with flow velocities of $0.4\text{-}1 \text{ ms}^{-1}$ observed (Figure 3.18i). Secondary flows of $<0.21 \text{ ms}^{-1}$ were measured, with flow in the flatter region to the east of the subsection ($\sim 3 \text{ m}$ depth) in a westerly direction whilst flow direction was reversed over the deeper bedforms at the west of the section (Figure 3.18v). The deeper eastern channel was measured after lower-low water (Trans029). Flow velocities were of a similar magnitude to those measured on the bar edge, with the greatest flow velocities at the eastern edge of the channel (Figure 3.18ii). Secondary flow velocities were stronger within the channel ($<0.36 \text{ ms}^{-1}$) and show recirculation as flow enters the channel from the bar top (Figure 3.18vi).

Midway between lower-low water and high water (Trans033-Trans034) a second set of measurements were made across the western bar edge. Flow was still in a seaward direction, although it had slowed from the previous measurements ($0.2\text{-}0.7 \text{ ms}^{-1}$), with the highest velocities observed near to the surface in the across the flatter central region (Figure 3.18iii). Secondary flow has also decreased (0.17 ms^{-1}), but shows the same flow pattern as at lowest low water (Figure 3.18vii). Before lower-high water the eastern channel repeat was collected (Trans011-Trans012). Primary flow within the channel has slowed to almost 0 ms^{-1} (Figure 3.18iv), but a weaker version of the secondary flow cell previously observed is visible (Figure 3.18viii).

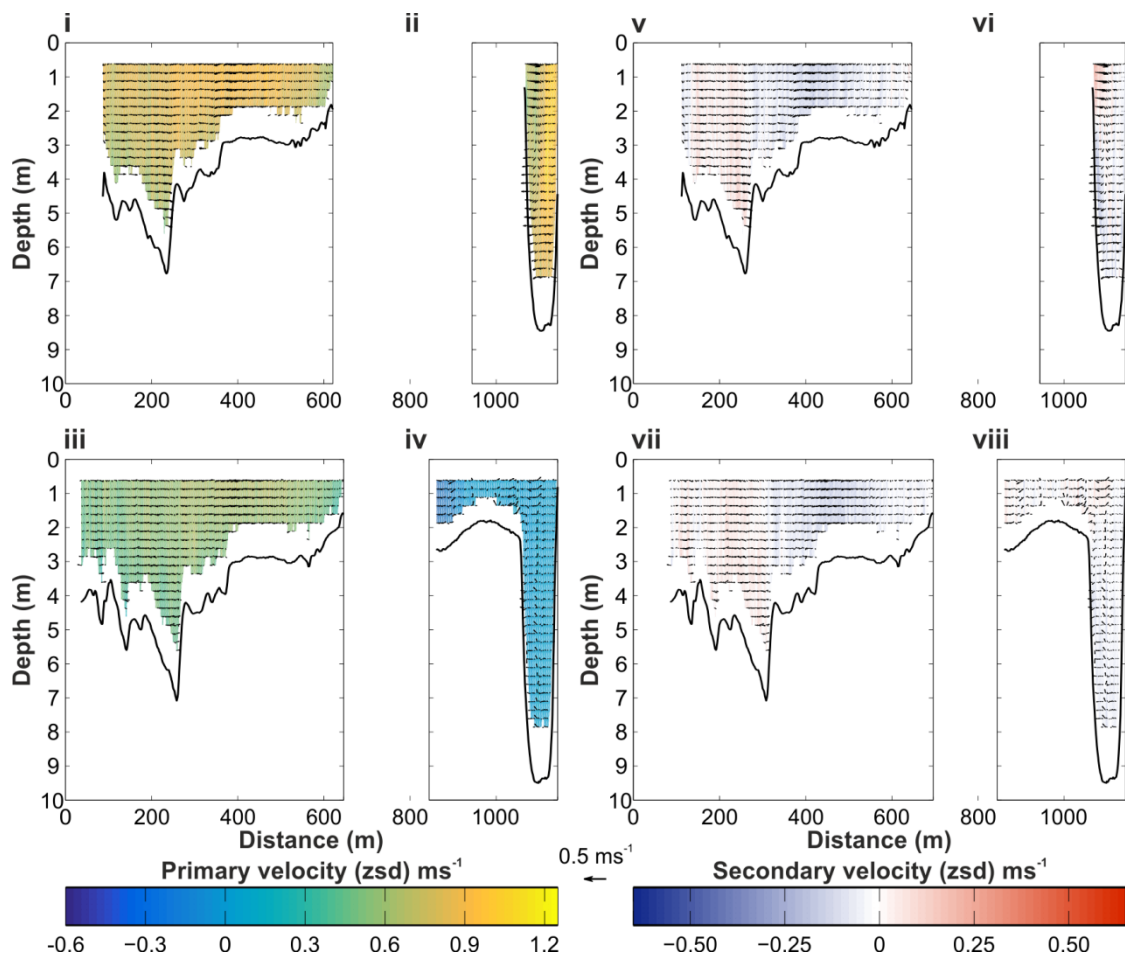


Figure 3.18 Flow data collected at cross-section C (located on Figure 3.2). Seaward flow is oriented out of the page and the barhead is emergent at low water: i & v) Lower-low water across the bar; ii & vi) after lower-low water in the eastern channel; iii & vii) midway between lower-low water and high water across the bar; iv & viii) before lower-high water within the eastern channel.

iv) Cross-section D

The final cross-section was measured at the seaward end of the emergent region of Wood Bar, from just after lower-low water to lower-high water (Table 3.2; Figure 3.19). The cross-section is 1100 m in length measuring across the tail end of the bar, marked by a 600 m wide relatively flat region (~4 m deep) in the centre of the cross-section, with deeper channels (<4 m below bar surface) at each end; to the west the channel is 300 m wide, whilst in the east the channel is 200 m wide. Comparison to the bathymetry in Figure 3.5 shows that this cross-section is seaward of the main bar top.

The repeat collected just after lower-low water (Trans031) shows strong seaward flow in both channels, with higher velocities seen in the eastern channel (<1 ms⁻¹). On the shallower bar surface, flow slows to 0 ms⁻¹ before reversing in the central region (500-650 m from north-west edge of cross-section) to show landward flow of 0.15 ms⁻¹ (Figure 3.19i). Within the two channels there is lateral secondary flow (<0.5 ms⁻¹)

towards the bar surface (Figure 3.19v). On the bar surface itself the direction of secondary flow reverses and the velocity decreases, forming two flow cells.

The second repeat was collected midway between lower-low water and lower-high water (Trans035). There is reduced seaward flow within both channels (0.74 ms^{-1} maximum), but the same pattern of slowing and reversed flow in a landward direction on the bar surface (Figure 3.19ii). The region of reversed flow at the centre of the cross-section has increased in velocity ($<0.25 \text{ ms}^{-1}$) and shifted slightly to the east as the central region has deepened. The secondary flow maintains a similar orientation to the lowest low water repeat, with the boundary between the two flow cells shifting to the east as in the primary flow reversal (Figure 3.19vi), although the maximum secondary velocity observed is only 0.31 ms^{-1} .

The third repeat was collected just before lower-high water (Trans010). The dual flow cells observed within the first two repeats are again found in these measurements (Figure 3.19iii). The region of reversed, landward directed, flow is now centred at 750 m from the north-west edge of the cross-section and has widened to 250 m; the associated region of no flow now extends halfway across the eastern channel, with seaward flow only observed within the eastern 150 m. Within the two channels, flow remains in a seaward direction with velocities $<0.4 \text{ ms}^{-1}$. The maximum secondary flow velocities are slightly higher than in the previous measurement (0.36 ms^{-1}), but secondary flow velocities are lower throughout the section (Figure 3.19vii).

The final repeat was collected at lower-high water (Trans017). This shows similar velocities in the channels, in some areas slowing to almost 0 ms^{-1} , but no flow reversal on the bar surface, where flow slows to 0 ms^{-1} (Figure 3.19iv). Secondary circulation shows divergence within both deeper channels, whilst also showing flow toward the centre of the bar top (Figure 3.19viii).

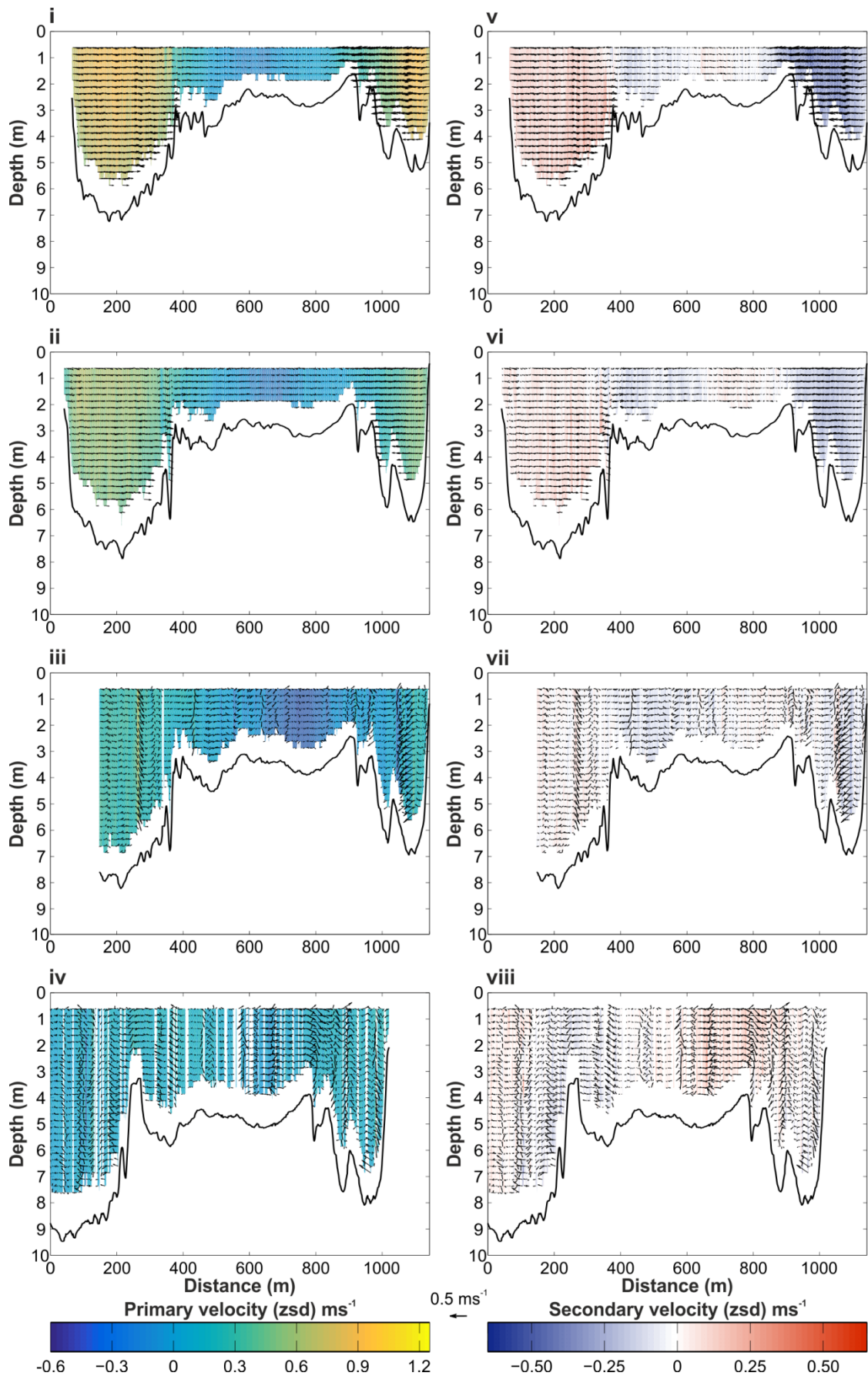


Figure 3.19 Flow data collected at cross-section D (located on Figure 3.2). Seaward flow is oriented out of the page: i & v) after lower-low water; ii & vi) midway between lower-low water and lower-high water; iii & vii) before lower-high water; iv & viii) lower-high water.

3.4 Discussion

Detailed bathymetry, GPR and flow measurements were made around a fluvially-dominated bar in a region of tidal influence. This revealed variations in bedform morphology associated both with the location of the barform and the general channel planform. Examination of flow patterns around the barform showed steering around the edges. Variations in flow arising from tidal and fluvial flow have resulted in variations in bedform orientation, with alignment varying with bedform scale.

3.4.1 Bedform morphology

The bathymetry measurements revealed two distinct bedform patterns: large-scale dunes oriented NE-SW (macroscale) and smaller scale dunes (mesoscale) oriented NW-SE (Figure 3.20). Superimposed on dune crests throughout the bathymetry measurements are smaller scale dunes (microscale) whose orientation does not necessarily match the larger bedforms. Macroscale longitudinal dunes were found in the landward region of the surveyed section, aligned roughly NE-SW, which had crest separations of up to 200 m and crest heights of 1.5 m. Cross-cutting these crests are sinuous dunes with a NW-SE orientation; the dune crests are highlighted in Figure 3.20. The macroscale dune features have formed with crests oblique to the local flow patterns and matches the orientation of dunes further landward within the same channel (Figure 2.25). The cross-cutting mesoscale dune crests are oriented with the local flow around the bar, showing the adaptation of sediment transport to the local topographic conditions. Although the bar is a significant feature within Prairie Channel the orientation of these mesoscale dune crests does not show any significant steering around the barhead. However, topographic forcing of the flow is clearly shown when the combination of bedform scales is considered.

The macroscale dunes located landward of the bar are revealed by GPR to extend underneath the bar itself (Figures 3.14-3.15). Large-scale dune stratification is observed underlying the landward region of the bar, with orientations appearing to correspond to the macroscale dune crests. At the eastern edge of the bar steep lateral accretions correspond to the bar edge, with a similar angle and morphology to the bar edge observed in the bathymetry measurements adjacent to them. Smaller-scale dune stratification corresponds to the bar top bathymetry observed adjacent to the bar limbs. In the western bar tail limb the large-scale dune stratification is found throughout; within the eastern limb lower angled beds are observed with steep accretions at the edges. The longitudinal GPR traces reveal the uppermost horizons are sub-horizontal, but appear to dip in a seaward direction.

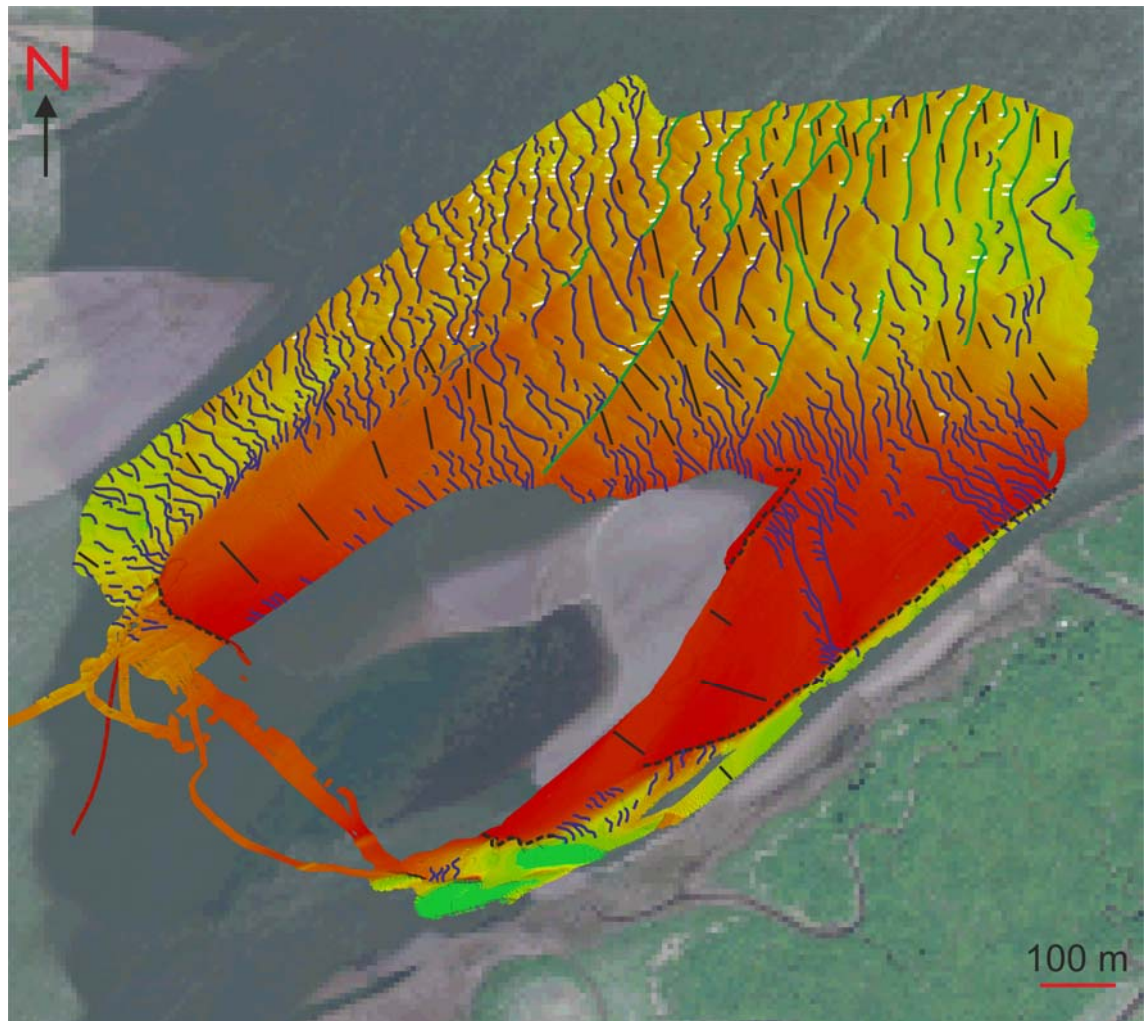


Figure 3.20 Crestlines of bedforms observed within the bathymetry data at Wood Bar; fluvial flow is from top right corner of the image (shown by black arrow). Green lines highlight macroscale crests which are oriented perpendicular to flow from within the channel to the south of Sandee Bar (not yet adjusted to presumed local flow); blue highlights main mesoscale dune crest orientation, consistent with flow in this area; black dashed lines highlight sharp changes in bathymetry at the edge of the bar top; black lines highlight dominant crest lines of microscale superimposed bedforms; white highlight dune spurs.

The bathymetry survey reveals that in the landward region of the Wood measurement zone straight crested longitudinal features are observed in the lee of both macroscale and mesoscale main bedforms at an oblique angle to the crestline. Up to 20 m in length, they are smaller in height than the adjacent larger dunes (Figure 3.20). These dune spurs were described by Allen (1982), where they were noted to have a variable profile and most commonly lie downstream of saddles on crest lines (Figure 3.21). Spurs are also found at other locations studied in the Columbia River, such as within the main Prairie Channel section, where they have a symmetrical profile and are oriented parallel to the main flow (and normal to the adjacent dune crests) in the channel as it moves around the bend (Figures 2.23-2.24).

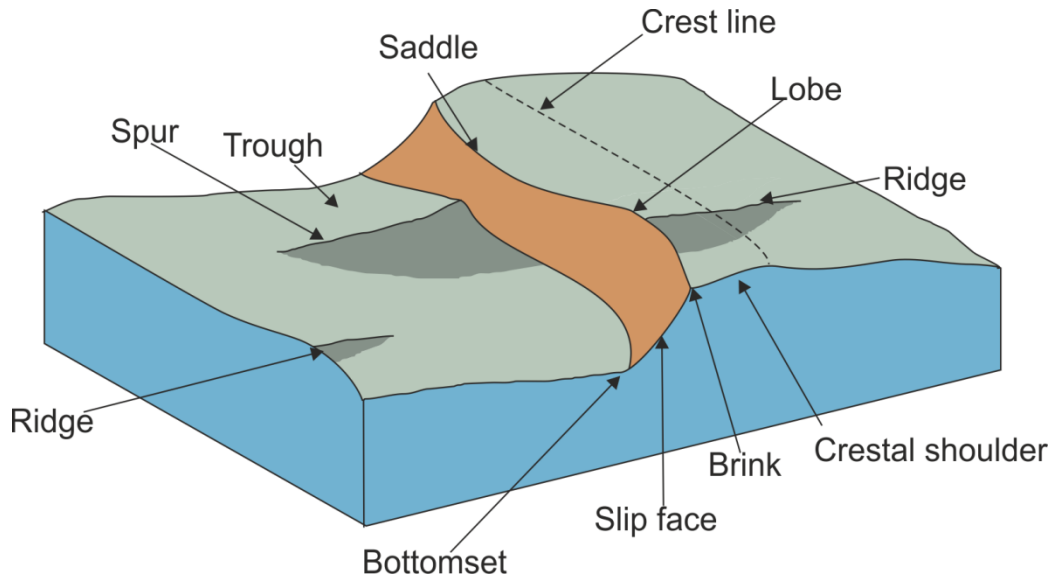


Figure 3.21 Morphological features of transverse bedforms (redrawn from Allen, 1982).

The general orientation of the spurs within the section studied at Wood Bar is neither normal to dune crest orientation nor parallel to the fluvial flow direction. They are found in the lee of both the largest scale longitudinal crests and the smaller crests and are found adjacent to both lobes and saddles. The orientation of large-scale dune crests in this region has already been noted to have an orientation inherited from further landward within the channel. Dalrymple and Rhodes (1995) suggest that spur orientation will lie parallel to the local flow direction. In the present location spur orientations can be split into three distinct groupings: i) in the eastern region, where flow enters the bathymetry measurement zone, spur direction reflects this incoming flow and has not yet adjusted to the local barforms (oriented east-west); ii) in the central region spur orientation indicates flow to the west of Wood Bar (oriented northeast-southwest); iii) in the northern region spur orientation suggests flow to the west, which would indicate flow into the channel which lies to the north of the second bar shown in Figure 3.20. At the northern end of the Wood bathymetry there is an overlap with the region of data collection made at Sandee during FS1, measuring 1 km by 100 m (Figure 2.25i). During the FS1 data several of these spurs were present in the same region, but not in the same number as during the Wood collection in FS2.

Cross-sectional profiles of the features collected normal to the crestline of the spur high reveal a large number of them to have an asymmetric shape (Figure 3.22). These spurs appear to be composed of highly mobile sediment which has been transported off dune crestlines, as is seen in the bathymetry at the Prairie Channel section. This available sediment has been preferentially reworked by tidal currents within this area,

representing the only landward oriented bedforms in the Wood measurement zone. As noted previously these dune spurs have been described within both fluvial and tidal environments, but are noted as forming parallel to flow. This location is unusual as flow is undergoing topographic steering, with fluvial flow and tidal flow not occurring parallel to each other. During periods of fluvial flow sediment is transported in a seaward direction into the trough of the large dunes where it is sheltered and does not undergo further transport. During periods of (much weaker) tidal flow this sediment is no longer sheltered and is instead transported along the “channels” formed by the dune troughs, forming asymmetrical spurs which have an asymmetrical profile. This results in a bi-directional pattern of bedforms, with large-scale fluvial dominance; the asymmetrical profiles of these secondary bedforms are the only indicators of tidal flow within this region.

Superimposed on top of both macroscale and mesoscale dune crests are smaller bedforms (microscale) up to 5 m in length with heights of <0.2 m. The crest orientations of these bedforms vary with position around the bar, with crest alignments north-south at the northern end of the bathymetry measurements, becoming more northwest-southeast as fluvial flow is steered around the bar (Figure 3.20). These superimposed bedforms are found at a range of depths throughout the bathymetry measurements but are never associated with dune spurs, even in regions where they are

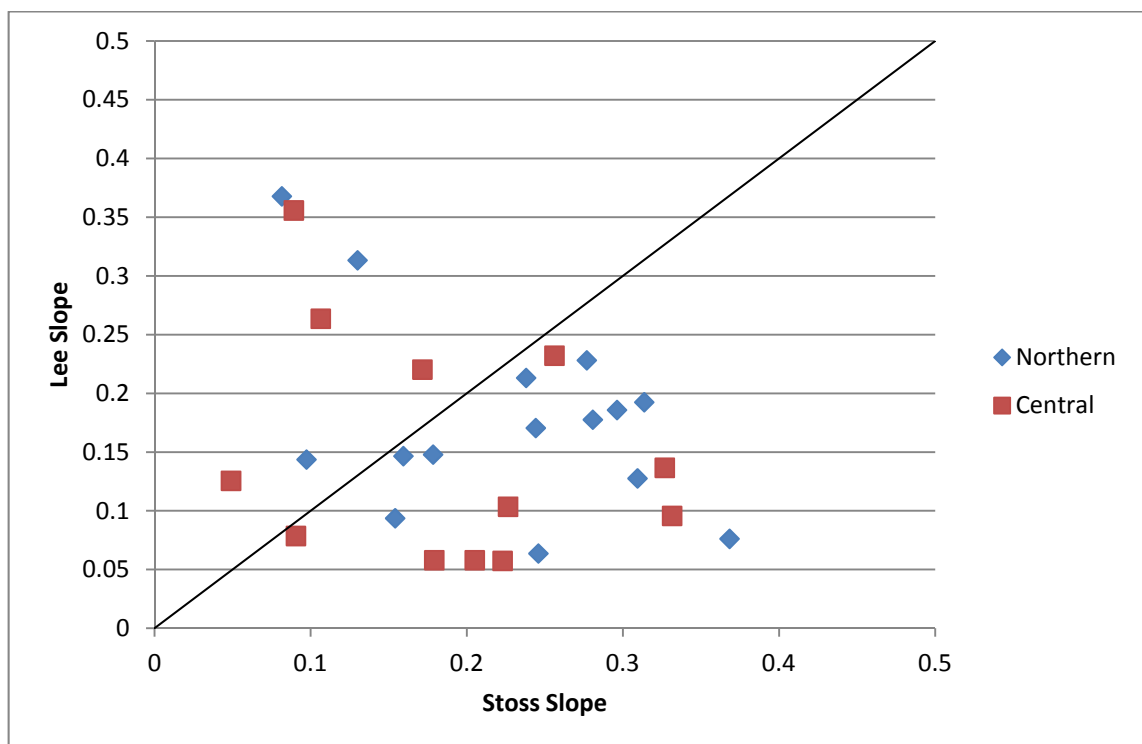


Figure 3.22 Spur asymmetries, showing variations in slope asymmetries. Central region is directly landward of the barhead, whilst northern region lies at the north of the bathymetry measurement zone.

of a comparable depth to the adjacent dune stoss slope. The superimposed microscale bedforms are aligned to the dominant fluvial current and topographic steering around the large barform. The cross-bedding arising from these compound bedforms will illustrate the variations in channel geometry through the bathymetry section; again, the spurs are shown to be sheltered from fluvial flows and are tidally modified in this zone.

3.4.2 Bedform migration

In addition to the main bathymetry survey, repeated surveys were made at a smaller subsection to investigate the rate and form of bedform migration at Wood Bar (Figures 3.7, 3.9, 3.11 and 3.13). The section selected for repeated bathymetry surveys had a depth of -2.6 m TP_MSL and contained both mesoscale and microscale bedforms (location shown in Figure 3.2). The bedforms observed during all surveys are of a similar size and distribution, with compound dunes composed of large-scale bedforms and smaller superimposed dunes. The central profile transect shows that between Epochs 1 and 2 there has been migration of the large bedforms in a seaward direction (Figure 3.9). Comparison of the transect profiles of Epochs 2 and 3 reveals that there has again been migration of the large bedforms, but this has occurred in a landward direction (<5 m). The shape of the main bedforms does not differ greatly from the previous repeats, with seaward oriented crests and the surface elevation varied by only 0.2 m across the profile section. This landward migration is concentrated at the centre of the repeated measurement section, with seaward migration occurring at the edges of the section. The height data collected at the Tongue Point gauge shows that the survey

Table 3.3 Mean discharges collected at the Beaver Army Terminal river gauge (USGS 14246900).

| Date | Mean discharge (m ³ s ⁻¹) |
|------------|--|
| 21/05/2013 | 12783909 |
| 22/05/2013 | 12466077 |
| 23/05/2013 | 12748594 |
| 24/05/2013 | 13560832 |
| 25/05/2013 | 13419573 |
| 26/05/2013 | 13172371 |
| 27/05/2013 | 13207685 |
| 28/05/2013 | 13490203 |
| 29/05/2013 | 13702091 |
| 30/05/2013 | 13454888 |
| 31/05/2013 | 13031112 |
| 01/06/2013 | 12395448 |
| 02/06/2013 | 11230064 |
| 03/06/2013 | 10629715 |

was collected prior to low water, following a period of relatively high water. However, the mean discharge measured at the Beaver Army Terminal river gauge (Table 3.3) was the highest recorded during the survey period.

The surface of the final repeat, Epoch 4, whilst still containing large-scale bedforms, has a different appearance to the other repeats. The surface has been extensively scoured, by up to 0.5 m in some locations, resulting in the removal of the smaller superimposed bedforms. The largest scale bedforms (40 m crest separation) have migrated up to 20 m seaward during the 94.5 hours since the previous measurements. The bed profile in Figure 3.13, shows the erosion of the surface, with some reforming of smaller bedforms ~0.2 m in height. Discharge data collected at the USGS gauge at Beaver Army Terminal (Gauge 14246900) shows that generally flows in the Lower Columbia River were high in late May to early June. However, the period between the final two repeat sections (29/05/2013 and 02/06/2013) shows a decrease in mean discharge (Table 3.3).

A series of profiles were made along a central transect, which are shown in Figure 3.23. This shows the evolving bed surface along a single transect line. A large dune trough can be observed at ~180 m landward of the profile start point. This trough can be observed to migrate at varying rates between the different measurements. Migration is generally in a seaward direction, although there appears to be some landward migration between Epochs 2 and 3 (Table 3.4). Comparison of dune crestlines between the repeats shows that dune migration occurs at differing rates across the measurement surface (Figure 3.23ii). Within the central region dunes have migrated upstream, whilst at the edges of the section they have migrated very little or stayed in the same position. Comparison of the bathymetry data shows that the bar has extended into the channel to the north west of the main bar (Figure 3.11).

Dune migration rates have previously been collected within regions of tidal influence. Surveys collected every two weeks in the Avon Estuary, Devon, UK, dune migration in a seaward direction, attributed to fluvial dominance at the survey location (Masselink *et al.*, 2009). Comparison of Epochs 1 and 4 in the present data would also reveal the same sense of bedform migration. However, this masks the intermediary landward migration which occurred between Epochs 2 and 3. Multiple bathymetry measurements were made by Nittrouer *et al.* (2008) within the lower Mississippi River, where there is limited tidal influence, to analyse bedform transport rates, finding migration of dunes in a seaward direction. Again, any tidal influence and possible landward migration of dune crests again may have been missed between surveys. Although net migration in all three locations is in a seaward direction the internal morphology of the dunes will be more complicated due to the short period of landward migration. These fluviially-

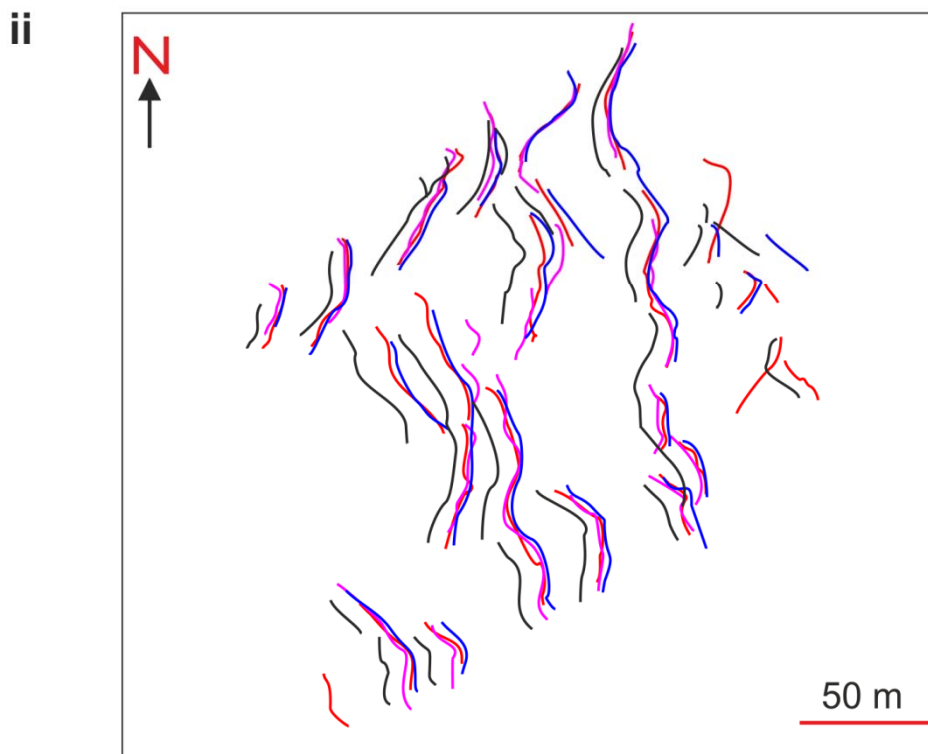
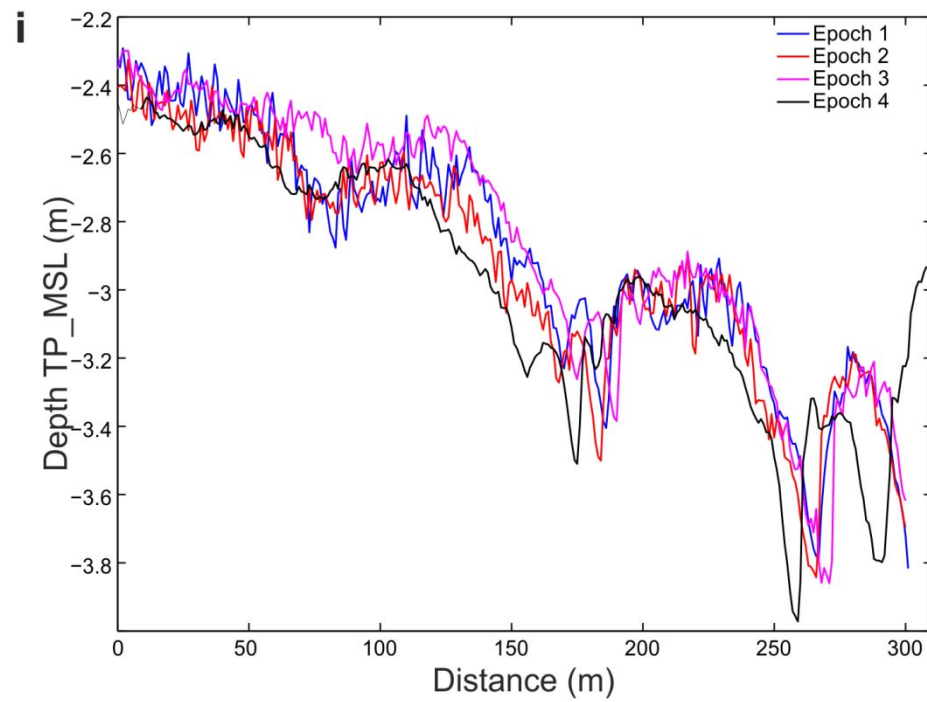


Figure 3.23 Dune crest migration at the repeat bathymetry location (Location shown in Figure 3.2): i) central bathymetry profiles (0 m is at landward end of profiles); ii) variations of crestline locations (fluvial flow from top right of image).

Table 3.4 Trough migration rates along central transect profile.

| Profiles | Migration | | |
|---------------------------|--------------|-----------|---------------|
| | Distance (m) | Direction | Rate (m/hour) |
| Epoch 1 to 2 (18 hours) | 1.66 | Seaward | 0.09 |
| Epoch 2 to 3 (23.5 hours) | 5.64 | Landward | 0.25 |
| Epoch 3 to 4 (94.5 hours) | 14.59 | Seaward | 0.15 |

dominated bedforms appear to undergo very little tidal modification, and net transport does occur in a seaward direction, when in fact there is a significant landward transport component which has been masked. The variable migration observed within a region only 150 m wide further highlights the difficulties in reconstructing tidal and fluvial influence, with tidal influence only observed within isolated sections.

Examination of the varying sizes of bedforms observed within the measurement zone reveals apparently different degrees of tidal modulation. The microscale bedforms recorded were superimposed on both mesoscale and macroscale bedforms to form compound dunes. These microscale bedforms, and the dune spurs observed within troughs, were found to be highly modified by tidal flows. The mesoscale bedforms, although aligned to the local fluvial flow, do not show much evidence of tidal influence although migration in a landward direction was observed in the repeated section. The macroscale bedforms within the measurement zone have not yet re-oriented to the local fluvial flow direction, instead maintaining a morphology linked to the landward channel; there is no evidence of tidal modification in these bedforms. As such, when bedform scale increases any evidence of tidal influence becomes lost. Within the context of the measurement zone the bedforms showing evidence of tidal influence are small and localised, reducing the likelihood of any evidence being recorded within geophysical surveys, where only the larger scale bedforms are observed (Figures 3.14-3.15), or within any sedimentary cores. The already subtle signatures of tidal modulation within systems such as this are therefore highly likely to be missed, leading to inaccurate reconstructions when using existing facies models (e.g., Dalrymple and Choi, 2007; van den Berg *et al.*, 2007).

3.4.3 Flow patterns

To investigate the interaction of flows with both the barform and the local bedforms, flow measurements were made at four cross-sections across the tidal cycle. At low water flow is aligned to the local channel, from the northeast and can be seen to diverge around the bar into the two deeper channels. The cross-cutting smaller dune crests observed in the bathymetry measurements are aligned to this local flow pattern (Figure 3.5). The western edge of cross-section C is located landward of the barform forming the edge of the western channel (Figures 3.2 and 3.19). Flow can be seen to divert

around this barhead, in a manner which aligns to the bedform steering observed in the bathymetry data. A helical flow cell is observed within the deeper channel to the east of the bar during low water at cross-sections A, B and C (Figures 3.16-3.18), with flow into the channel from the bar top. However prior to lower high water when flow begins to slow and at lower high water when flow is reversed this secondary circulation cell weakens and is replaced by linear flow to the east. Landward of the bar this channel is curved, which has probably induced the circulating cell; seaward of the bar the channel is straighter, so any induced circulation effects have weakened when the bar channel is reached. McLelland *et al.* (1999) examined the flow patterns around a fluvial braid bar and found that flow occurred parallel to the bar edges with no helical circulation cells, although cross-bar flow was observed. Similar flow patterns were observed by Parsons *et al.* (2007) within channels surrounding a fluvial bar, finding that flow steering occurring at the base of the channel is transmitted throughout the flow depth, rather than inducing a helical cell. At the present bar helical circulation is only observed within the narrow deep channel which continues from the landward section at Sandee (Figure 2.25ii) and has a curved planform.

In addition to flow steering effects around the barform itself, flow is also seen to be diverted by the bedforms surrounding the bar. At cross-section A, the most landward location flow just before lowest high water has slowed considerably to $\sim 0 \text{ ms}^{-1}$, but occurs predominantly in a seaward direction (Figure 3.16iii). However there are vertical regions of stronger landward ($< 0.5 \text{ ms}^{-1}$) and seaward ($< 0.45 \text{ ms}^{-1}$) flow found within the section, associated with stronger secondary and vertical flow patterns. These flow variations are associated with the underlying bed topography, with landward, downwelling flow occurring adjacent to dune crests, whilst seaward upwelling flow is associated with the dune crestline (Figure 3.16iii). Secondary flow within the wider western channel appears to be controlled by local bedform morphology, with regions of upwelling adjacent to the longitudinal dune crests with northeast-southwest alignment. This indicates that this inherited bedform orientation is steering the seaward directed flow.

At the seaward end of the bar, a region of primary flow recirculation is observed, with flow diverting around the bar tail as two counter-rotating flow cells. At lower-high water this flow at the bar tail slows to almost 0 ms^{-1} , whilst flow into the channels has been reversed in a seaward direction. Cross-stream flow in the western channel at lower-high water contains a weak region of recirculation, with flow from the central region into the channel. Depth averaged flow patterns reveal that flow around the bar is variable across the tidal cycle, with recirculation around the bar tails occurring before lower-high water (Figure 3.24ii-iii). Between lower-low water and lower-high water

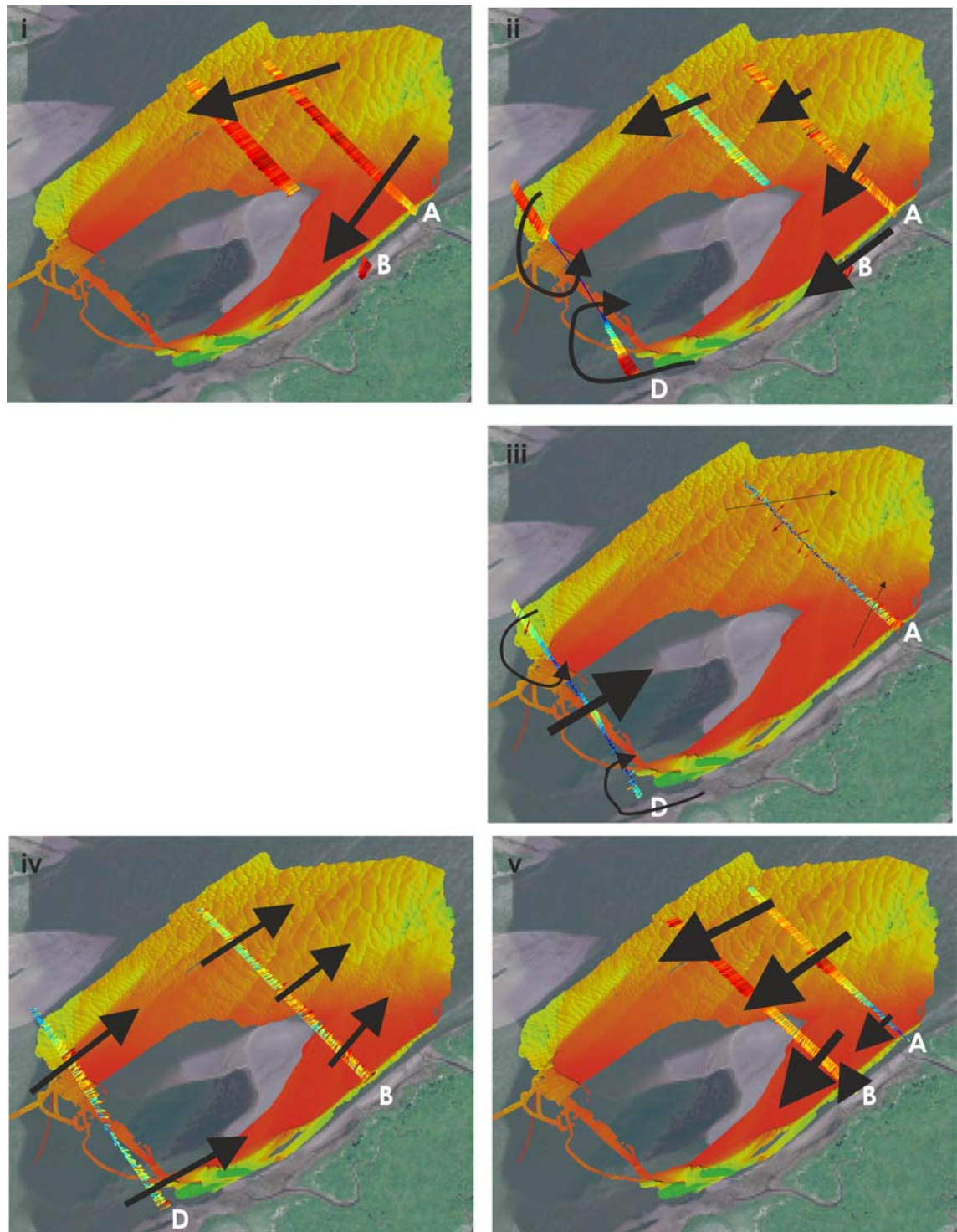


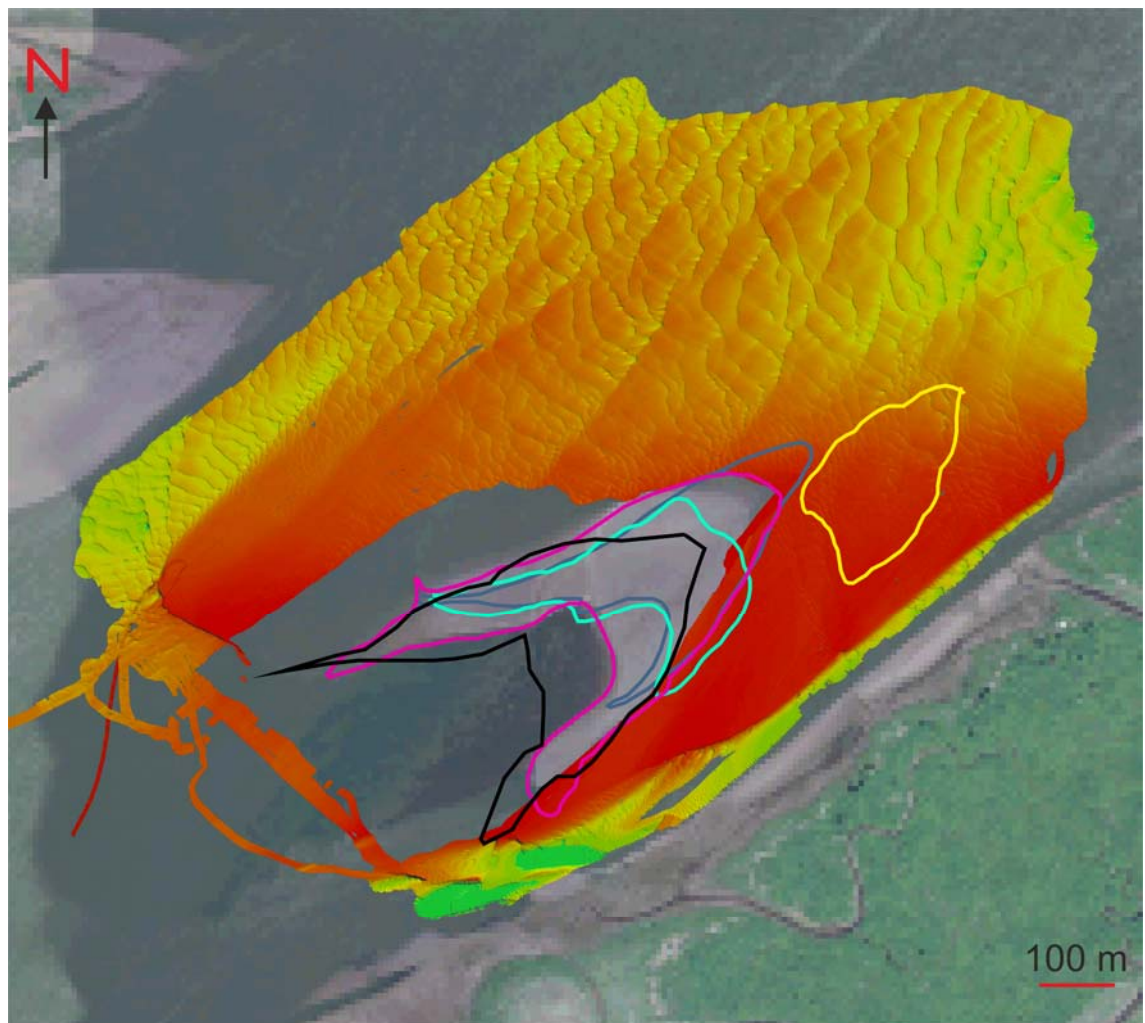
Figure 3.24 Depth averaged flow patterns at the 4 cross-sections measured at: i) lower-low water; ii) after lower-low water; iii) between lower-low water and lower-high water; iv) lower-high water; v) after lower-high water.

flow is diverted around dune crests in the region landward of the bar (Figure 3.24iii), whilst at lower-high water landward directed flow is diverted around a local high, which is the extension of the western bar tail (Figure 3.24iii).

3.4.4 Bar formation

The planform of Wood Bar is lobate in nature, with elongated bar tails visible at the seaward end. This would suggest that the bar has either formed due to the amalgamation of two elongate barforms to form a U-shaped bar, or that bi-directional flow has caused a delta bar-shield to form (Hayes, 1975; Dalrymple and Rhodes, 1996). The Plassac Bar, a large lobate barform with delta bar-shield morphology within the Gironde Estuary, was described by Billy *et al.* (2012) as a rare example of a bay-head delta situated tidally-dominated bar with some fluvial-influence. The internal architecture derived from seismic profiles by Chaumillon *et al.* (2013) revealed horizons dipping normal to the channel; the bar has formed by lateral accretion, indicative of tidal bar formation rather than tidal dune formation (cf. Olariu *et al.*, 2012). Whilst highly angled horizons are observed adjacent to the eastern channel in the present bar (Figure 3.20) the underlying presence of large-scale dunes overlain by smaller bedforms would suggest that the bar has formed due to transport of fluvial sediment (*sensu.* Villard and Church, 2005). Horizons are dipping in a seaward direction, again suggesting tidal dune deposition rather than bar deposition (Olariu *et al.*, 2012).

A series of aerial photos collected by the United States Department of Agriculture (USDA) allows the migration of the bar over the course of 10 years to be estimated, although only the bar top visible at the water surface can be commented on (Figure 3.25). These show that the bar initially was rounded in shape, with no visible bar tails. As the bar has migrated seawards it has elongated and longer tails have become visible. Whilst the bar length has varied considerably, bar width can be seen to remain constant throughout the surveys, suggesting stable flow widths at the region. The recent locations of the bar all lie at relatively shallow depths (<-1.5 m relative to TP_MSL), with bedforms aligned NW-SE; this bar top does not contain any of the largest scale bedforms with the landward channel alignment of NE-SW. This suggests that the inherited alignment predates formation of the bar and has not been fully modified by flow around the bar top. The bar lies within a region of fluvial-dominance with some tidal influence and whilst it superficially resembles the delta-bar shield morphology observed at the Plassac Bar the amount of tidal flow at this point in the system is much lower. It is more likely that the incoming tide has modified the seaward region of the bar, forming the small inflection visible in the earliest aerial survey. This in turn has



Barform date

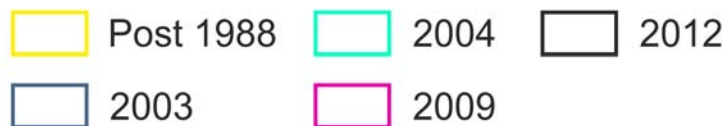


Figure 3.25 Summary of bar position in aerial surveys carried out by the USDA. Bar shows migration in a seaward direction consistent with fluvial dominance.

resulted in the recirculation of fluvial flow observed at cross-section D in the flow data which has elongated the bar tails (Figure 3.19).

Estuarine bars are known to have a wide variety of sizes, morphologies and internal architectures (Dalrymple and Rhodes, 1995), making the reconstruction of palaeoenvironments based on bar morphology problematic. Barforms within the Columbia River estuary show a range of morphologies (Figure 2.32), but the most common is that exemplified by Wood Bar. In the creation of facies models of the region of tidal influence primary fieldwork is often expanded into other regions by the use of aerial photography (e.g., Archer, 2012; Billy *et al.*, 2012; Dalrymple *et al.*, 2012). Extrapolating these models based on the planform appearance of the bar studied herein

suggests a degree of tidal influence which is not supported by the measurements reported, revealing that care must be taken when applying local findings to other systems. Variations in system size, fluvial flow and tidal strength are not measured by remote sensing methods, therefore resulting in a suggested model of barform creation which would not be supported by field measurements. This further complicates palaeogeographical reconstruction if these field reconstructions are not properly applied.

3.5 Conclusions

Understanding the range of flow and depositional patterns within the tidal-fluvial transition zone is currently of high interest due to various social and economic factors (Xie *et al.*, 2009; Fustic *et al.*, 2012). The variation of the tidal-fluvial boundary results in a complex depositional region, with spatially distinctive patterns. The wide range of tidally-influenced barforms which have been reported within this zone makes quantification of these facies more difficult, and to date there has been little focus on the region of fluvial dominance with some tidal influence.

The large tidal bar studied herein is of fluvial origin but with a small tidal effect, confirmed by the flow data, has developed a distinct planform suggestive of a more tidally-dominated position (Dalrymple and Rhodes, 1995; Billy *et al.*, 2012). The apparently tidal planform was not unexpected as previous flow data reveals a strong tidal influence at this location. The internal structure of the bar and its pattern of migration, however, reveal its fluvial origin. The small tidal input measured at this location has resulted in bar tails, which have become elongated due to the recirculation of the dominant fluvial flow. The fluvial depositional dominance of the location is further confirmed by the observation of seaward migration rather than laterally as is often the case in tidal bars (Olariu *et al.*, 2012), although it should be noted that the delta bar-shield morphology is more pronounced than would be expected. The discrepancy between the apparent system morphology revealed in isolated aerial images and the internal structure of the bar highlight the pitfalls of over reliance on such remote sensing methods in regions of complex flow.

There is widespread steering of bedforms around the bar by the dominant fluvial flow, which is dependent on bedform scale. The largest scale bedforms are aligned to flow from the channel located landward of the section; medium scale bedform crests are aligned to flow into the channels adjacent to the barform; the smallest superimposed bedforms are aligned to flow at the time of the survey. This reveals the lag in bedform reorientation to local flow patterns over time. However, although it was expected that tidal flows would also be steered around the bar there is no evidence of this within

either the flow data or the bedform morphology. Whilst the presence of a series of bedforms with a landward orientation arising from tidal flow, or the extensive modification of fluvially-dominated bedforms were expected due to the apparently tidal nature of the bar planform these were not observed. Although the flow measurements reveal reversals at this location, the only depositional evidence of tidal flow is the predominantly asymmetrical profile of dune spurs and their lack of superimposed bedforms. This reveals that tidal flow is predominantly routed along the troughs of the much larger fluvial bedforms.

To fully understand the nature of the tidal-fluvial transition it is necessary to also describe the region of fluvial-dominance, such as the region studied herein. The present work has examined the flow patterns occurring within this region, which is coupled to the resulting bedforms and their evolution over 12 months. This combination of process and product reveals that the present models of the tidal-fluvial transition, whilst describing in detail the expected variations in bedforms and deposition occurring in regions of tidal dominance, do not describe those occurring within regions of fluvial dominance in detail (Dalrymple *et al*, 1992; Dalrymple and Choi, 2007; van den Berg *et al.*, 2007; Archer, 2013). This area is currently under-reported or reported only in terms of the system planform. The present work reveals the presence of a region of apparently fluvial deposition which needs to be examined in detail for more subtle indications of tidal influence such as flow steering around dune crests and the variations in orientation of bedforms dependent on bedform scale must be recognised as a feature of tidal-fluvial systems in addition to features such as tidal rhythmites. The addition of this fluvially-dominated deposition with subtle tidal modification would allow the present models of the tidal-fluvial transition to more accurately inform workers within ancient systems who may misinterpret such features as lacking in any tidal component.

Chapter 4

Three-dimensional meander bend flow within the tidally-influenced fluvial zone¹

4.1 Abstract

Although three-dimensional bend flow within fluvial meanders is well known and the linkages between the flow field, bend morphodynamics and resultant floodplain sedimentology well connected, there is limited knowledge on the dynamics of flows in bends that are subject to tidal forcing or tidal influence. This paper presents measurements of three-dimensional flow around a tightly curved meander bend in the tidally-influenced fluvial zone within the River Severn, UK. Repeat measurements were taken at two hydrological conditions: i) high river flows and neap tides, and ii) lower fluvial discharge and spring tide. These two cases thus highlighted the end members of the flow forcing distributions experienced at the bend, with the former showing the maximum fluvial influence and the latter the maximum tidal influence on bend flow processes. Results show that during a period of higher river flow at neap tides there was very little tidal influence experienced at the bend. During the second set of measurements, made during a period of low river flow and at high spring tides, a full flow reversal occurred, indicating that the tidal-fluvial transition had moved landward of the bend. In both cases the maxima primary flow velocities measured were of a similar magnitude, even though flow was fully reversed during the spring tides. However, the secondary flow velocities increased notably during the flow reversal at spring tide. These flow patterns provide an explanation of the often observed stability of meander bends within the tidally-influenced fluvial zone, with the location and focus of maximum flow shear migrating around the bend during reversals, likely hindering bar push processes that can drive meander migration processes.

¹ This chapter has been published as:

Keevil, C.E., Parsons, D.R., Ainsley, M. and Keevil, G.M., 2015. Three-dimensional meander bend flow within the tidally-influenced fluvial zone. In: Ashworth, P.J., Best, J.L. and Parsons, D.R. (Eds), *Developments in Sedimentology 68: Fluvial-Tidal Sedimentology*, 127-148.

4.2 Introduction

The transition zone between fully-fluvial and fully-estuarine environments is a region of complex flow and sediment transport processes that can extend from 10s to 100s of km and ultimately produces composite sedimentological structures and facies (Dalrymple *et al.*, 1992; Dalrymple and Choi, 2007; van den Berg *et al.*, 2007; Fustic *et al.*, 2012). Whilst the sediment transport processes and morphodynamics occurring within fully-fluvial and fully-tidal systems have been studied in some detail (e.g., Allen, 1991a; Bridge, 1993; van den Berg *et al.*, 2007; Kostaschuk *et al.*, 2010; Rennie and Church, 2010; Uncles, 2010; Blanckaert, 2011), and the sedimentological facies produced are reasonably well understood, the complex tidally-influenced fluvial zone (TIFZ) between them has yet to be fully explored.

Understanding the processes within the TIFZ is important as they are often host to large centres of population and industry as well as being the sites of important ecological habitats (Xie *et al.*, 2009). Moreover, the low-lying nature of tidally-influenced systems means that they will be among the first, and perhaps most sensitive, zones to be affected by climate change, sea level rise (Kirby, 2010; Phillips and Crisp, 2010) and storminess (Uncles, 2010), meaning that understanding the controls on their dynamics has immediate and pressing relevance related to mitigation and adaptation management of a range of climate change impacts. Moreover, there is also a drive to understand the detailed processes within the TIFZ in order to better constrain such systems in the ancient for commercial exploitation (e.g., Townend *et al.*, 2007, Smith *et al.*, 2009).

Despite the complex range of influences acting within the tidal-fluvial transition zone, many workers have noted that these regions appear to have a fairly stable planform morphology. For example, Dalrymple *et al.* (1992) examined the morphology of tidally-dominated estuarine systems and found them to have a characteristic “straight-meander-straight” geometry, particularly at the head of estuaries. Dalrymple *et al.* (2012) suggest that with increasing tidal influence the fluvial channel begins to meander tightly, resulting in “double meander” formations. Within this tightly meandering region, neither fluvial nor tidal processes are thought to dominate over the other (Archer, 2013), although the same pattern has been found within tidal creeks with little fluvial influence, with the reasons governing this geometry presently poorly constrained and largely unknown. The meanders in the “straight-meander-straight” region tend to be tighter in terms of curvature than within other systems, possibly arising from the bi-directional flow. However, the effects of this bi-directional flow on

the bend-induced secondary flows and bend migration and morphodynamics has not to date been investigated in any detail.

The geometry of a meander bend is known to induce a secondary circulation that is superimposed on the downstream flow, forming a three-dimensional helical flow structure (Dietrich and Smith, 1983), with the extent and magnitude of this secondary circulation controlled by the bend curvature and width:depth ratio of the channel (Dietrich, 1987; Markham and Thorne, 1992). At the apex of a bend this will characteristically be in the form of secondary flows that are outwardly directed near the surface and inwardly directed near the bed. This flow structure is generated by the balance between the centrifugal forces (acting in a cross-stream direction) and a pressure gradient produced through a cross-stream tilting of the water surface and super-elevation of fluid at the outer bank (Rozovskii, 1957). Secondary flow cells in a reversed direction may also be formed close to the outer bank, with the size and strength controlled by bank slope and the aspect ratio of the channel (Bathurst *et al.*, 1979, Blanckaert, 2011; Blanckaert *et al.*, 2012). Flows over the inner-bank point bar of a meander bend have been identified as key in generating outwardly directed flows (Dietrich and Smith, 1983), with the geometry of the point bar influencing the extent of these flow secondary flow patterns (Nanson, 2010).

The influence of bend shape on three-dimensional flow structure was examined in detail by Frothingham and Rhoads (2003). In a study of an asymmetrical bend, they described how the bend shape resulted in an induced asymmetry of the core of high velocity around the bend, and they linked this effectively to channel bank erosion processes and the overall morphodynamics of their reach. Asymmetry of individual meander bends was also previously found to increase the intensity of secondary circulation cells around the bend, this in turn being proportional to the rate of bend migration (Hickin and Nanson, 1975), with erosion often forming downstream of the bend apex through the influences of spatial lag in the force balance between centrifugal and pressure gradient terms (Furbish, 1988). Changes in discharge and the resulting accommodation within the channel has also been shown to alter the bend flow patterns. In channels where increased discharge is accommodated by an increase in channel width, but only small increase in depth, the effects of centrifugal force will dominate flow patterns. When the channel is confined in terms of width, any increase in discharge will cause the flow to deepen with only a small increase in width and the pressure-gradient forces will tend to dominate flow patterns (Markham and Thorne, 1992), resulting in an increase in flow separation at the outer and inner banks.

Bi-directional flows acting within individual meander bends will, by their nature, show a range of flow patterns. Investigations of estuarine flows and their interactions with

curved channels have been carried out in the past, but these measurements are often made close to the estuary mouth, where flows are split into subsidiary channels or around islands, or on smaller channels within tidal flats (e.g., Seim and Gregg, 1997; Lacy and Monismith, 2001; Marani *et al.*, 2002; Nidzeiko *et al.*, 2009). Flows through a curved channel within zones of bi-directional flow have been shown to produce similar cross-channel secondary circulation patterns as those found in purely fluvial bends, with the effects of fluid stratification produced by salinity and temperature changes shown to modify the force balance in some instances (Seim and Gregg, 1997).

Lacy and Monismith (2001) measured flow within a curved subsidiary channel within San Francisco Bay. They found that the tide-averaged flows on both flood and ebb tides were highly stratified, with upwelling occurring near the deepest section of the channel. High seaward velocities were measured near the centre of the channel on the flood tide, and on the ebb tide the highest velocities were observed nearer to the flow surface (Lacy and Monismith, 2001). They concluded that the short distance travelled by flows did not allow the forces acting on the flow to reach equilibrium, resulting in the differences observed compared with those found in the classical fluvial bend flow described above. In a more recent study, Nidzeiko *et al.* (2009) examined the flow induced by a pair of bends approximately 1.5 km landward from an estuary mouth. The seaward bend had a curve of 100° with a radius of curvature of 225 m and a maximum depth of 7 m; the landward bend had a curve of 60° with a radius of curvature of 375 m and a maximum depth of 5 m. Measurements were made of flow velocity from a fixed, bottom-mounted, Acoustic Doppler Current Profiler (ADCP) in the straight stretch between the bends; a Conductivity Temperature Depth probe (CTD) was also mounted at the surface at the same point. Their results reveal a coherent secondary circulation through the bend, with flow towards the inside of the bend at the base of the channel, matching that found and described in fluvial bends. Stratification of the flow was observed during some tides due to density differences and, under these circumstances, the ebb tide showed a three-layered flow towards the outside of the bend at the surface and base of the channel, with flow towards the inside of the bend in the centre of the channel. On the flood tide a two-layer flow developed, but with flow towards the outside of the bend at the base of the channel, returning to the inside of the bend at the surface (Nidzeiko *et al.*, 2009), with implications for the long-term evolution of the system's morphology.

The influence of tidal flows on the morphology of meanders was investigated by Marani *et al.* (2002), who found that the wavelength, width:depth ratios and radius of curvature of meanders appeared to alter as the system became more tidally-dominated. Their study investigated channels within coastal wetlands, and found that these changes were driven by local hydrodynamic patterns, resulting in characteristic

planforms in fluvially- or tidally-dominated regions. Tidally-dominated regions showed an exponential increase in channel width seaward, whilst meander width to length ratios remain roughly comparable to those seen in fluvially-dominated regions (Marani *et al.*, 2002). Whilst these show some of the effects of tides on flow around bends, the patterns observed within the landward tidal-fluvial transition zone will be further complicated by the movement of the region of tidal influence. Fagherazzi *et al.*, (2004) investigated the effect of tidal flows in salt-marsh bound meander bends. They were able to quantify a fully bi-directional system that was actively undergoing bank collapse and channel migration. They found that meander geometries became skewed in their planform patterns as either flood or ebb flows began to dominate within the system.

The study presented herein investigates the detailed three-dimensional flow structure around a tightly curved symmetrical meander bend within the tidal-fluvial transition zone of the River Severn, UK. The bend is known to experience reversed (landward) flows at high tides and the aim of the work presented is the quantification of the differences in the three-dimensional flow at different points in the fluvial and tidal forcing. Measurements were repeated at the same locations upstream of the bend at high fluvial discharge during a neap tide and at low fluvial discharge during a high spring tide, allowing direct comparison of these different conditions on the flow velocities. In order to investigate the evolution of the flow field at the bend apex during flow reversal a series of repeated measurements were also made at the apex section during the spring tide to quantify the changes in flow through the changing tidal conditions. The results are discussed in light of the differences from flow structures found within classical fluvial bends and the implications for bend morphodynamics and longer-term sedimentary evolution of bends within the TIFZ.

4.3 Methods

4.3.1 Field Area

The Severn Estuary is a megatidal estuary in the southwest of the UK, with a maximum tidal range of 13.5 m at Avonmouth and an average river discharge of $100 \text{ m}^3\text{s}^{-1}$ (Figure 4.1; Kirby, 2010; Uncles, 2010). The estuary is funnel shaped with a south-westerly orientation within a wide fault bounded valley, which acts to direct the local prevailing winds up the system (Manning *et al.*, 2010). The full estuary system combines the Bristol Channel and lower River Severn, with Dyer (1996) defining the outer limit of the estuary as being between Barry and Minehead (Figure 4.1). The River Severn is said to end at the Severn Bridge, whilst the inner estuary limit is defined as Maisemore Weir, north of Gloucester (Dyer, 1996; Uncles, 2010). As a consequence the system is usually described as an outer or lower estuary, from Barry and Minehead in the Bristol Channel

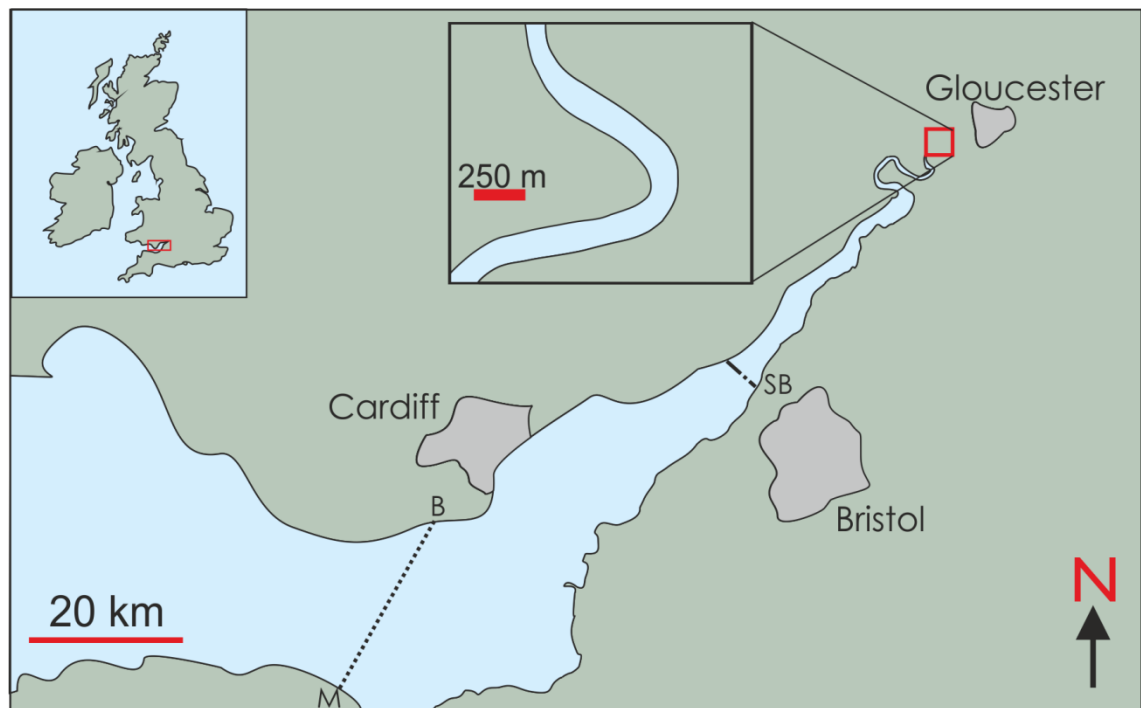


Figure 4.1 Map of tidal Severn Estuary showing study bend. Outer estuary extends from Barry (B) - Minehead (M) to Severn Bridge (SB). Inner estuary ends at Maisemore Weir (MW). E shows the location of the Environment Agency gauge at Epney. ADCP measurement cross-sections are shown on the inset of the study bend.

to the Severn Bridge and an inner or upper estuary from this point inland to the Maisemore Weir (Dyer, 1996; Uncles, 2010; Archer, 2013).

The combination of the rapidly narrowing funnel shape of the estuary and the shallowing of the system (from 50 m at the outer point of the outer estuary to less than 10 m at the boundary with the inner estuary) and the high tidal range result in tidal flows of over 5.5 ms^{-1} (Manning *et al.*, 2010). Tidal bores are regular occurrences on the River Severn (Rowbotham, 1983; Chanson, 2012; Archer, 2013) and prior to the construction of weirs close to Gloucester they were regularly witnessed as far landward as Worcester (Archer, 2013); during high spring tides flow reversals may still be observed this far landward. Flow features within the Severn Estuary system were investigated from a number of stations by Uncles (2010). The inner estuary was found to have a vertically well mixed salinity profile during high tides, with a well-developed estuarine turbidity maximum beyond the region of salt water influence, landward of the current field area. Storage of water and fine sediment following high tides was also observed, released on the following tidal cycle (Uncles, 2010).

The Severn Estuary has a mixed sediment content of mud, sand and gravels (Manning *et al.*, 2010), with the fine suspended primarily composed of marine sediment and sand and gravels with a fluvial source (Kirby, 2010). Regions of sand and gravel occur primarily on the north of the outer estuary on the Welsh coast (Duquesne *et al.*, 2006;

Manning *et al.*, 2010), although there are locally sourced regions of gravel also within the inner estuary (Carling *et al.*, 2006). The estuary has a high concentration of fine suspended sediment (Carling *et al.*, 2009), and due to the extreme tidal nature of the Severn Estuary it has two turbidity maxima (Manning *et al.*, 2010): landward of Sharpness, in the inner estuary, a zone of suspended particulate matter concentrations can be found of 0.5-10 g l⁻¹; within the outer estuary in the region of Bridgwater Bay higher salinity concentrations of up to 100 g l⁻¹ have also been observed (Manning *et al.*, 2010). Fine sediment deposition occurs in the outer estuary at Newport Deeps and Bridgwater Bay, which are both rapidly filling with sediment (Kirby, 2010). Fieldwork was carried out on a symmetrical channel bend in the inner Severn Estuary approximately 18 km south of Gloucester, UK (Figure 4.1). The river is 100 m wide at this point and the bend has a curve of 135° and a radius of curvature of 225 m. It is of a similar size and geometry as the bend studied by Nidzeiko *et al.* (2009). The channel width does not vary around the bend or for several hundred metres landward or seaward of the field site. The bend investigated herein is fully within the TIFZ of a mega-tidal estuary, experiencing flow reversals (landward) during spring tides but only modulation of seaward flows at high river discharges and neap tides. Salinities of 15-20 g l⁻¹ were reported in this area at high water during a high spring tide with low river flow (Uncles, 2010).

4.3.2 Field methods

Flow measurements were collected using a Teledyne RD Instruments RioGrande 1200 Hz Acoustic Doppler Current Profiler (ADCP) deployed from the side of a small research vessel. Data were collected at vertical intervals (bins) of 0.25 m through the water column; blanking distances due to instrument deployment and acoustic interference effects were 0.61 m down from the water surface and 0.5 m up from the base of measurements. Data were collected at a rate of ~1 Hz across a series of channel wide cross-sections. A series of repeated ADCP transects were conducted at each cross-section (mean number of repeats was 5, with a minimum of 2 repeats, maximum of 8 repeats), as recommended by a number of works (e.g., Yorke and Oberg, 2002; Muste *et al.*, 2004a; Muste *et al.*, 2004b; Szupiany *et al.*, 2007). Such multiple transect repeats are needed to remove data fluctuations and ensure that the data reveal the finer details of the secondary flow structure, as a single transect is only able reveal general flow patterns (Szupiany *et al.*, 2007). Corrections must be made to boat motion relative to the water column, as the velocities returned will be a combination of those of the water column and the vessel (Yorke and Oberg, 2002; Parsons *et al.*, 2005). The present measurements were performed using a vector track and speed over ground derived (VTG-derived) dGPS correction for the boat velocity.

All ADCP data were post-processed using the Velocity Mapping Toolbox (Parsons *et al.*, 2013). This toolbox allows the analysis of ADCP data collected from moving vessels, that includes averaging over multiple transects with an irregular shiptrack transect. The transects can be rotated to compute secondary circulation fields and herein the zero-net secondary discharge method, where the cross-section is re-oriented so that there is no lateral flux through the cross-section, was applied (Parsons *et al.*, 2013). This method was chosen as it allows improved visualisation of the cross-stream flow patterns, without the complication of any residual cross-stream discharge being within the rotation.

4.4 Results

Data were collected during two separate field periods: i) during a neap tide at high river level; and ii) during a spring tide at low river level (Figure 4.2). The high river level flow data were collected following a period of heavy rain within the upper Severn catchment, resulting in high fluvial discharge. The arrival of a neap tide at the study bend slowed the flow of the river considerably, but did not cause the river flow to reverse within the section of the tidal-fluvial transition zone studied (high river-neap tide (HRNT)). The

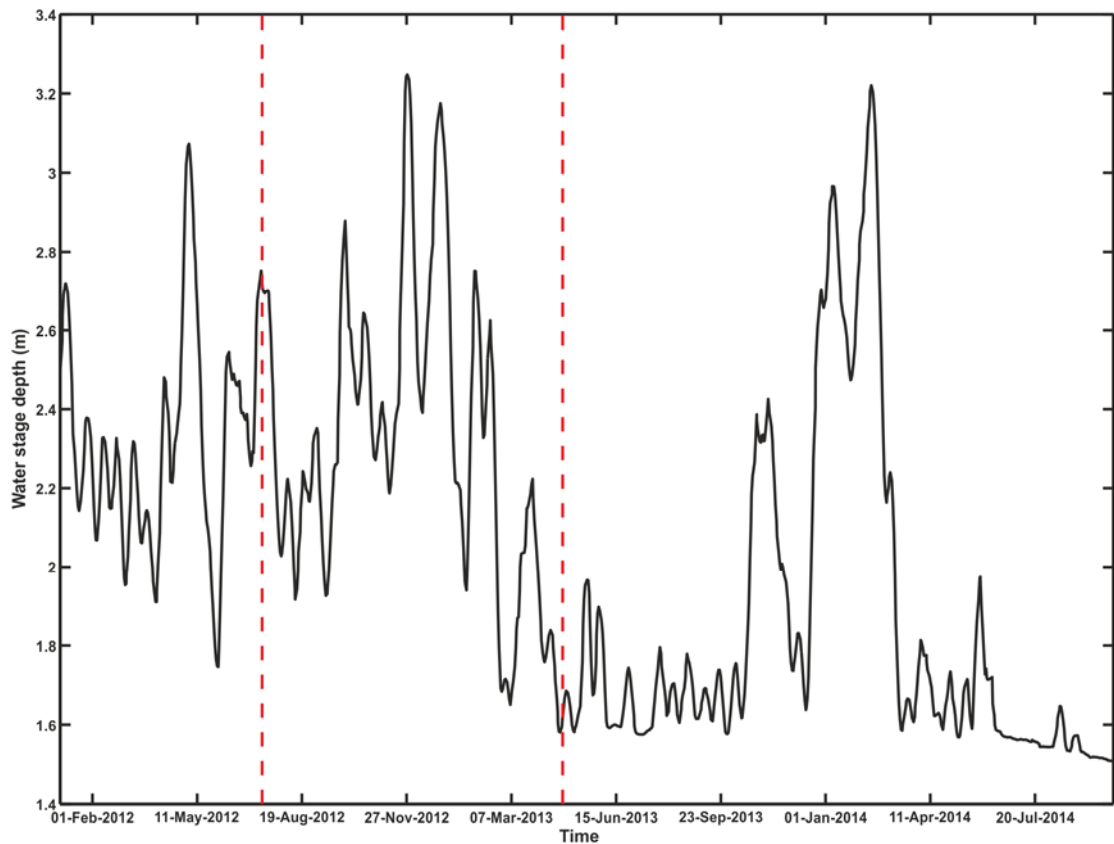


Figure 4.2 Base river flow measured at Epney Gauge (Site ID – 2059). Red dashed lines show the dates of the fieldwork reported on here. *Contains Environment Agency information © Environment Agency and database right*

second dataset was collected at low river flow and a high spring tide (low river-spring tide (LRST)), during some of the lowest river flow in the two year period shown in Figure 4.2. The spring tides were associated with a tidal bore on the river, following which river flow fully reversed around the bend investigated. During both periods repeated transect measurements were made at several cross-sections around the bend. Additional to this, a series of repeat cross-section transect sets were also collected at the bend apex section during the LRST measurement period, to investigate the evolution of flow structure during the flood-ebb reversal. Primary flow is reported as being in a seaward or landward direction as the spring tide caused the flow to reverse during some of the measurements.

i) High River – Neap Tide (HRNT)

Flow measurements were collected over 65 minutes in July 2012, during a period of high river flow following a period of high rainfall in the upper Severn catchment. Measurement times of each cross-section are shown in Table 4.1. Base river flow at the Environment Agency gauge at Epney, 4.5 km seaward of the measured bend, was 2.5 m, with a flood height of 0.2 m occurring with the arrival of the neap tide 20 minutes prior to the collection of the ADCP transect data (Figure 4.3). Flow was measured at 6 cross-sections (A-F) around the bend during the neap tide flood (Figure 4.4). Three cross-sections were measured landward of the bend apex (Figure 4.4i-iii & vii-ix), a cross-section at the bend apex itself (Figure 4.4iv & x) and two cross-sections seaward of the bend apex (Figure 4.4v-vi & xi-xii). At all cross-sections flow was in a seaward direction

Table 4.1 Data collection times at high river-neap tide (HRNT) and low river-spring tide (LRST). Flow was reversed (primary velocities in a landward direction) during the first four measurements at LRST.

| Time | River condition | Location |
|------------------|---------------------|-----------------|
| 14:19 11/07/2012 | HRNT | Cross-section A |
| 14:33 11/07/2012 | HRNT | Cross-section B |
| 14:46 11/07/2012 | HRNT | Cross-section C |
| 14:56 11/07/2012 | HRNT | Cross-section D |
| 15:06 11/07/2012 | HRNT | Cross-section E |
| 15:15 11/07/2012 | HRNT | Cross-section F |
| 08:01 25/04/2013 | LRST: Flow reversed | Apex (T20) |
| 08:27 25/04/2013 | LRST: Flow reversed | Cross-section C |
| 08:44 25/04/2013 | LRST: Flow reversed | Cross-section B |
| 09:02 25/04/2013 | LRST: Flow reversed | Cross-section A |
| 09:21 25/04/2013 | LRST | Apex (T100) |
| 10:16 25/04/2013 | LRST | Apex (T155) |
| 11:01 25/04/2013 | LRST | Apex (T200) |

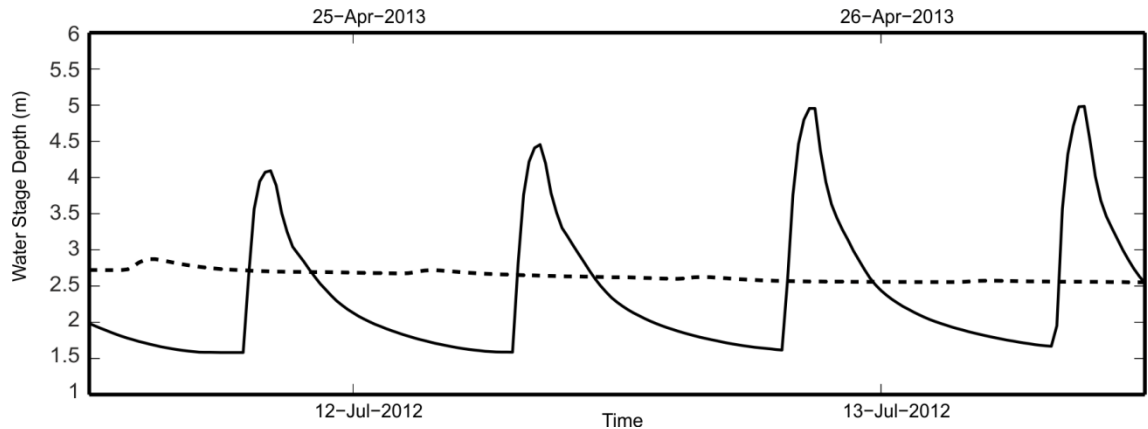


Figure 4.3 Stage data collected every 15 minutes by Environment Agency Epney Gauge (Site ID – 2059). The dotted line shows data for 12:00 11/07/2012 to 12:00 13/07/2012; solid line shows data for 12:00 24/04/2013 to 12:00 26/04/2013. Contains Environment Agency information © Environment Agency and database right.

at all times, generally in the range of 0.60-1.2 ms⁻¹. Seaward of the bend apex (Figure 4.4v-vi), the fastest velocities were measured in the deepest section of the channel, with slower velocities close to both banks; this pattern of flow is also detected at the most landward cross-sections (Figure 4.4i-ii). Secondary velocities are much slower than the primary (seaward) velocities, approaching a maximum of ~0.15 ms⁻¹ and mean absolute values of 0.05 ms⁻¹ (5 % of the primary flow). Flow at the channel edges and base is towards the inside of the bend, with a region of outward directed flow within the main channel (Figure 4.4xi-xii).

Cross-section A shows secondary flows of up to 0.2 ms⁻¹, with flow at the base of the channel towards the western bank, with return flow close to the flow surface of the channel (Figure 4.4vii). This was likely produced by the helical flow which would be expected to be produced at the bend immediately landward and then advected through the reach. Cross-sections B (Figure 4.4viii) and C (Figure 4.4ix), located landward of the bend apex, show a region of slower velocities in the centre of the cross-section. In this region of the bend a large subaqueous bar is present in the channel. This divides the flow into a region of strong seaward-directed primary flow in the western channel at the inside of the bend, whilst at the outer bank a small region of flow reversal is observed. Associated with this flow reversal is a change in the orientation of secondary circulation within the channel, with cross-stream secondary flow directed towards the inner bank within the main channel, but directed towards the outer bank as the channel shallows and divides over the bar (Figure 4.4viii-ix).

The velocities measured at the bend apex, due in part to a larger cross-sectional area (Figure 4.4iv), are generally slower than in the other cross-sections measured reaching

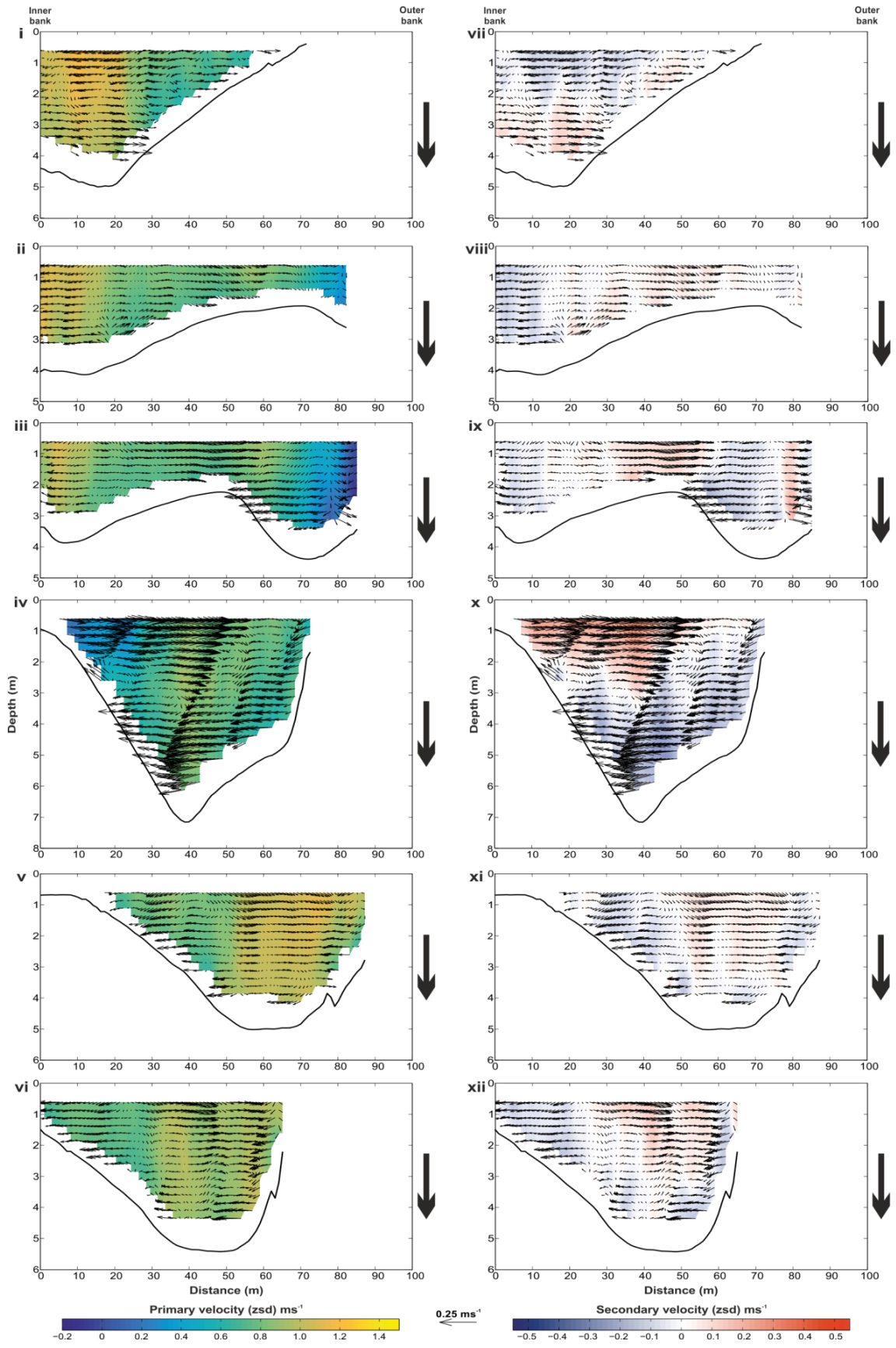
a maximum velocity of only 0.95 ms^{-1} . A region of slower velocity flow is also measured near the inner bank, with some very slow velocities at the base of the flow. However, this cross-section showed some of the fastest secondary circulation velocities measured in any of the data, with cross-stream velocities over 0.5 ms^{-1} (~50 % of primary flow). A strong reversed recirculation cell is also visible (cf. Blanckaert *et al.*, 2012), with flow towards the outside of the bend at the surface and in the opposite direction at the base.

ii) Low River – Spring Tide (LRST)

A second series of flow measurements were collected in April 2013, a time of low river flow during high spring tides. Data was collected over 200 minutes following the passage of the tidal bore which marked the incoming tide; the flow effects of the tidal bore were not measured. A similar set of cross-sections to the HRNT measurements (A-C) were made during the flood tide (measurement times for each cross-section are shown in Table 4.1). A repeated set of cross-section measurements were collected at the bend apex over a portion of the tidal cycle (see details in section below) to investigate the evolution of flow structure in the bend during the flood-ebb switch. Over the period of the measurements the Epney gauge showed a base river stage of 1.6 m, with a rapid incoming flood tide of nearly 3 m elevation, which then slowly decayed (Figure 4.3) through time. Cross-section measurements were collected again after the initial flood tide had passed, which revealed flow in a landward direction immediately after the incoming tide in all sections (Figure 4.5i-vi), showing that the tidal-fluvial transition during this second set of measurements had moved landward.

Flow velocities were generally slower than those detected during the HRNT measurements. Cross-section A shows primary flow in a landward direction, predominantly between $0.2\text{-}0.4 \text{ ms}^{-1}$ with some areas of faster velocity at the surface of up to 0.5 ms^{-1} (Figure 4.5i). A small region of seaward flow can be found at the western edge of the cross-section; this corresponds to the centre of the channel in Figure 4.4i. However, these slower flow velocities may be due to the waning of the flood tide before re-establishment of flow in a seaward direction as this cross-section was collected 80 minutes after arrival of the incoming flood tide, shortly before seaward oriented flow

Figure 4.4 (next page) Flow velocities at six cross-sections at high river-neap tide conditions: i-vi show primary flow velocities (zero secondary discharge) in ms^{-1} ; vii-xii show secondary flow velocities (zero secondary discharge), also shown as black arrows. Cross-section A is shown in i and vii; cross-section B in ii and viii; cross-section C in iii and ix; cross-section D in iv and x; cross-section E in v and xi; cross-section F in vi and xii. Flow is in a seaward direction at all cross-sections. Locations of the cross-sections are shown in Figure 4.1.



was fully re-established (Table 4.1). Cross-sections B and C show faster primary flow velocities than cross-section A ($<1.1 \text{ ms}^{-1}$), again in a landward direction. The fastest velocities were observed towards the outer edge of the channel (Figure 4.5i-iii), whilst the secondary circulation observed had the same orientation as those detected during HRNT conditions, even though primary flow was reversed. The secondary flow was found to be significantly faster (Figure 4.5iv-vi), with maximum velocities observed an average of 50% higher than at HRNT.

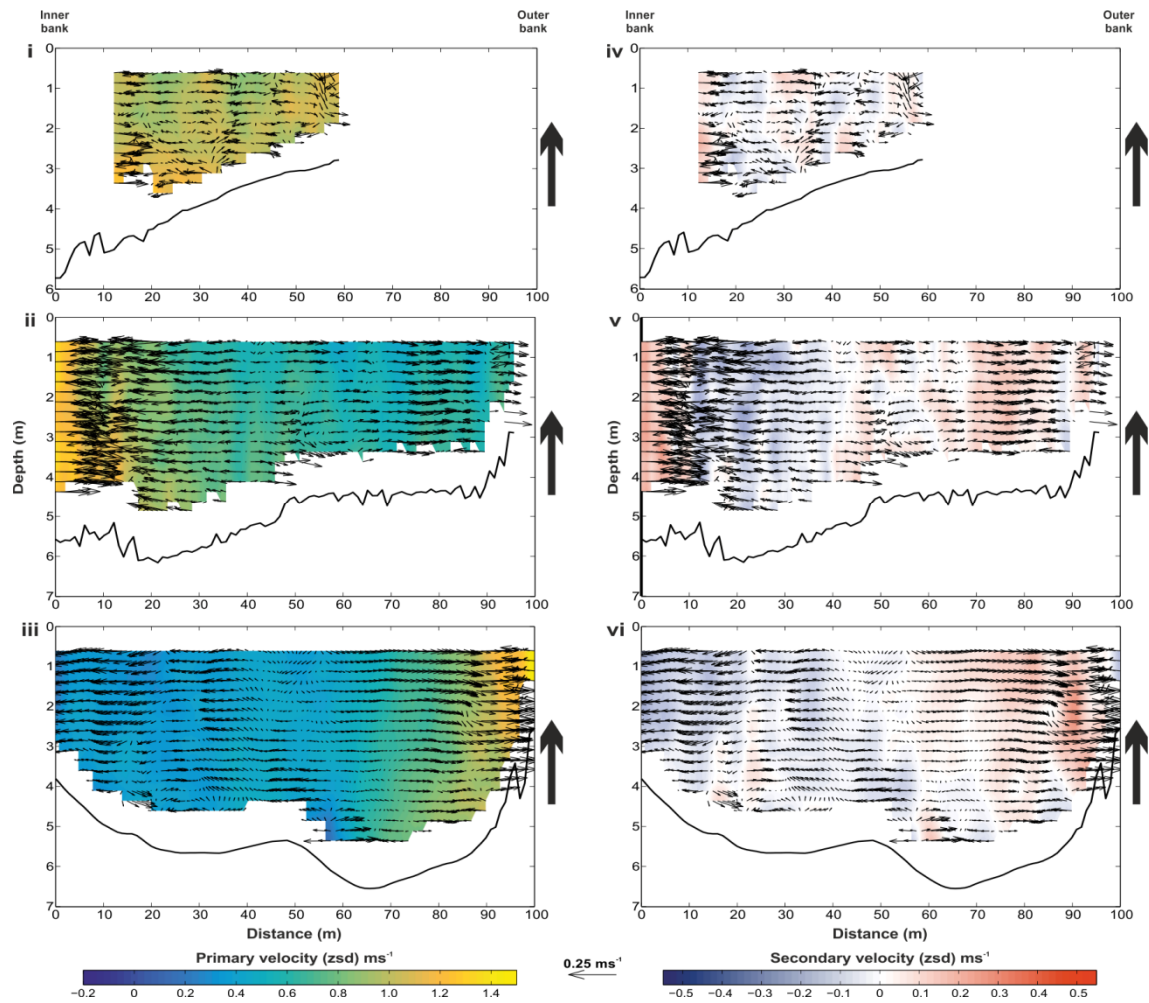


Figure 4.5 Flow velocities at three cross-sections, landward of the bend apex at LRST conditions: i-iii show primary flow velocities (zero secondary discharge) in ms^{-1} , where flow is in a landward (reversed) direction due to the incoming flood tide; iv-vi show secondary flow velocities (zero secondary discharge), also shown as black arrows. Cross-section A is shown in i and iv; cross-section B is shown in ii and v; cross-section C is shown in iii and vi. Flow is in a landward direction (reversed to normal river flow) at all cross-sections. Locations of the cross-sections are shown in Figure 4.1.

The large bar observed in cross-sections B and C during the HRNT measurements (Figure 4.4) had flattened and occupies less of the channel base (Figure 4.5ii-ii & v-vi) since the HRNT measurements. The flow division and the region of flow reversal measured in during HRNT at cross-section C (Figure 4.4) is again observed in the LRST measurements, even though flow is in a landward direction in these measurements (Figure 4.5iii). Although flow is in a landward direction during the LRST case, the maximum primary flow velocities measured in the cross-sections are generally around the same magnitude as the maximum primary flow velocity in the HRNT case. However, the secondary flow velocities observed at LRST are much faster than those at HRNT.

iii) Repeated Bend Apex measurements at LRST

During the LRST measurements, repeated cross-sections were also collected at the bend apex (close to the position of cross-section D in Figure 4.4) to monitor the flow evolution with the changing conditions on the flood tide and switch to ebbing conditions (Figure 4.6). The first measurements were made 20 minutes (T20) after the arrival of the incoming flood tide, with a maximum channel depth of 8 m. The cross-section shows flow in a landward direction, as the flood tide reversed all fluvial flow (Figure 4.6i). The primary flow velocities are the fastest measured during the fieldwork at 1.50 ms^{-1} (Figure 4.6i), with much lower velocities at the channel margins (0.1 ms^{-1}). There is a very strong secondary circulation cell that extends nearly 80 m across the cross-section before down-welling at the outer bank, where the slowest primary velocities were measured ($<0.5 \text{ ms}^{-1}$). Cross-stream velocities measured are the fastest detected in any of the cross-sections measured with a maximum of 0.54 ms^{-1} (Figure 4.6v). An outer bank recirculation cell is also present extending 30 m from the outer bank (cf. Bathurst *et al.*, 1987). This pattern of secondary circulation is the same as that observed in the apex measurement collected at HRNT (Figure 4.4iv), where the fastest cross-stream velocity measured was only 0.32 ms^{-1} .

Flow measurements at the apex section were repeated 80 minutes later (T100) (Figure 4.6ii). The primary flow was no longer reversed by the flood tide and was now re-established in a seaward direction. The maximum depth of the channel had decreased to 6.5 m. The pattern of flow velocity had altered significantly, with the fastest velocities now detected at the channel margins, particularly the 40 m closest to the inner bank, where there were regions of $>0.8 \text{ ms}^{-1}$. Flow in the centre of the channel was $\sim 0.5 \text{ ms}^{-1}$, showing very little variation with depth. Secondary flow velocities were significantly slower than at T20, with a maximum of $\sim 0.2 \text{ ms}^{-1}$ observed (Figure 4.6vi). The fastest secondary flow velocities were recorded at the surface in the centre of the channel,

where flow was towards the outer bank. Flow at the base of the channel was directed towards the inner bank. There was no outer bank recirculation cell observed.

A third cross-section repeat was performed 55 minutes later (T155), by which time the river stage had decreased further, with a mean channel depth of 6 m (Figure 4.6iii). Primary flow velocities were in the same range as those measured at T100, but with the fastest velocities now observed in the centre of the channel and regions of slower velocity at the outer bank. Cross-stream velocities were faster than those observed at T100 ($\sim 0.3 \text{ ms}^{-1}$) showing a different pattern of spatial distribution, with outward flow dominating the outer portion of the channel and inward directed flow at the inside of the bend (Figure 4.6vii), perhaps revealing an increasing effect of bed topography as the flow shallowed during the ebb.

A final repeat cross-section was collected 45 minutes later, 200 minutes (T200) after the arrival of the incoming flood tide (Figure 4.6iv). The mean channel depth had decreased to just under 6 m with slower velocities than previously measured. The fastest flow velocities at this time were observed in the upper region of the channel, with lower velocities at the channel margins and base. Cross-stream velocities are similar to those at T100 ($\sim 0.2 \text{ ms}^{-1}$) with a similar spatial distribution (Figure 4.6viii). Flow directed towards the inside of the bend only extends 10 m into the channel in this case, whereas at T100 this flow extended up to 20 m (Figure 4.6v). There is also a small region of secondary flow reversal/recirculation 10 m from the outer bank, where flow downwells at the bank.

Although the initial water depth was lower during the LRST, the volume of water brought landward by the spring flood tide resulted in an overall higher water depth. During the HRNT measurements, Transect D in Figure 4 shows a maximum water depth of 7 m at the base of the channel, with Transect E just beyond the bend apex showing a depth of 5 m (Figure 4.4). In the LRST measurements 20 minutes after the arrival of the flood tide at the bend apex, the maximum flow depth measured was nearly 8 m. At 200 minutes after the arrival of the flood tide this maximum water depth had decreased to just under 6 m (Figure 4.6). The repeat cross-sections collected during the LRST conditions show flows generally 1 m deeper than those collected at HRNT (Figures Figure 4.4-Figure 4.6). The post-flood river flow in the spring tide measurements is considerably slower than those in the neap tide measurements, as demonstrated in the flow velocities shown in Figure 4.6ii-iv.

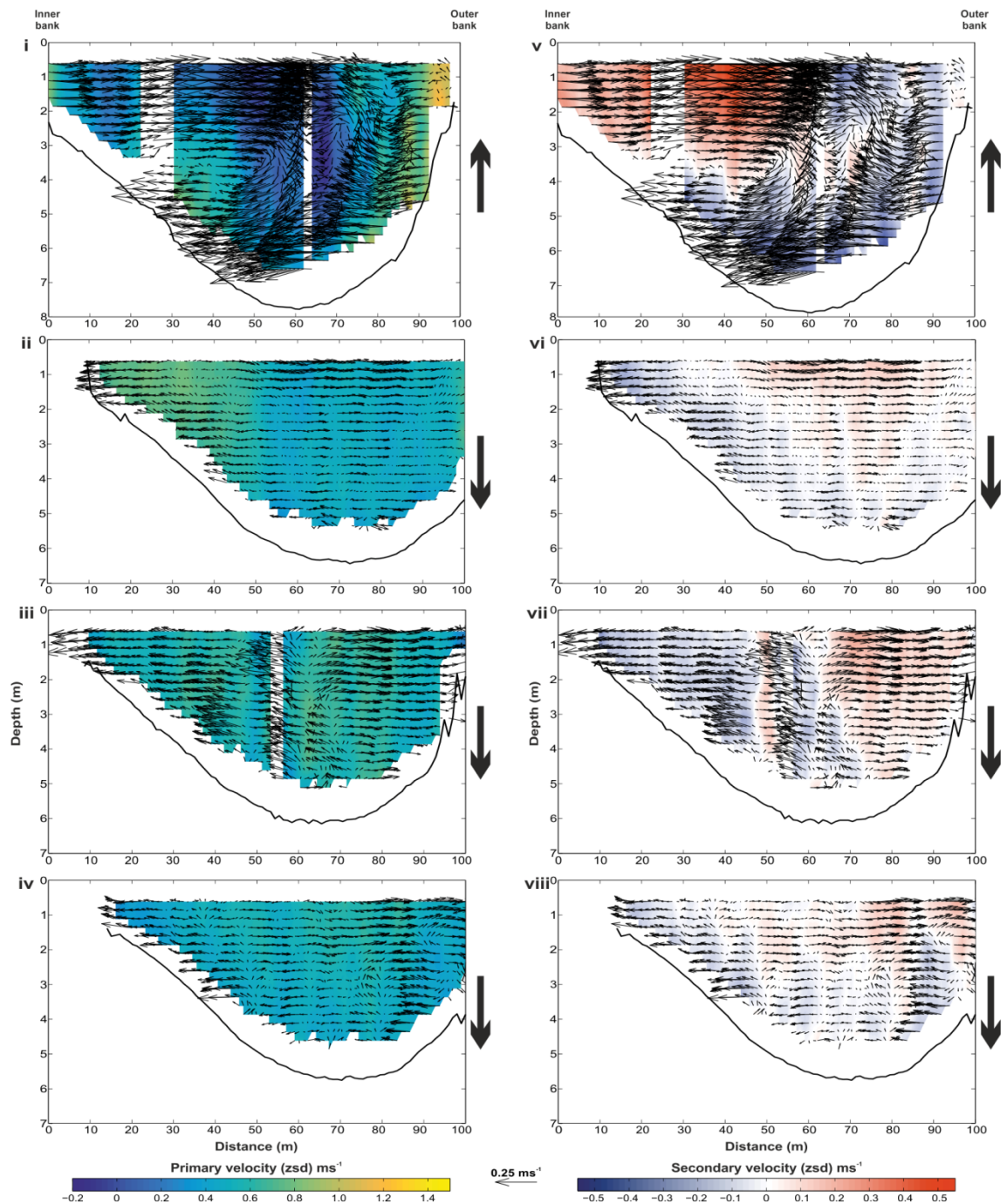


Figure 4.6 Flow velocity collected close to the position of cross-section D (Figure 4.1) during one spring tidal cycle at low river discharge. i-iv show primary flow velocities (zero secondary discharge) in ms^{-1} ; v-vii show secondary flow velocities (zero secondary discharge). Cross-sections were collected 20 minutes after tidal bore, where flow is in a landward direction (i and v); 100 minutes after tidal bore, when seaward flow had re-established (ii and vi); 155 minutes after tidal bore (iii and vii); 200 minutes after tidal bore (iv and viii). Gaps in the data are due to high suspended sediment concentrations during data collection.

4.5 Discussion

The three-dimensional flow structure was quantified in a 100m wide meander bend, with a symmetrical planform, situated within the TIFZ during two different fluvial-tidal conditions. There are profound changes in the fluid dynamics of bend flow as a result of the tidal backwater and flow reversal during the flood tide, which highlight that there will be notable modifications to the classical model of flow fields in channel bends and their subsequent morphodynamics within these zones.

The flows measured at high river-neap tides (HRNT) show well-developed flow patterns, with distinct regions of high primary velocity in the main channel and secondary circulation forming at bend apexes and continuing into the straighter inter-bend straight reaches (Figure 4.4). In contrast to this, the same cross-sections measured during the low river-spring tide (LRST) period do not show such clearly defined flow velocity patterns (Figure 4.5), although a strong and coherent secondary circulation cell was in evidence at the bend apex itself (Figure 4.6). Although the underlying river stage was 1 m lower than in the HRNT measurements, the maximum flow depth in each of the LRST cross-sections was over 1 m deeper. Flow velocities in the cross-sections landward of the bend apex showed lower maximum flow velocities whilst flow was reversed by the incoming flood tide than those measured in the seaward flow during the HRNT measurements, and did not show clear and coherent secondary circulation cells. In contrast, cross-stream velocities in the LRST measurements, whilst flow was in a seaward direction, were higher than those observed at corresponding HRNT cross-sections.

The highest flow velocities measured were seen at the bend apex during LRST conditions 20 minutes after the arrival of the flood tide (Figure 4.6). The maximum velocity measured was $\sim 1.5 \text{ ms}^{-1}$ during a full reversal of flow in the system, with strong secondary circulation that had cross-stream flows over 0.5 ms^{-1} . However, this period of flow reversal was relatively short-lived, with seaward flow re-establishing itself about 100 minutes after the arrival of the flood tide. The short-lived nature of the flow reversal could be argued to limit its influence on the overall bend morphology and morphodynamics, but as the velocities seen were the highest measured at any time across all the measurement periods, its influence is likely to be disproportionately greater. The similar magnitude of flow velocities during the LRST flow reversal ($>1.5 \text{ ms}^{-1}$) and the HRNT flow (1.2 ms^{-1}) will combine to control point bar dynamics at the inside of the bend. Comparison of the spatial positioning of the maximum velocities measured at each cross-section relative to the centreline reveals the dramatic effect on the flow structure through the bend during the different flow conditions (Figures 4.4

and 4.5). During HRNT conditions the highest flow velocities are found in the deepest parts of the channel at all times, close to the inner bank landward of the bend apex and crossing to the outer back seaward of the bend apex (Figure 4.4). At LRST conditions measurements were made landward of the bend apex whilst the flow was reversed by the flood tide. The region of highest flow velocities were found close to the outer bank landward of the bend apex (in the shallower part of the channel), reflecting the changed flow forcing and topographic acceleration through the bend during reversal of flow direction. Comparison of the position of these areas of highest velocity is shown in Figure 4.7. The maximum velocity values observed landward of the bend apex during LRST, whilst the flow was reversed, and are approximately 80% of the maximum velocities measured in the same position at HRNT whilst flow was in a seaward direction. This would result in a pattern of flow strength variation counter to that

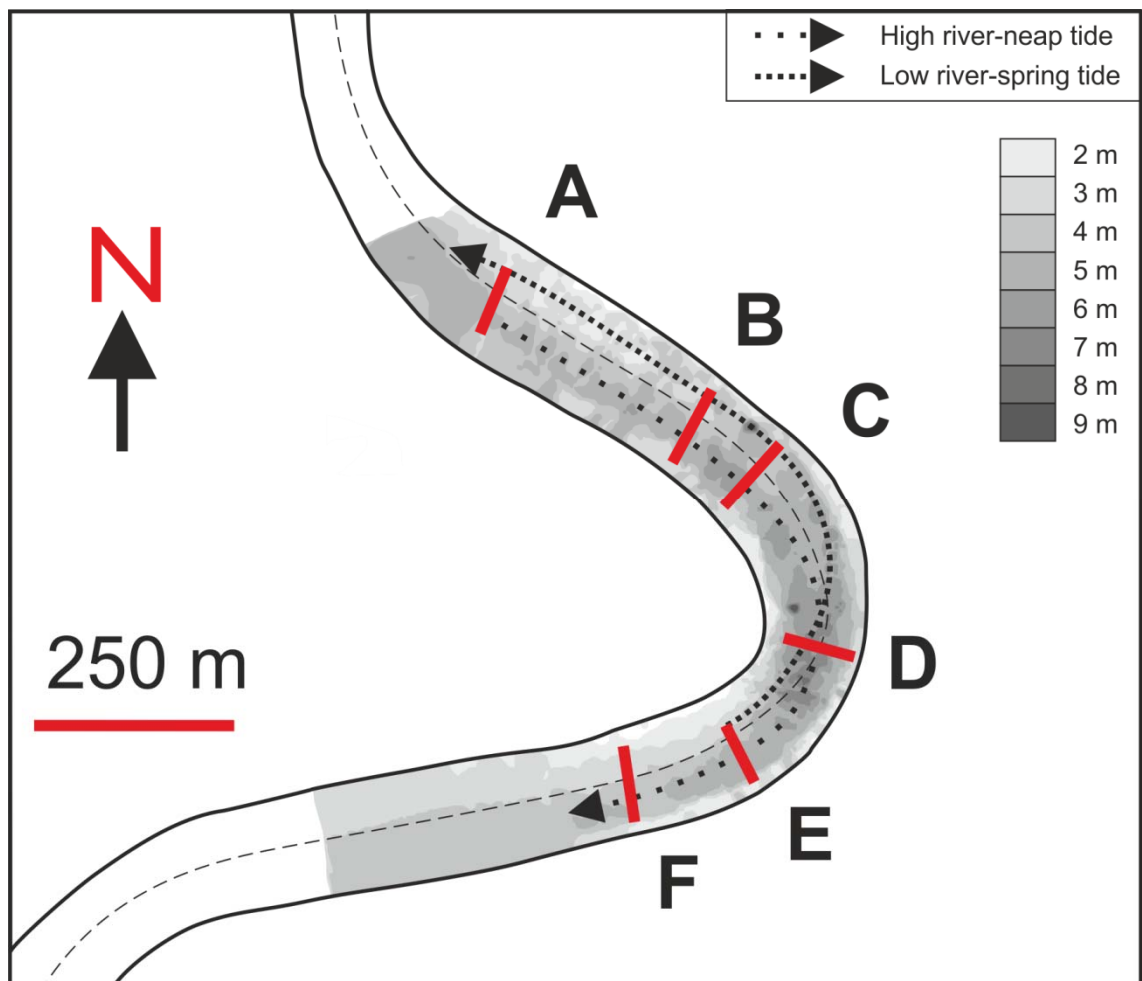


Figure 4.7 Regions of highest flow velocity within the bend measured, relative to the centreline (shown as grey dashed line) showing bed bathymetry. Landward of the bend at high river-spring tide flow is adjacent to the inner bank, whilst at low river-high tide flow is adjacent to the outer bank.

predicted by van den Berg *et al.* (2007) for these zones, with coarser sediment transport likely occurring during the shorter flood tide than during conditions where there was a dominant fluvial flow.

It is likely that the combined influence of the bi-directional flow has altered the point bar in this bend, with this development preventing the evolution of any bend asymmetry, such as those seen in fluvial systems (Furbish, 1988). As a result, bends within tidal-fluvial zones may remain relatively stable with very little large scale migration as the point-bar push effect (Eke *et al.*, 2014) is effectively removed by the switching of flow direction in the ebb and flood tides. This pattern of symmetrical meanders when flood and ebb flows are of similar magnitude is analogous to channels observed within tidal-creek bends (e.g., Fagherazzi *et al.*, 2004). The current data suggest that the balance between the maximum fluvial and tidal flows, combined with the duration and strength of the secondary currents, appear to be significant to the geometry and migration of meander bends within this zone. As noted previously, the Severn Estuary contains a mixed sediment content of mud, sand and gravels (Manning *et al.*, 2010), with regions of locally sourced gravel found within the upper estuary (Carling *et al.*, 2006). It is possible that there is a local gravel deposit present at this location creating a stable core to the point bar (Carling *et al.*, 2015), which could only be moved at the maximum flow velocities in both landward and seaward directions. At lower flow velocities only finer material would be moved within the system. The differences in the flow forcing produced by these changes remove any long term morphodynamic trends as the point-bar adjusts to the sequence of flood and ebb flows. Additionally, the outer bank reversed secondary circulation cells that have been suggested as mechanisms to reduce outer bank erosion in fluvial systems (Blanckaert, 2011), were observed at the bend apex during the primary flow reversal at LRST, however this cell was not present during measurements at HRNT. The planform geometry of the bend is symmetrical, with the adjacent bends landward and seaward having similar geometries as well. Any protection of the outer bank by a secondary circulation cell, such as those described in Blanckaert (2011), would therefore only occur at LRST.

Within this field area the effect of the spring tide is likely to be erosive in nature, with increased sediment available for deposition during the subsequent re-establishment of fluvial flow, allowing coarser material to be moved by the flood tide. The flood pulse at this site is very short lived, with flow in a seaward direction re-established ~100 minutes after the tidal bore has passed in the spring tide. Any sedimentation, particularly of finer material, that occurs will be predominantly governed by fluvial, seaward directed, processes, with some modification by the high velocities observed

during the flood tide. There will be a large amount of sediment transported with erosion of existing (seaward orientated) bedforms and some smaller superimposed bedforms, which are short-lived. Bedforms will be mainly of fluvial origin, but will also see some modification by the incoming flood. Van den Berg *et al.* (2007) suggested that tidal influence on the tidal-fluvial transition zone will result in fluctuations of fluvial flow strength. Deposition of finer sediments in the LRST case will occur following flood tides when seaward flow has re-established. The resultant variations in cross-bedding architecture may be characteristic of the landward region of the tidal-fluvial transition zone, with seaward orientated bedforms becoming washed out by stronger landward directed flows, but also showing overlying finer seaward orientated beds, with coarser material moved landward of this region. This coarser material would form the core of the point bar, with overlying finer material reworked throughout the normal tidal cycles. Moreover, bar push processes, that are important for meander migration, are thus lessened by this constant re-working. There would also likely be little depositional evidence of the high flux, but temporally limited, landward flows observed in the present study. Conversely, these findings highlight the potential importance of the relative balance of flow forcing in relation to the calibre of the sediments through the TIFZ. For example weaker, more frequent flows may rework finer sediments continually, but the morphology and morphodynamics of the system will depend upon the calibre of the sediments making up the core of the deposits and the relative maxima, and relative frequency, of the flow forcing, from either a tidal or fluvial source, and the capability of these flows to entrain the coarser fractions.

The increase in discharge through the bend due to the incoming tide is accommodated entirely by an increase in water depth. The channel at this point is largely steep sided, preventing any significant widening of the flow. This will lead to an increase in the pressure gradient around the bend, but no real redistribution of the centrifugal forces. The constant width of the channel within this field area and the similar geometry of the bend at the landward and seaward ends mean that any width induced secondary circulation effects would be expected to be observed in both HRNT and LRST cases. The helical flow cell initiated at the bend apex when the flow is reversed (Figure 4.6i) does not seemingly continue into the channel landward of the bend, even though the measurements at this location were collected whilst flow was still reversed (Figure 4.5). This is in contrast to the HRNT measurements where the established flow cell at the bend apex continued and was advected some distance seaward of the bend apex (Figure 4.4). The measurements made by Nidzeiko *et al.* (2009) were carried out on a pair of fluvial bends of similar size and geometry to the bend measured here. Measurements were made from a fixed position at the centre of the channel, roughly in a position equivalent to cross-section B in the present measurements. The tidal range in the

Nidzeiko *et al.* (2009) system was lower than that in the present measurements, and was situated further down the estuary system. The system measured by Nidzeiko *et al.*, (2009) was able to accommodate increased river discharge and incoming tides by expansion into a wider channel geometry, whilst the present measurements were made in a steeper sided channel, which deepened with increasing discharge. The velocities in the present measurements for both HRNT and LRST were generally higher than in the measurements by Nidzeiko *et al.* (2009). At LRST conditions the secondary circulation observed in the present measurements was stronger than at HRNT. Flow towards the outside of the channel is only observed in the outer 40 m, whilst in the high river-neap tide only the inner 10 m flows towards the inner bank; most flow is directed towards the outer bank. The cross-stream flows in the present measurements were generally stronger than those measured by Nidzeiko *et al.* (2009). However, cross-section B does not show the flow recirculation cells observed by Nidzeiko *et al.* (2009) in either of the tidal conditions measured. Nidzeiko *et al.* (2009) show that secondary circulation resulted from density differences due to increased salinity on the flood tide, an effect which was not observed during a period of high fluvial flow. As noted, the present measurements although showing a higher tidal range, were further from the estuary mouth, so probably did not have a high density difference due to a saline wedge. When considering a preserved system, these density effects would not be immediately apparent, and could result in very different interpretations of the relative position of the two bends within the tidal-fluvial transition zone.

4.6 Conclusions

Detailed process mechanics of flow and sediment transport within the TIFZ is of increasing interest to a range of stakeholders in order to constrain better TIFZ deposits in the ancient and predict better changes in TIFZ in the modern as an outcome from climate change and sea-level rise. The present study measured the three-dimensional flow within a tightly curved symmetrical meander bend during two distinct hydrological conditions: i) during high river discharge and neap tide (HRNT), and ii) during lower river discharge and spring tide (LRST).

Measurements made at HRNT showed little tidal influence on the flow structure. As the tidal-fluvial boundary was located seaward of the meander bend the flow structure was similar to that found in fully-fluvial bends. However, measurements made at LRST revealed a full reversal of flow around the bend. In this second set of measurements the tidal-fluvial boundary was located landward of the bend. As both sets of measurements were collected in the same location they are directly comparable and reveal that although the bend flows remain of a similar magnitude across the conditions in terms

of primary flows there is a distinct and important strengthening of secondary flows during flow reversal. Although the secondary circulation induced by the bend geometry across the point bar at the bend apex was much stronger during flow reversal at LRST, this pattern of secondary circulation was not observed landward of the bend apex. The persistence of the secondary flow helix landward during flow reversals is thus shorter than that typically found for fluvial bends.

The short-lived flow reversal and the therefore transient strengthening of the secondary flow may have a significant effect on point bar evolution, hindering the longer-term development of an asymmetric planform typical of fluvial bends. This possibly explains the low rates of meander migration often highlighted for bends within the TIFZ (e.g., Dalrymple *et al.*, 1992). This being attributable to the effective removal of the point-bar push effect as the evolution of asymmetry is curtailed. This curtailment may also arise as a result of local gravel deposits. These deposits would only be reworked at higher flow velocities - at very high, but infrequent, fluvial flows or during the more frequent, but shorter lived, spring tides. This raises important questions in terms of the need to explore the relative balances of flow forcing in relation to the calibre of the sediments through the TIFZ. For example weaker flows may rework finer sediments continually, but the morphology and morphodynamics of the systems will depend upon the calibre of the sediments making up the deposits and the relative maxima, and relative frequency, of the flow forcing produced by tidal or fluvial origins.

Chapter 5

The influence of tidal bores on bar morphology

5.1 Introduction

River-estuary systems exhibit a complex transition between fully-fluvial and fully-tidal conditions, resulting in variable hydrodynamics, morphodynamics and water chemistry throughout. Tidal flows will be amplified as estuarine systems narrow, whilst fluvial flows are modulated or even reversed by tides (Figure 1.3). The interaction of tidal and fluvial flows will act to modify the system planform with a region of balanced tidal and fluvial flows postulated to result in a region of tight meanders, with straighter channels landward (fluvially-dominated) and seaward (tidally-dominated) of this (Dalrymple *et al.*, 1992; Dalrymple and Choi, 2007). Salinity values will vary throughout the river-estuary system, decreasing to zero within the fluvially dominated system, although the position of this will vary with relative fluvial input, e.g. within the Severn Estuary salinities of 35 were measured in the outer estuary, decreasing in the tidal river (Uncles, 1983; Uncles, 2010). This transition is not fixed in position due to the variations in fluvial and tidal flow magnitudes, resulting in a transitional zone containing composite sedimentological structures and facies which may be 10s to 100s of km in length (Boyd *et al.*, 1992; Dalrymple *et al.*, 1992; Dalrymple and Choi, 2007; van den Berg *et al.*, 2007; Fustic *et al.*, 2012). Although there is recognition of these process complexities, the effect of the river-estuary transition on the sedimentological characteristics of these systems are, at present, poorly understood.

Morphological and facies models of tidal-fluvial systems have been developed (Dalrymple and Choi, 2007; Archer, 2013), with Archer (2013) examining six river-estuary systems with hypertidal ranges, subdividing each into three sedimentological zones. Their outer zone consists of longitudinal bars, whilst the middle zone has extensive sand flats throughout. The innermost tidal zone marks the landward limit of tidal flows and the formation of estuarine point bars, with cycles of spring and neap tides observed. It is important to note that these zones do not necessarily tie to the straight-meander-straight morphology of the model presented by Dalrymple and Choi (2007), where the central part of the tightly meandering section is thought to mark the position of bedload convergence and hence the outer limit of the tidal-fluvial transition (Figure 1.3). The innermost zone of Archer's (2013) framework lies landward of the meandering section and would not differentiate between sandflats of tidal, fluvial or mixed origin.

An often undescribed feature of some river-estuary systems is the formation of tidal bores. These are known to occur in areas with a high tidal range and a rapidly shallowing, narrowing planform geometry (Fielding and Joeckel, 2015). Bores are mobile hydraulic jumps that propagate upstream as a series of waves at the leading edge of flood tides and may be undular or breaking in nature, occurring as a series of waves. Tidal bores have been observed in locations around the world (Bartsch-Winkler and Lynch 1988, Chanson, 2012), with the highest bores occurring in the Qiantang Estuary, China. Studies have shown that the passage of a tidal bore may cause soft-sediment deformation within the underlying surface such as erosion surfaces, folding, flame structures and dewatering of the underlying sediments (Tessier and Terwindt, 1994; Greb and Archer, 2007; Fan *et al.*, 2014).

Within tidally-influenced regions, alternating deposits of coarse and fine material are commonly found, attributed to alternating high and low energy conditions. Dalrymple *et al.* (2015) suggest that any fluviially-derived sedimentation within a tidal-fluvial transition will result from periods of high energy flow, such as river floods arising from high rainfall. Lower energy interflood horizons are eroded by the arrival of these river flood events. Laminations of varying thickness may also be observed, with coarse grained deposition during flood and ebb tides (the dominant tide forming thicker bands) whilst fine grained material is deposited during slack water (Kuecher *et al.*, 1990). The spring-neap tidal sequence may also be preserved within these tidal rhythmities due to variations in the lamination thickness.

Depending on the ratios of coarse to fine material within the system this may take the form of flaser, wavy or lenticular bedding (Reineck and Wunderlich, 1968). In systems with a greater amount of coarser material flaser bedding commonly forms; fine grained mud or silt settles during slack water conditions into the troughs of ripples which have previously formed at either high or low tide. However, where fine material dominates lenticular bedding will primarily form, where lenses of coarse material, which may be discontinuous, are found within a finer grained deposit (Reineck and Wunderlich, 1968). Investigations of these tidal-fluvial deposits and any interaction with tidal bores are, however, limited. Greb and Archer (2007), working in Turnagain Arm, Alaska, described deformation horizons 5-19 cm thick of fine sand and silt (representing two daily tides) lying between undeformed horizons of laminated sands and silts. This suggests that only the upper horizons were affected by the tidal bore, or that some horizons are more susceptible to liquefaction or folding. Fan *et al.*, (2014) investigated the interaction of the bore of the Qiantang Estuary with localised sediments, finding that deposits modified by tidal bores were generally coarser and less sorted than surrounding deposits.

Although tidally-influenced features such as estuaries have a high preservation potential, as they contain large amounts of sediment from both fluvial and tidal sources and are often contained within older valleys, they have not always been well recognized within the geological record (Dalrymple *et al.*, 1992). Estuaries commonly form during periods of high sea level when older valleys are flooded, and are often confined within these spatially limited features. Active sediment transport and deposition will cause the system to infill, particularly as the rate of sea level rise begins to slow or fall, often resulting in several cycles of stacked estuarine facies with sea level fluctuations (Reinson, 1992; Dalrymple *et al.*, 1992). The relatively rapid rate of formation and infilling of such systems results in a range of facies which are representative of a short geological time period but have a high likelihood of preservation (Dalrymple *et al.*, 1992; Boyd *et al.*, 1992). However, following the formulation of more comprehensive facies models, their signatures are now being recognized more frequently within the geological record (Boyd *et al.*, 1992; Dalrymple *et al.*, 1992; Dalrymple and Choi, 2007) and the need for identifying the complexities recorded in order to better interpret palaeoenvironments has recently become a significant research focus. There have been some limited reports of tidal bores preserved within the ancient record, (Martinius and Gowland, 2011; Fielding and Joeckel, 2015), which are broadly in agreement with modern descriptions (Fan *et al.*, 2014), although their identification is sometimes limited by a lack of modern examples and process based understanding. Interpretation of bores in the ancient therefore holds great promise for regional interpretations from isolated outcrops, both of system geometries and tidal range.

The present study investigates the sedimentological characteristics of a large bar within the region of tidal-fluvial transition within the Severn Estuary, UK, and the interaction of a tidal bore with the bar. This region is known to experience full reversal of flow during high tides, with tidal bores a regular occurrence in this stretch of the inner estuary. Flow measurements were made during a spring tide at a time of low fluvial flux, allowing the influence of the incoming flood tide on the bar to be quantified. Measurements of the passage of a single tidal bore were carried out within the channel and at the seaward end of the bar, allowing direct comparison of the same bore front in these two locations. Finally, a series of cores retrieved from the bar surface at low tide allow the variations in fluvial and tidal influence on the bar sedimentology to be investigated in detail. The study investigates tidal influence on this bar and the preservation potential, along with the interaction and relationships with the deposits produced by passage of a tidal bore.

5.2 Field location

The Severn Estuary, UK shows the second highest tidal range in the world, with a tide height of 9 m observed at Sharpness. The Bristol Channel-Severn Estuary-River Severn system rapidly narrows and shallows, causing an amplification of tide height at the upper reaches of the estuary system, producing a significant bore at spring high tides (Rowbotham, 1983; Chanson, 2012; Keevil *et al.*, 2015b; Carling *et al.*, 2015). Within the inner estuary there is a high concentration of suspended sediment, approaching the order of 0.5-10 gl^{-1} , along with fluvially sourced sands and gravels (Carling *et al.*, 2006; Carling *et al.*, 2009; Manning *et al.*, 2010; Kirby, 2010; Carling *et al.*, 2015). The incoming tide of the Severn Estuary is now halted at Gloucester by the presence of a weir; previously the highest tides would occasionally reach as far upstream as Worcester (Archer, 2013; Uncles, 2010).

Fieldwork was carried out on and around Longney Sands, a large sand bar within the tidally influenced zone, 15 km downstream of Gloucester (Figure 5.1). Archer's (2013) study of hypertidal systems places this location within a region which

“includes the innermost extent of tides and estuarine point bars. Annual and neap–spring cycles have been documented in Zone 3 and are probably the most indicative features of hypertidal systems.” (page 1)

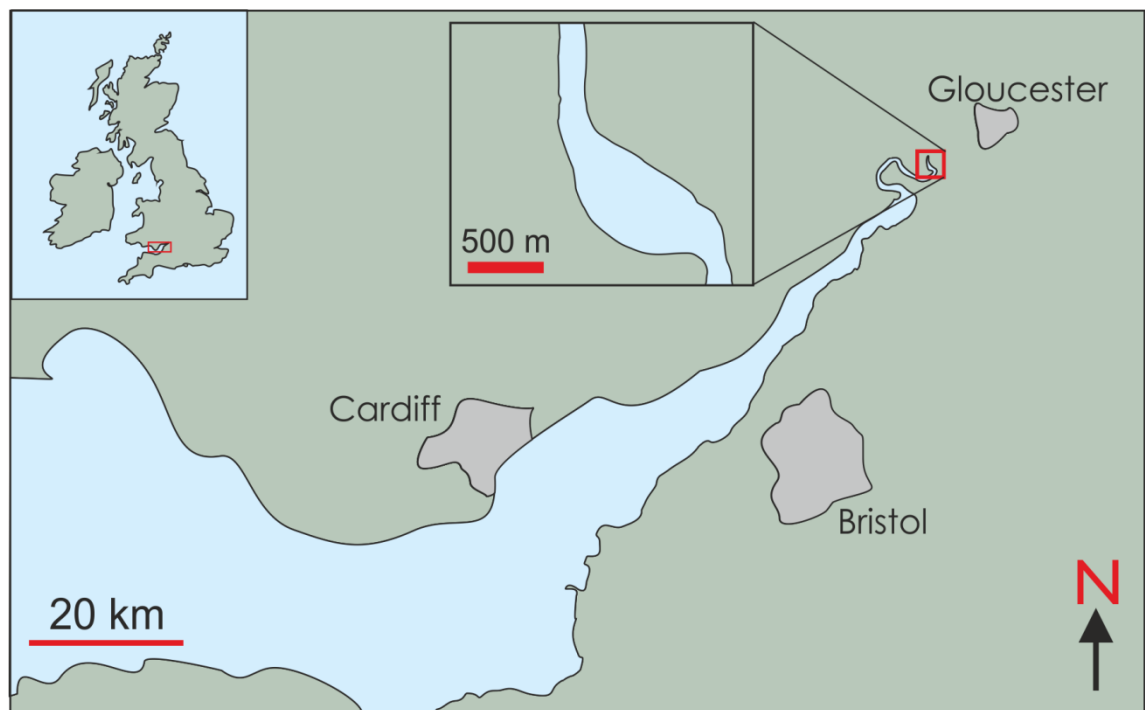


Figure 5.1 Location of Longney Sands, River Severn, UK. The bar is located 3 km seaward of the bend investigated in Chapter 4. River flow is from the North.

Laminations of varying thickness, indicative of a tidal system have been found within this zone (Archer, 2013), although it is unclear the exact location at which these were observed. Using the straight-meander-straight model of Dalrymple *et al.* (1992), it would be expected that this field site lies within the mixed-energy region of the estuary system. Dalrymple *et al.* (2013) suggest that this location would lie upstream of the position of bedload convergence within the Severn Estuary.

The inner Severn Estuary has been extensively engineered, with flood protection levees built at the location along much of the banks from the Roman period onwards (Allen, 1991b). As a result, much of the planform geometry of the system has remained relatively fixed for an extended period. An exception to this is the region around Longney, where the studied bar is located, with historic maps showing that this bend has moved in position by over 100 m in the last 150 years.

The study bar is 1.2 km long and 500 m wide, without a fixed morphology, illustrated in the Google Earth imagery in Figure 5.2. Images collected over seven years show the main river channel switching from the west bank to the east bank and back again. The earliest image (31/12/1999), shows a bar occupying most of the bend with a small channel to the west and bank attachment to the east (Figure 5.2i). Although the second image is less clear, by 17/04/2005 the channel has moved away from the west bank, leaving a smaller attached bar at the southern end (Figure 5.2ii). 18 months later, in the image dated 31/12/2006, the bar has now become fully attached to the western bank, with a wide channel to the east of bar (Figure 5.2iii), whilst by 13/07/2013 a bar morphology similar to the original image is observed (Figure 5.2iv). Longney Sands is a long-lived feature of the Severn Estuary, being present on the earliest Ordnance Survey maps in the 1850s. During fieldwork, navigation around the bar was difficult as at low water the channels were very shallow and cryptic. There is no current maintenance of the river channel as it is not commonly used for shipping, although the banks have been raised for flood protection.

Fieldwork was carried out in September 2014, during a period of relatively low river flow. Records from the Environment Agency gauge at Epney, 1 km downstream of the survey site, shows river flow variation of up to 1.7 m over the course of 2012 – 2014, with the lowest flows observed during the present fieldwork (Figure 5.3i). The bar top was completely exposed during low tide as a consequence of this low flow. Fieldwork was conducted during a series of Spring Tides within the estuary, when the incoming tide caused a rise in water level of over 3.5 m (Figure 5.3ii). The tidal flow at the site is highly asymmetrical, with a flow reversal for approximately 1 hour on the flood tide, after which seaward flow is re-established and the system begins to drain.

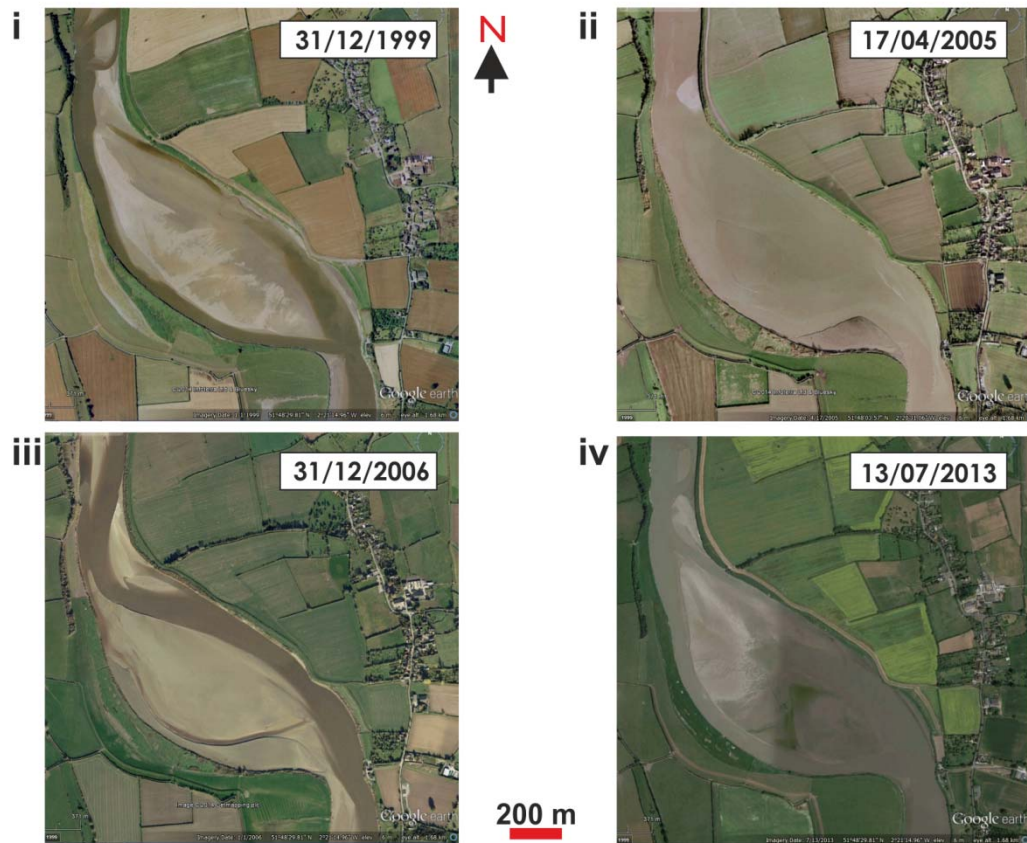


Figure 5.2 Evolution of Longney Sands shown via Google Earth imagery: i) shows a single bar with 2 channels; ii) the bar has become bank attached to the east with the western channel cutting through the previous bar; iii) the bar is now bank attached to the west with a wider eastern channel, smaller surface channels are also visible; iv) the bar is now centralised again.

5.3 Field methods

A variety of measurements were made around Longney Sands during the fieldwork reported herein (Figure 5.4). Flow velocity measurements were obtained as cross-sections and at fixed locations, both downstream of the bar and along a central transect, using a Teledyne RD Instruments RioGrande 1200 Hz Acoustic Doppler Current Profiler (ADCP) deployed from the side of a small research vessel. The instrument collects data at vertical intervals (bins) of 0.25 m through the water column at a rate of ~1 Hz; blanking distances due to instrument deployment and acoustic sidelobe interference effects were 0.61 m down from the water surface and 0.5 m up from the base of measurements (Figure 5.5). Two series of ADCP data were obtained: firstly, a series of channel cross-sections were measured to the east of the bar; secondly, measurements were collected from a fixed position during the incoming flood tide on the morning of 09/09/2015, as the tidal bore passed and for 20 minutes following.

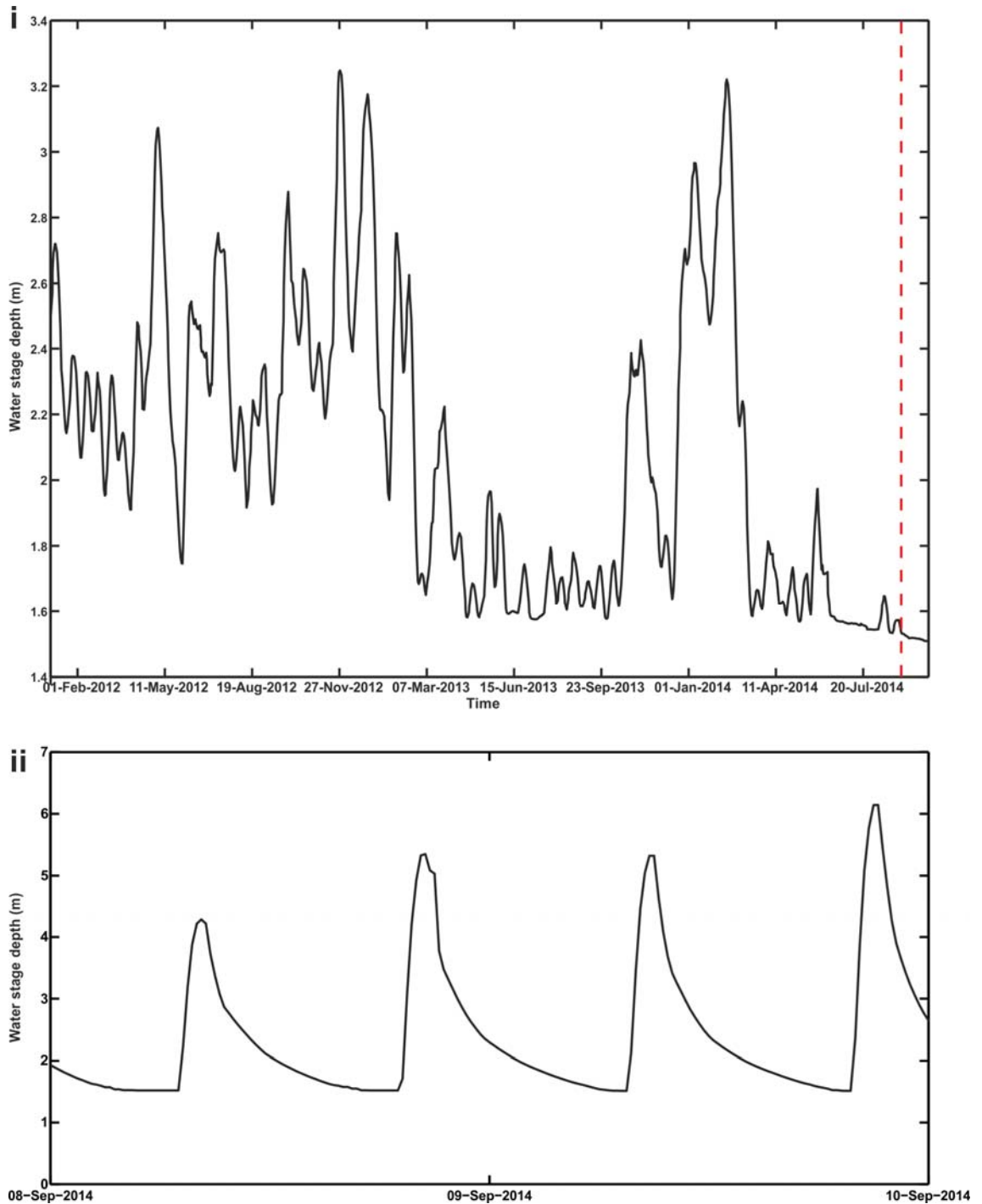


Figure 5.3 Stage data measured at Environment Agency Epney Gauge (Site ID – 2059): i) Base river flow for the period 01/01/2012 – 10/10/2014- red dashed line shows the fieldwork reported on here (08-09/09/2014); ii) Stage data collected every 15 minutes for the period of the present work 00:00 08/09/2014 to 00:00 10/09/2014. *Contains Environment Agency information © Environment Agency and database right.*

Repeated transects were collected where possible as recommended by a number of works (e.g. Yorke and Oberg, 2002; Muste *et al.*, 2004a; Muste *et al.*, 2004b; Szupiany *et al.*, 2007), to remove larger scale fluctuations; the moored tidal data was only able to reveal more general flow patterns (Szupiany *et al.*, 2007). A vector track and speed over ground derived (VTG-derived) dGPS correction was applied to correct for the motion of the boat relative to the water column (Yorke and Oberg, 2002; Parsons *et al.*, 2005).

The cross-sectional flow data was post-processed within the Velocity Mapping Toolbox (Parsons *et al.*, 2013). Transects were rotated using the zero-net secondary discharge method to remove lateral flux through the cross-section to allow improved visualisation of cross-stream flow (Parsons *et al.*, 2013). The moored data was not processed using VMT, as it was collected from a fixed position. The raw data was analysed to ascertain the dominant flow direction during fluvial flow and then the downstream (northern oriented) and cross-stream (eastern oriented) velocities were rotated relative to this

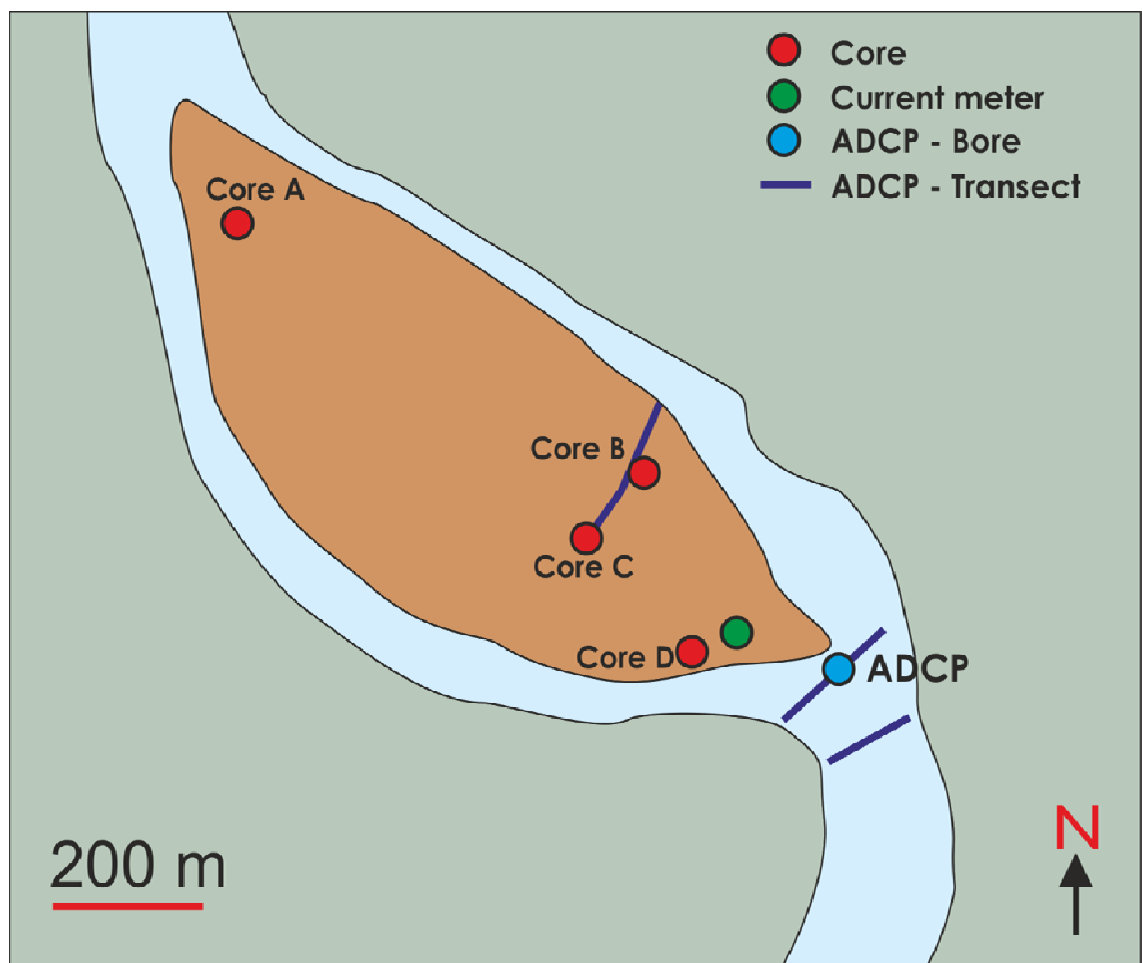


Figure 5.4 Locations of field measurements. Cores are red circles, the current meter as a green circle. ADCP transects are shown as blue lines, with the blue circle showing the mooring location during the tidal bore.

obtain true downstream and cross-stream velocity values. ADCP data was collected along three separate transects before and after the arrival of a tidal bore, and also at a moored position during the passage of the bore (Table 5.1). The approximate positions of these transects are shown in Figure 5.4.

As the fieldwork coincided with the spring tides, measurements were also made of the incoming tidal bore and the following flood tide, at a fixed position. An electromagnetic current meter (Valeport Midas ECM +CTD) was deployed at the seaward end of the bar (Figures 5.4 and 5.5), for 24 hours (two tides) to measure current speed (ms^{-1}), conductivity, from which salinity is derived in Practical Salinity Units (1 PSU \sim 1 g/kg), temperature ($^{\circ}\text{C}$) and pressure (DBar), whilst a flux gate compass allows for the orientation of flow to be derived. The instrument is battery powered, allowing it to be deployed in the field and collected later (Figure 5.6). The current meter was placed within a small hollow at the downstream end of the bar. When sited the top of the instrument was left exposed above the water level (Figure 5.6ii); following the first tide measured the instrument was left in a small pool and was not exposed at low water. When the instrument was recovered it was still within the pool (Figure 5.6iii). Data

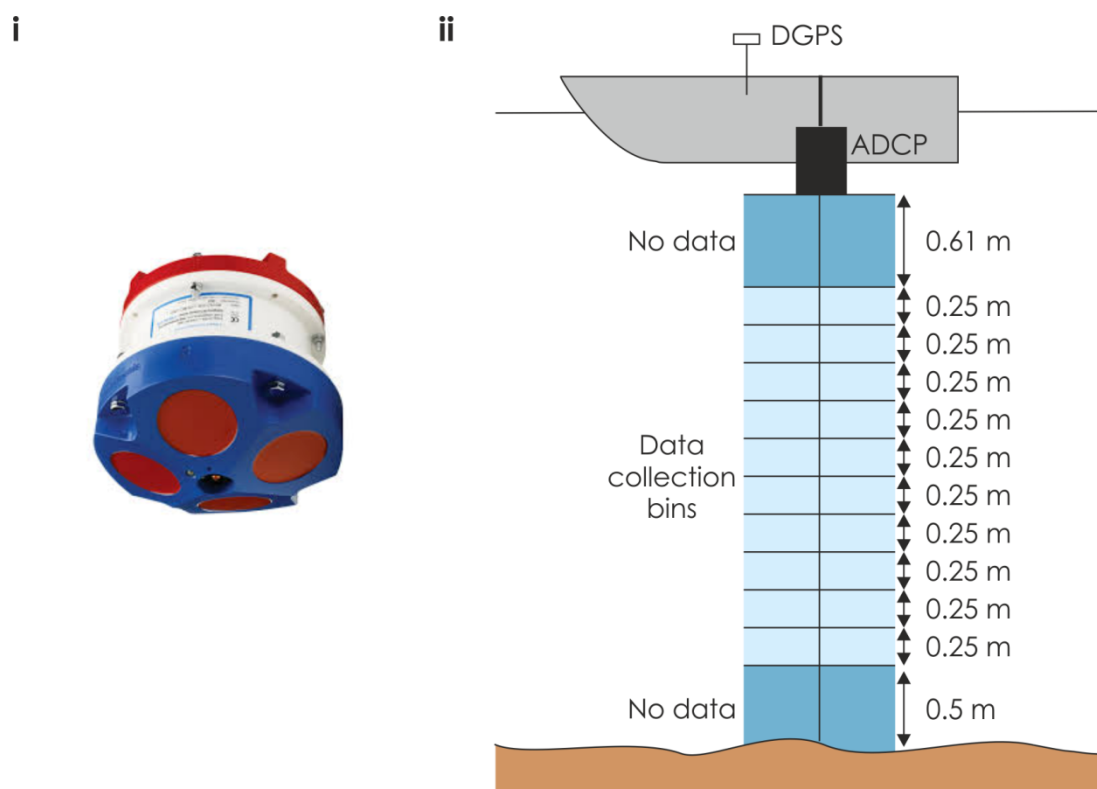


Figure 5.5 ADCP setup: i) Teledyne RD Instruments Rio Grande 1200 Hz ADCP; ii) schematic of instrument setup showing position of instrument and data collection bins.

Table 5.1 Timings of ADCP data

| Time | Transect | River condition | Location | Primary vel (zsd) ms ⁻¹ | |
|---------------------|----------|---|------------------------|------------------------------------|------|
| | | | | Min | Max |
| 08:39 08/09/2014 | Trans001 | After bore – flow reversed | Downstream of bend (a) | 0.60 | 2.57 |
| 09:45 08/09/2014 | Trans004 | After bore – flow re-established in seaward direction | Central transect (c) | 0.13 | 0.44 |
| 10:04 08/09/2014 | Trans006 | After bore – flow re-established in seaward direction | Seaward end of bar (b) | 0.36 | 0.66 |
| 08:04 09/09/2014 | Trans009 | Before bore – flow in seaward direction | Seaward end of bar (b) | 0.04 | 0.62 |
| 08:34 09/09/2014 | Trans010 | Bore – flow reversed | Moored at location (d) | - | - |
| 09:41 09/09/2014 | Trans013 | 55 minutes after bore – central region reversed | Downstream of bar (b) | 0.01 | 1.54 |
| 10:26 09/09/2014 | Trans014 | After bore – flow re-established in seaward direction | Central transect (c) | 0.28 | 0.68 |

were collected at a point ~0.2 m above the bar top at a rate of 8 Hz. Data were post-processed to re-orientate flow data relative to the dominant fluvial flow direction at the bar.

In contrast to an ADCP which measures a velocity profile through a water column, an electromagnetic current meter makes an at a point velocity measurement. An alternating magnetic current is generated by the instrument and using Faraday's Law of induction when water (a conductor) flows around it a voltage is induced. This voltage is detected by the instrument and as it is proportional to the flow velocity this is calculated

$$E = B\bar{v}b$$

Equation 5.1

where E = the electromagnetic field generated in volts;

B is the magnetic flux density in teslas (T);

\bar{v} is the average velocity of the conducting fluid (ms⁻¹);

b is the length of the conductor (m).

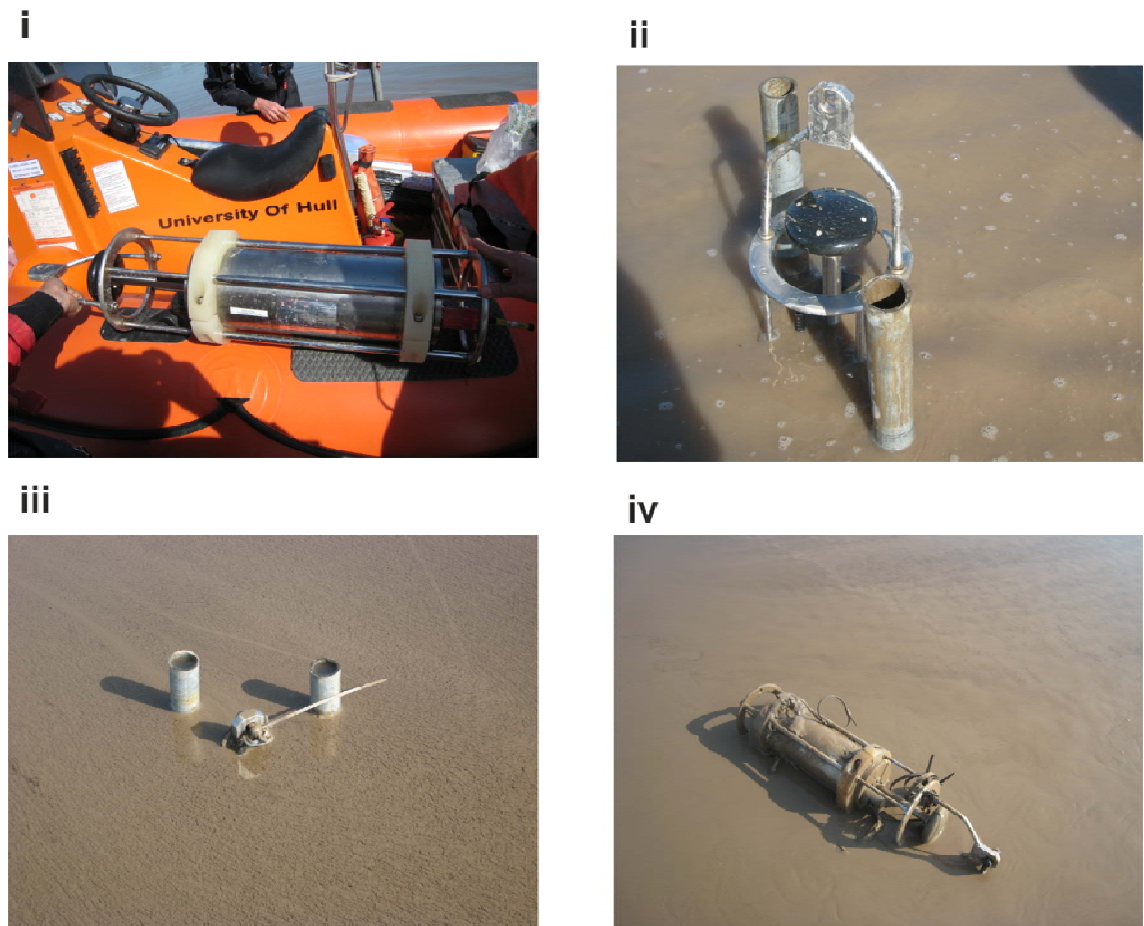


Figure 5.6 Midas ECM current meter: i) Instrument before deployment; ii) Instrument in situ; iii) Instrument in situ at time of recovery; iv) Instrument following recovery.

Four sediment cores were recovered, using a custom built vibracoring rig, at the landward and seaward ends of the bar and 2 along the central ADCP transects. The core furthest downstream was located close to the position of the current meter (Figure 5.4). The collection of sedimentary cores and the creation of relief peels from these allows for the interpretation of sub-surface sediments within a system. These cores also allow the accurate grain-sizing of sediments to be carried out. This combination of cores and flow data will allow the interplay between flow processes and sedimentary deposits on a bore-influenced tidal bar to be examined.

The vibrocorer consisted of an Oztec BP50a concrete poker, which was clamped to the core pipe to provide the necessary vibration to drive the pipe into the substrate. The concrete poker is formed of a Honda 2 ½ HP engine mounted on a backpack for ease of transport. Connected to this is a flexible shaft with a steel head at the end. This head was mounted in a repositionable custom clamp which was attached to the core pipe and used drive the core into the bed (Figure 5.7i). The core pipe was 4 m long aluminium tube with a 76.2 mm outer diameter and a wall thickness of 1.626 mm (16 swg).

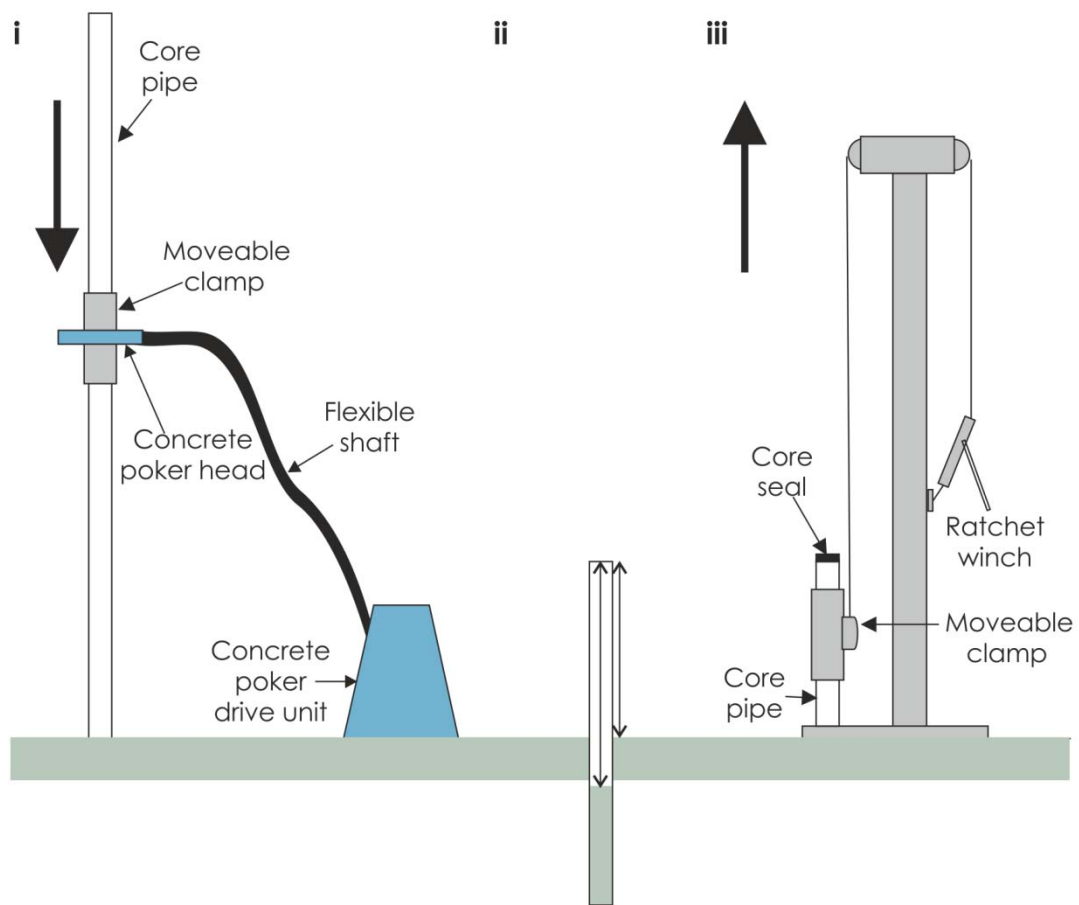


Figure 5.7 Coring rig set up: i) the pipe driving rig using a moveable clamp with a concrete poker head attached; ii) shows the measurements taken; iii) the retrieval rig using a ratchet winch with the cable passed over the top of a fixed frame.

Once the core pipe had been fully driven into the bed the depth from the pipe top (trimmed if necessary) to the top of the bed and the sample within were measured (Figure 5.7ii); following this the top of the pipe was filled with water and sealed using a pipe seal. The pipe retrieval rig was assembled around the pipe core and the winch cable passed through a set of rollers at the top and attached to the clamp on the pipe. In this way the core can be gradually extracted with repositioning of the clamp on the pipe. When the pipe has been fully retrieved the bottom of the core was sealed to prevent loss of material, whilst the water was removed from the top of the core which was marked and back filled to maintain core integrity before sealing.

The cores were cut using a small handheld circular saw (Bosch PKS16) and split in half. Approximately 1 cm of material was removed from one half of the core material, forming a smooth surface. This was filled with West System Epoxy (105 Epoxy Resin and 205 Hardener in a 5:1 mix) with wooden battens to act as a support. The epoxy penetrates the pore spacings between grains and acts to preserve sedimentary

structures and grain-size differences (Burger *et al.*, 1969). The length of cure time was not an issue as the cores were not prepared on the bar surface. Once the epoxy resin had hardened the core slice was removed and excess sediment washed off to show the core surface clearly. These cores were photographed using a Nikon D810 DSLR with a Nikon Nikkor 60 mm macro AF-D F2.8 lens and a Kaiser RS1 copy stand to minimize image distortions and then logged.

Sediment samples were taken every 5 cm from the remaining half of the core for grain-sizing. These samples were dried in a small oven; regular stirring of the samples was necessary to prevent aggregates from forming. Grain-sizing was carried out using a Retsch CamSizer XT with X-Dry X-Jet module, which has a measurement range of 2 μm to 3.5 mm (Retsch, 2012). The dry sample is fed into a vibrating hopper into a venturi, and from there is passed through the analysis window by positive air pressure from a compressed air source (in this case at 20kPa). The analysis window is imaged by two cameras (one of which is zoomed in) and illuminated by two LEDs, allowing grain-size and shape to be analysed by the software in real time.

Finally, several water samples were collected using a Van Dorn water sampler. These were subsequently analysed using a Sympatec QicPic Lixell system to examine grain-size, which uses a water dispersal system. The residual water samples were then filtered and dried using 0.2 μm cellulose nitrate filter papers and the sediment sample weighed to find the suspended sediment concentration.

5.4 Results

5.4.1 Flow measurements

ADCP flow data was collected at several locations around the bar during the reported fieldwork (Figure 5.4 and Table 5.1). To investigate the flow around the seaward end of the bar, depth-averaged flow data was collected for 30 minutes before the arrival of the tidal bore (Figure 5.8i). The bar at this time was exposed but the strongest flow was observed in the central region of transect. Flow velocities were in the range of 0.04 – 0.62 ms^{-1} . During the tidal bore flow within the river completely reversed (Figure 5.8ii). At the most seaward transect strong flow in a landward direction is observed across the entire width of the channel, with flow velocities of 0.6-2.57 ms^{-1} . The transect at the seaward end of the bar also shows flow in a landward direction within the central region of the channel (corresponding to the earlier strong seaward flow). However, at the edges of the transect where flow steering had previously been observed, flow was found to be in a downstream direction. This flow was much slower than in the central region ($\sim 0.15 \text{ms}^{-1}$), whilst the maximum landward flow velocity was 1.54 ms^{-1} . Flow

i



ii



iii



100 m



Figure 5.8 Depth averaged ADCP measurements: i) prior to the arrival of the tidal bore, ii) during flow reversal following tidal bore, iii) following re-establishment of flow in a seaward direction.

was eventually re-established in a downstream direction, the central transect and downstream of the bar again show maximum flow velocities of $\sim 0.7 \text{ ms}^{-1}$ (Figure 5.8iii).

ADCP data was also collected whilst anchored at a point during the passage of a tidal bore and the following flood tide (for location see Figure 5.4). Downstream flow velocities rapidly reverse on the arrival of the tidal bore (Figure 5.9), accompanied by a rise in water level of over 0.5 m. The downstream flow velocity immediately following the bore head fluctuates rapidly, varying from $\sim 0.2 \text{ ms}^{-1}$ to 1.5 ms^{-1} in a landward direction over the course of 2 minutes. Following this the flow velocity increases to a maximum of 3 ms^{-1} , which corresponds to the highest flow depth observed 8 minutes after the arrival of the bore head (Figure 5.9). Cross-stream flow velocities also fluctuate on the arrival of the bore head, but these variations are much smaller ($< 0.5 \text{ ms}^{-1}$). Cross-stream velocities gradually increase until the maximum flow depth height is reached after 8 minutes ($< 1.75 \text{ ms}^{-1}$), after which they begin to fluctuate more widely ($0.2\text{-}2.5 \text{ ms}^{-1}$) (Figure 5.9). This variation in cross-stream velocity is likely to result from the inundation of the bar top, which lies to the northwest of the anchor position (Figure 5.4), and the diversion of the flow onto the bar.

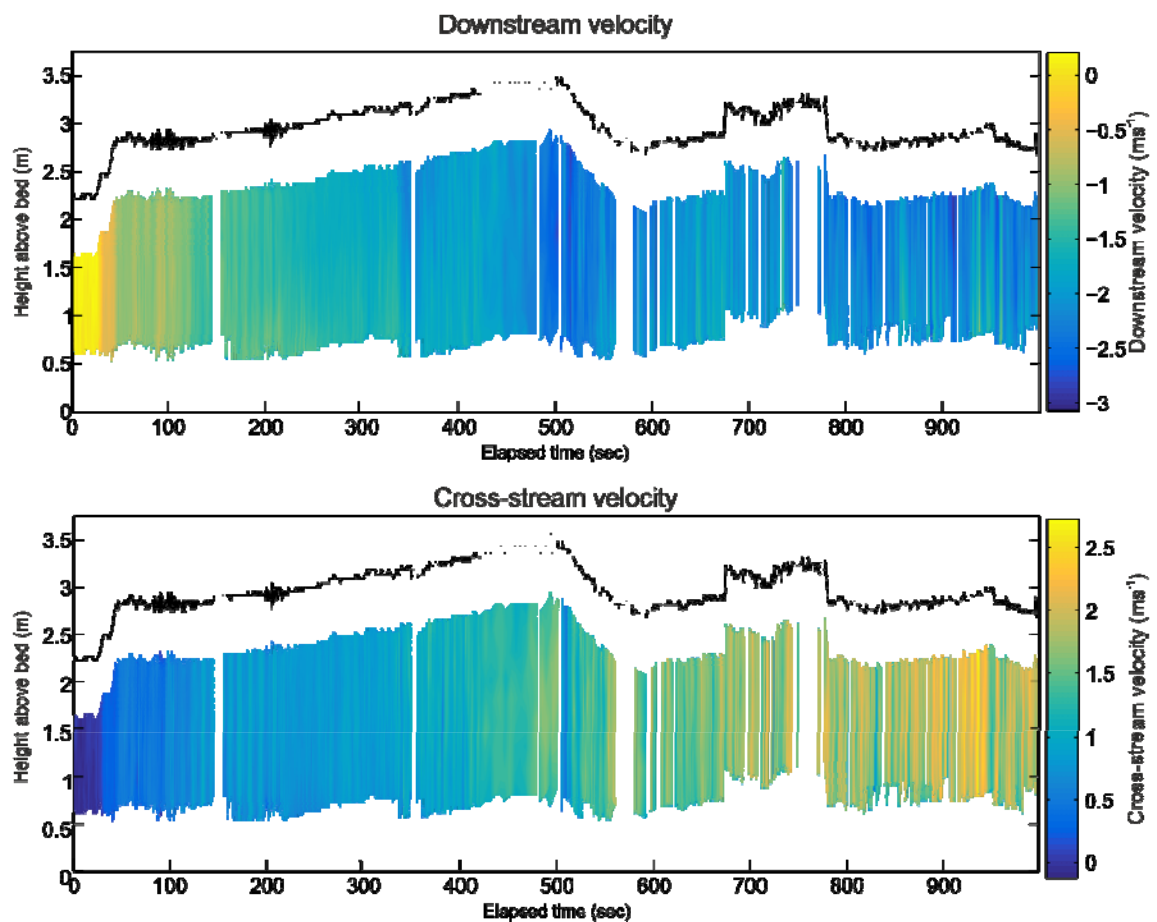


Figure 5.9 ADCP velocity data collected during the first 15 minutes of the passage of a tidal bore from an anchored boat. Initial anchor position is shown in Figure 5.4, following which the boat was carried landward by the incoming tide. Positive downstream velocity is in a seaward direction whilst positive cross-stream velocity is towards the western bank.

Further flow measurements were made at the seaward end of the bar. The ECM collected at a point flow measurements over two tides; downstream and cross-stream flow data were collected by the instrument during deployment. The Epney gauge data shows that the tides measured were of a similar magnitude (Figure 5.3ii). The arrival of the incoming flood tide, in the form of a tidal bore, is marked by a rapid cycling of downstream flow in landward and seaward directions (Figure 5.10). After these initial fluctuations the flow can be observed to increase in a landward direction, before slowing a returning to a seaward direction. The downstream flow velocities were of a similar magnitude in both tides measured. Cross-stream flow shows the deflection of flow as it meets the bar head and as the bar is exposed when the tide falls, although cross-stream velocities were of a higher magnitude during the first tide measured (Figure 5.10).

The current meter was also able to measure pressure, temperature and conductivity data. The pressure data curve shows the incoming of both tides with the same general shape visible (Figure 5.11). The slightly higher initial pressure observed before the second tide is due to the fact that the instrument remained submerged after the previous tide. The initial rise in pressure during the first 1000 seconds measured is

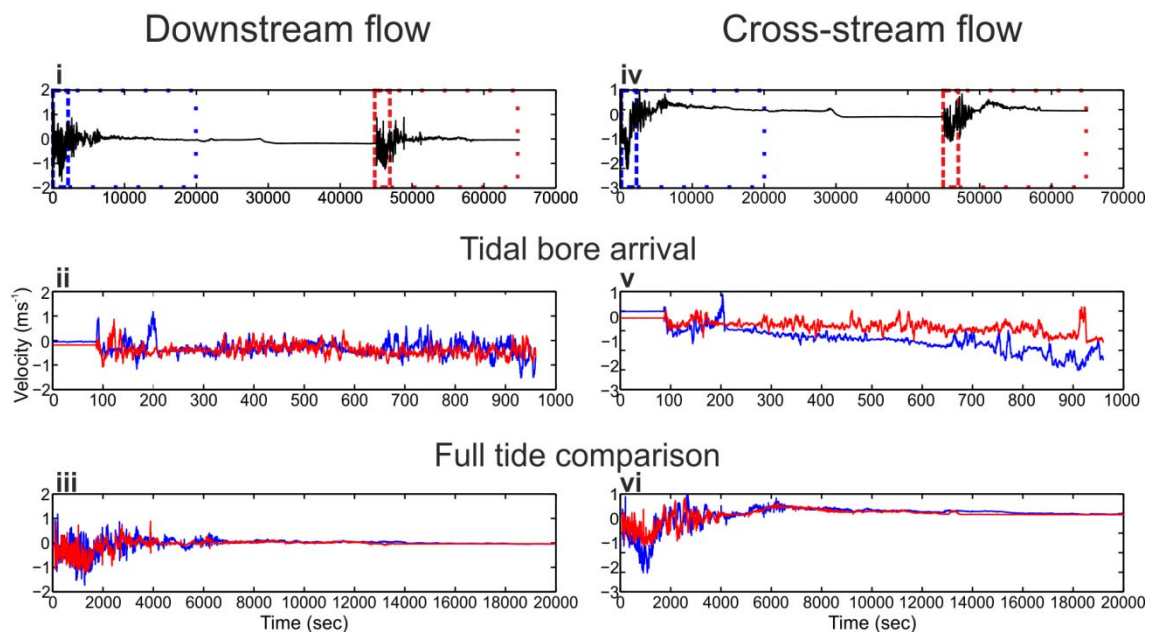


Figure 5.10 Flow data collected by the Midas ECM (location shown in Figure 5.4). Downstream flow is in i-iii, cross-stream flow in iv-vi (data in blue is from the first tide, data in red from the second tide). Data from the full deployment is shown in i and iv; the first 1000 seconds of data following the arrival of a tidal bore are shown in ii and v (dashed box on i and iv); the full tide comparison is shown in iii and vi (dotted box on i and iv).

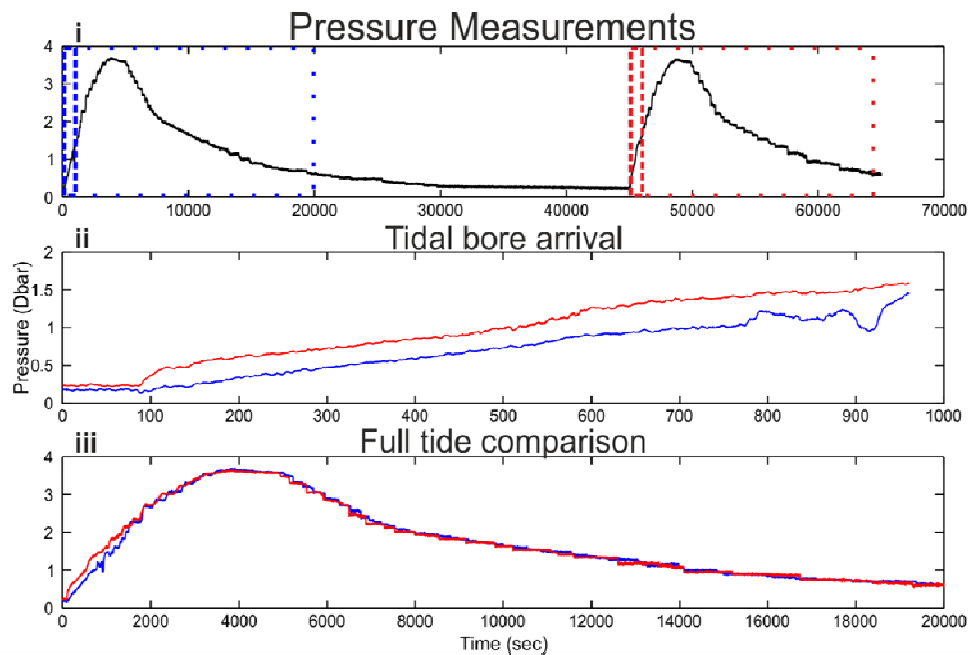


Figure 5.11 Pressure measurements from the Midas ECM: i) all data measured; ii) comparison of the arrival of both tidal bores (data in blue is from the first tide, data in red from the second tide); iii) the full incoming tide for both tides (start point of tidal bore and tide plots is the same).

lower during the first bore (08/09/2014 pm), but the overall tide shows the same pressure rise to a maximum of 3.5 DBar, equivalent to a water depth of ~0.35 m on the bar top at this time. The river height measure at the Epney gauge shows that both these tides were of the same magnitude, so the correspondence of the maximum pressure is not unexpected (Figure 5.3ii).

Calculated salinity values also show the effects of the incoming tides on flow mixing through the zone (Figure 5.12). The exposed instrument prior to the first bore (08/09/2014 pm) shows a sharp rise in salinity during the arrival of the bore to 5 psu before decaying back to 1 psu; the salinity levels were much higher (10 psu) before the arrival of the second bore (09/09/2014 am), suggesting that the submerged instrument was located within a pool of residual water from the previous flood tide at the seaward end of the bar between the two tides. The arrival of this bore shows an initial sharp drop in salinity to ~5 psu, before following the same decreasing pattern as that observed during the first bore. Comparison of both tides shows that after the initial salinity changes produced by the arrival of the bore, the salinity level only shows a slight rise for the next 1500 seconds. Following this, the salinity rises from 1 psu to 18 psu in the next 2500 seconds showing a large scale turbulence pattern; the salinity value then slowly decreases to 10 psu.

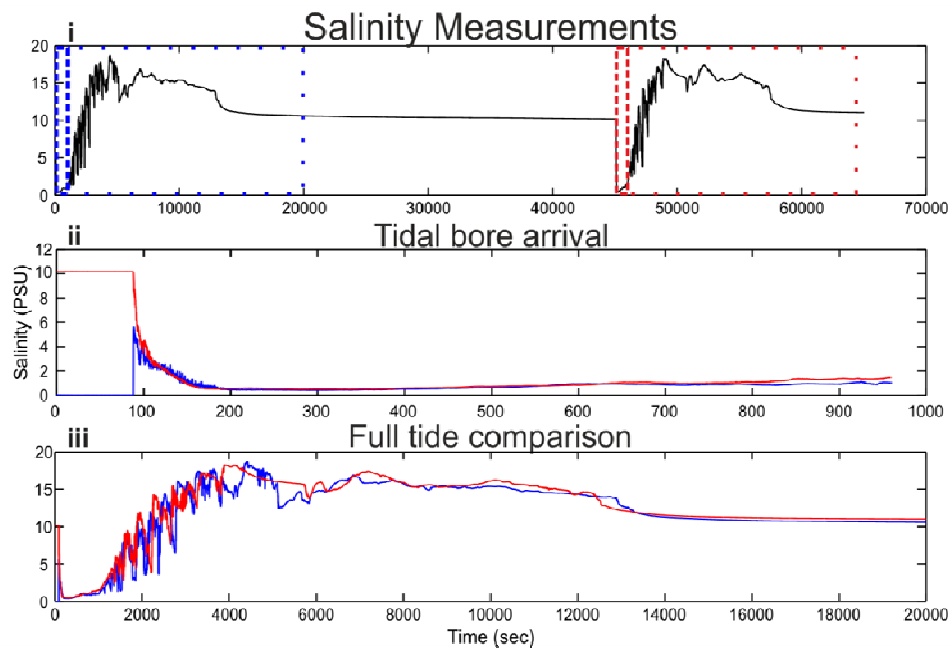


Figure 5.12 Salinity measurements from the Midas ECM: i) all data measured; ii) comparison of the arrival of both tidal bores (data in blue is from the first tide, data in red from the second tide); iii) the full incoming tide for both tides (start point of tidal bore and tide plots is the same).

Temperature measurements show that the first bore was measured in the evening (08/09/2014 pm) and the second the next morning (09/09/2014 am) (Figure 5.13). On the arrival of the first bore the temperature rose sharply from $\sim 15^{\circ}\text{C}$ to a peak of 18°C , followed by some smaller fluctuations. The water temperature then decreased slowly over the next 10 hours. The arrival of the second bore shows a drop in temperature from 17.6°C to 16°C , followed by a rise of 1°C over 3 minutes to a maximum of 17°C , lower than the temperature following the first bore. This period of stabilisation was the same duration following both bores.

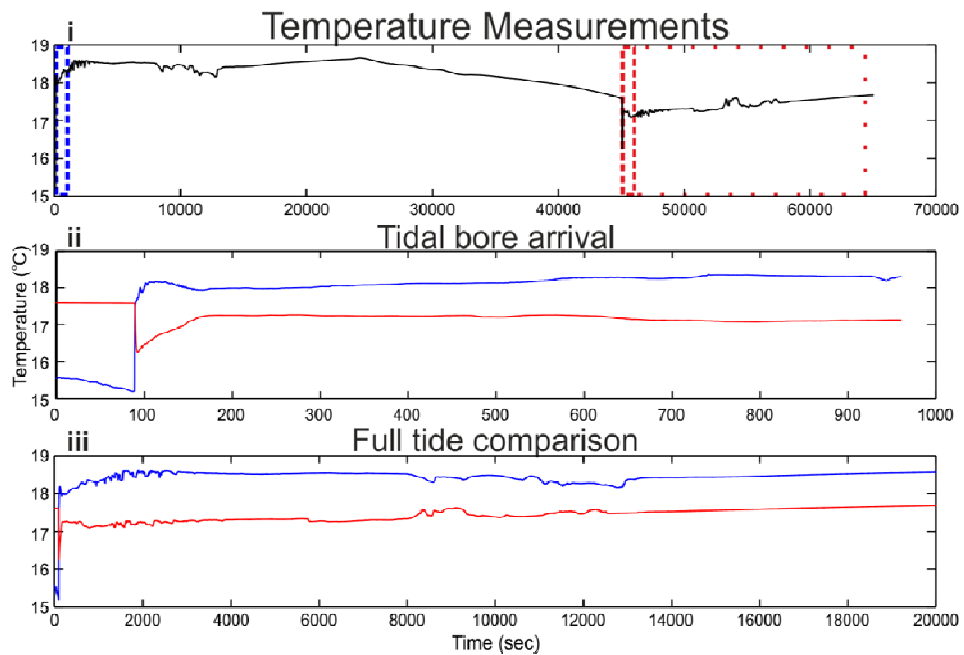


Figure 5.13 Temperature measurements from the Midas ECM: i) all data measured; ii) comparison of the arrival of both tidal bores (data in blue is from the first tide, data in red from the second tide); iii) the full incoming tide for both tides (start point of tidal bore and tide plots is the same).

5.4.2 Deposits

The variations in deposition occurring within the bar at Longney Sands was investigated by a visual inspection of the bar top and the recovery of four vibrocores. These cores were located at the landward and seaward ends of the bar and also along the central ADCP transect (Figure 5.4). Table 5.2 contains details of the cores recovered and their exact locations.

Table 5.2 Cores recovered. Locations are shown on Figure 5.4.

| Core | Latitude | Longitude | Date | Length recovered | Notes |
|--------|------------|-------------|------------|------------------|--|
| Core A | 51°48.561' | 002°21.564' | 08/09/2014 | 1.45 m | At landward end of bar |
| Core B | 51°48.360' | 002°21.108' | 09/09/2014 | 2.39 m | 300 m from seaward end of bar, next to channel. Bottom of core had hit a layer of gravel. Flat rounded clasts <5 cm. |
| Core C | 51°48.326' | 002°21.150' | 09/09/2014 | 1.9 m | At bar centre, 300 m from seaward end of bar |
| Core D | 51°48.238' | 002°21.024' | 08/09/2014 | 1.0 m | At seaward end of bar, 60 m from current meter. |

i) Core A – landward bar region

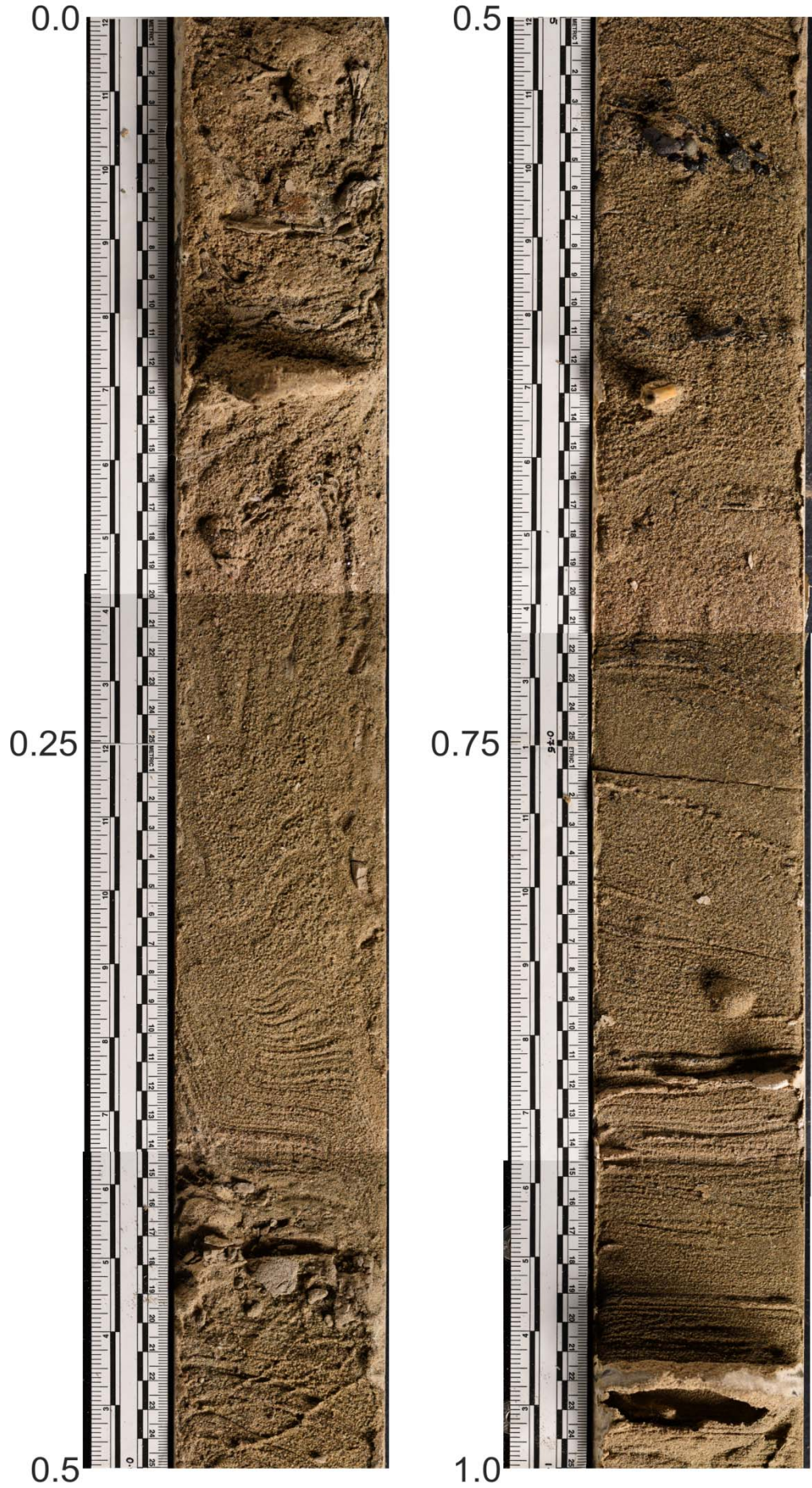
The core collected at the landward end of the bar (Core A) was 1.45 m in length (Figure 5.14). The core is predominantly formed of fine sands, comprising >80 % of most horizons. The lowest 0.65 m of the core shows horizontally oriented fine laminations throughout, with erosional surfaces often overlain by horizons of climbing ripples, approximately 0.01 m thick. The base of this section is coarser, fining upwards to a very fine sand in the upper 0.3m, with coarser coal particles in observed in some horizons. The coal particles are not observed within the ripples, mainly forming the horizontal laminations. Towards the top of this section some finer grained horizons are observed, with the angle of the laminations becoming steeper in the top 0.05 m (~ 30°).

Directly overlaying these laminations (0.98 m from top of core) is a finer-grained band that is ~3.5 cm thick, the base of which drapes the underlying laminar region, whilst the top surface is flat with a horizontal orientation. Above this the sand coarsens again, with less defined laminations observed for ~0.25 m. This region contains a 1 cm thick gravel band (0.53 m from top of core) and some organic material. The sediment rapidly fines upwards to a very fine sand showing some laminations and a mud horizon. At 0.4 m from the top of the core there is a grain-size break to a coarse sand layer 0.27 m thick which shows fine laminations at the base (with some deformation) and is more massive above. A 0.01 m thick very fine grained sand horizon is found 0.13 m from the top of the core, above which a fine grained sand horizon, with incorporated mud deposits that have been strongly deformed is found (Figure 5.14).

The grain-sizes contained within Core A were analysed and the mean grain-size (50th percentile of the data or D₅₀), fine grained fraction (10th percentile or D₁₀) and coarse grained fraction (90th percentile or D₉₀) were output. Core A had a D₅₀ of ~140 µm in the upper 1 m of the core; below this, in the region of the core containing the laminations, the D₅₀ is finer at ~130 µm (Figure 5.15). The upper 0.85 m of the core has a finer component (D₁₀) grain-size of 105 µm, but fines below this to 90 µm. The coarse component (D₉₀) is more variable, with some noticeably coarse horizons at 0.45 m possibly connected to the gravel band observed in Figure 5.14.

Figure 5.14 (next page) Core retrieved at landward end of bar (Core A on Figure 5.4).

Core A Part 1: Surface to 1.0 m



Core A Part 2: 1.0 m to 1.40 m

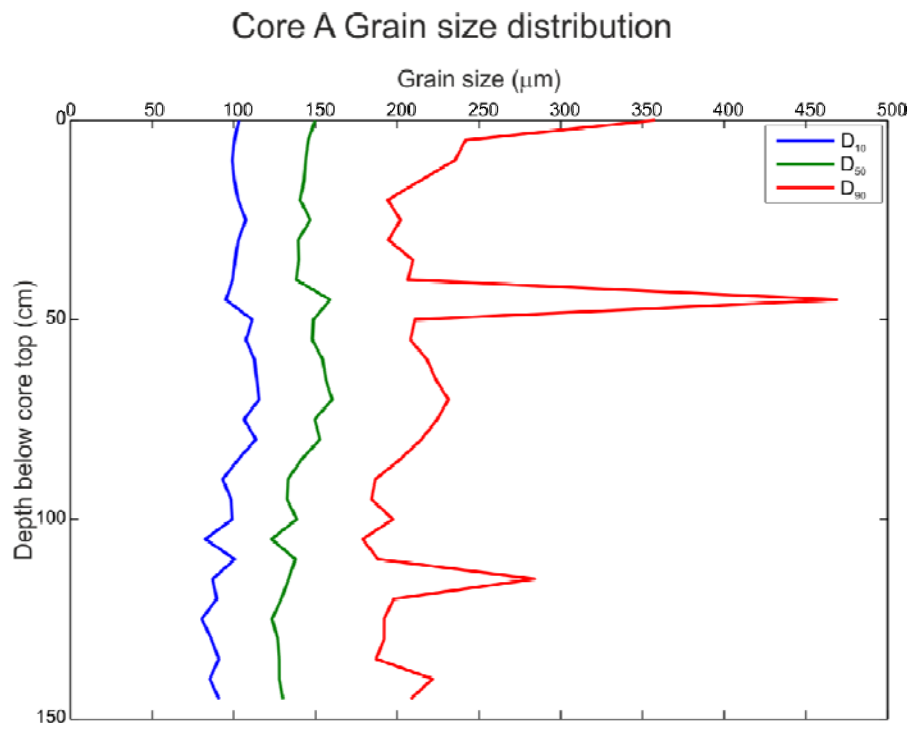
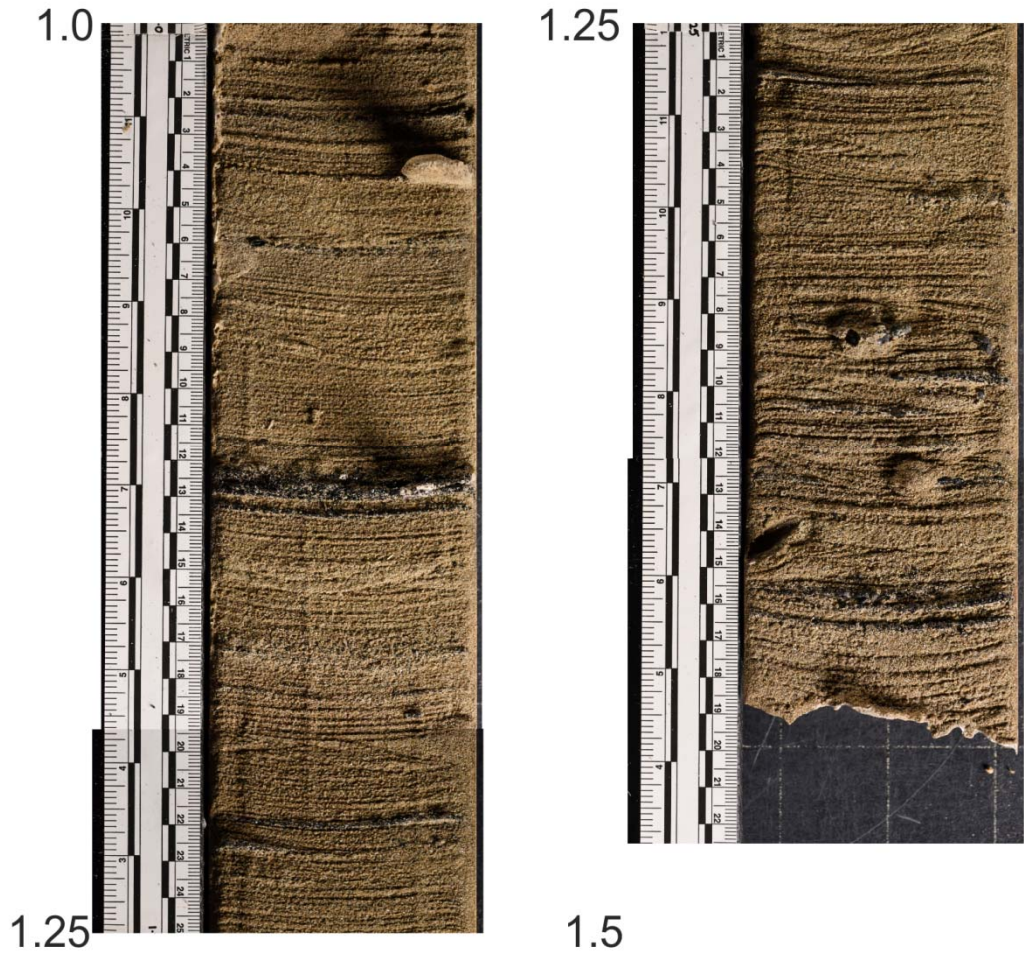


Figure 5.15 Grain-size statistics for the landward core showing D₁₀, D₅₀ and D₉₀.

ii) Core B – Channel adjacent to bar centre

The second core retrieved (Core B) was 2.39 m in length, the longest core recovered during the present work (Figure 5.16). This core was located within the channel region approximately 300 m northeast of the seaward end of the bar, lying on the furthest landward ADCP transect (Core B on Figure 5.4). This location was completely submerged at high tide and for several hours following. Whilst the upper 1.25 m of the core is composed of medium to coarse sands, the bottom 1.1 m dominated by rounded gravel clasts. These gravel clasts formed a plug which prevented the vibrocore rig from penetrating deeper into the sub-surface. The gravel layers form a series of coarsening upwards bands, up to 10 cm thick, supported in a matrix of coarse sand. Between the gravel bands mud layers up to 0.05 m thick can be found. There is a 0.3 m thick very coarse sand layer below 1.25 m, with coal clasts at the top of this section, showing some deformation in sediment structures. The upper 1.25 m of the core shows fine laminations throughout; these are generally horizontal, although in some regions they become angled at $\sim 45^\circ$ or show some deflections towards the edge of the core. There are some fine grained coal laminations and also some fine grained mud horizons. The top 0.1 m of the core lies above one of these mud horizons and does not show any structure.

Grain-size analysis of Core B (Figure 5.17) revealed a D_{50} of $\sim 140 \mu\text{m}$ in the upper 1 m of the core, very similar to that of Core A (Figure 5.14); below this, in the region of the core containing the laminations, the D_{50} is finer at $\sim 130 \mu\text{m}$. The finer grained component of the core (D_{10}) has a grain-size of $105 \mu\text{m}$ in the upper 0.85 m of the core, but fines below this to $90 \mu\text{m}$; there are two finer grained horizons ($\sim 23 \mu\text{m}$) observed at 0.25 m and 0.45 m from the top of the core. The coarse component (D_{90}) is more variable ($185 - 1013 \mu\text{m}$), with some noticeably coarser D_{90} values observed at 0.25 m and 0.45 m possibly connected to the gravel band (Figure 5.14).

Figure 5.16 (next page) Core retrieved within channel, 300 m from seaward end of bar (Core B on Figure 5.4).

Core B Part 1: Surface to 1.0 m

0.0



0.25

0.5

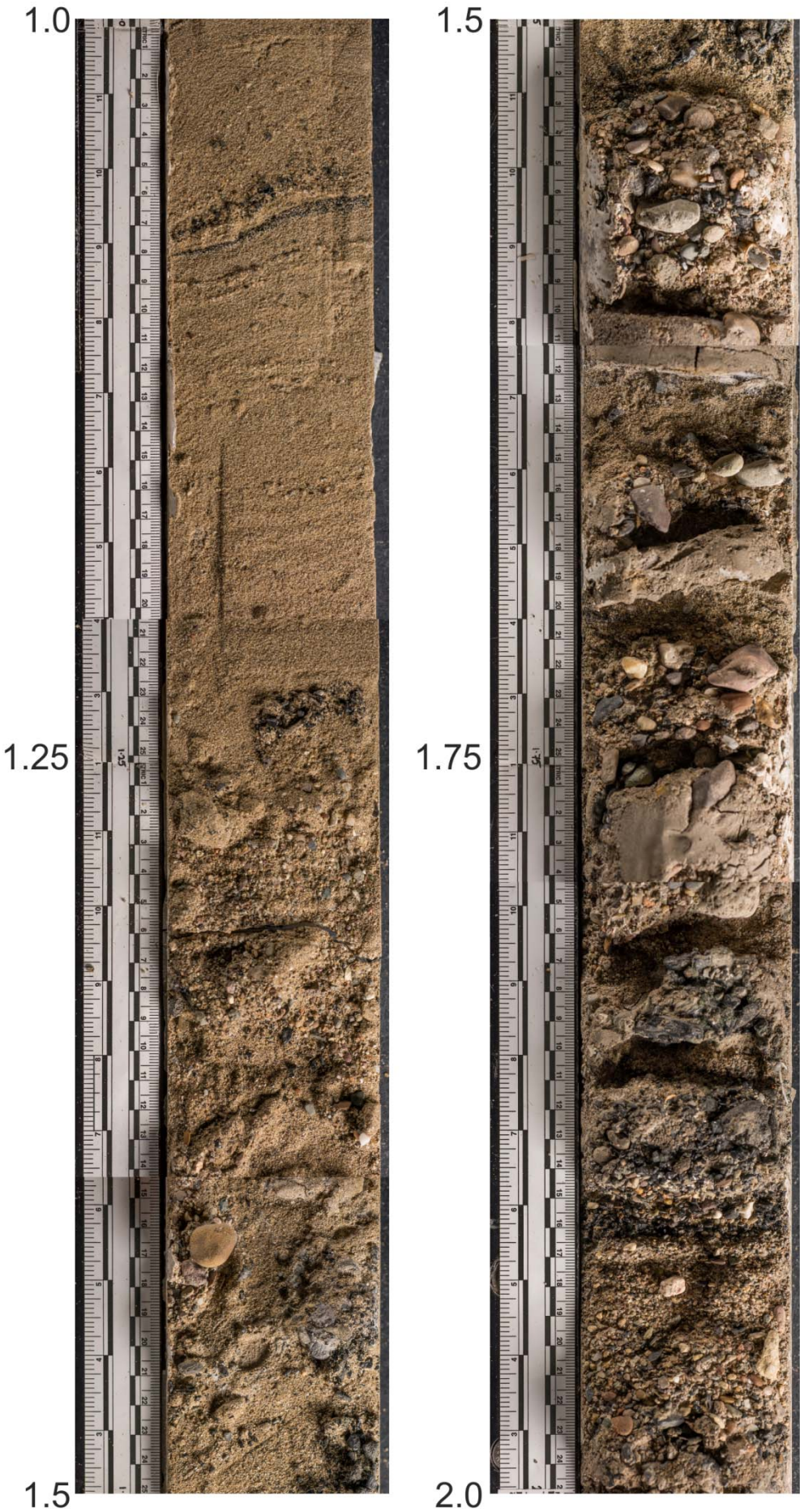
0.5



0.75

1.0

Core B Part 2: 1.0 m to 2.0 m



Core B Part 3: 2.0 m to 2.18 m

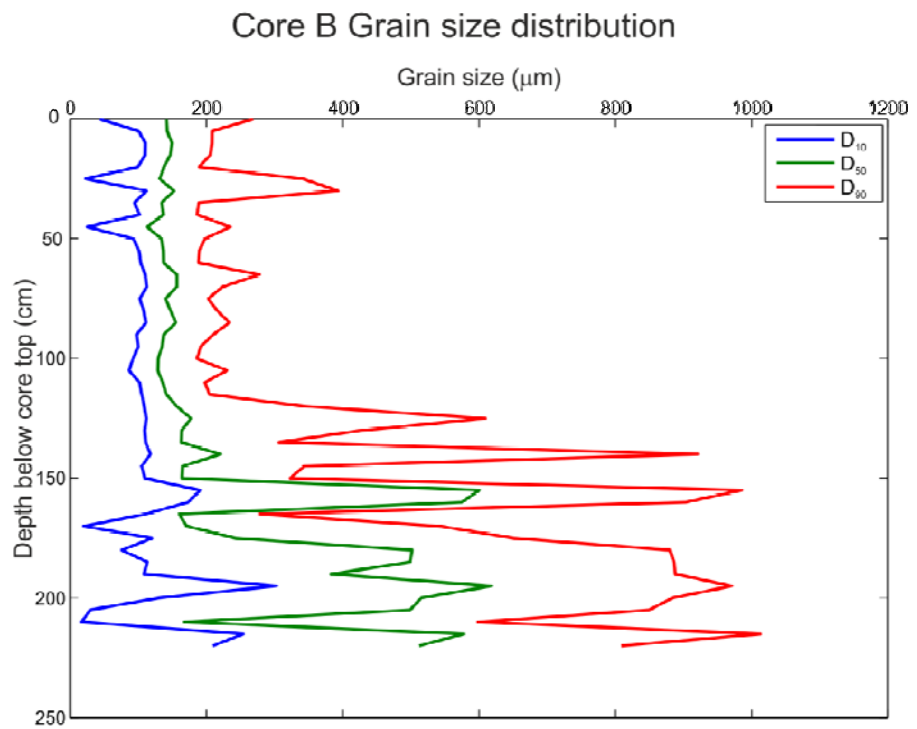


Figure 5.17 Grain-size statistics for the central channel core (Core B) showing D_{10} , D_{50} and D_{90} .

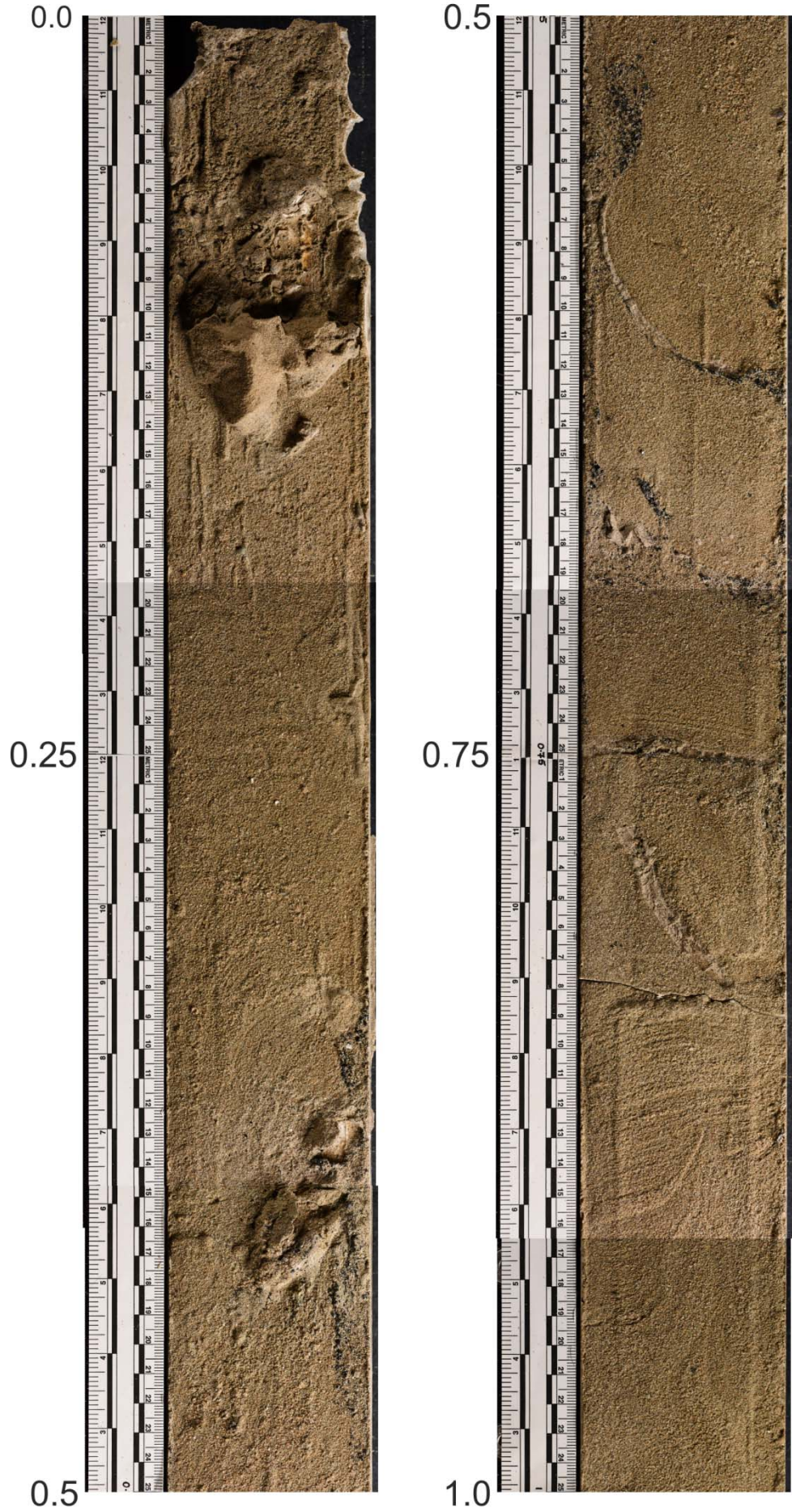
iii) Core C – Bar centre

Core C was also recovered at the centre of the bar 300 m landward of the bar end (Core C on Figure 5.4; Figure 5.18). Unlike Core B this location was only covered at the highest tide; the bar top was re-exposed within 2 hours of the bore passage. Core C is 1.9 m in length and the base is marked by a very coarse coal horizon that was 0.03 m thick and shows laminations marked by finer sand grains. Overlying this is 0.7 m of fine to medium sand showing laminations throughout with some coarser coal horizons. A coal horizon found 1.53 m from the top of the core, which intrudes 0.05 m into the overlying laminations. Above this is a more structureless fine to medium sand horizon 0.4 m thick with occasional indistinct laminations. A 0.08 m thick structureless layer of sand overlies this, containing an angled mud layer 5 mm thick and 6 cm long. No laminations are observed in the top 0.7 m of the core, although occasional mixed mud and coal horizons are observed, some of which show fluid escape features.

Grain-size analysis of Core C (Figure 5.19) reveals a narrower grain-size range within this core than within the two cores previously examined, with a D_{50} of $\sim 140 \mu\text{m}$ observed throughout the core length. The only notable exception to this occurs at 0.75 m from the core top where a D_{50} of $116 \mu\text{m}$ is observed. D_{10} and D_{90} show more variations in values, but these only occur at distinct horizons (e.g. at the surface where D_{10} is $43 \mu\text{m}$ and D_{90} is $269 \mu\text{m}$ and at 0.4 m below the surface where D_{10} is $31.1 \mu\text{m}$ and D_{90} is $421 \mu\text{m}$). The variation of grain-size at 0.4 m corresponds to a coal and mud fluid escape horizon within the core.

Figure 5.18 (next page) Core retrieved at bar centre, 300 m from seaward end of bar (Core C on Figure 5.4).

Core C Part 1: Surface to 1.0 m



Core C Part 2: 1.0 m to 1.96 m

1.0



1.25

1.5

1.5



1.75

2.0

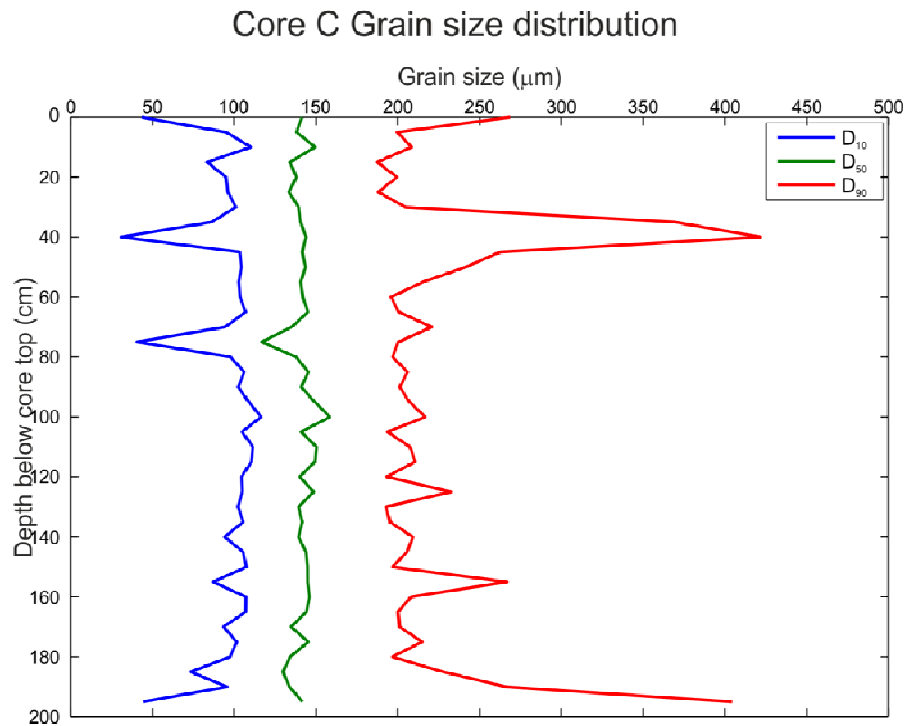


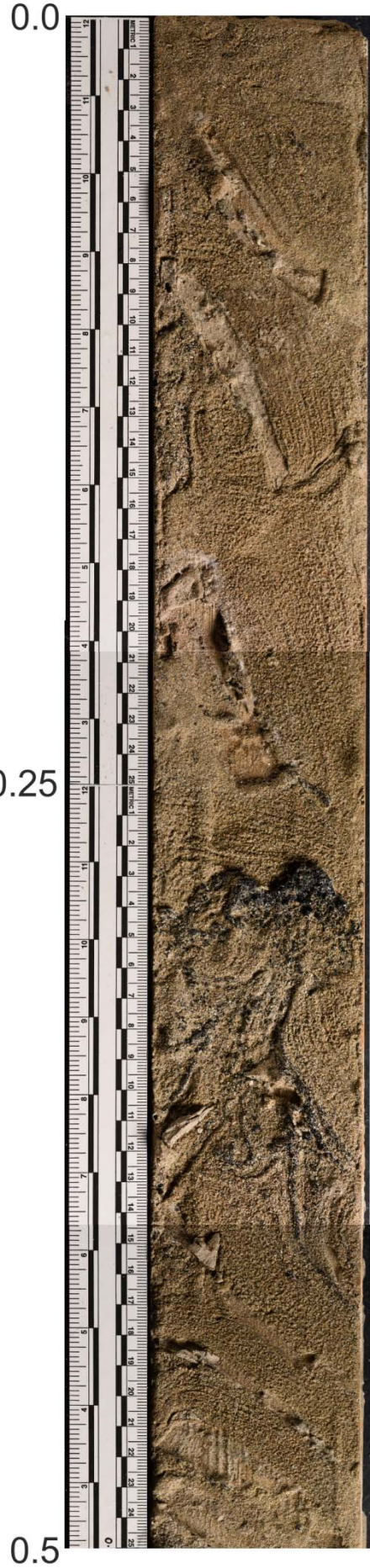
Figure 5.19 Grain-size statistics for the core collected at the centre of the bar, 300 m from seaward end of bar (Core C) showing D₁₀, D₅₀ and D₉₀.

iv) Core D – Seaward bar region

The most seaward of the cores recovered was also the shortest, at 1.0 m in length (Figure 5.20). This core was located at the end of the bar, 60 m west of the position of the electromagnetic current meter (Core D on Figure 5.4). This core was formed of medium grained sand for most of its length, with some smaller horizons of other sediments. The basal 0.4 m of the core exhibit no sedimentary structures and are overlain by 0.06 m of horizontal laminations. Above this the laminations become laminated and contain mud horizons 0.01 m thick oriented with the laminations. 0.4 m from the top of the core lies the base of a highly convoluted horizon composed of finer grained material and coal clasts. This convoluted horizon is 0.13 m thick, with the greatest concentration of coal particles at the top. Overlying these convoluted beds are horizontally laminated sands 0.03 m thick. Three further angled mud horizons, which don't extend across the width of the core, but show laminated in the adjacent sand appear above this horizon, with horizontal laminations between them. The top 0.04 m of the core is comprised of massive sands which fine upwards.

Figure 5.20 (next page) Core retrieved at seaward end of bar (Core D on Figure 5.4).

Core D: Surface to 1.0 m



Grain-size analysis of Core D (Figure 5.21, revealed a D_{50} of $\sim 130 \mu\text{m}$ throughout the core. The D_{10} value is generally $\sim 90 \mu\text{m}$, finer than that observed at a similar depth in the landward core, although similar to that of the two central cores (Figure 5.17 and Figure 5.19). A finer D_{10} value of $27 \mu\text{m}$ (and corresponding coarser D_{90} value of $384 \mu\text{m}$) is observed 0.5 m from the top of the core. This corresponds to a deformed mud clast within the core. The convoluted coal and mud horizons 0.3 m from the top of the core shows an increase in D_{90} values ($< 270 \mu\text{m}$), but no variation in D_{10} or D_{50} .

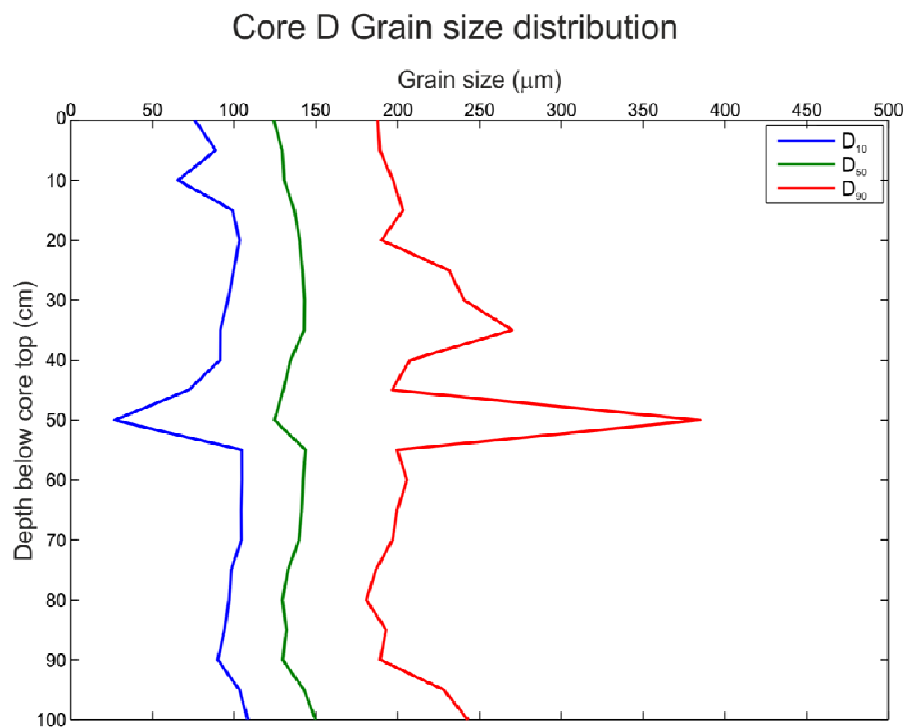


Figure 5.21 Grain-size statistics for the seaward core showing D_{10} , D_{50} and D_{90} .

To complement the core data, a survey was carried out of bedforms visible on the bar surface at low tide. These were highly variable within a few 10s of metres. At the landward end of the bar 2D and 3D seaward oriented ripples were observed in close proximity (Figure 5.22i-ii). These ripples were of a similar scale, with some showing coarser grained coal particles within the troughs (Figure 5.22iii). At the seaward end of the bar ~ 50 m west of Core D, imbricated gravels were observed adjacent to the western channel (Figure 5.22iv). These gravels were aligned to local flow in a seaward direction. Also at the seaward end rounded cohesive mud clasts were observed on the surface of the bar, often lying in small hollows. These ranged in size from 0.02 m to 0.3 m and often had coarse coal particles on the surface (cf. grain-size analysis of Core D in Figure 5.21) and lay in small hollows. Covering most of the surface of the seaward end of the bar (from the central ADCP transect to the bar tail) was a layer of liquid mud.

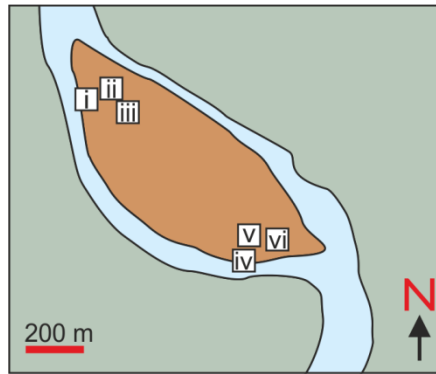


Figure 5.22 Bedforms observed on the bar top: i) 2D ripples; ii) 3D ripples; iii) ripples showing coal detritus; iv) gravel lags; v) rip up clasts; vi) overlaying fluid muds.

The suspended sediment carried by the flows were also investigated. The locations and timings of these samples are in Table 5.3, along with the D_{10} , D_{50} , D_{90} and concentrations. The D_{50} of all samples is very similar ($\sim 15 \mu\text{m}$), as is the D_{10} ($\sim 6\mu\text{m}$). There is more variation in the D_{90} value, with samples showing a range of values from 24-68 μm . The sample containing a D_{90} of 68.26 μm was collected at low water, shortly before the arrival of a tidal bore and is likely due to flocculation or biotic effects. There is more variation in the suspended sediment concentration of the samples. At time of low water the concentration is 0.3-0.45 gl^{-1} ; the arrival of the tidal bore results in an increase in concentration, up to a maximum of 2.84 gl^{-1} in Sample 8. Once flow has fully re-established in a seaward direction following the tide concentrations again fall to 0.3 gl^{-1} . The sample collected during the passage of the tidal bore (Sample 7) was obtained at the water surface due to the high flow velocities and has a similar concentration to the sample collected before the bore's arrival.

Table 5.3 Suspended sediment samples

| | Time | Location | River Conditions | Depth | D_{10} (μm) | D_{50} (μm) | D_{90} (μm) | Conc (gl^{-1}) |
|---|---------------------|------------------------|---|---------|-------------------------------|-------------------------------|-------------------------------|------------------------------|
| 1 | - | Central transect (c) | Low Water | Surface | 7.16 | 16.38 | 68.26 | 0.32 |
| 2 | 08:57 08/09/2014 | Channel | After bore – flow reversed | 2 m | 8.20 | 16.41 | 38.56 | 2.05 |
| 3 | 09:45 08/09/2014 | Central transect (c) | After bore – flow re-established in seaward direction | | 4.91 | 10.51 | 24.74 | 0.29 |
| 4 | 11:41 08/09/2014 | Bend landward of bar | After bore – flow re-established in seaward direction | 3 m | 5.56 | 12.77 | 33.71 | 1.45 |
| 5 | 08:05 09/09/2014 | Seaward end of bar (b) | Low water – prior to bore | 1.5 m | 5.34 | 12.42 | 33.88 | 0.45 |
| 6 | 08:38 09/09/2014 | Moored | Low water – prior to bore | 1 m | 5.38 | 11.59 | 24.59 | 0.35 |
| 7 | 08:49 09/09/2014 | Moored | During bore | Surface | 5.10 | 11.56 | 26.44 | 0.31 |
| 8 | 09:44 09/09/2014 | Downstream of bar (b) | 55 minutes after bore – central region reversed | 1.5 m | 5.86 | 13.05 | 27.70 | 2.84 |
| 9 | 10:38 09/09/2014 | Central transect (c) | After bore – flow re-established in seaward direction | | 7.30 | 15.12 | 32.23 | 0.32 |

5.5 Discussion

A tidal bore and the associated flow structures around a large bar, and the resultant sedimentary deposits, were examined within the tidally-influenced fluvial region of the River Severn. The passage of two tidal bores were measured; these tides were of a similar magnitude and duration, as observed in the data at the Epney gauge (Figure 5.3). The flow data clearly show that the bar reported on herein lies within a region with a significant tidal influence although it is fluvially dominated.

Measurements of flow during the passage of a single tidal bore were made in two locations, allowing direct comparison of the interaction of the bore with a bar and within the lateral channel (Figure 5.23). Downstream velocity in both sets of measurements show a rapid reversal from flow in a seaward direction prior to the incoming tide to flow in a landward direction on the arrival of the tidal bore. Downstream velocities measured within the eastern channel are generally higher at higher than those measured by the ECM at the seaward end of the bar (Figure 5.23). During the first 15 minutes following the passage of the tidal bore, during the initial flow reversal, the maximum velocity measured within the channel is -3 ms^{-1} , whilst at the seaward end of the bar the maximum velocity is only 1.5 ms^{-1} . This corresponds to the steering of the incoming tide around the end of the bar, with most of the flow initially diverted into the deeper channel before inundating the bar top.

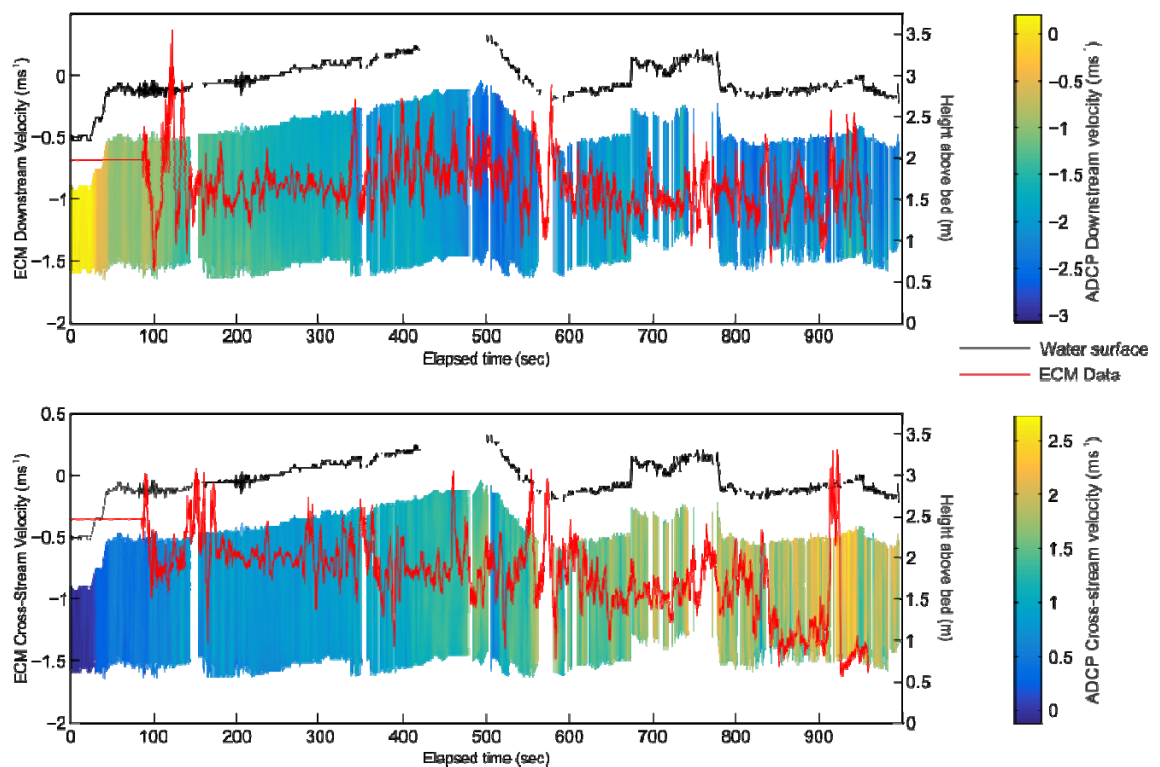


Figure 5.23 Combined ADCP and ECM flow data

A 0.75 m increase in flow depth is observed within the ADCP data, with some small variations (~0.1 m) following the arrival of the bore, followed by a 1 m decrease 9 minutes after the passage of the bore. This variation is likely due to topographic effects as the bar top has become completely covered as the channel overflows. The maximum water depth observed at the seaward end of the bar by the ECM is ~0.35 m (Figure 5.11), whilst the variation in flow depth measured at the Epney gauge is ~3.5 m (Figure 5.3). These variations in flow depth reflect the variations in local system geometry and the ability of the system to accommodate high flows by inundating the bar, resulting in lower flow depths on the bar top.

Sedimentary cores were recovered from both the landward and seaward ends of the studied bar. The cores were all sandy in nature, with gravel clasts at the base of the two central cores. The top 1.5 m of the cores show D_{50} values of 120-150 μm in all cores. The base of the central channel core (Core B), has a much coarser grain-size. Thin laminations were observed in all cores, the most distinct found in Core A, the most landward sample. Core A also showed evidence of ripple cross-laminations, which weren't observed elsewhere. There was no clear evidence of erosion surfaces observed in any of the cores. However, the deformed mud horizons observed in the seaward and central cores (Figure 5.18; Figure 5.20) appear to be rip up clasts observed on the bar top (Figure 5.22) incorporated into the bar sedimentology. Within the seaward core there is a clast observed at a depth of 0.5 m (Figure 5.20). The grain-size data shows this horizon to have a D_{10} of 26.7 μm and a D_{90} of 384.8 μm . This observation corresponds to the fine-grained rip up clasts with a coarser grained coating observed on the bar top (Figure 5.22). In both cores they have been flattened and are at an angle of ~45°. The clasts in the seaward core have overlying laminations which are at the same angle as the upper surface, whilst in the central core no laminations are present. This angle could be due to deformation of the core sediments during the vibracoring process. However, the clasts observed in the upper part of the seaward core is cross-cutting the underlying laminations. Whilst there may be some deformation of the core this would not appear to be the cause in this case.

Carling *et al.* (2015) noted Longney Sands as the limit of estuarine sands within the Severn Estuary, however the fine grained material observed by them at a point bar 2 km seaward of Longney Sands were not present in the cores obtained here. The point bar contained heterolithic stratifications of sand and mud (Carling *et al.*, 2015), whilst any laminations observed in the present work were composed of sand with some occasional coal horizons. Although there were some fine grained horizons and clasts within the cores, there was no evidence of tidal rhythmites or flaser bedding which are commonly described in tidal settings and used as indicators of these environments (e.g.

Reineck and Wunderlich, 1968; Carling *et al.*, 2015). The Severn Estuary is known to have a mixed sediment content of sands, muds and gravels (Carling, 2009), but the finest grained material does not appear to be deposited at this location. Liquid mud was observed on the top of the bar, but there was no evidence of these within the cores themselves. The variable position of the boundary between fully-tidal and fully-fluvial flow in the Severn was discussed in detail by Keevil *et al.* (2015b), investigating flow around a bend 3 km landward of the present work. The current field location lies within this transition zone, so will show fully-fluvial flow during periods of low tidal influence. However, the movement of this tidal-fluvial boundary does not fully account for the lack of tidal deposits observed here. The lack of these common tidal indicators would imply that the cores recovered were fluvial in origin, even though the flow data reported herein is clearly of a tidal nature.

The soft sediment deformation observed in the upper section of the seaward core Core D is most likely as a result of the action of the incoming tidal bore. The deformed surface is cut by the edge of the core so is clearly not a result from the action of the vibracore. There is a similarly shaped upper boundary to the coarse bottom of Core B. Due to the lack of deformation structures observed in the landward core (Core A) and the location of the cores where deformation is observed it is suggested that these arise from the interaction of the tidal bore with the bar top. Previous examples of soft sediment deformation produced by a tidal bore within Mont St Michel bay were observed within a fine grained substrate comprising tidal couplets of silt and carbonate sediments (Tessier and Terwindt, 1994). Fan *et al.* (2014) also observed similar structures within the Qiantang Estuary, China within fine grained sands and silts (Figure 5.24). Fan *et al.*, (2014) describe a tidal bore cycle of irregular erosion overlain by homogeneous sands and parallel sandy laminations, with soft sediment deformation structures in the upper section. The load-flame structures observed by Fan *et al.* (2014) show a strong resemblance to the convolute structure observed in Core D (Figure 5.20), as does the deformation and draping of parallel laminations above the convolute structures. The present deformation occurs within a horizon of predominantly fine grained sand, but containing a noticeably coarser fraction ($D_{90} = 230\text{-}270 \mu\text{m}$). This may be due to the presence of coal particles within the deformation structure – although the particles are larger than the surrounding fine sand matrix they have a lower density. However, Fan *et al.* (2014) reported that tidal bore deposits were generally coarser grained with poorer sorting than other tidal deposits present.

The ECM measurements made at the seaward end of the bar showed rapid flow reversals during the incoming tidal bore, which are not observed within the ADCP data (Figure 5.23). This is likely due to the blanking distance at the base of the ADCP

the landward core contains fine grained laminations and evidence of ripple formation indicating flow within this region.

Smaller scale deformation structures were observed by Carling *et al.* (2015) at Rodley Sands, which were not as well developed as those observed herein. This may be related to their location on a point bar, rather than at the seaward end of a bar at the centre of the channel as in the present work. The moored ADCP data was used to calculate the shear stress within the channel during the passage of the tidal bore (Figure 5.25). This data reveal large peaks in shear stress which correspond to the arrival of the tidal bore and also to the velocity fluctuations previously observed. Following the bore as the water depth increases there are some small fluctuations in shear stress, but not as great as in the initial observations.

Temperature variations were observed following both bores, due to the heating and cooling effects of the main estuary. The incoming bore flow exhibiting a rise in temperature in the evening measurements, whilst the measurement the next morning showed a fall in temperature on arrival of the bore. After this initial temperature

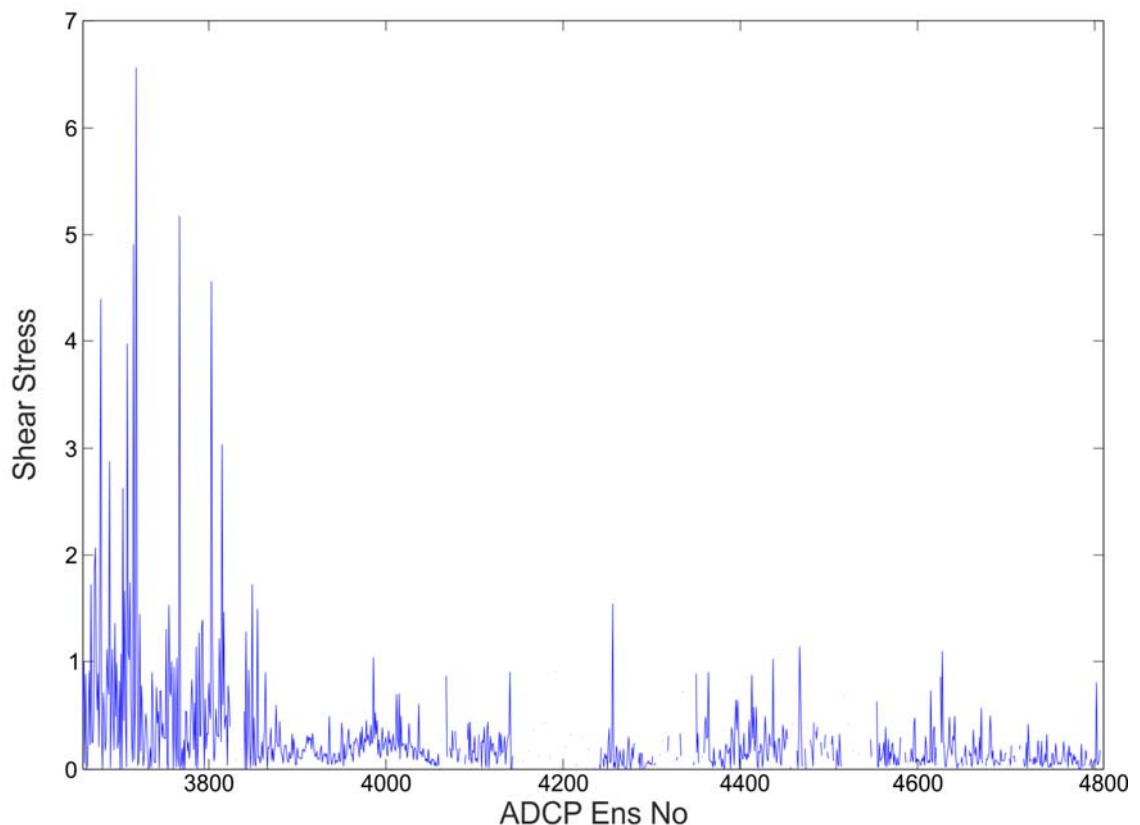


Figure 5.25 Shear stress calculated from ADCP data.

change there was a period of temperature stabilisation following both bores lasting ~ 3 minutes, following which there is a gradual increase in temperature of about 1 ° over the entire tide (Figure 5.13). A relatively small salinity change (to ~ 6 PSU) is observed in the first minute of each bore's passage (a rapid increase in the case of the exposed ECM when the first bore arrives and a rapid decrease when the second bore arrives, before which the ECM was located in a pool of water), which then decreases to ~0.5 PSU suggesting that some small amount of saline water has been carried by the head of the tide. During both bores this corresponds to the temperature variations noted above. It is not until 30 minutes after the arrival of the tidal bore that the salinity begins to rapidly rise (<18 PSU), in a series of turbulent fluctuations (Figure 5.12), which correspond to some small temperature fluctuations of <0.2 °C (Figure 5.13).

The delay in the maximum salinities measured after the passage of the tidal bore suggests that the local incursion of the salt wedge follows the head of the flood tide (Figure 5.12). These turbulence patterns do not correspond to fluctuations observed in the velocity measurements (Figure 5.10), but do occur at the same time as the maximum pressures observed in Figure 5.11, suggesting that the incoming salt wedge is present when the river is at its maximum depth. Uncles (2010) measured the salinity at high tide in this location as 15-20 g l^{-1} , which is in agreement with the maximum value measured in the present work of 19 PSU, where 1 g l^{-1} ~ 1 PSU (Unesco, 1981). A value of 10 PSU was measured following the flood tide, but this was due to the instrument being left in a pool of water after the tide had turned, rather than becoming exposed on the bar top (Figure 5.12). This pooling of water at the seaward end of the bar may lead to changes in the fine grained material deposited due to increased effects of flocculation in still, slightly saline water. Measurements of salinity during the passage of a tidal bore on the Garonne River (Reungoat *et al.*, 2014, 2015) show a slight decrease in salinity on the arrival of the bore, followed by a rapid increase in the following 5 minutes and then a decrease. Salinity measurements on the Garonne River were made at the surface, whereas the present work measured at a fixed position above the bed. Unlike the present work, the salt wedge in the Garonne River arrives at approximately the same time as the tidal bore, with the decrease in salinity on bore arrival due to the pushing of a freshwater plume above the salt wedge.

The temperature and salinity measurements presented herein show the importance of tidal bores in the mixing of fluvial and tidal flow at the base of the water column within the Severn Estuary. Salinity measurements show turbulent variations revealing large scale mixing during the main flood tide (<1 hour after the passage of the tidal bore) as the salt wedge passes this location (Figure 5.12). However, the presence of smaller fluctuations on the arrival of the tidal bore, with an accompanying variation in

temperature suggest that although the majority of the salt wedge is transported later in the tide there appears to be a component contained within the bore itself. The variation in salinities was the same for both bores measured, so is not likely to arise from localised salinity accumulations on the bar tail. This salinity transport would also infer that the bore is likely to transport a small volume of pollutants (such as dissolved metals and particulates) and nutrients at the head of the incoming tide leading to a more landward incursion than may be expected if transport was only occurring during the main body of the tide.

Tidal bores are known to form under only a limited range of conditions, dependent on a delicate balance between the size of incoming tides, the volume of river flow, channel geometry and bathymetry (Fielding and Joeckel, 2015). They are observed in macro-tidal systems, when the tidal range exceeds 6 m, in locations with a rapidly narrowing geometry and gently sloping bathymetry (Chanson, 2012; Bonneton *et al.*, 2016). Even in systems which are favourable to tidal bore generation they will not occur during every tide, usually only forming at the highest tides and in times of low river flow. Modifications of local bathymetry can result in changes in the tidal bores generated, e.g. following the 1964 Alaskan earthquake the Turnagain inlet subsided 2.4 m after which the tidal bores observed have been much smaller (Chanson, 2012). As such, the presence of sedimentary structures which can be attributed to the passage of a tidal bore is a useful indicator of general system size, shape and tidal range. However, tidal bore deposits are not commonly recognised within ancient systems with only two examples published to date (Martinius and Gowland, 2011; Fielding and Joeckel, 2015). These published examples both describe horizons with a stepped erosive base, they do not describe the soft sediment deformation which has been described in addition to erosive surfaces in modern environments which are known to result from tidal bores (Tessier and Terwindt, 1994; Fan *et al.*, 2014). This lack of recognition of tidal bore deposits and their use as a marker of tidal influence misses a useful tool in the interpretation of tidal-fluvial systems, especially within the transition zone between fully-fluvial and fully-tidal systems.

The tidal bore deposits described by Fielding and Joeckel (2015) illustrate the usefulness of tidal bores as a system indicator, as the deposits they describe lie 200 km inland of the palaeoshoreline, and indicate that the system must have had a tidal range of <6 m. The variations in flow patterns observed herein during a single tidal bore event illustrate the difficulties in predicting the interaction of tidal bores with local bathymetry. Interactions with bathymetry alter the form of a tidal bore, with deeper channels forming an undular bore and regions of shallow bathymetry a breaking bore. Within the area of Longney Sands during the present measurements a breaking bore

was generated across the width of the system, although it travelled at higher velocity in the channels surrounding the bar than when it flowed across the bar top. The single tide and the leading tidal bore front generated widely differing velocities and flow depths at the two flow measurement location and would therefore generate very different deformation or erosion patterns.

Suspended sediment concentrations observed in the present work are similar to those reported by Uncles (2010) for this location at high tide (Table 5.3). With the exception of some higher D_{90} values at low water, which probably are due to aggregation or biological effects, the grain-sizes measured were very similar across all samples. Comparison of suspended sediment concentrations to those measured during the passage of a tidal bore on the Garonne River (Keevil *et al.*, 2015a) show a similar 10 fold increase in concentration following the arrival of the bore. However, the Garonne River at the field location reported is much finer grained than the present field location, which accounts for the much higher suspended sediment concentrations observed there. Fine grained sediments are known to transport heavy metal pollutants (e.g. Ciffroy *et al.*, 2010) and act as depositional sinks for them. Jonas and Millward (2010) examined the metal distributions present within the Severn Estuary and noted that while dissolved metal concentrations were generally low, the concentrations of copper have not declined as their input has lowered. They attribute this to local hydrodynamics altering the locations of contamination. Allen (1987) described the presence of fine grained coal dust within muddy sediments in the lower Severn Estuary, noting that although the system interacts with local coal fields these particles were probably had an anthropogenic origin from the South Wales Coalfield. The presence of coal particles within the bar at Longney Sands illustrates the widespread distribution of these particles. Tidal bore interaction with a surface underlain by a buried source of pollutants may induce their release into the system by erosion or soft sediment deformation (e.g. fluidisation of underlying material) will result in redistributions of pollutants in a landward direction.

Although the bar was predominantly composed of sand, gravels were observed within the channel regions of the bar at the base of Core B (Figure 5.16) and adjacent to the seaward end of the bar (Figure 5.20). Whilst the Severn Estuary predominantly contains mud and sand there are locally sourced regions of gravel throughout (Carling *et al.*, 2006; Manning *et al.*, 2010). At the seaward end of the bar they were observed to be imbricated and aligned with flow in a seaward direction (i.e. fluvially dominated); the gravels within Core B were smaller in size with little preserved structure (Figure 5.16). However, it should be noted that the recovery any sediment below the base of Core B was prevented due to the gravels locking the base of the core pipe, so any structural

information may have been lost or lies below this horizon. Landward of the bar at a bend with a symmetrical planform it was suggested that a gravel core to the point bar is only transported at times of high flow, i.e. seaward during periods of high fluvial flux and landward during very high tides (Keevil *et al.*, 2015b; Chapter 4), effectively fixing the position of the bend spatially. The gravels observed at the present location preserve markers of flow in a seaward direction, suggesting that although the fluvial flow within the study area is of sufficient magnitude to transport large clasts, the tidal flow is comparatively weaker and unable to rework these deposits. This suggests that different grain-size distributions within the Severn Estuary will preserve varying evidence of tidal influence. Sand dominated deposits will be more likely to preserve evidence of bi-directional flow; however gravel dominated deposits will appear to be fluvial in origin. Therefore it is important when analysing ancient deposits for indications of tidal influence that the effect of grain-size on the preservation of palaeoflow direction indicators is also assessed.

The position of the bar and channels at Longney Sands is highly dynamic (Figure 5.2), however the presence of these gravel lags may act to prevent some tidally induced migration of the channels, with erosion of the channel edges only possible during high flows at spring tides. As such, the movement of the bar would appear to be fluvially-dominated, as is evident from the cores reported here, with only limited movement due to incoming tides. Also present both on the bar top and within Cores B and D were fine grained rip-up clasts (Figure 5.17, Figure 5.20 and Figure 5.22). The bar itself is formed of sand, indicating that they have been transported from elsewhere within the River Severn, possibly at the channel edge. The surface clasts were highly rounded with coal clasts incorporated on their surface, indicating that they had been transported within the system for some time. Their large size indicates that they are only transported at times of high flow, before eventually being incorporated into the substrate (Figure 5.22v). Their presence only at the seaward end of the bar would suggest a source from either local banks or from a source further seaward in the system. Whilst the clasts themselves are relatively large and will only be transported by high-energy flows, they are preserved as lenses of fine-grained material. Within a core this may be interpreted as a fine-grained low energy horizon or as evidence of a feature such as flaser bedding which is found in systems with a more mixed sediment content (Reineck and Wunderlich, 1968), rather than the sand-dominated relatively high energy environment examined herein. In contrast to the bar studied herein, extensive mud drapes and flaser bedding were found within the tidal-fluvial deposits examined by van den Berg *et al.* (2007). Whilst these have been commonly found in other systems, the lack of tidal rhythmites and associated deposits at the present location illustrate that these are not the only indicators of a fluvially-dominated region with tidal influence.

The landward zone of hypertidal systems discussed by Archer (2013) contains laterally extensive tidal rhythmites. However, although the Severn Estuary was one of the systems described, and the present work lies within this landward zone (Zone 3), this description appears to have been based on satellite imagery. The location of the single field image is described as “in Zone 3”, with no further information whilst the accompanying references to cyclicity describe sites much further seaward than the suggested location (Allen, 1990; Allen, 2004; Archer, 2013). This further illustrates the need for field based studies of the tidal-fluvial transition and the accurate placement of this field data to allow description of the transition. As noted previously, whilst tidal rhythmites are a common feature of the tidal-fluvial transition from the present work they do not appear to be found within the fluvially dominated region of all systems.

5.6 Conclusions

Investigations were made of the flow patterns and sedimentary deposits of a large tidally-influenced bar in the fluvially-dominated region of the Severn Estuary. Deposition shows the bar to be primarily composed of sand, with fluvial deposition occurring. The cores recovered show few of the commonly described indicators of tidal influence (e.g. heterolithic bedding, flaser bedding, tidal couplets), instead appearing fluvial in nature with structureless sand bodies dominating. Coarse gravels also support the fluvially-dominant nature of this location.

Flow data collected at the seaward end of the bar and within the channel reveal a short-lived but significant tidal influence in this area, with a tidal bore forming during at low river flow during a spring tide. This bore is steered around the bar head, resulting in deeper flows and higher flow velocities within the channel. However, the interaction of the tidal bore with the seaward region of the bar has resulted in characteristic soft sediment deformation which, along with the presence of fine grained rip-up clasts, are the only sedimentological indicators of tidal influence observed. The formation of tidal bores is limited to certain conditions (high tidal range, shallowing bathymetry, narrowing planform); therefore the presence of these deposits can be used to infer tidal influence even in systems which appear to be fluvial in nature, along with wider scale system morphology. Mixing at the head of the bore, seen in salinity and temperature data, will act to transport sediment, pollutants and nutrients at the head of the tide resulting in landward transportation which may exceed that of the main body of the flood tide.

The combined flow and depositional data obtained at this bar can be used to update the landward region of the tidal-fluvial transition model. Within the facies model of Dalrymple and Choi (2007) this region would appear to be fluvial in origin, with no

tidal influence. However the data collected herein shows that the apparently fluvial deposition lies within a region of tidal flow. Whilst the previously described bedforms, such as thinly laminated horizons of fine and coarser grained material must still form a part of the model within the region of fluvial dominance, it must be recognised based on the present flow data that these are not the only bedforms present. The landward region of the tidal-fluvial transition model therefore needs to be updated to reflect this tidally-modified region of deposition with the addition of these apparently fluvial bedforms.

Tidal bores would also be a useful addition to the fluvially-dominated but tidally-influenced region of tidal-fluvial transition models. Although tidal bores are relatively rare their presence is a strong indicator of system size and tidal conditions which would assist palaeogeographical reconstruction (e.g. Bonneton, *et al.*, 2016). As an estuary system becomes infilled the conditions necessary for the formation of a tidal bore may be removed from the system, resulting in the loss of any tidal bore signature. This will allow the development of systems to be tracked. In a similar manner, changing system geometries arising from variation in sea level would result in the movement of these tidal bore deposits, with tidal bore deposition moving landward during periods of sea level rise, such as those arising from climate change and seaward at times of regression. This moving pattern of tidal bore deposits would allow further information about system geometries to be deduced.

Chapter 6

Discussion

This thesis has considered the flow and morphology within two different tidally-influenced systems and the resultant barforms and bedforms through these zones. The variation in bedform morphologies which arise due to interaction with varying tidal and fluvial flows, and local barforms have been examined in detail. Whilst tidally-influenced estuarine systems have been previously described at a system level (e.g., Dalrymple *et al.*, 1992; Longhitano, *et al.*, 2012; Webb *et al.*, 2015), the processes within a region of fluvial-dominance which is undergoing some degree of tidal-influence has not yet been fully quantified.

Whilst both the field areas studied lie within a region which is tidally-modulated fluvial the two systems possess very different morphologies. The area of the Columbia River estuary investigated has a complex braided pattern, with multiple sand bars and braided channels. The wide, relatively deep nature of the estuary (<22 m in the bathymetry measurements reported herein), has resulted in the formation of large-scale bedforms with crests <3.5 m high with separations of <300 m. In contrast, the region of the Severn studied contains a single channel 100 m wide at the bend section, 500 m wide at the bar section, with a maximum depth of 9 m reported at high fluvial flow, with both tidal and fluvial flow contained within this channel.

6.1 Tidal modification of fluvial flow within fluvially-dominated systems

The variable position of the tidal-fluvial boundary is evident at both study areas, although the maximum tidal and fluvial flow velocities measured are roughly comparable. Flow measurements at a symmetrical bend in the inner Severn estuary were collected at both high river flow during a neap tide and at low river flow during a spring tide. Flow completely reversed during the spring tide at low river flow, but at high river flow the neap tide had a minimal effect on the seaward directed fluvial flow. The maximum flow velocities measured in both landward and seaward directions were 1.5 ms^{-1} (Figures 4.4-4.6). This illustrates a movement of the tidal-fluvial boundary between the two sets of measurements, lying landward of the bend during low river flow but seaward of the bend during high river flow. A similar movement of the tidal-fluvial boundary was observed in the flow measurements collected in the Columbia River estuary. The flow data collected at the Sandee section during the first field season (FS1), whilst there was relatively high fluvial flow, show limited reversal of flow at high

water $<0.35 \text{ ms}^{-1}$ and have a maximum seaward velocity of 1.1 ms^{-1} (Figures 2.28-2.31). In contrast flow measurements collected at Wood bar have maximum seaward flow velocities of 1.25 ms^{-1} and landward velocities during high water of 0.6 ms^{-1} (Figures 3.16-3.19). Whilst it could be considered that there is a fixed boundary between the tidal-fluvial boundary occurring between these two locations, their close proximity (1 km) and the higher fluvial flow measured during FS1 reveals that again this represents a movement of the tidal-fluvial transition, as has been previously described (Dalrymple and Choi, 2007; van den Berg, 2007). It should therefore be expected that bedform and barform morphology within both systems will reflect the movement of the tidal-fluvial transition.

Although the flow velocities measured at the two study locations are of similar magnitude the resultant bedform morphologies observed are different. Using the depth trace of the ADCP data it was possible to output a bathymetry map of the bend measured on the Severn (Figure 4.7), but the resolution is insufficient to allow detailed bedform patterns to be discerned. However, it is possible to visualise local deposition and erosion patterns which reveal that although the bend has an asymmetric planform typical of a meander bend, a large scour has formed at the inside of the bend apex and there has been modification of a local region of higher bathymetry situated landward of the outer bend between the two field seasons. The bathymetry measurements collected at a bend within the Prairie Channel section in contrast show the deepest bathymetry is adjacent to the outside of the bend at the bend apex (Figures 4.23 and 4.24). This channel is much wider (400 m) and is deeper ($<13.5 \text{ m}$) than the bend on the Severn. Large-scale bedforms clearly show fluvially-dominant flow with superimposed bedforms on dune crests. This suggests that the flows occurring within this wider channel will have a different structure to those observed in the Severn. There is a variation in width:depth ratio of the two bends, 11.1 in the case of the Severn and 29.6 in the Columbia. The secondary circulation arising as a consequence of the system geometry can be expected to be different, with a relative decrease in circulation occurring at higher width:depth in Prairie Channel (Parsons *et al.*, 2007; Nanson, 2011).

The previously discussed model of the tidal-fluvial transition zone describes the variations in deposition as fluvial and tidal flow varies whilst referring to the zones of tidal and fluvial energy (Figure 1.3; Dalrymple *et al.*, 1992; Dalrymple and Choi, 2007). However, the relative flows are not quantified at any point within this model or the actual balance between them described. This lack of data within the model causes difficulties when applying it to both ancient and modern systems as this becomes a qualitative measure. Dalrymple *et al.* (2015) apply a schematic representation of

varying tidal and fluvial currents during periods of river flood which are used to interpret ancient deposits, but comparisons to modern systems with these patterns of flows is not made. The large river floods postulated within this schematic representation acts to move the position of the tidal-fluvial transition in a seaward direction. As noted previously the two systems described herein are of very different sizes and geometries, yet comparable maximum flow velocities. The combination of flow velocity measurements and the resultant bedforms described herein allows a more accurate reconstruction of the expected facies within the region of fluvially-dominated but tidally-modified flow. While the addition of quantified flow regime data to the model of the tidal-fluvial transition would result in a more accurate understanding of the zones of deposition, this process data must be couple to the resultant product to be of any use to the understanding of such systems: this is discussed further in the following sections.

6.2 Steering of tidally-influenced flows

Comparison of the flow data at Sandee and Wood reveals that splitting of the flow around the barhead is initiated some distance landward of the barhead. Sandee cross-section A was collected ~400 m landward of the barhead with seaward flow velocities of 1.1 ms^{-1} at lower-low water, slowing to 0.18 ms^{-1} at lower-high water (Figure 2.27). At lower-low water there is a distinct divergence in secondary flow with velocities of $< 0.2 \text{ ms}^{-1}$ (Figures 2.27). This could be suggested to arise from flow diverting into the large channel to the east of the section, however whilst this flow divergence is also observed at cross-section B (Figure 2.28), with similar primary and secondary flow velocities, it is not present at cross-section C (Figure 2.29) which lies seaward of the bar crest. Here the observed cross-stream flow of $< 0.25 \text{ ms}^{-1}$ shows drainage from the bar top into the deeper channel to the east. The divergence is located 100 m from the western bar edge at cross-section A, moving out to 200 m from the western edge at cross-section B, as the minor channel to the west of the measurement section begins to widen. The location of this flow divergence corresponds to the steering of bedforms observed in the bathymetry measurements (Figure 2.27). The secondary channel which has formed to the north of the barhead is relatively minor in comparison to Prairie channel, with a maximum depth of 5 m at high water. At high water flow is diverted past the channel mouth, as illustrated by the lack of flow divergence measured and no evidence of flow from this channel. The bathymetry difference observed at this location between FS1 and FS2 (Figure 2.32) show the building of the bar head onto the previous flat bar shelf. This corresponds to some of the flow steering, suggesting that in addition to the existing channels steering flow some minor bed variations have initiated further depositional patterns at this point.

The flow measurements collected around Wood Bar during FS2 also show flow divergence around the barhead. The furthest landward of the cross-sections, cross-section A, is located ~150 m landward of the barhead observed in the bathymetry measurements (Figure 3.2). Flow velocities measured at this cross-section range from 1.0 ms^{-1} at lower-low water, slowing to almost 0 ms^{-1} just before lower-high water (Figure 3.16). A region of flow divergence is observed ~500 m from the north-western edge of the cross-section with maximum secondary flow velocities of 0.65 ms^{-1} observed after lower-low water and no significant cross-stream flow at lower-high water (Figure 3.16). The ADCP data shows the bed to be sloping at this point (Figure 3.16), directly landward of the barhead (Figure 3.5). Whilst the splitting of the secondary flows is clear, the location is not as precisely defined as within the Sandee Bar, probably due to the more complicated bathymetry at this location. At high water there is no obvious flow divergence observed. During periods of fluvial flow cross-section B, located 150 m seaward of the barhead, is split by the exposed bar (Figure 3.17). However, during high water the bar top was submerged allowing flow measurements to be made across the length of the cross-section. Secondary flow velocities of $<0.17 \text{ ms}^{-1}$ were measured, similar to those at high water in cross-section A, with flow divergence occurring 750 m from the north-western edge of the cross-section. Regions of helical flow are observed within the deeper channel at the eastern edge of all cross-sections, probably induced by the curvature of the channel upstream from Wood Bar; there is no helical flow observed during high water when flow has reversed (Figure 3.16 and 3.17).

The flow measurements at both Sandee and Wood bars reveal that during periods of low water (fluvial flow dominant) flow is parallel to the bar edges, as observed in previous work measuring flow around fluvial bars (McLelland *et al.*, 1999; Parsons *et al.*, 2007). The location of the two bars with relation to the incoming tides differs significantly: Wood Bar is a mid-channel bar within the main Prairie Channel, whilst the measurements at Sandee Bar were made around a bar at the edge of a bar complex adjacent to Prairie Channel (Figure 2.5). Although the effects of flow steering around the bar at low water is directly comparable, at high water the tidal flow will be different, with flow over and around Wood Bar exhibiting some steering effects. Sandee Bar will only see significant flow reversal effects due to tidal flow within Prairie Channel, which can be seen to bypass the secondary channel (Figure 2.30). This steering of tidal flows is considered within the tidally-dominated region of estuaries by Dalrymple and Choi (2007). Within more fluvially-dominated regions tidal flow is only proposed to fully reverse within a channelised region, resulting in the modification of bedforms preserved as grain-size variations. Consideration of the interaction of strong tidal flows with barforms within more fluvially-dominated regions is essential for the interpretation of any deposition which arises.

Flow measurements collected at two locations during the passage of a single tidal bore at a bar in the Severn reveal the variations in flow arising from interaction with the barform (Figure 5.23). Measurements collected at the landward end of the bar top reveal flow velocities of $<1.5 \text{ ms}^{-1}$, whilst flow within the channel is faster, $<3 \text{ ms}^{-1}$. This variation arises due to the diversion of most flow into the channel itself rather than onto the bar top. As a consequence any tidal modification to bedforms within the channel will be noticeably different to bedforms at the bar tail due to this interaction with the barform itself, with the channel deposits exhibiting a more tidally-influenced signature. These local variations in apparent tidal modifications should be expected within other systems, instead of assuming that tidal influence gradually varies with position. The possible presence of tidal bores is not considered within any models of tidal fluvial systems (Rahmani, 1988; Allen, 1991a; Dalrymple and Choi, 2007; Archer, 2013), even when the model describes a system in which they occur, as is the case in the model based on the Gironde Estuary (Allen, 1991a; Reungoat *et al.*, 2015; Keevil *et al.*, 2015a). The limited conditions under which tidal bores form reveal important information about system morphology, scale and tidal range. As such recognition of the possibility that tidal bores may have been present within a system should be included within such models.

6.3 Variations in bedform morphology

Bathymetry measurements made within the Columbia River estuary reveal variations of dune morphology with location. Within the main navigation channel bedform length varies in a seaward direction, with maximum lengths observed at Taylor Sands (Figure 2.34). Although no samples were made within the channel previous work has suggested that there is little variation in grain-size between these locations, reported to be mainly medium sand (Sherwood and Creager, 1990). Whilst dune heights may be undergoing hysteresis (c.f. Kostaschuk and Best, 2005), the variations in length with relative position are postulated to arise due to variations in tidal input. Variations in bedform morphology observed at Wood Bar do not appear to be tidal in origin, but instead arise due to steering of bedforms around a bend landward of the section. Bedforms are present on three scales, with the largest bedforms aligned to flow from the channel located landward of the section, medium bedforms aligned to flow around the barform (including steering around the bar head) and superimposed bedforms aligned to local flow patterns. The scale of the bedforms present within this region of the Columbia River estuary (the largest bedforms had crest separations of up to 200 m and crest heights of 1.5 m) may mean that these multiple scales of alignment are unusual. Further bathymetry measurements would be required within smaller systems to confirm that this is a general process trend. These dunes will appear to be fluvial in

origin, but the internal structure will preserve a more complicated flow structure in the form of grain-size variations and cross-bedding (Figure 6.1). Whilst this is reported as a facies observed within more tidally-dominated channels this hasn't been considered in detail in the tidal-fluvial transition model of Dalrymple and Choi (2007) and would be a useful addition when interpreting fluvially-dominated tidally-influenced beds.

In addition to these fluvial bedforms, which will give rise to complicated cross-bedding patterns, a series of dune spurs are observed within the lee of the large and medium bedforms. Dune spurs usually form parallel to the dominant flow, and variation in the orientation of the spurs across the measurement zone reflects this (Figure 3.20; Allen, 1982; Dalrymple and Rhodes, 1995). However, there are no superimposed bedforms on these spurs, suggesting active migration, and they often have an asymmetric profile, indicating that tidal flow has been forced preferentially along the existing fluvial dune troughs. Flow reversals were observed at high water in the ADCP data collected during bathymetry measurements. Thus, the reworked dune spurs appear to be the only indicator of tidal flow at this location. A series of repeated bathymetry measurements collected adjacent to Wood Bar reveal that whilst the bedforms appear to have a morphology indicative of fluvially-dominated flow crest migrations occur in both seaward and landward directions (Figure 3.23). The final repeat had a noticeably smoother eroded surface, lacking the superimposed bedforms observed previously (Figure 3.12). The seaward migration of dune crests indicates suggest that this is due to an increased fluvial flow, however without studying the underlying bed morphology or local flow patterns this is unclear.

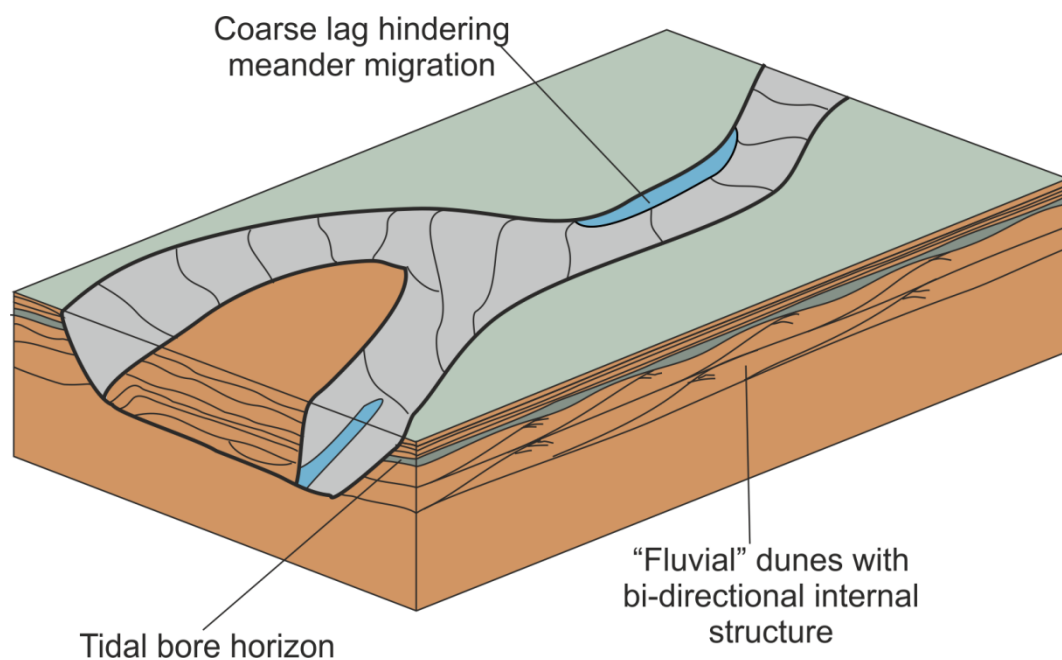


Figure 6.1 Summary diagram of expected bedforms within the fluvially-dominated region of the tidal-fluvial transition. Active channel is shown in grey.

The bathymetric measurements made within the Columbia River estuary reveal topographic steering around the landward barhead at several locations, with dune crests deflecting and steering around bars (Figures 2.22, 2.25, 2.27 and 3.5). In contrast there is no steering observed at the seaward end of barforms, suggesting that either tidal flows are not of a magnitude to influence bedform orientation or that any tidal steering is rapidly reset by the dominant fluvial flow. It is most likely that a mixture of these processes is responsible, with minimal modification of large-scale fluvially-dominated bedforms occurring during periods of landward flow which is re-set when fluvial flow becomes re-established. The seaward end of Wood bar shows fluvial flow recirculating around two elongated bar tails. Although superficially this resembles bars seen within more tidal regions (Hayes, 1975; Dalrymple and Rhodes, 1995), the internal structure and recent seaward migration of the bar reveal that it is of fluvial origin with some tidal modification. This highlights the need to base general models on field data rather than using satellite or aerial imagery (Archer, 2012; Billy *et al.*, 2012; Dalrymple *et al.*, 2012). The seaward migration of Wood bar observed in Figure 3.25 also clearly shows that before 1988 the exposed region of the bar did not possess bar tails. As with all data this represents a snapshot of the processes occurring within the Columbia River estuary, and the assumption of a more tidal origin would not have been made using this earlier data. Bathymetry data was not collected at the point of recirculation at the bar tails, due to the shallow nature of the system, but any landward oriented bedforms present will be of fluvial origin.

In present models of the tidal-fluvial transition, whilst the variation in barform morphologies with increasing tidal influence is often described, the steering effects of flows around these barforms is not usually considered, particularly at the seaward end where any tidal effects may be measured (Dalrymple and Choi, 2007; van den Berg *et al.*, 2007; Archer, 2013; Dalrymple *et al.*, 2015). Whilst tidal inputs may be rapidly overprinted by fluvial flows within this region any steering of flows around the seaward end of bars, and the relative scale of this in comparison to fluvial steering, may be an important indicator of tidal influence which at present is missed. This suggests that careful observation of seemingly fluvial deposits should be made as there may be a degree of tidal influence which is not apparent (Figure 6.1). The present models of tidal-fluvial transition whilst describing the modification of fluvial systems where there is a significant tidal influence do not adequately describe the expected flows and structures where there is a significant fluvial flow (Dalrymple and Choi, 2007; Archer, 2013; Dalrymple *et al.*, 2015). This would be an important addition to models describing the transition between tidal and fluvial systems, raising awareness of the more complicated nature of this seemingly relatively simple flow regime.

The bar sedimentology observed in the Severn appears to be fluvial in origin, with no evidence of tidal rhythmites, flaser bedding or heterolithic beds, all indicators of tidal influence (Reineck and Wunderlich, 1968; van den Berg *et al.*, 2007). The presence of a tidal bore was measured at this location using both ADCP and an ECM. Temperature, salinity and pressure measurements reveal the turbulent nature of the bore passage over the bar top (Figures 5.9-5.12). Soft sediment deformation arising from the passage of a tidal bore has previously been observed in modern systems, but there are currently limited reports of this (Tessier and Terwindt, 1994; Greb and Archer, 2007; Fan *et al.*, 2014). The presence of deformation structures in Core D, at the seaward end of the bar, demonstrate the interaction of the tidal bore with the bar top; at the landward end of the bar the bore is deflected around the bar top (Figure 5.21).

As a consequence of the narrow range of conditions under which a tidal bore forms (shallowing bathymetry, narrowing planform, high tidal range) the presence of this deformation is a useful indicator of palaeosystem morphology. Again, a barform which is seemingly fluvial in origin is revealed to contain subtle indications of tidal flow. The addition of tidal bore deposits to models of the tidal-fluvial transition would be a useful indicator of system morphology within apparently fluvial systems, although it should be noted that tidal bores will only be present in a limited number of systems (Figure 6.1). Recent work by Bonneton *et al.* (2016) to quantify the conditions for tidal bore formation will further aid this reconstruction. There have only been two reports of ancient tidal bores, in part due to the relative lack of modern descriptions (Martinius and Gowland, 2011; Fielding and Joeckel, 2015). Continued work to describe modern tidal bore deposits will enable further recognition within ancient systems, allowing them to be used as indicators of palaeoflow.

The symmetrical bend studied in the Severn estuary has a fixed position and planform morphology due to a balance between the tidal and fluvial flows. As previously discussed, the maximum seaward flows observed during high river flows at a neap tide were of a similar magnitude to the much shorter landward flow observed during low river flows at a spring tide when the flow in the river completely reversed. This fixed bend position is suggested to arise due to the combined effects of the balanced bi-directional flow altering point bar morphology limiting bend asymmetry, the presence of a coarser grained core to the bar which is only modified during periods of high flow and the short-lived strengthening of secondary flows reducing point bar-push effects. Sediment is suggested to be continually re-worked by both tidal and fluvial flows, similar to the superimposed bedforms within the Columbia River. As a consequence the evolution of the system will not follow expected fluvial or tidal pattern. Meander bends within the fluvially-dominated region of tidal-fluvial systems may become fixed. The

model of Dalrymple and Choi (2007) describes a “straight-meander-straight” planform, with the fluviially-dominated region lying within the landward straight region. However, if the planform within this region becomes fixed it would further complicate system evolution during periods of sea-level change where the tidal incursion will be reset. Recognition of the possibility that portions of the system may become fixed is important when such models are used to interpret ancient deposits (e.g., Hubbard *et al.*, 2011; Fustic *et al.*, 2012; Shiers *et al.*, 2014). Further fieldwork identifying the extent of these fixed features and the identification of the relative grain-size differences which result in hindered migration would further inform any changes to the model.

Variations in grain-size will also have an impact on the preserved apparent tidal modification of fluvial flows. Within systems of comparable fluvial flux, coarser grained regions are likely to preserve less evidence of tidal differences than finer grained areas, as is apparent due to the fixed bend planform and the regions of gravel imbrication observed in the Severn. This is summarised in Figure 6.2, which shows the variable apparent flow energy observed within different grain-sizes. The full range of grain-sizes present within a system must therefore be considered when creating a palaeotidal model and grain-size variations must be taken into account when comparing apparently similar systems. Dune and ripple cross-lamination were described by Archer (2013) as a common indication of hypertidal systems, particularly within the innermost regions of deposition such as those studied herein. However, although this model described some facies observed within the Severn Estuary, this pattern of deposition is revealed within laminations of sands and finer grained muds which are not seen within the present work, further illustrating the influence of grain-size on perceived tidal influence.

Tidally-influenced systems with large palaeoflood deposits were found to contain finer interflood deposits, but coarse grained flood deposition (Dalrymple *et al.*, 2015). It was assumed that the only evidence of tidal flow occurs in the interflood deposits, however this does not account for variations as described in Figure 6.2. As the coarser grained flood intervals have not been extensively reworked, it would suggest that there was less tidal influence than stated. While broad regional grain-size patterns have been described within tidal-fluvial systems the recognition that they may preserve differing tidal information is not currently considered (e.g., Rahmani, 1988; Allen, 1991a).

The superimposed bedforms observed within the Columbia River were smaller in scale with rounded crests, often at an oblique angle to the dominant crestlines. They reflect the flow conditions at the time the bathymetry data was collected, representing the dominant fluvial or tidal flow at this time. The eroded repeat surface measured adjacent

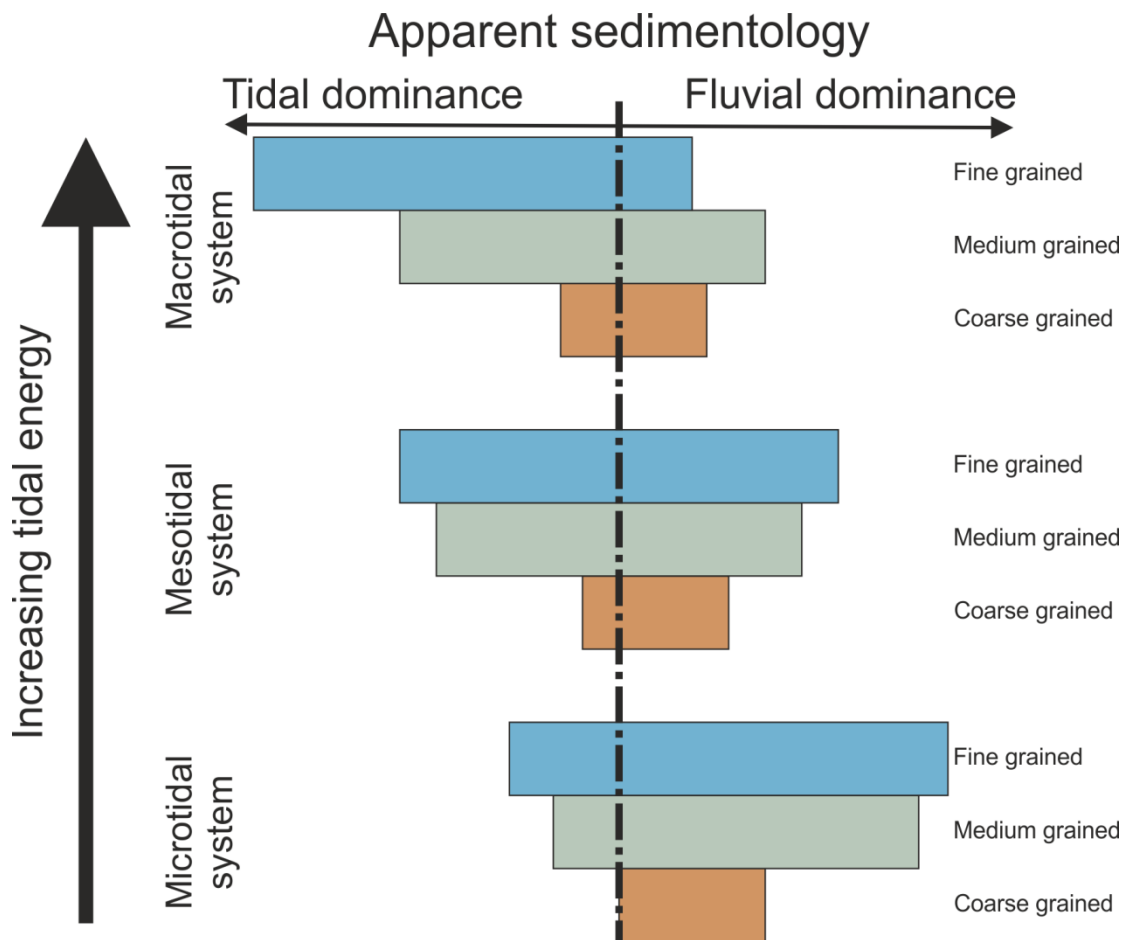


Figure 6.2 Variations in perceived flow energies with grain-size. Fluvial flow is the same for all tidal conditions. As tidal influence decreases coarser material is not reworked and evidence of tidal influence decreases.

to Wood Bar (Figure 3.12) illustrates the transient nature of these superimposed bedforms: although they reflect local flow patterns and may transport large amounts of sediment, ultimately they are reworked into the large bedforms characterising the mean flow at this region. This is further evidence of the varying tidal preservation, as any bedforms arising from tidal modification are rapidly reworked by fluvial flows during periods of lower tidal flux, dependent on the local grain-size distributions (Figure 6.1), and local sediment competence.

Tidal flows within the Columbia River estuary appear to be relatively sediment starved, reworking existing bedforms (modification of large-scale dune crests, movement of superimposed bedforms, reworking of dune spurs). However, large featureless sand sheets with an orientation suggesting transport in a landward direction were observed at both Taylor Sands and Jubilee Channel (Figures 2.15, 2.18 and 2.20). Scour features were associated with both these sand sheets, along with another sheet with no discernible orientation at Desdemona North (Figure 2.10), although the largest scours were associated with Taylor Sands and Jubilee Channel. The Taylor Sands scour was

observed in both field seasons with very little modification of its shape, maintaining a relative depth of 8 m in comparison to the local bathymetry (Figure 2.18). The sand sheets were associated with erosion of the adjacent barforms, the cause of which is unknown. This suggests that in addition to barforms influencing local bedforms by steering fluvial flows as previously discussed, erosion of bar edges releases a large amount of sediment which becomes available to be reworked by tidal flows.

6.4 Effects of system morphology on perceived tidal influence

The present work reveals comparable tidal and fluvial flows are located at a relatively landward position in a macrotidal estuary (Severn) with relatively low fluvial flow where the system has narrowed considerably, and located close to the mouth of a high fluvial flux mesotidal estuary (Columbia). This illustrates the difficulty in assessing the effects of tidal modulation within fluvially-dominated systems. Due to the variations in system size the underlying fluvial signatures of the two systems at the field locations are very different, resulting in different forms of tidal modification with flows of the same magnitude (Figure 6.3). Throughout the field sites the morphology of the bedforms and barforms appear to indicate a purely fluvial origin. However, as previously discussed the flow data reveals that both systems have a significant tidal-influence. Subtle indications of this tidal influence are present, but are overshadowed by the more dominant fluvial processes. This variation in system morphology has not previously been discussed within the description of the tidal-fluvial transition, instead focussing on recognition of facies at certain locations. The modern systems described are generally large in scale, as is the case in both the Columbia River and River Severn, to allow easy identification and quantification of the systems. Whilst the interaction of fluvial flows with barforms can be observed to steer the adjacent bedforms, tidal flows within the region are fluvially-dominated and will be diverted around bar tails, but are of insufficient magnitude to result in the steering of bedforms. However, it is possible for this balance of tidal and fluvial flows to modify point bars, effectively retarding the migration of meander bends. This retardation has been observed within the meandering region of river-estuary systems, which corresponds to the middle estuary (Rahmani, 1988; Allen, 1991a; Archer, 2103), or mixed-energy region (Figure 1.3; Dalrymple and Choi, 2007). However the retarded migration of meanders lying within the fluvially-dominated “straight” landward region has not been previously discussed in detail as flows are expected to be mainly fluvial in nature (Dalrymple and Choi, 2007).

In both field areas the smaller tidal component acts to modify fluvially-dominated bedforms at a variety of scales, resulting in modified large-scale dune shapes and soft-sediment deformation. At all scales this tidal modification is subtle in nature, making

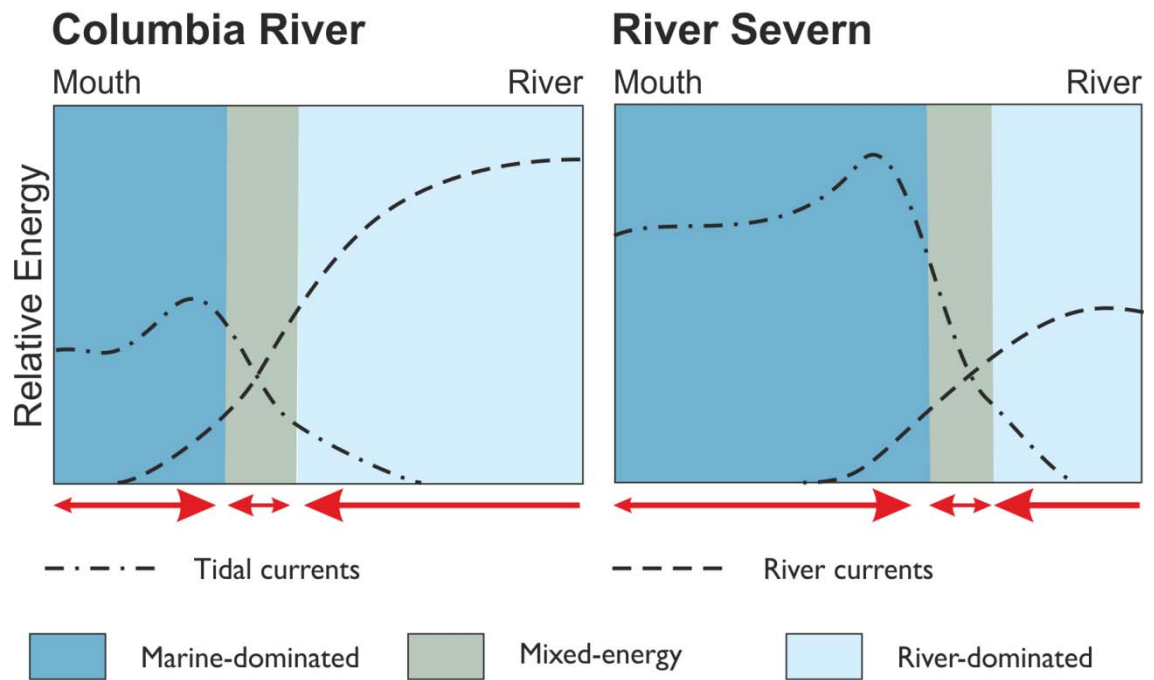


Figure 6.3 Comparison of the relative strengths of tidal and fluvial energy with distance from the mouth of the Columbia River and the River Severn. Red arrows show the dominant flow directions, throughout each system. Whilst the tidal and fluvial flows are balanced at both field locations, which lie within the mixed energy region, overall system flows are very different. Adapted from Figure 1.3 (Dalrymple and Choi, 2007).

recognition of tidally-influenced facies problematic in palaeoenvironments (e.g., Fielding and Joeckel, 2015). This variable response to tidal modification with bedform size is exemplified by the interaction of bedforms on three different scales at the head of Wood Bar (Figure 3.6v). The largest scale bedforms do not appear to have formed in a region with any tidal influence whilst the smallest scale bedforms are modified by the local tidal currents. Therefore, when reconstructing ancient systems, the size of bedforms must also be considered when assessing the amount of tidal influence. This perceived variation in tidal influence with bedform size is summarised in Figure 6.4 which shows simplified variations in microtidal, mesotidal and macrotidal systems, assuming that in other respect the systems are identical (equal fluvial flux, constant grain-size and bedforms of similar sizes). The perceived tidal influence is highly dependent on the size of the bedforms and barforms being studied, with different bedform scales preserving varying tidal-fluvial processes; smaller scale bedforms preserve a higher degree of tidal influence than larger scale bedforms at the same location. Dalrymple and Choi (2007) consider the effects of cross-stratification arising from flow regimes, stating that within fluvial regions ripples and dunes will migrate in a seaward direction. In regions with some degree of tidal influence the only indicators present are likely to be preserved as grain-size changes as bedforms adjust to reversals

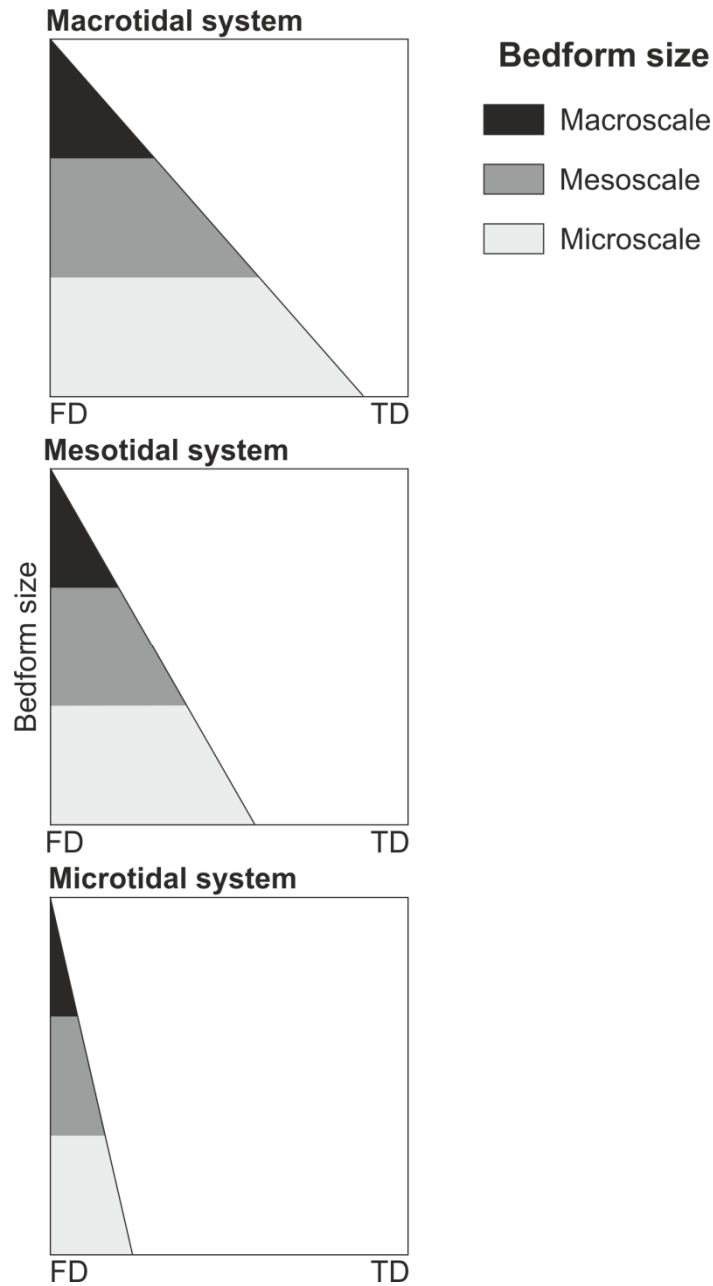


Figure 6.4 Summary of the variations in perceived tidal influence arising due to bedform size within identical tidal systems (fluvial input, grain-size, planform geometry) with varying tidal energy. TD = Tidal dominance, FD = Fluvial dominance.

in flow due to tidal variations. This model does not consider that bedform patterns may be more complicated than simple superimposition with flow reversing along a single axis. The consideration of these multiple bedform scales and their preservation of different flow regimes rather than a simplistic flow reversal (Figure 6.4) would be an important addition particularly within the region of fluvial dominance.

The reduction of bedform scale with increasing tidal influence observed in the Columbia River (Figure 2.34) is also an important system wide indicator of tidal

influence, which further complicates the reconstruction of both the perceived tidal influence and system size. Recognition of this systematic scaling of bedforms with tidal influence would be an important addition to the models of the tidal-fluvial transition such as Dalrymple and Choi (2007). Presently this model refers to a region of tidal bars and channelised deposits with no discussion of their scale or any variations arising with tidal influence.

The similarity of perceived tidal influence preserved within these two very different systems illustrates that the resultant subtle indications of tidal influence do not arise as a consequence of a very high tidal flow within a region of relatively low fluvial flux, or due to lower tides interacting with a high fluvial flux. The results described herein can be applied to all tidal-fluvial transition zones, allowing for a more accurate reconstruction of the region of fluvial dominance. Models of the tidal-fluvial transition have to date focussed on the more tidal regions of systems, describing the bedforms and barforms of these in some detail (e.g., Dalrymple and Choi, 2007; van den Berg *et al.*, 2007; Archer, 2013; Dalrymple *et al.*, 2015). Whilst this is useful for the understanding of systems with a very obvious tidal influence it results in poor interpretation of more fluvially dominated regions such as those studied here. This region of fluvial dominance will result in a large amount of deposition within the tidal-fluvial transition, so it is important that it is fully recognised (Figure 6.1). As discussed previously, it is suggested that the following would be useful additions to the tidal-fluvial transition model (Dalrymple and Choi, 2007), particularly within the fluvially-dominated tidally-influenced region:

- A fuller understanding of the flow regimes which govern the tidal-fluvial transition and the resultant bedforms and the recognition of the effects of the balance between different tidal and fluvial flow (Figure 6.3). Further fieldwork on systems of varying size and tidal range will allow further quantification of the processes and product to be made, allowing a more accurate model to be created.
- The recognition of tidal bore facies as indicators of system scale, morphology and tidal range (Figure 6.1).
- Hindrance of meander migration due to balanced tidal and fluvial flows, resulting in different patterns of point bar deposition, which may be of importance when searching for reservoir facies (Figure 6.1). Identification of such meander bends and an investigation of the facies occurring at the point bar to confirm the suggestion that movement is hindered by coarse lags is needed.

- Consideration of multiple scales of bedforms and their preservation of differing temporal snapshots of the flow regime (Figure 6.4) and variations in internal structure (Figure 6.1). Investigation of further systems will confirm whether this is a general finding or restricted to the system studied herein.
- Recognition of tidal steering around fluvial bedforms when fluvial processes are dominant. This steering was observed around large-scale fluvial bedforms. Further investigations are required to confirm if this finding is applicable within smaller river-estuary systems.
- The variation of bedform scale with increased tidal modulation throughout the tidal-fluvial transition.

These additions will create a model which describes the full length of the tidal-fluvial transition from fully tidal to fully fluvial. Further work is required to fully describe the nature of the fluvially-dominated tidally-influenced region, both flow regime and bedform information, as it is this scarcity of data points which has resulted in the lack of detail within the present model. The present work has studied two modern systems (River Severn and Columbia River) with different tidal ranges (macrotidal and mesotidal) and fluvial flux (low and high fluvial flux). While studies have been made of other tidal systems they have often concentrated on either flow data (e.g., Lacy and Monismith, 2001; Nidzeiko *et al.*, 2009) or deposition (e.g., van den Berg *et al.*, 2007; Billy *et al.*, 2012; Dashtgard and La Croix, 2015). Further work studying both flow and the resultant bedforms will improve the model of the tidal-fluvial transition.

Chapter 7

Conclusions

Although the Columbia River estuary and the River Severn are systems with very different tidal and fluvial inputs, the regions studied in the present work have comparable tidal and fluvial fluxes. Whilst the energy flux of each system is comparable, this results in very different patterns of bedforms and barforms. Flow measurements show that the locations investigated lie within the transitional zone, with the boundary between fully-fluvial and tidal flow varying between measurements. However, at each location whilst the overall morphology appears to be fluvial in nature there are subtle indicators of the tidal influence:

- Bi-directional migration of dunes which was only revealed by repeated bathymetry measurements. The short period of tidally-influenced landward migration is rapidly overprinted by the dominant fluvial flow. However, the internal structure of the dunes will maintain evidence of this bi-directional migration which is not revealed otherwise, and will be of importance when interpreting ancient deposits with reference to modern systems. Closer examination of preserved bedforms will reveal if these subtle distinctions have been missed in previous descriptions, allowing a more accurate palaeogeographic reconstruction.
- Dune spurs located in the lee of dunes which are undergoing topographic steering may undergo tidal modification due to protection by the parent bedform from the dominant fluvial flow and channelling of the tidal flow along troughlines. The resultant spur asymmetry may be the only clear indicator of tidal flow at this location.
- Barforms with a lobate planform are found throughout the Columbia River estuary. Investigations around a single barform at the landward end of the study are found that whilst it appears to be tidally-influenced it is fluvial in origin. The small tidal flow interacting with the seaward end of the bar may have formed a small defect which initiated the lobate form, but bar migration and the elongation of the bar tails arises due to fluvial processes. Recirculation of fluvial flow around the bar tails will result in bedforms with an apparently landward flow direction, however this is not due to any tidal flow.

- The modification of meander point bar results in the slowing of meander migration. The highest flow velocities measured during high river flow at neap tide were comparable to the reversed flow measured during low river flow at spring tide. The re-setting of the point bar may not be obvious within the point bar deposits as the short lived tidal flows are gradually reworked by the dominant fluvial flows. It should be recognised that the position of meander bends within the region of fluvial dominance may be more fixed than in fluvial bends of a similar geometry. As a consequence the resultant deposits will be less laterally extensive than previously proposed.
- Flow measurements of a single bore made both at the bar tail and within the channel reveal that the bore is more turbulent when interacting with the bartop. This interaction has resulted in characteristic soft sediment deformation. Tidal bores form in a limited number of systems with a high tidal range, shallowing bathymetry and narrowing system geometry. As such, the presence of depositional signatures arising from tidal bores is of importance to palaeogeographical system reconstruction and should be added to more general models of the region of tidal-fluvial transition.

The two systems studied provide useful analogues for the region of fluvial dominance with tidal influence. Whilst they are not comparable in system size or relative fluvial and tidal flows, the similar balance of flows and resultant bedforms found in each system reveals that they are not unusual, possibly representing two flow end member. As a consequence the results reported herein can be considered directly applicable to the fluvially-dominated region of the tidal-fluvial transition of other systems. Tidal modification of apparently fluvial bedforms will be found within this region of all systems, although at present this modification has been missed due to the subtle nature of the modification and the previous lack of linked flow and bedform data. The temporal and spatial development of such regions will not be fluvial in nature, as suggested by the apparent bedform architecture, but will be modified by tides, e.g. due to the fixing of meander bends by coarser grained deposits or flow steering in both fluvial and tidal directions. The addition of tidal bores to the model will allow more accurate reconstruction of system morphology. Although tidal bores are present in only a small number of systems they should still be highlighted as a useful indicator of tidal modification, although their relative scarcity should also be noted.

7.1 Further work

This thesis has demonstrated that within the fluvially-dominated tidally-influenced region of river-estuary systems there is variation in barform and bedform morphology.

Further work is suggested to investigate these apparently fluvial deposits which show cryptic tidal modification:

- Further bathymetry measurements to investigate bedform morphology arising from further combinations of fluvial and tidal flow (e.g. higher and lower fluvial fluxes, different tides). This would allow the modification of bedforms under different flow conditions to be further quantified and further inform amendments to the present model of the tidal-fluvial transition (Dalrymple and Choi, 2007) within the region of fluvial dominance with some tidal influence.
- The repeated bathymetry measurements were made at a single location, allowing the seaward and landward migration of bedforms to be investigated. Further series of bathymetry measurements at different locations within the tidal-fluvial transition zone, coupled with flow measurements at the repeat location, will allow this migration to be further quantified. This would allow further quantification of the effects of tidal flow within the region of fluvial dominance in the tidal-fluvial transition. The Columbia River estuary contains bedforms on a number of scales; choosing a location where bedforms are of a different size to those at Wood Bar would further inform these migration rates, as would choosing a channel location. In addition to bedform migration the modification of dune spurs should also be investigated further.
- Wood Bar lies at the landward end of the Columbia River estuary. Further investigations around a bar at a more tidal location would allow a fuller understanding of the tidal-fluvial interaction in this system and further quantify the variations in bedform and barform migration in response to these flows. This will enable a more accurate model of the Columbia River estuary to be created, which will further inform the understanding of tidal interaction within a region of fluvial dominance.
- Further coring and flow work across the tidal cycle to investigate the interaction of tidal bores with underlying barforms would allow a fuller model of tidal bore processes to be investigated. This could be achieved with a series of flow measurements made over several months at a single location, coupled with further coring. Shallow cores would allow bore interaction with the surface to be further understood, whilst a series of deeper cores would fully quantify the bar morphology.

References

- Allen, J.R.L., 1982. *Developments in Sedimentology 68: Sedimentary structures: their character and physical basis*. Elsevier, Amsterdam
- Allen, J.R.L., 1987. Coal dust in the Severn Estuary, Southwestern UK. *Marine Pollution Bulletin* 18, 169-174, doi: 10.1016/0025-326X(87)90241-4
- Allen, J.R.L., 1990. Salt-marsh growth and stratification: A numerical model with special reference to the Severn Estuary, southwest Britain. *Marine Geology* 95, 77-96, doi: 10.1016/0025-3227(90)90042-I
- Allen, G.P., 1991a. Sedimentary processes and facies in the Gironde estuary: a recent model for macrotidal systems. In: Smith, D.G., Reinson, G.E., Zaitlin, B.A., Rahmani, R.A. (Eds.), *Clastic Tidal Sedimentology*, Canadian Society of Petroleum Geologists Memoir 16, pp 29-40.
- Allen, J.R.L., 1991b. Salt-marsh accretion and sea-level movement in the inner Severn Estuary, southwest Britain: the archaeological and historical contribution. *Journal of the Geological Society* 148, 485-494, doi: 10.1144/gsj.148.3.0485
- Allen, J.R.L., 2004. Annual textural banding in Holocene estuarine silts, Severn Estuary Levels (SW Britain): patterns cause and implications. *The Holocene* 14, 536-552, doi: 10.1191/0959683604hl729rp
- Allison, M.A., Nittrouer, C.A. and Kineke, G.C., 1995. Seasonal sediment storage on mudflats adjacent to the Amazon River. *Marine Geology* 125, 303-328, doi: 10.1016/0025-3227(95)00017-S
- Archer, A.W., 2004. Recurring assemblages of biogenic and physical sedimentary structures in modern and ancient extreme macrotidal estuaries. *Journal of Coastal Research* SI43, 4-22. <http://www.jstor.org/stable/25737019>
- Archer, A.W., 2013. World's highest tides: Hypertidal coastal systems in North America, South America and Europe. *Sedimentary Geology* 284-285, 1-25, doi: 10.1016/j.sedg.2012.12.007

- Ashworth, P.J., 1996. Mid-channel bar growth and its relationship to local flow strength and direction. *Earth Surface Processes and Landforms* 21, 103-123, doi: 10.1002/(SICI)1096-9837(199602)21:2<103::AID-ESP569>3.0.CO;2-O
- Baas, J.H., 1994. A flume study on the development and equilibrium morphology of current ripples in very fine sand. *Sedimentology* 41, 185-209, doi: 10.1111/j.1365-3091.1994.tb01400.x
- Bartsch-Winkler, S. and Lynch, D.K., 1988. *Catalog of worldwide tidal bore occurrences and characteristics*. US Geological Survey Circular, No. 1022, 17pp.
- Bathurst, J.C., Thorne, C.R. and Hey, R.D., 1979. Secondary flow and shear stress at river bends. *Journal of Hydraulic Engineering Division-ASCE* 105, 1277-1295
- Bathurst, J.C., Thorne, C.R. and Hey, R.D., 1987. Turbulent structure in a river bend. *Journal of Hydraulic Engineering* 113, 1484-1485, doi: 10.1061/(ASCE)0733-9429(1987)113:11(1484)
- Best, J.L. and Ashworth, P.J., 1997. Scour in large braided rivers and the recognition of sequence stratigraphic boundaries. *Nature* 387, 275-277.
- Best, J.L., Ashworth, P.J., Bristow, C.S. and Roden, J., 2003. Three-dimensional sedimentary architecture of a large, mid-channel sand braid bar, Jamuna River, Bangladesh. *Journal of Sedimentary Research* 73, 516-530, doi: 10.1306/010603730516
- Billy, J., Chaumillon, E., Féliès, H. and Poirier, C., 2012. Tidal and fluvial controls on the morphological evolution of a lobate estuarine tidal bar: The Plassac Tidal Bar in the Gironde Estuary (France). *Geomorphology* 169-170, 86-97, doi: 10.1016/j.geomorph.2012.04.015
- Blanckaert, K., 2011. Hydrodynamic processes in sharp meander bends and their morphological implications. *Journal of Geophysical Research* 116, F01003, doi: 10.1029.2010JF001806
- Blanckaert, K., Duarte, A., Chen, Q. and Schleiss, A.J., 2012. Flow processes near smooth and rough (concave) outer banks in curved open channels. *Journal of Geophysical Research*. 117, F04020, doi: 10.1029/2012JF002414
- Blondeaux, P. and Vittori, G., 2011. Dunes and alternate bars in tidal channels. *Journal of Fluid Mechanics* 670, 558-580, doi: 10.1017/S0022112010005458

- Bonneton, P., Filippini, A.G., Arpaia, L., Bonneton, N. and Ricchiuto, M., 2016. Conditions for tidal bore formation in convergent alluvial estuaries. *Estuarine, Coastal and Shelf Science* 172, 121-127, doi: 10.1016/j.ecss.2016.01.019
- Boyd, R., Dalrymple, R. and Zaitlin, B.A., 1992. Classification of coastal depositional environments. *Sedimentary Geology* 80, 139-150, doi: 10.1016/0037-0738(92)90037-R
- Bridge, J.S., 1993. Description and interpretation of fluvial deposits: A critical perspective. *Sedimentology* 40, 801-810, doi: 10.1111/j.1365-3091.1993.tb01361.x
- Bristow, C.S. and Jol, H.M., 2003. An introduction to ground penetrating radar (GPR) in sediments. In: Bristow, C.S. and Jol, H.M. (Eds.), *Ground Penetrating Radar in Sediments*. Geological Society, London, Special Publications 211, 1-7.
- Bryce, S., Larcombe, P. and Ridd, P.V., 1998. The relative importance of landward-directed tidal sediment transport versus freshwater flood events in the Normanby River estuary, Cape York Peninsula, Australia. *Marine Geology* 149, 55-78, doi: 10.1016/S0025-3227(98)00013-9
- Burger, J.A., Klein, G. de V. and Sanders, J.E., 1969. A field technique for making epoxy relief-peels in sandy sediments saturated with saltwater. *Journal of Sedimentary Petrology* 39, 338-341
- CARIS, 2012. *HIPS and SIPS 7.1 Service Pack 2 User Guide*, 542pp.
- CARIS, 2013. *Technical Note: Sound Velocity Correction for Reson PDS Data*, 100pp.
- Carling, P.A., Chateau, C.C., Leckie, D.A., Langdon, C.T., Scaife, R.G. and Parsons, D.R., 2015. Sedimentology of a tidal point-bar within the fluvial-tidal transition; River Severn Estuary, UK . In: Ashworth, P.J., Best, J.L. and Parsons, D.R. (Eds.), *Developments in Sedimentology 68: Fluvial-Tidal Sedimentology*. Elsevier, Amsterdam, pp 149-189.
- Carling, P.A., Radecki-Pawlik, A., Williams, J.J., Rumble, B., Meshkova, L., Bell, P., Breakspear, R., 2006. The morphodynamics and internal structure of intertidal fine-gravel dunes. *Sedimentary Geology* 183, 159–179, doi: 10.1016/j.sedgeo.2005.07.007
- Carling, P.A., Williams, J.J., Croudace, I.W. and Amos, C.L., 2009. Formation of mud ridge and runnels in the intertidal zone of the Severn Estuary, UK. *Continental Shelf Research* 29, 1913-1926, doi: 10.1016/j.csr.2008.12.009

- Chanson, H., 2012. *Tidal Bores, Aegir, Eagre, Mascaret, Pororoqa: Theory and Observations*. World Scientific, Singapore, 201pp.
- Chaumillon, E., Féliès, H., Billy, J., Breilh, J.-F. and Richetti, H., 2013. Tidal and fluvial controls on the internal architecture and sedimentary facies of a lobate estuarine tidal bar (The Plassac Tidal Bar in the Gironde Estuary, France). *Marine Geology* 346, 58-72, doi: 10.1016/j.margeo.2013.07.017
- Ciffroy, P., Moulin, C. and Gailhard, J., 2000. A model simulating the transport of dissolved and particulate copper in the Seine river. *Ecological Modelling* 127, 99-117, doi: 10.1016/S0304-3800(99)00182-9
- Culver, S.J., 1980. Differential two-way sediment transport in the Bristol Channel and Severn Estuary, UK. *Marine Geology* 34, M39-M43, doi: 10.1016/0025-3227(80)90135-8
- Dalrymple, R.W. and Choi, K., 2007. Morphologic and facies trends through the fluvial-marine transition in tide-dominated depositional systems: A schematic framework for environmental and sequence-stratigraphic interpretation. *Earth-Science Reviews* 81, 135-174, doi: 10.1016/j.earscirev.2006.10.002
- Dalrymple, R.W. and Rhodes, R.N., 1995. Estuarine dunes and bars. In: Perillo, G.M.E. (Ed.), *Developments in Sedimentology 53: Geomorphology and Sedimentology of Estuaries*. Elsevier, Amsterdam, pp 359-422.
- Dalrymple, R.W., Kurcinka, C.E., Jablonski, B.V.J., Ichaso, A.A., Mackay, D.A., 2015. Deciphering the relative importance of fluvial and tidal processes in the fluvial-marine transition. In: Ashworth, P.J., Best, J.L. and Parsons, D.R. (Eds.), *Developments in Sedimentology 68: Fluvial-Tidal Sedimentology*. Elsevier, Amsterdam, pp 3-45.
- Dalrymple, R.W., Mackay, D.A., Ichaso, A.A., Choi, K.S., 2012. Processes, morphodynamics, and Facies of tide-dominated estuaries. In: Davis, R.A. and Dalrymple, R.W. (Eds.), *Principles of Tidal Sedimentology*. Springer, Heidelberg, pp 79-107.
- Dalrymple, R.W., Zaitlin, B.A. and Boyd, R., 1992. Estuarine facies models: Conceptual basis and stratigraphic implications. *Journal of Sedimentary Petrology* 62, 1130-1146.
- Dark, P. and Allen, J.R.L., 2005. Seasonal deposition of Holocene banded sediments in the Severn Estuary Levels (southwest Britain): palynological and sedimentological

evidence. *Quaternary Science Reviews* 24, 11-33, doi: 10.1016/j.quascirev.2004.08.001.

Dashtgard, S.E. and La Croix, A.D., 2015 Sedimentological trends across the tidal-fluvial transition, Fraser River, Canada: A review and some broader implications. In: Ashworth, P.J., Best, J.L. and Parsons, D.R. (Eds.), *Developments in Sedimentology 68: Fluvial-Tidal Sedimentology*. Elsevier, Amsterdam, pp 111-126

Davis, J.L. and Annan, A.P., 1989. Ground-penetrating radar for high-resolution mapping of soil and rock stratigraphy. *Geophysical Prospecting* 37, 531-551.

Davis, R.A., 2012. Tidal signatures and their preservation potential in stratigraphic sequences. In: Davis, R.A. and Dalrymple, R.W. (Eds.), *Principles of Tidal Sedimentology*. Springer, Heidelberg, pp 35-55.

Dietrich, W.E., 1987. Mechanics of flow and sediment transport in river bends. In: Richards, K. (Ed.), *River Channels*, Blackwells, Oxford, pp 179-227.

Dietrich, W.E. and Smith, J.D., 1983. Influence of the point bar on flow through curved channels. *Water Resources Research* 19, 1173-1192.

Dinehart, R.L. and Burau, J.R., 2005. Repeated surveys by acoustic Doppler current profiler for flow and sediment dynamics in a tidal river. *Journal of Hydrology* 314, 1-21, doi: 10.1016/j.jhydrol.2005.03.019

Duquesne, S., Newton, L.C., Giusti, L., Marriott, S.B., Stark, H.-J., Bird, D.J., 2006. Evidence for declining levels of heavy-metals in the Severn Estuary and Bristol Channel, U.K. and their spatial distribution in sediments. *Environmental Pollution* 143, 187-196, doi: 10.1016/j.envpol.2005.12.002

Dyer, K.R., 1996. The definition of the Severn Estuary. *Proceedings of the Bristol Naturalists Society* 56, 53-66.

Dyer, K.R., 1997. *Estuaries: A Physical Introduction* (2nd Edition). John Wiley & Sons, Chichester, 195pp.

Ellis, E.R. and Church, M., 2005. Hydraulic geometry of secondary channels of lower Fraser River, British Columbia, from acoustic Doppler profiling. *Water Resources Research* 41, W08421, doi: 10.1029/2004WR003777

Elliott, M. and McLusky, D.S., 2002. The need for definitions in understanding estuaries. *Estuarine, Coastal and Shelf Science* 55, 815-827.

- Eke, E., Parker, G. and Shimizu, Y., 2014. Numerical modeling of erosional and depositional bank processes in migrating river bends with self-formed width: Morphodynamics of bar push and bank pull. *Journal of Geophysical Research Earth Surface* 119, 1455-1483, doi:10.1002/2013JF003020
- Fagherazzi, S., Gabet, E.J. and Furbish, D.J., 2004. The effect of bidirectional flow on tidal channel planforms. *Earth Surface Processes Landforms* 29, 295-309, doi: 10.1002/esp.1016
- Fain, A.M.V., Jay, D.A., Wilson, D.J., Orton, P.M. and Baptista, A.M., 2001. Seasonal and tidal monthly patterns of particulate matter dynamics in the Columbia River Estuary. *Estuaries* 24, 770-786, doi:10.2307/1352884
- Fan, D., Tu, J., Shang, S. and Cai, G., 2014. Characteristics of tidal-bore deposits and facies associations in the Qiantang Estuary, China. *Marine Geology* 348, 1-14, doi:10.1016/j.margeo.2013.11.012
- Fenies, H., de Resseguier, A. and Tastet, J.-P., 1999. Intertidal clay-drape couplets (Gironde estuary, France). *Sedimentology* 46, 1-15, doi: 10.1046/j.1365-3091.1999.00196.x
- Fielding, C.R. and Joeckel, R.M., 2015. Recognition of tidal-bore deposits in the rock record: towards a facies model. *Journal of Sedimentary Research* 85, 118-123, doi: 10.2110/jsr.2015.14
- FitzGerald, D., Buynevich, I. and Hein, C., 2012. Morphodynamics and facies architecture of tidal inlets and tidal deltas. In: Davis, R.A. and Dalrymple, R.W. (Eds.), *Principles of Tidal Sedimentology*. Springer, Heidelberg, pp 301-333
- Franzetti, M., Le Roy, P., Delacourt, C., Garlan, T., Cancouët, R., Sukhovich, A. and Deschamps, A., 2013. Giant dune morphologies and dynamics in a deep continental shelf environment: Example of the banc du four (Western Brittany, France). *Marine Geology* 346, 17-30, doi: 10.1016/j.margeo.2013.07.014
- Frothingham, K.M. and Rhoads, B.L., 2003. Three-dimensional flow structure and channel change in an asymmetrical compound meander loop, Embarras River, Illinois. *Earth Surface Processes and Landforms* 28, 625-644, doi: 10.1002/esp.471
- Furbish, D.J., 1988. River-bend curvature and migration: How are they related? *Geology* 16, 752-755, doi: 10.1130/0091-7613(1988)016<0752:RBCAMH>2.3.CO;2

- Fustic, M., Hubbard, S.M., Spencer, R., Smith, D.G., Leckie, D.A., Bennett, B., Larter, S., 2012. Recognition of down-valley translation in tidally influenced meandering fluvial deposits, Athabasca Oil Sands (Cretaceous), Alberta, Canada. *Marine and Petroleum Geology* 29, 219-232, doi: 10.1016/j.marpetgeo.2011.08.004
- Gingras, M.K. and MacEachern, J.A., 2012. Tidal ichnology of shallow-water clastic settings. In: Davis, R.A. and Dalrymple, R.W. (Eds.), *Principles of Tidal Sedimentology*. Springer, Heidelberg, pp 57-77.
- Ginsberg, S.S. and Perillo, G.M.E., 1999. Deep-scour holes at tidal channel junctions, Bahia Blanca Estuary, Argentina. *Marine Geology* 160, 171-182, doi: 10.1016/S0025-3227(99)0019-5
- Gray, M., Xu, Z. and Masliyah, J., 2009. Physics in the oil sands of Alberta. *Physics Today* 62, 31-35.
- Greb, S.F. and Archer, A.W., 2007. Soft-sediment deformation produced by tides in a meizoseismic area, Turnagain Arm, Alaska. *Geology* 35, 435-438, doi: 10.1130/G23209A.1
- Hayes, M.O., 1975. Morphology of sand accumulation in estuaries: An introduction to the symposium. In: Cronin, L.G. (Ed). *Estuarine Research Volume II: Geology and Engineering*, Academic Press, Inc, London, pp 3-22
- Hibma, A., Stive, M.J.F. and Wang, Z.B., 2004. Estuarine morphodynamics. *Coastal Engineering* 51, 765-778, doi: 10.1016/j.coastaleng.2004.07.008
- Hickin, E.J. and Nanson, G.C., 1975. Character of channel migration on the Beatton River, northwest British Columbia, Canada. *Geological Society of America Bulletin* 86, 487-494.
- Hubbard, S.M., Smith, D.G., Nielsen, H., Leckie, D.A., Fustic, M., Spencer, R.J. and Bllow, L., 2011. Seismic geomorphology and sedimentology of a tidally influenced river deposit, Lower Cretaceous Athabasca oil sands, Alberta, Canada. *AAPG Bulletin* 95, 1123-1145, doi: 10.1306/1231010111
- Hughes, Z.J., 2012. Tidal channels on tidal flats and marshes. In: Davis, R.A. and Dalrymple, R.W. (Eds.), *Principles of Tidal Sedimentology*. Springer, Heidelberg, pp 269-300
- Jay, D.A., Giese, B.S. and Sherwood, C.R., 1990. Energetics and sedimentary processes in the Columbia River Estuary. *Progress in Oceanography* 25, 157-174.

- Jay, D.A., Leffler, K. and Degens, S., 2011. Long-term evolution of Columbia River Tides. *Journal of Waterway, Port, Coastal, and Ocean Engineering* 137, 182-191, doi: 10.1061/(ASCE)WW.1943-5460.0000082
- Jonas, P.J.C. and Millward, G.E., 2010. Metals and nutrients in the Severn Estuary and Bristol Channel: Contemporary inputs and distributions. *Marine Pollution Bulletin* 61, 52-67, doi: 10.1016/j.marpolbul.2009.12.013
- Keevil, C.E., Chanson, H. and Reungoat, D., 2015a. Fluid flow and sediment entrainment in the Garonne River bore and tidal bore collision. *Earth Surface Processes and Landforms* 40, 1574-1586, doi: 10.1002/esp.3735
- Keevil, C.E., Parsons, D.R., Ainsley, M. and Keevil, G.M., 2015b. Three-dimensional meander bend flow within the tidally-influenced fluvial zone. In: Ashworth, P.J., Best, J.L. and Parsons, D.R. (Eds.), *Developments in Sedimentology 68: Fluvial-Tidal Sedimentology*. Elsevier, Amsterdam, 127-148.
- Kirby, R., 2010. Distribution, transport and exchanges of fine sediment, with tidal power implications: Severn Estuary, UK. *Marine Pollution Bulletin* 61, 21-36, doi: 10.1016/j.marpolbul.2009.12.011
- Kjerfve, B., Shao, C.-C. and Stapor, F.W., 1979. Formation of deep scour holes at the junction of tidal creeks: an hypothesis. *Marine Geology* 33, M9-M14
- Kostaschuk, R. and Best, J., 2005. Response of sand dune to variations in tidal flow: Fraser Estuary, Canada. *Journal of Geophysical Research* 110, F04S04, doi: 10.1029/2004JF000176
- Kostaschuk, R., Best, J. and Villard, P.V., 2010. The influence of dunes on mixing in a migrating salt-wedge: Fraser River estuary, Canada. *Earth Surface Processes and Landforms* 35, 460-465, doi: 10.1002/esp.1928
- Kostaschuk, R., Best, J., Villard, P., Peakall, J., and Franklin, M., 2005. Measuring flow velocity and sediment transport with an acoustic Doppler current profiler. *Geomorphology* 68, 25-37, doi: 10.1016/j.geomorph.2004.07.012
- Kuecher, G.J., Woodland, B.G. and Broadhurst, F.M., 1990. Evidence of deposition from individual tides and of tidal cycles from the Francis Creek Shale (host rock to the Mazon Creek Biota), Westphalian D (Pennsylvanian), northeastern Illinois. *Sedimentary Geology* 68, 211-221, doi: 10.1016/0037-0738(90)90113-8

- La Croix, A.D. and Dashtgard, S.E., 2015. A synthesis of depositional trends in intertidal and upper subtidal sediments across the tidal-fluvial transition in the Fraser River, Canada. *Journal of Sedimentary Research* 85, 683-698, doi: 10.2110/jsr.2015.47
- Lacy, J.R. and Monismith, S.G., 2001. Secondary currents in a curved, stratified, estuarine channel. *Journal of Geophysical Research* 106, C12, 31283-31302.
- Longhitano, S.G., Mellere, D., Steel, R.J. and Ainsworth, R.B., 2012. Tidal depositional systems in the rock record: A review and new insights. *Sedimentary Geology* 279, 2-222, doi: 10.1016/j.sedgeo.2012.03.024
- Manning, A.J., Langston, W.J., Jonas, P.J.C., 2010. A review of sediment dynamics in the Severn Estuary: Influence of flocculation. *Marine Pollution Bulletin* 61, 37-51, doi: 10.1016/j.marpolbul.2009.12.012
- Marani, M., Lanzoni, S., Zandolin, D., Seminara, G. and Rinaldo, A., 2002. Tidal meanders. *Water Resources Research* 38, 1225, doi:10.1029/2001WR000404
- Markham, A.J. and Thorne, C.R., 1992. Geomorphology of gravel-bed rivers. In: Billi, P., Hey, R.D., Thorne, C.R., Tacconi, P. (Eds.), *Dynamics of Gravel-bed Rivers*. Wiley and Sons, Chichester, 433-450
- Martinius, A.W. and Gowland, S., 2011. Tide-influenced fluvial bedforms and tidal bore deposits (Late Jurassic Lourinhã Formation, Lusitanian Basin, western Portugal). *Sedimentology* 58, 285-324, doi: 10.1111/j.1365-3091.2010.01185.x
- Masselink, G., Cointre, L., Williams, J., Gehrels, R. and Blake, W., 2009. Tide-driven dune migration and sediment transport on an intertidal shoal in a shallow estuary in Devon, UK. *Marine Geology* 262, 82-95, doi: 10.1016/j.margeo.2009.03.009
- McLelland, S.J., Ashworth, P.J., Best, J.L., Roden, J. and Klaassen, G.J., 1999. Flow structure and transport of sand-grade suspended sediment around an evolving braid bar, Jamuna River, Bangladesh. In: Smith, N.D. and Rogers, J. (Eds.), *Fluvial Sedimentology VI*, Special Publication of the International Association of Sedimentologists 28, 43-57
- Muste, M., Yu, K., Pratt, T. and Abraham, D., 2004a. Practical aspects of ADCP data use for quantification of mean river flow characteristics; Part II: fixed-vessel measurements. *Flow Measurement and Instrumentation* 15, 17-28, doi: 10.1016/j.flowmeasinst.2003.09.002

- Muste, M., Yu, K. and Spasojevic, M., 2004b. Practical aspects of ADCP data use for quantification of mean river flow characteristics; Part I: moving-vessel measurements. *Flow Measurement and Instrumentation* 15, 1-16, doi: 10.1016/j.flowmeasinst.2003.09.001
- Naik, P.K. and Jay, D.A., 2005. Estimation of Columbia River virgin flow: 1879 to 1928. *Hydrological Processes* 19, 1807-1824, doi: 10.1002/hyp.5636
- Naik, P.K. and Jay, D.A., 2011. Human and climate impacts on Columbia River hydrology and salmonids. *River Research and Applications* 27, 1270-1276, doi: 10.1002/rra.1422
- Nanson, R.A., 2010. Flow fields in tightly curving meander bends of low width-depth ratio. *Earth Surface Processes and Landforms* 35, 119-135, doi: 10.1002/esp.1878
- Neal, A., 2004. Ground-penetrating radar and its use in sedimentology: principles, problems and progress. *Earth-Science Reviews* 66, 261-330, doi: 10.1016/j.earscirev.2004.01.004
- Nidzieko, N.J., Hench, J.L. and Monismith, S.G., 2009. Lateral circulation in well-mixed and stratified estuarine flows with curvature. *Journal of Physical Oceanography* 39, 831-851, doi: 10.1175/2008JPO4017.1
- Nittrouer, J.A., Allison, M.A. and Campanelle, R., 2008. Bedform transport rates for the lowermost Mississippi River. *Journal of Geophysical Research* 113, F03004, doi: 10.1029/2007JF000795
- NOAA, 2014. Datums for 9439040, Astoria, OR. (Accessed 01/07/2014)
<http://tidesandcurrents.noaa.gov/datums.html?units=1&epoch=0&id=9439040&name=Astoria&state=OR>
- Olariu, C., Steel, R.J., Dalrymple, R.W. and Gingras, M.K., 2012. Tidal dunes versus tidal bars: The sedimentological and architectural characteristics of compound dunes in a tidal seaway, the lower Baronia Sandstone (Lower Eocene), Ager Basin, Spain. *Sedimentary Geology* 279, 134-155, 10.1016/j.sedgeo.2012.07.018
- Olariu, C., Steel, R.J., Olariu, M.I. and Choi, K., 2015. Facies and architecture of unusual fluvial-tidal channels with inclined heterolithic strata: Campanian Neslen Formation, Utah, USA. . In: Ashworth, P.J., Best, J.L. and Parsons, D.R. (Eds.), *Developments in Sedimentology 68: Fluvial-Tidal Sedimentology*, 353-394.

- Parsons, D.R., Best, J.L., Lane, S.N., Orfeo, O., Hardy, R.J. and Kostaschuk, R., 2007. Form roughness and the absence of secondary flow in a large confluence-diffuence, Rio Parana, Argentina. *Earth Surface Processes and Landforms* 32, 155-162, doi: 10.1002/esp.1457
- Parsons, D.R., Best, J.L., Orfeo, O., Hardy, R.J., Kostaschuk, R. and Lane, S.N., 2005. Morphology and flow fields of three-dimensional dunes, Rio Paraná, Argentina: Results from simultaneous multibeam echo sounding and acoustic Doppler current profiling. *Journal of Geophysical Research* 110, F04S03, doi: 10.1029/2004JF000231
- Parsons, D.R., Jackson, J.A., Czuba, J.A., Engel, F.L., Rhoads, B.L., Oberg, K.A., Best, J.L., Mueller, D.S., Johnson, K.K., Riley, J.D., 2013. Velocity Mapping Toolbox (VMT): a processing and visualisation suite for moving-vessel ADCP measurements. *Earth Surface Processes and Landforms* 38, 1244-1260, doi: 10.1002/esp.3367
- Phillips, M.R. and Crisp, S., 2010. Sea level trends and NAO influences: The Bristol Channel/Severn Estuary. *Global and Planetary Change* 73, 211-218, doi: 10.1016/j.gloplacha.2010.06.005
- Prokocki, E., Best, J.L., Ashworth, P.J., Parsons, D.R., Sambrook Smith, G.H., Nicholas, A.P., Simpson, C.J., Wang, H., Sandbach, S.D. and Keevil, C.E., 2015. Mid to late Holocene geomorphological and sedimentological evolution of the fluvial-tidal zone: Lower Columbia River, WA/OR, USA. In: Ashworth, P.J., Best, J.L. and Parsons, D.R. (Eds.), *Developments in Sedimentology 68: Fluvial-Tidal Sedimentology*, 193-226.
- Rahmani, R.A., 1988. Nearshore sedimentation of a late Cretaceous epicontinental sea. In: de Boer, P.L., van Gelder, A. and Nio, S.D. (Eds.), *Tide-Influenced Sedimentary Environments and Facies*, 433-471.
- Rahmani, R.A., 2000. Facies and types of river deltas and estuaries: perspective of a practicing clastic sedimentologist. *Proceedings of the annual meeting of GAC/MAC held in Calgary, May 29-June 1, 2000*.
- Reesink, A.J.H. and Bridge, J.S., 2009. Influence of bedform superimposition and flow unsteadiness on the formation of cross strata in dunes and unit bars – Part 2, further experiments. *Sedimentary Geology* 222, 274-300, doi: 10.1016/j.sedgeo.2009.09.014

- Reineck, H.-E. and Wunderlich, F., 1968. Classification and origin of flaser and lenticular bedding. *Sedimentology* 11, 99-104, doi: 10.1111/j.1365-3091.1968.tb00843.x
- Rennie, C.D. and Church, M., 2010. Mapping spatial distributions and uncertainty of water and sediment flux in a large gravel bed river reach using an acoustic Doppler current profiler. *Journal of Geophysical Research* 115, F03035, doi: 10.1029/2009JF001556.
- RESON, 2007. *SeaBat 7125 Multibeam Echo Sounder Operator's Manual version 5.00*, 100pp.
- Reungoat, D., Chanson, H. and Keevil, C., 2014. Turbulence, sedimentary processes and tidal bore collision in the Arcins Channel, Garonne River (October 2013). *Hydraulic Model Report No. CH94/14*, School of Civil Engineering, The University of Queensland, Brisbane, Australia, 145pp.
- Reungoat, D., Chanson, H. and Keevil, C., 2015. Field Measurements of Unsteady Turbulence in a Tidal Bore: the Garonne River in October 2013. *Journal of Hydraulic Research* 53, 291-301, doi: 10.1080/00221686.2015.1021717
- Rowbotham, F.W., 1983. *The Severn Bore*. David and Charles, Dawlish, 3rd edition, 104pp.
- Rozovskii, I.L. 1957. Flow of Water in Bends of Open Channels. Academy of Sciences of the Ukrainian SSR: Kiev (translated from Russian by the Israel Program for Scientific Translations, Jerusalem, 1961).
- Sambrook Smith G.H., Ashworth, P.J., Best, J.L., Woodward, J. and Simpson, C.J., 2006. The sedimentology and alluvial architecture of the sandy braided South Saskatchewan River, Canada. *Sedimentology* 53, 413-434, doi: 10.1111/j.1365-3091.2005.00769.x
- Sambrook Smith G.H., Best, J.L., Ashworth, P.J., Lane, S.N., Parker, N.O., Lunt, I.A., Thomas, R.E. and Simpson, C.J., 2010. Can we distinguish flood frequency and magnitude in the sedimentological record of rivers? *Geology* 38, 579-582, doi: 10.1130/G30861.1
- Seim, H.E. and Gregg, M.C., 1997. The importance of aspiration and channel curvature in producing strong vertical mixing over a sill. *Journal of Geophysical Research* 102, C2, 3451-3472, doi: 10.1029/96JC03415

- Sherwood, C.P. and Creager, J.S., 1990. Sedimentary geology of the Columbia River Estuary. *Progress in Oceanography* 25, 15-79, doi: 10.1016/0079-6611(90)90003-K
- Sherwood, C.P., Jay, D.A., Harvey, R.B., Hamilton, P. and Simenstad, C.A., 1990. Historical changes in the Columbia River Estuary. *Progress in Oceanography* 25, 299-352, doi: 10.1016/0079-6611(90)90011-P
- Shiers, M.N., Mountney, N.P., Hodgson, D.M. and Cobain, S.L., 2014. Depositional controls on tidally influenced fluvial successions, Neslen Formation, Utah, USA. *Sedimentary Geology* 311, 1-16, doi: 10.1016/j.sedgoc.2014.06.005
- Simenstad, C.A., Small, L.F., McIntire, C.D., Jay, D.A. and Sherwood, C., 1990. Columbia River Estuary studies: An introduction to the estuary, a brief history, and prior studies. *Progress in Oceanography* 25, 1-13, doi: 10.1016/0079-6611(90)90002-J
- Simenstad, C.A., Burke, J.L., O'Connor, J.E., Cannon, C., Heatwole, D.W., Ramirez, M.F., Waite, I.R., Counihan, T.D., and Jones, K.L., 2011. *Columbia River Estuary Ecosystem Classification—Concept and Application: U.S. Geological Survey Open-File Report 2011-1228*, 54 pp.
- Simmons, S.M., Parsons, D.R., Best, J.L., Orfeo, O., Lane, S.N., Kostaschuk, R., Hardy, R.J., West, G., Malzone, C., Marcus, J. and Pocwiardowski, P., 2010. Monitoring suspended sediment dynamics using MBES. *Journal of Hydraulic Engineering* 136, 45-49, doi: 10.1061/(ASCE)HY.1943-7900.0000110
- Simon, B., 2013. Effects of tidal bores on turbulent mixing: a numerical and physical study in positive surges. Unpublished Phd Thesis, pp 259.
- Smith, D.G., Hubbard, S.M., Leckie, D.A. and Fustic, M., 2009. Counter point bar deposits: lithofacies and reservoir significance in the meandering modern Peace River and ancient McMurray Formation, Alberta, Canada. *Sedimentology* 56, 1655-1669, doi: 10.1111/j.1365-3091.2009.01050.x
- Szupiany, R.N., Amsler, M.L., Best, J.L. and Parsons, D.R., 2007. Comparison of Fixed- and Moving-Vessel Flow Measurements with an aDp in a Large River. *Journal of Hydraulic Engineering* 133, 1299-1309, doi: 10.1061/(ASCE)07933-9429(2007)133:12(1299)
- Teledyne RD Instruments, 2007. *WorkHorse Rio Grande Acoustic Doppler Current Profiler: Technical Manual*, 264pp.

- Tessier, B. and Terwindt, J.H.J., 1994. An example of soft-sediment deformations in an intertidal environment: the effect of a tidal bore. *Comptes Rendus de l'Academie des Sciences Serie II* 319, 217-233
- Townend, I.H., Wang, Z.B. and Rees, J.G., 2007. Millennial to annual volume changes in the Humber Estuary. *Proceedings of the Royal Society A* 463, 837-854, doi: 10.1098/rspa.2006.1798
- Uncles, R.J., 2002. Estuarine physical processes research: some recent studies and progress. *Estuarine, Coastal and Shelf Science* 55, 829-856.
- Uncles, R.J., 2010. Physical properties and processes in the Bristol Channel and Severn Estuary. *Marine Pollution Bulletin* 61, 5-20, doi: 10.1016/j.marpolbul.2009.12.010
- Uncles, R.J., Easton, A.E., Griffiths, M.L., Harris, C., Howland, R.J.M., King, R.S., Morris, A.W. and Plummer, D.H., 1998. Seasonality of the turbidity maximum in the Humber-Ouse estuary, UK. *Marine Pollution Bulletin* 37, 206-215, doi: 10.1016/S0025-326X(98)90157-6
- van den Berg, J.H., Boersma, J.R. and van Gelder, A., 2007. Diagnostic sedimentary structures of the fluvial-tidal transition zone – Evidence from deposits of the Rhine and Meuse. *Geologie en Mijnbouw-Netherlands Journal of Geosciences* 86, 287-306
- van der Mark, C.F. and Blom, A., 2007. *A new and widely applicable bedform tracking tool*. University of Twente, 48pp.
- van der Mark, C.F., Blom, A., and Hulscher, S.J.M.H., 2008. Quantification of variability in bedform geometry. *Journal of Geophysical Research* 113, F03020, doi: 10.1029/2007JF000940
- van Rijn, L.C., 2007. Unified View of Sediment Transport by Currents and Waves. I: Initiation of Motion, Bed Roughness, and Bed-Load Transport. *Journal of Hydraulic Engineering* 133, 649-667.
- Villard, P.V. and Church, M., 2005. Bar and dune development during a freshet: Fraser River Estuary, British Columbia, Canada. *Sedimentology* 52, 737-756, doi: 10.1111/j.1365-3091.2005.00721.x

- Webb, N.D., Seyler, B. and Grube, J.P., 2015. Geologic reservoir characterization of Carboniferous fluvio-tidal deposits of the Illinois Basin, USA. In: Ashworth, P.J., Best, J.L. and Parsons, D.R. (Eds.), *Developments in Sedimentology 68: Fluvial-Tidal Sedimentology*, 395-444.
- Woodward, J., Ashworth, P.J., Best, J.L., Sambrook Smith, G.H. and Simpson, C.J., 2003. The use and application of GPR in sandy fluvial environments: methodological considerations. Bristow, C.S. and Jol, H.M. (Eds.), *Ground Penetrating Radar in Sediments*. Geological Society, London, Special Publications 211, 127-142.
- Xie, D., Wang, Z., Gao, S. and De Vriend, H.J., 2009. Modeling the tidal channel morphodynamics in a macro-tidal embayment, Hangzhou Bay, China. *Continental Shelf Research* 29, 1757-1767, doi: 10.1016/j.csr.2009.03.009
- Yang, Z. and Khangaonkar, T., 2008. Modeling of salt intrusion, intertidal mixing, and circulation in a braided estuary. *Journal of Coastal Research* Special Issue 52, 171-180.
- Yorke, T.H., Oberg, K.A., 2002. Measuring river velocity and discharge with acoustic Doppler profilers. *Flow Measurement and Instrumentation* 13, 191-195, doi: 10.1016/S0955-5986(02)00051-1

Appendix I

Reungoat, D., Chanson, H. and Keevil, C., 2015. Field Measurements of Unsteady Turbulence in a Tidal Bore: the Garonne River in October 2013. *Journal of Hydraulic Research* 53, 291-301, doi: 10.1080/00221686.2015.1021717

Fieldwork was carried out between 18th-20th October 2013 at Bras d'Arcins near Bordeaux, France. Data was calibrated and interpreted by the authors, and the paper written following discussions. This work was carried out during the author's PhD studies, but does not form part of the main thesis.

Appendix II

Keevil, C.E., Chanson, H. and Reungoat, D., 2015a. Fluid flow and sediment entrainment in the Garonne River bore and tidal bore collision. *Earth Surface Processes and Landforms* 40, 1574-1586, doi: 10.1002/esp.3735

Fieldwork was carried out between 18th-20th October 2013 at Bras d'Arcins near Bordeaux, France. Data was calibrated and interpreted by the authors, and the paper written following discussions. This work was carried out during the author's PhD studies, but does not form part of the main thesis.